BNL-90897-2009

Progress on Nuclear Data Covariances: AFCI-1.2 Covariance Library

P.Oblo˘zinsk´y, C.M.Mattoon, M.Herman, S.F.Mughabghab, M.T.Pigni
National Nuclear Data Center, BNL, Upton, NY 11973, USA

P. Talou, G.M. Hale, A.C. Kahler, T.Kawano, R.C. Little, P.G. Young
LANL, Los Alamos, NM 87545, USA

September 28, 2009

Energy Sciences & Technology Department
National Nuclear Data Center
Brookhaven National Laboratory
P.O. Box 5000
Upton, NY 11973-5000
www.bnl.gov

Notice: This manuscript has been co-authored by employees of Brookhaven Science Associates, LLC under Contract No. DE-AC02-98CH10886 with the U.S. Department of Energy. The publisher by accepting the manuscript for publication acknowledges that the United States Government retains a non-exclusive, paid-up, irrevocable, world-wide license to publish or reproduce the published form of this manuscript, or allow others to do so, for United States Government purposes.

This preprint is intended for publication in a journal or proceedings. Since changes may be made before publication, it may not be cited or reproduced without the author's permission.

DISCLAIMER

This report was prepared as an account of work sponsored by an agency of the United States Government. Neither the United States Government nor any agency thereof, nor any of their employees, nor any of their contractors, subcontractors, or their employees, makes any warranty, express or implied, or assumes any legal liability or responsibility for the accuracy, completeness, or any third party's use or the results of such use of any information, apparatus, product, or process disclosed, or represents that its use would not infringe privately owned rights. Reference herein to any specific commercial product, process, or service by trade name, trademark, manufacturer, or otherwise, does not necessarily constitute or imply its endorsement, recommendation, or favoring by the United States Government or any agency thereof or its contractors or subcontractors. The views and opinions of authors expressed herein do not necessarily state or reflect those of the United States Government or any agency thereof.

Progress on Nuclear Data Covariances: AFCI-1.2 Covariance Library

P.Obložinský, C.M.Mattoon, M.Herman, S.F.Mughabghab, M.T.Pigni
National Nuclear Data Center, BNL, Upton, NY 11973, USA

P. Talou, G.M. Hale, A.C. Kahler, T.Kawano, R.C. Little, P.G. Young
LANL, Los Alamos, NM 87545, USA

September 28, 2009

Abstract

Improved neutron cross section covariances were produced for 110 materials including 12 light nuclei (coolants and moderators), 78 structural materials and fission products, and 20 actinides. Improved covariances were organized into AFCI-1.2 covariance library in 33-energy groups, from 10^{-5} eV to 19.6 MeV.

BNL contributed improved covariance data for the following materials: ^{23}Na and ^{55}Mn where more detailed evaluation was done; improvements in major structural materials ^{52}Cr, ^{56}Fe and ^{58}Ni; improved estimates for remaining structural materials and fission products; improved covariances for 14 minor actinides, and estimates of mubar covariances for ^{23}Na and ^{56}Fe.

LANL contributed improved covariance data for ^{235}U and ^{239}Pu including prompt neutron fission spectra and completely new evaluation for ^{240}Pu. New R-matrix evaluation for ^{16}O including mubar covariances is under completion.

BNL assembled the library and performed basic testing using improved procedures including inspection of uncertainty and correlation plots for each material. The AFCI-1.2 library was released to ANL and INL in August 2009.

Contents

1 Introduction **3**

2 Progress in nuclear data covariances **5**

2.1 BNL progress in covariance methodology . . . 5

2.1.1 Resonance region . . . 5

2.1.2 Fast neutron region . . . 6

2.2 LANL progress in covariance methodology . . . 6

2.3 BNL covariance work . . . 8

2.3.1 ^{23}Na . . . 8

2.3.2 ^{55}Mn . . . 12

2.3.3 ^{52}Cr and ^{58}Ni . . . 15

2.3.4 ^{56}Fe . . . 16

2.3.5 Mubars for ^{23}Na and ^{56}Fe . . . 18

2.3.6 Other structural materials . . . 24

2.3.7 Fission products . . . 24

2.3.8 Minor actinides . . . 26

2.4 LANL covariance work . . . 27

2.4.1 Light nuclei . . . 27

2.4.2 Actinides Improvements . . . 30

2.4.3 Prompt fission neutron spectrum for n(0.5 MeV)+^{239}Pu. . . . 35

2.4.4 n+^{240}Pu . . . 37

3 AFCI-1.2 covariance library **45**

3.1 Creation of library . . . 45

3.2 Quality assurance . . . 46

3.2.1 Data checking . . . 46

3.2.2 Data testing . . . 50

3.2.3 Some issues identified by QA . . . 52

4 Conclusions **56**

Bibliography **58**

A AFCI-1.2 covariances **60**
A.1 Contents of the library 60
A.2 Covariance plots 65
A.2.1 Light nuclei 66
A.2.2 Structural materials and fission products 87
A.2.3 Actinides 165
A.2.4 Mubars and Fission Spectra 205

B ^{240}Pu evaluation **206**

Chapter 1

Introduction

The present M2 Report (Milestone 2) describes FY2009 results of the BNL-LANL effort to produce covariances of neutron-induced reactions for the AFCI data adjustment project. The scope and deliverables were explained in detail in our M2 FY2008 Report [1] and can be summarized as follows:

- List of materials covers 110 materials, including 12 light nuclei (LANL responsible), 78 structural materials and fission products (BNL responsible) and 20 actinides (LANL responsible).
- Reactions include four main channels (elastic, capture, inelastic, n2n) for all materials, plus charged particle emission for light nuclei, and fission and $\bar{\nu}$ (nubars) for actinides.
- Covariances (uncertainties and correlation matrices) should be delivered in 33-energy group structure, covering the energy range from 10^{-5} eV to 19.6 MeV.

In FY2008 and partly also in FY2009 our work was conducted under the Global Nuclear Energy Partnership (GNEP) that aimed to combine the closed nuclear fuel cycle concept with the development of new types of reprocessing plants and fast reactors. Late in FY2009 GNEP technical activities metamorphosed into the Advanced Fuel Cycle Initiative (AFCI) and the covariance library name was changed from GNEP to AFCI accordingly.

The initial version of the covariance library, GNEP-1.0, was released in October 2008 and contained starter files for 108 materials, most of which were taken from the low-fidelity covariance project. Based on the feedback from the AFCI user group at ANL and INL we produced improved covariances for 11 important materials (including ^{53}Cr omitted from the original list) as well as mubars for ^{23}Na and ^{56}Fe. These 13 files were released in April 2009 and together with the earlier files they constituted GNEP-1.1 covariance library. Afterwards, we worked on numerous other improvements, added yet another missing laterial, ^{168}Er, and produced the AFCI-1.2 library.

The report is organized as follows. In Chapter 2 we describe the progress achieved in FY2009 and discuss BNL and LANL contributions. In Chapter 3 we describe the improved covariance library, its assembly and testing. Conclusions are given in Chapter 4 and complete set of

covariance plots is shown in the Appendix A. In Appendix B we reproduce recent report by LANL on new evaluation of ^{240}Pu.

Chapter 2

Progress in nuclear data covariances

Covariance evaluation capabilities at BNL and LANL are complementary, allowing them to cover all covariance data needs for AFCI. The only exception are the low energy covariances for major actinides, where we also rely on the work of the ORNL group that traditionally supplies resonance parameters for actinides and also produces covariances in this region.

2.1 BNL progress in covariance methodology

BNL covariance methodology is described in detail in the recent paper by Herman *et al* [2] and a broader description containing seven other reports can be found in our M3 FY2008 Report [3]. The methodology covers the thermal energy, resolved resonance, unresolved resonance and fast neutron regions and builds on the three major components, (i) Nuclear reaction model code EMPIRE [4], (ii) Atlas of Neutron Resonances [5], and (iii) Kalman filtering code [6]

2.1.1 Resonance region

the EMPIRE code system includes a newly-developed resonance module that extends its covariance capability to the thermal and resonance ranges. The module utilizes the recently published Atlas of Neutron Resonances and makes use of uncertainties in both thermal values and resonance parameters. These uncertainties are used to produce covariances of resonance parameters in the ENDF-6 formatted file MF32. Then, processing codes NJOY-99 or PUFF-IV are employed to collapse MF32 into cross section covariances into a suitable multi-group representation [7].

In FY2009 we addressed the following issues in the resonance region:

- Decline in (n, γ) uncertainties due to collapsing of data into 33-groups. This effect increases with the energy due to the growing number of resonances. We managed to remedy this decline by introducing full correlation among radiative widths, Γ_γ, of all resonances. This is illustrated in Section 2.3 for the case of ^{58}Ni, but further study is needed to justify this approach.

- Decline in (n,el) uncertainties due to collapsing. Our attempt for a similar solution as above, introducing full Γ_n correlations, failed due to complex nature of elastic processes such as strong interference effects and strong tails of (n,el) resonances.

- Introducing uncertainty of reduced scattering radius, R'. At the moment there is no provision in ENDF-6 format to handle $\Delta R'$, though it is expected that it might contribute meaningfully to uncertainties in the thermal region as well as in the areas of large gaps between resonances. This is illustrated in Section 2.3 in the case of ^{23}Na. An international effort is under way to update the ENDF-6 format as well as NJOY and PUFF.

- Developing alternative way of generating uncertainties from the Atlas of Neutron Resonances. The idea is to replace MF32 fully or partly with MF33 containing fairly simple step-function of uncertainties directly deduced from Atlas, likely with a fully correlated matrix. This work is currently under way.

2.1.2 Fast neutron region

In the fast neutron region, EMPIRE can produce both cross section and covariance *priors* using the latest library of input model parameters, RIPL-3, with estimates of parameter uncertainties. One can choose among three possibilities of increasing complexity: purely model-based estimate, where nuclear reaction model parameter uncertainties are propagated into MF33 covariances; model-based estimate combined with limited inclusion of experimental data; and the full-scale (rigorous) approach with model-based priors and detailed inclusion of experimental data.

In FY2009 our methodology work focused on two areas:

- Development of evaluation procedure based fully on nuclear physics parametrization coupled to code EMPIRE. We selected ^{23}Na as a trial case, more details can be found in Section 2.3. This procedure appears to be pretty complex, but it has future potential of providing direct coupling between microscopic nuclear physics parametrization and large-scale integral quantities.

- Attempt to understand peculiarities of rigorous methods, which tend to produce small uncertainties. These are usually attributed to inadequate inclusion of systematic uncertainties (in a single experiment, among different experiments, in nuclear reaction models, etc), which poses a considerable challenge also to the present project. We contributed to the international effort that studied these issues under WPEC Subgroup 24.

2.2 LANL progress in covariance methodology

LANL has long-term expertise in neutron cross section evaluations for actinides in the fast neutron region and light nuclei in the entire energy range, and this expertise is being extended

to produce covariances. For the actinides, the Uncertainty Quantification (UQ) methodology is based on the Kalman filtering technique that has been presented elsewhere [8]. It follows closely the evaluation procedure itself, combining sources of uncertainties both from model calculations and experimental information that enter into the evaluation. Sensitivity calculations are performed to assess the sensitivity of the results (e.g., cross sections) on the model parameters. On the other hand, differential experimental data also constrain the values of those parameters and introduce additional correlations due to systematic experimental uncertainties. The Kalman filter applies a Bayesian update to combine both model-based and experimental covariances. The end result is a covariance matrix that well represents the evaluation process.

In FY 2009, most of LANL's focus was on adopting this methodology to the issue of prompt fission neutron spectrum uncertainties, in the case of actinides, and to $\overline{\mu}$ (the mean scattering cosine) uncertainties for light nuclei.

The uncertainty quantification methodology used to evaluate cross section uncertainties was adopted for the prompt fission neutron spectrum (PFNS). In this case however, the nuclear reaction models used to compute reaction cross sections have to be replaced by a model predicting the PFNS. In the ENDF/B-VII.0 library, as well as in all evaluated libraries around the world, use the so-called Los Alamos or Madland-Nix (MN) model at its core [9]. This model was developed in the 1980's by D.G.Madland and J.R.Nix in our nuclear theory group at LANL. While some improvements have been made over the years by several groups, all evaluated data on PFNS still rely on the fundamental MN model equations.

In the present work, we are interested in calculating the covariance matrix associated with a particular evaluated file, i.e., ENDF/B-VII.0. To be consistent, the PFNS evaluation and its uncertainties should be computed using the same model and the same model parameters. The ENDF/B-VII.0 evaluations were done prior to the present UQ work of course, however we tried to ensure that the most important ingredients entering in the evaluation were kept identical.

During FY09, we developed an entirely new code, which implements the MN equations. This code was written in a modern language, is flexible and has been benchmarked very accurately against D.G.Madland's own calculations. This new code is also very flexible and can be used with the KALMAN code that we use for combining experimental and model parameters uncertainties.

Results obtained in the case of the prompt fission neutron spectrum of n+^{239}Pu at 0.5 MeV incident neutron energy are presented in Section 2.4.

2.3 BNL covariance work

In FY2009 BNL contributed improved covariance data for the following materials: ^{23}Na and ^{55}Mn where more detailed evaluation was done; ^{52}Cr, ^{56}Fe and ^{58}Ni based mostly on analysis and improvement of other evaluations; improved estimates for remaining structural materials and fission products; and improved covariances for 14 minor actinides. In addition we also produced estimates of covariances for mubar (average scattering cosines) for ^{23}Na and ^{56}Fe.

2.3.1 ^{23}Na

AFCI-1.2 covariances

The resonance module of EMPIRE was used both at the thermal energy and in the resonance region up to 985 keV. Uncertainties for parameters of 38 resonances (including the bound state) were retrieved from the electronic version of the Atlas of Neutron Resonances [5]. The Kalman filter technique was used to adjust parameter uncertainties so that the uncertainties of the thermal values were reproduced. This adjustment created correlations between parameters of a few low-energy resonances and generated changes in the parameter uncertainties. The first effect is visible in the correlation matrix of (n,el) where strong anti-correlations were created. The second one is in (n,γ) where the uncertainty of Γ_γ for the 2.8 keV resonance is about 5% (original Atlas value 11.7%). The uncertainty $\Delta\sigma_\gamma = 0.7\%$ at the thermal energy given in Atlas was considered underestimated and we increased it by about a factor of 2. Also for the elastic channel, in the energy range about 50-900 keV, we felt that the cross section uncertainties deduced from Atlas (about 2%) are too optimistic and increased them to $\approx$5%.

In the fast neutron region the sensitivity calculations were performed with EMPIRE [4]. Three nuclear reaction models were adopted to describe the physics of nuclear reactions at neutron energies from 0.5 MeV to 20 MeV. The spherical optical model takes care of the total cross sections and neutron scattering, Hauser-Feshbach statistical model describes the bulk of particle emission, and the exciton pre-equilibrium model describes major features of fast particle emission at higher incident energies. Altogether, we varied 21 model parameters in the fast neutron region with the parametrization taken from RIPL library [10]. We varied 8 optical-model parameters as well as two optical-model scaling parameters of total and absorption cross sections (TotRed and FusRed) used primarily to reproduce fluctuations in the MeV energy region. Eleven additional parameters were used to describe the Hauser-Feshbach and the exciton model.

The Bayesian update procedure was performed by the KALMAN code [6] by taking into account the sensitivity calculations and selected experimental data (Larson 1976, Perey 1971, Liskien 1965, Williamson 1961, Bass 1966). Due to large fluctuations in the experimental data, particularly (n,tot) and (n,n$'$), the experimental cross sections included in the Bayesian update were averaged over broader bins. In the Appendix the results for the four reaction channels are shown in the graphical form. For (n,el) in the energy region above 1 MeV, the uncertainties are between 5% and 12%. The same is true for (n,n$'$), except for the threshold

energy (about 40%). ^{23}Na(n,2n) cross section uncertainties were estimated to be about 20%, while for (n,γ) the estimates at $E_n > 1$ MeV are about 50-60%. The fit was relatively modest and square root of $\chi^2 \approx 7$ was applied as multiplicative factor to get cross section uncertainties.

Future development in the resonance region

In order to resolve the problem of low ^{23}Na(n,el) uncertainties in the energy range of 50-900 keV we intend to add the uncertainty due to the scattering radius, R', which for a light nucleus such as ^{23}Na might represent a non-negligible contribution. Fig. 2.1 shows uncertainties in 33-groups propagated from the resonance parameters in Atlas, compared to uncertainties which included also $R' = 4.9 \pm 0.2$ fm. The contribution of $\Delta R'$ is limited to the resonance region (file MF=32), it is strong far from the resonances and small at strong resonances as evident in groups containing the dominant 2.8 keV resonance.

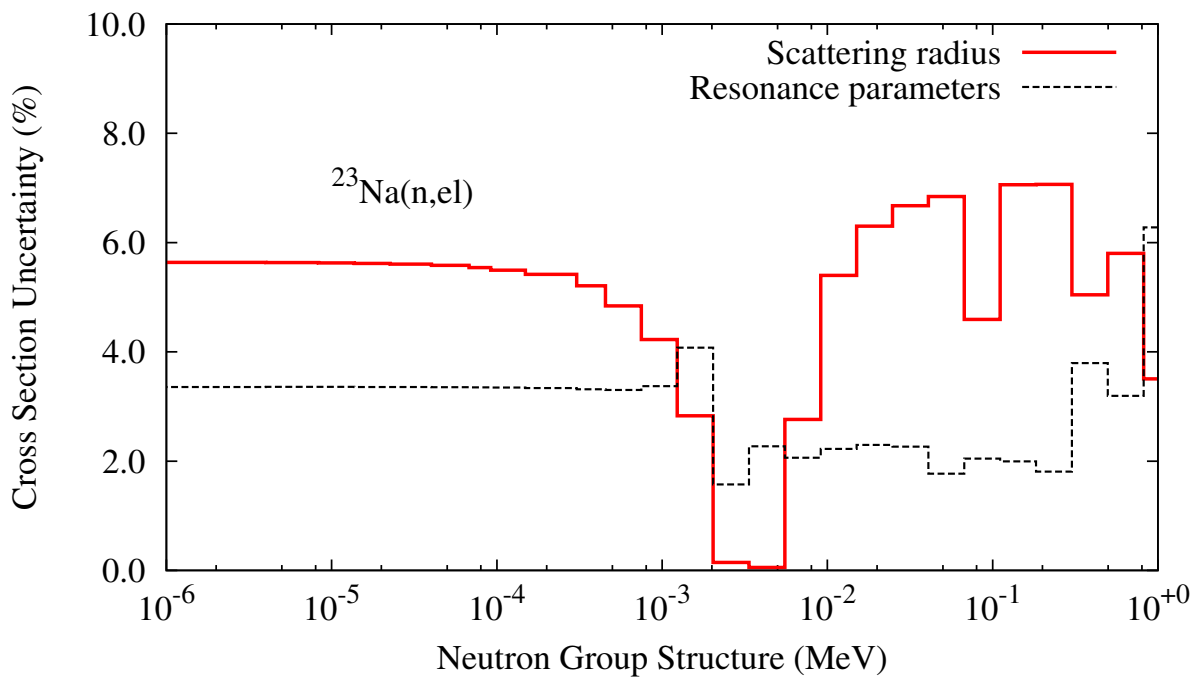

Figure 2.1: ^{23}Na(n,el) uncertainties in 33-groups propagated from the resonance parameters [5] only, compared to uncertainties due to the scattering radius, $R' = 4.9 \pm 0.2$ fm.

Another issue, still under investigation, is the role of correlations between the resonance parameters. This information, not present in the Atlas, can be essential in preventing the drop of the cross section uncertainties. In Fig. 2.2 we consider three different cases of correlations among the parameters of 38 resonances: default calculation where we assume uncorrelated parameters, Γ^i_γ correlation between all resonances set to corr(Γ^i_γ,Γ^j_γ)=0.9, and Γ^i_γ also strongly correlated to Γ^j_n.

As shown in Fig. 2.2, the inclusion of Γ_γ correlations produces consistent increase in capture cross section uncertainties. However, this is not the case for the elastic channel. The results shown in Fig. 2.2 were obtained with the LANL processing code, NJOY-99.296. We note that results obtained with the ORNL code, PUFF-IV version 6.1.0, provide very similar, albeit not identical results. The different approach in calculating partial derivatives of cross sections with respect to the resonance parameters, numerical for NJOY and analytical for PUFF, might explain such a difference.

Future development in the fast neutron region

A part of our effort is to develop evaluation procedure fully based on nuclear physics parametrization coupled to code EMPIRE. The work is not yet completed and the results described below are not yet part of the AFCI library.

Compared to AFCI-1.2 library, our initial estimates of cross section uncertainties in the fast neutron region were improved by explicit treatment of the fluctuating cross sections. We also improved the parametrization and alltogether varied 33 model parameters, mostly taken from RIPL [10] including 19 optical model parameters. Two additional parameters were introduced, optical-model scaling of total and absorption cross sections (TotRed and FusRed), to reproduce the fluctuations of high-resolution measurements (Larson 1976, Perey 1971) in the MeV region. Parametrization for the Hauser-Feshbach and the exciton model added 12 parameters. The prior values of the model parameters are carefully chosen in order to ensure physically meaningful results for cross sections. An overestimation of the prior model uncertainties, for instance, might affect the agreement between calculated and experimental cross sections in the Bayesian update procedure. The uncertainties were also used to compute the sensitivity matrix elements

$$s_{i,j} = \frac{\partial \sigma(E_i, \mathbf{p})}{\partial p_j} \,, \tag{2.1}$$

where σ is the cross section, E_i is the energy, and $\mathbf{p}$ is the vector of the prior model parameter. The partial derivatives were calculated numerically and they were used in the Bayesian update procedure.

We used KALMAN code to calculate cross section uncertainties and their covariance matrices at incident energies between 0.5 - 20 MeV. We considered seven most important reaction channels, total, elastic, inelastic, (n,2n), capture, (n,p), and (n,α) and selected experiments (Larson 1976, Perey 1971, Liskien 1965, Menlove 1967).

The fit was improved and the square root found in the Bayesian procedure was $\chi^2 = 2$. This factor was then used as a multiplicative factor in the cross section uncertainties plotted in Figs. 2.3-2.6. For ^{23}Na(n,tot) in Fig. 2.3, we found cross section uncertainties (red line) of about 6-10% in the fluctuating energy region, which decreases to about 4% above 10 MeV. In the elastic channel (Fig. 2.4) the uncertainty is almost constant at about 7-9%. For (n,n$'$) the uncertainties are about 15-20% close to threshold and in the fluctuating energy

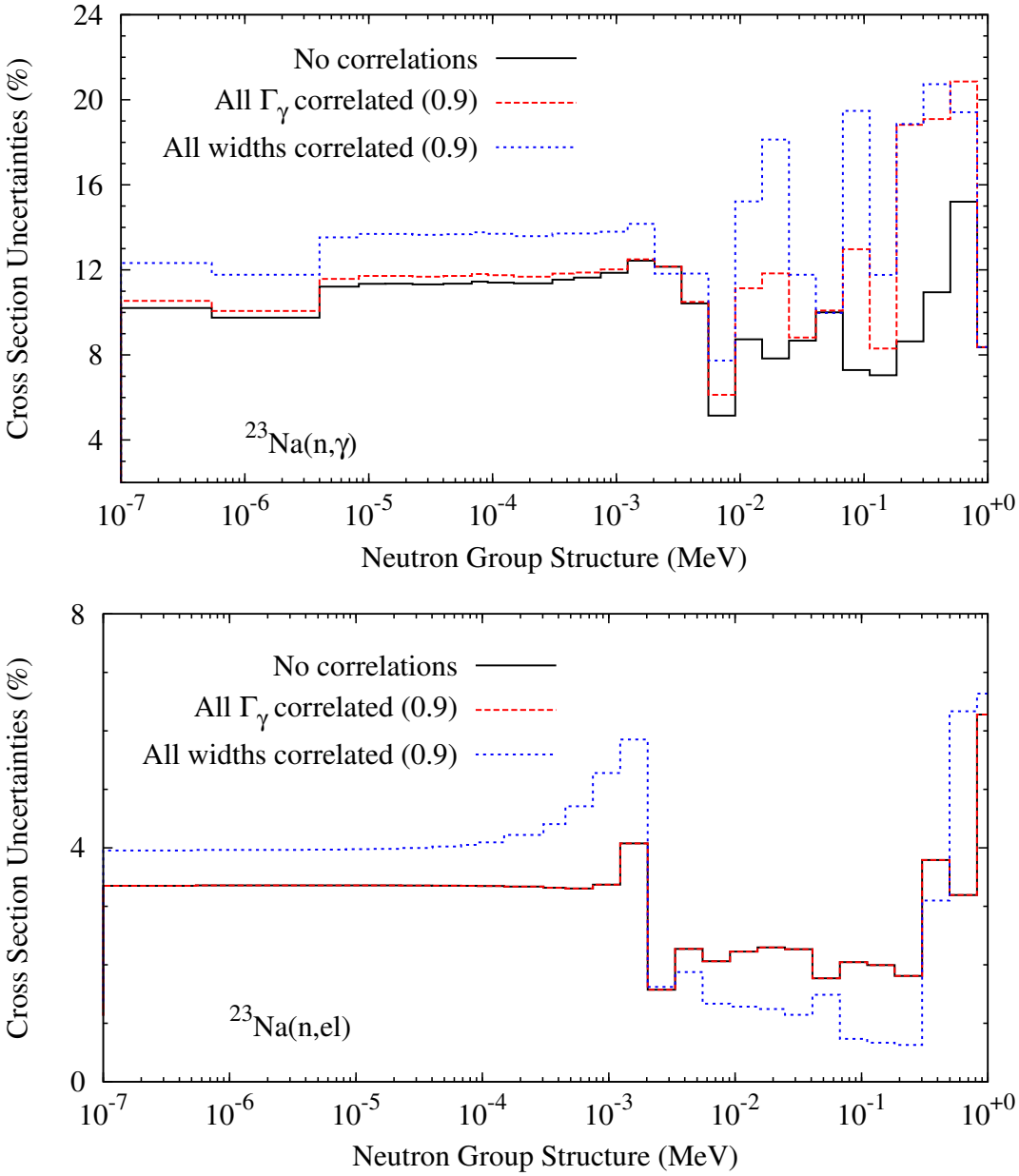

Figure 2.2: ^{23}Na(n,el) and ^{23}Na(n,γ) uncertainties in 33-groups calculated from resonance parameters [5]. Impact of different correlations among resonance parameters is shown. Processed by NJOY-99.296. Results by PUFF-IV yield somewhat different values, e.g, for capture they are higher by about 2 percentage points.

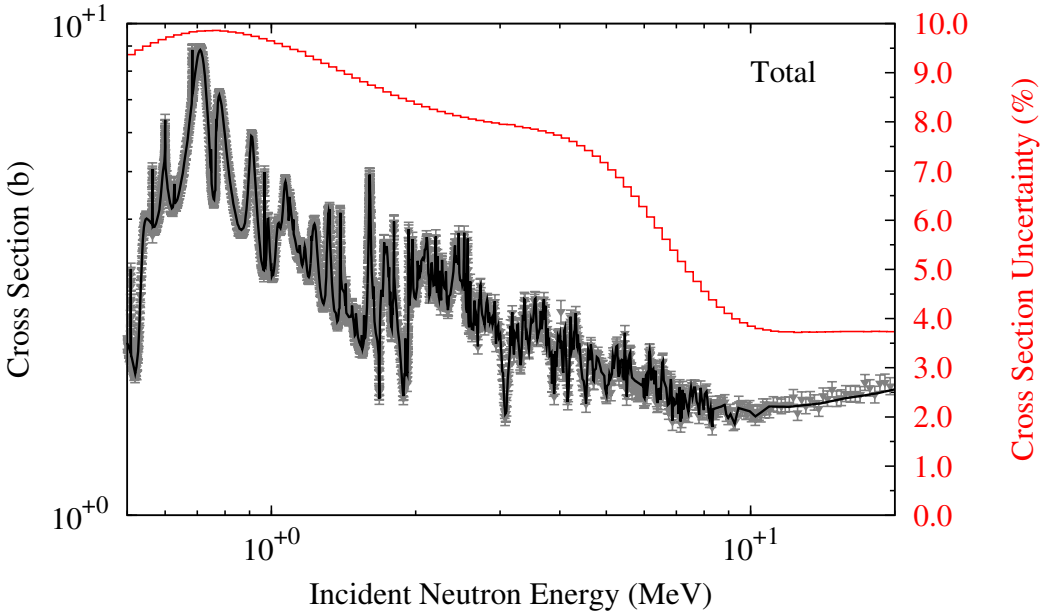

Figure 2.3: Reaction ^{23}Na(n,tot). Point-wise cross sections are compared with experimental data of Larson 1976. Relative uncertainties in % are shown in red.

region, and decrease to about 6% above 2 MeV. The (n,2n) uncertainties are between 7-16%.

In summary, the above results suggest that future refinement of AFCI will differ from our AFCI-1.2 values with some tendency towards more conservative uncertainties.

2.3.2 ^{55}Mn

Recent covariance estimates for ^{55}Mn have been made at both BNL (resonance region, fast neutron region), and at ORNL (resonance region only) [11]. Improved cross sections and covariances for ^{55}Mn are desired mainly in the resonance region, driven by the need for detailed input to Nuclear Criticality Safety calculations.

At Brookhaven, covariances were produced using the resonance parameters and uncertainties tabulated in the Atlas of Neutron Resonances [5]. Information from the Atlas was used along with the new covariance module of EMPIRE [2] in order to create an ENDF file with resonance parameters (MF2) and uncertainties (MF32, the resonance parameter covariance matrix). Using the covariance module, an adjustment was also made to the experimental thermal uncertainty for the (n,γ) and (n,elastic) reaction channels. This adjustment effectively generated correlations or anti-correlations between the bound resonance(s) and positive-energy resonances, modifying the thermal uncertainty to desired value.

Covariances for ^{55}Mn were also recently evaluated by ORNL as part of a new evaluation in the resolved resonance region. The evaluation is based on a recent neutron capture cross section measurement performed at ORELA by Guber 2007. Data from this experiment were

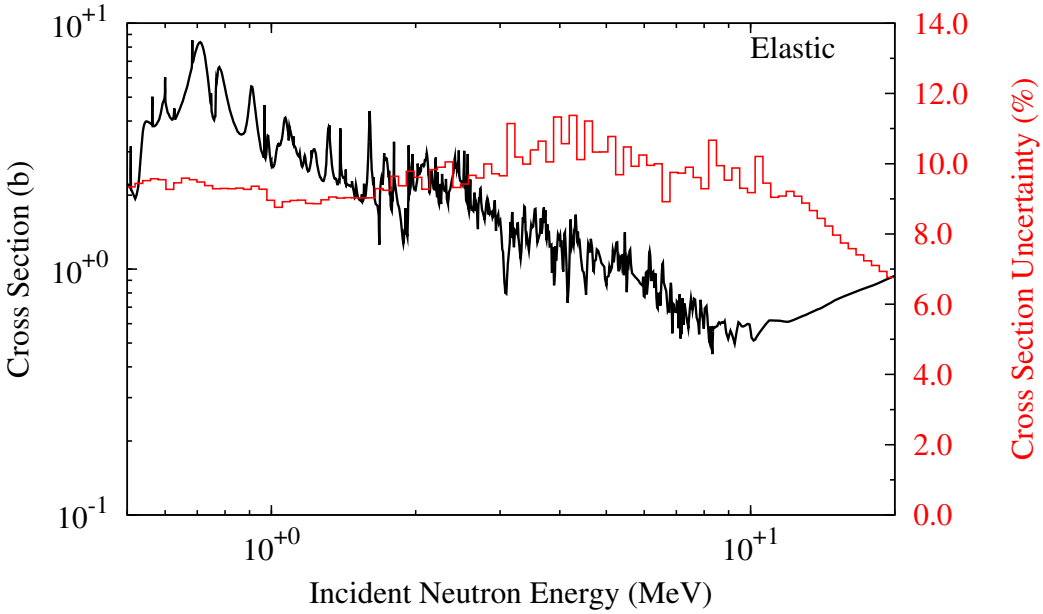

Figure 2.4: Reaction ^{23}Na(n,el). Shown are point-wise cross sections in black and relative uncertainties (%) in red.

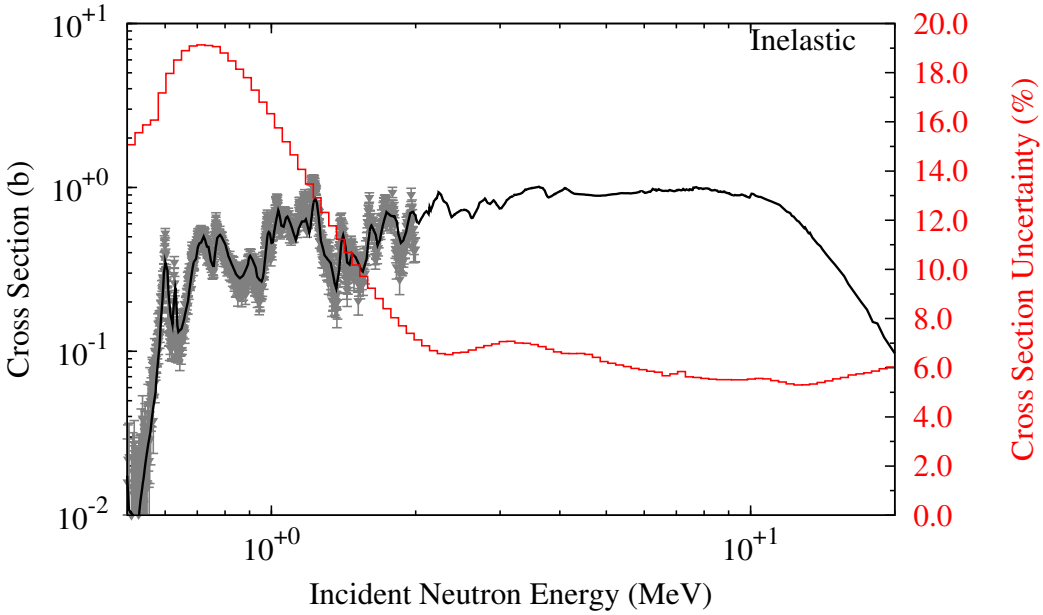

Figure 2.5: Reaction ^{23}Na(n,n′). Point-wise cross sections are compared with experimental data of Perey 1971. Relative uncertainties in % are shown in red.

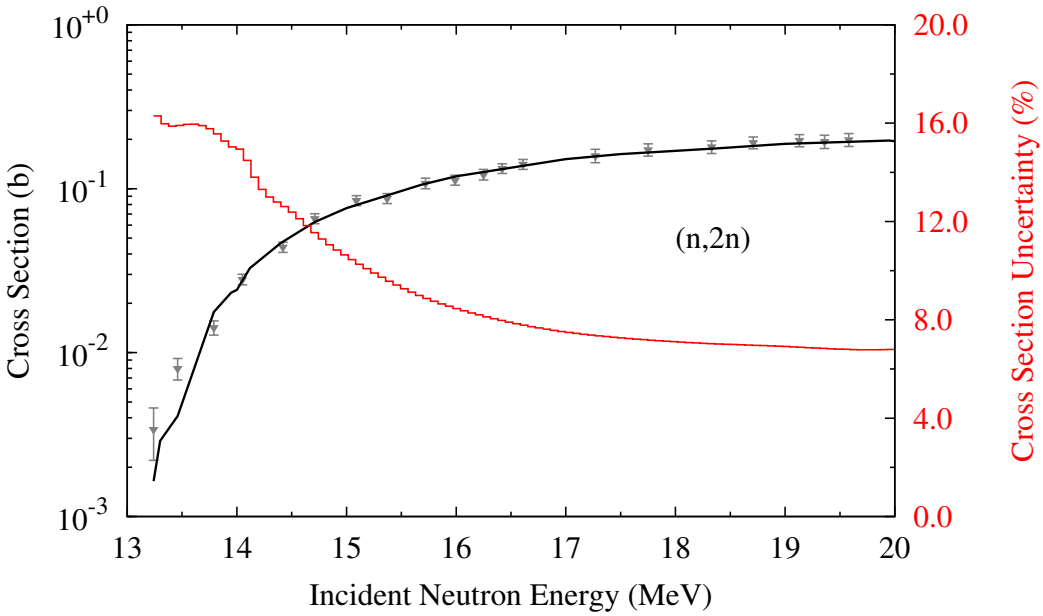

Figure 2.6: Reaction ^{23}Na(n,2n). Point-wise cross sections are compared with experimental data of Liskien 1965. Relative uncertainties in % are shown in red.

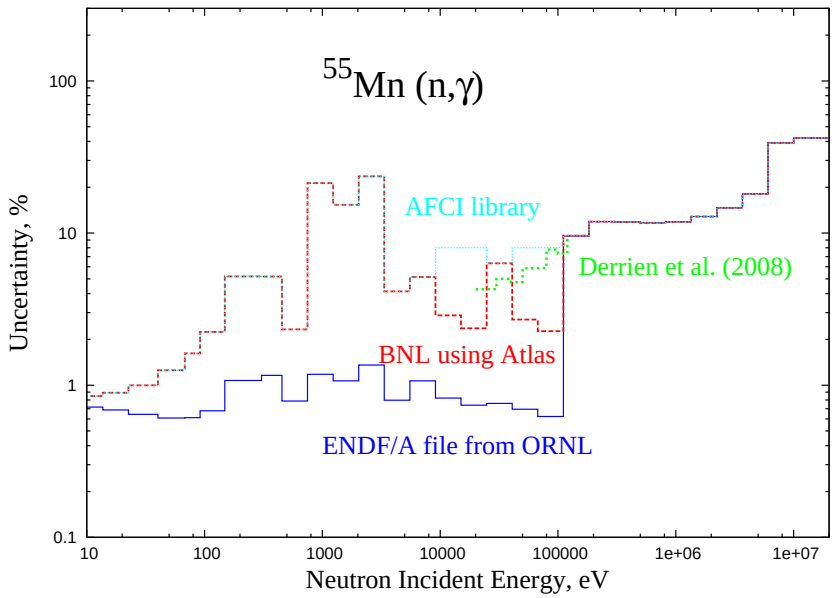

Figure 2.7: ^{55}Mn (n,γ) uncertainties in 33-groups. Both BNL (red) and ORNL (blue) evaluations are shown, together with uncertainties quoted from Derrien (green). The fast neutron energy region starts at 1 MeV and shows BNL data. To remedy decline of uncertainties at about $10^4 - 10^6$ keV we adopted higher values shown as AFCI.

analyzed by Derrien et al [11] using the code SAMMY to fit the resonance parameters in Reich-Moore representation (MF2) and acquire the resonance parameter covariance matrix (MF32). The results were submitted to ENDF/A library in May 2008 [12].

We analyzed the ORNL evaluation and found that it contains very low uncertainties, less than 1%, in the resonance region, which are not in agreement either with the BNL work or with the uncertainties quoted by the experimental description by Derrien et al [11]. A future update to the ENDF/A file from ORNL is expected to resolve this issue by adding a large component of systematic uncertainty using MF33 (Port Jeff, June 2009, private communication by D. Wiarda).

In view of the above for AFCI-1.2 we adopted BNL evaluation after some additional increase of uncertainties at the upper end of the resonance region as shown in Fig. 2.7.

2.3.3 ^{52}Cr and ^{58}Ni

Like ^{55}Mn, the structural materials ^{52}Cr and ^{58}Ni have been improved in the resonance region using the Atlas of Neutron Resonances and the covariance module of EMPIRE. In both cases, the isotopes were originally treated using a low-fidelity approach. This approach is based on simple step function of uncertainties defined by the thermal uncertainty up to 0.5 eV, followed by the resonance integral uncertainty assuming that the resolved resonance region ends at 5 keV. For these structural materials, however, resolved resonances extend to much higher energies, 1 MeV for ^{52}Cr and 811 keV for ^{58}Ni. Therefore, this approach was improved to take the full resonance region into account along with individual resonance parameter uncertainties.

^{58}Ni

Problems remain with the current approach, however: at the top of the resolved resonance region, the density of resonances increases, so that if the resonance uncertainties are uncorrelated the groupwise uncertainty decreases substantially. This effect is clearly seen in ^{58}Ni (n,γ) and (n,elastic) reactions from approximately 10 keV to 1 MeV, Figs. 2.8 (a). and 2.8 (b). In both cases the uncertainties decrease in the wide 33-group representation if no correlations are present. Adding correlations between all Γ_γ in the resonance parameter correlation matrix increases the (n,γ) uncertainty, but correlations are not effective in raising the 33-group (n,elastic) uncertainty as seen in figure 2.8 (b). Possibilities for addressing this reduced uncertainty might include:

- Switching from resonance parameter (MF32) to cross section (MF33) covariances after the first few resonances,
- Replacing MF32 with MF33 containing uncertainty step function deduced readily from the Atlas combined with full correlations, and
- Introducing $\Delta R'$, which would contribute to elastic uncertainties and thus make the issue less pronounced.

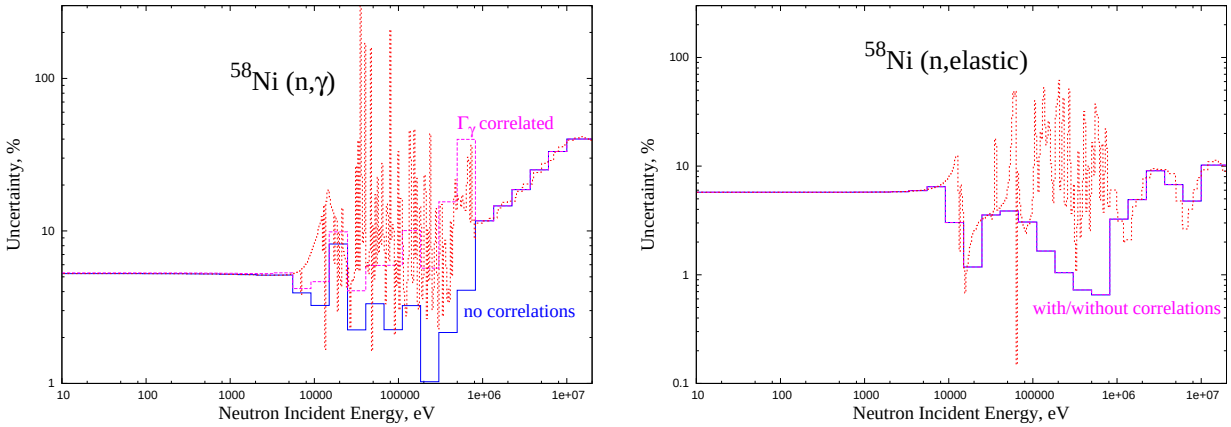

Figure 2.8: ^{58}Ni(n,γ) and (n,elastic) uncertainties. Detailed 618-group representation is compared with 33-groups illustrating the effect of collapsing. When Γ_γ are fully correlated the decrease of uncertainties is prevented. For (n,elastic) however, correlations fail to prevent the decrease in uncertainty.

^{52}Cr

Similar problems also appeared in ^{52}Cr, although the level density is lower than in ^{58}Ni and hence the drop in uncertainties in both (n, γ) and (n,el) is much less dramatic. The capture and elastic uncertainties are shown in Fig. 2.9, where one can also see how we handled the drops in uncertainty.

To remedy drop of uncertainties in the resonance region, changes in the uncertainties for both ^{52}Cr ^{58}Ni were made *after processing* as deemed necessary. Details of these changes to the groupwise uncertainties will be further discussed in Chapter 3.

2.3.4 ^{56}Fe

^{56}Fe is the most important structural material. Its natural abundance of 91.8% makes it the dominant isotope of elemental iron, followed by ^{54}Fe with 5.8% and ^{57}Fe with 2.1%. Evaluations of cross sections along with their covariances are available in every major evaluated library as summarized in Table 2.1. ENDF/B-VII.0 cross section evaluation below 20 MeV is based on both data and model analysis dating back to ENDF/B-V work at ORNL with the last update by Fu et al [13] in 1986, followed by the covariance update by Hetrick, Larson and Fu [14] in 1991 largely based on the experimental data.

JEFF-3.1 evaluation was done by Pronyaev-Vonach in 1995 [15] and consists of fairly simple covariance estimates in the resonance region up to about 820 keV, followed by very extensive evaluation in the fast neutron region based on rigorous analysis of data. JENDL-3.3 is based on estimates of covariances by Shibata in 1997 [16], while BROND-3 is based on new analysis of Pronyaev in 2006 [17] who adopted 1995 Pronyaev-Vonach covariance evaluation.

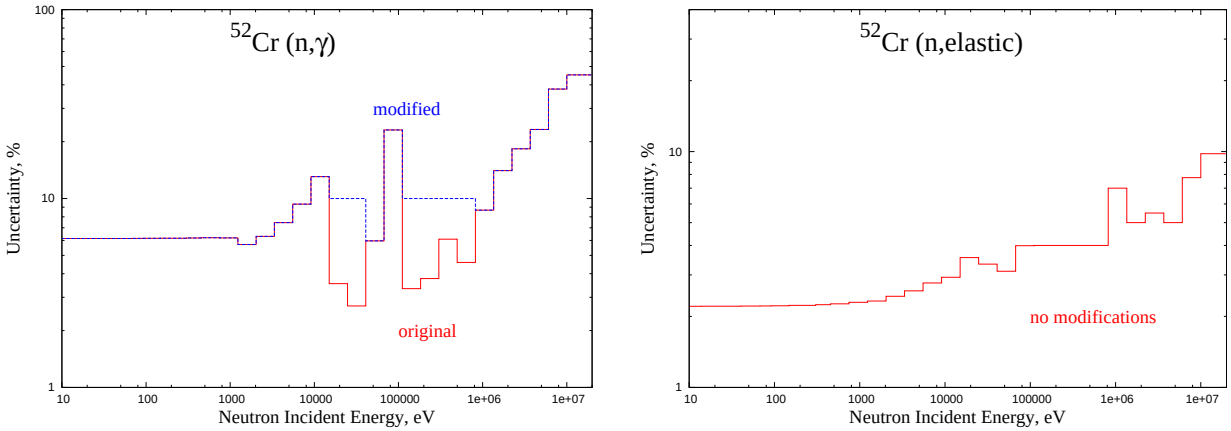

Figure 2.9: ^{52}Cr(n,γ) and (n,elastic) uncertainties. In (n,γ), two dips seen in the original values produced by EMPIRE were increased to approximately 10%. In (n,elastic), the dip produced by EMPIRE at about 70-700 keV was replaced by a flat estimate of 4%.

Table 2.1: ^{56}Fe covariance evaluations in major libraries. Covariances for elastic scattering are calculated as (n,el) = (n,tot) - (n,nonel).

Library	1st author	Year	Resonances	Fast region
ENDF/B-VII	Hetrick	1991 [14]	Estimate	tot,γ, $\bar{\mu}$=data
JEFF-3.1	Pronyaev	1995 [15]	Estimate <820 keV	all=data
JENDL-3.3	Shibata	1997 [16]	Data <250 keV	tot=data; inl,γ, $\bar{\mu}$=model
BROND-3	Pronyaev	2006 [17]	Estimate <820 keV	all=data

We reviewed these evaluations and came to conclusion that the best evaluation is included in BROND-3 and JEFF-3.1. We note that BROND-3 has not been released, but several BROND-3 evaluations including ^{56}Fe are available in the recent Russian library of selected evaluations, ROSFOND. We chose BROND-3 as the reviewers' careful methodology and analysis of data, coupled with the Bayesian least squares approach in the well known code GLUCS was an appropriate approach to this important structural material. These covariance data were therefore adopted in the GNEP-1.1 library. However, upon review some of the uncertainties are found to be quite small: total around 1% or less, inelastic about 1.5% and elastic about 2%. This is typical consequence of "rigorous" methods that tend to predict very small uncertainties, widely believed to be caused by the lack of full inclusion of systematic uncertainties. The AFCI users raised their concerns and therefore we re-examined our choice for AFCI-1.2.

We have done additional analysis and looked specifically to ^{56}Fe(n,el) and ^{56}Fe(n,inl). To this end we performed comparison of processed cross sections in 33-groups between major

evaluated libraries with two ideas in mind:

- Our covariances refer to ENDF/B-VII.0 library and they should be consistent with the basic cross sections in this library. However, adopting the covariance evaluation from another library leads to breaking this consistency requirement. To take care of this issue one should take into consideration the difference between cross sections of the two evaluations and enlarge the uncertainties to bridge the difference.

- Evaluations of priority materials in major data libraries represent mature products of highly experienced evaluators and dispersion between the evaluated cross sections reflects genuine uncertainties in both data and methods. Dispersion can thus be used for estimate of cross section uncertainties. This dispersion method has been advocated and used years ago by H. Vonach, IRK Vienna, who argued that it gives pretty realistic estimate of uncertainties.

Comparison of major libraries for elastic and inelastic cross sections is shown in Figs. 2.10 and 2.11. One can see that dispersion is significant for both ^{56}Fe(n,el) and (n,inl). For (n,el) at energies above about 1 MeV it is in the range of 2-4%. For (n,inl) dispersion is in the range of 5% in the first three bins above threshold which extend up to almost 4 MeV, followed by about 2.5% at higher energies. In view of this we corrected GNEP-1.1 uncertainties by multiplying (n,el) by a factor of 2 and also (n,inl) by a factor of 2. We note, however, that for (n,inl) multiplying by a factor of 3 would be even more suitable solution for fast reactor applications. More detailed analysis is needed in order to arrive at a more refined solution.

We also fixed the resonance region, $E_n < 850$ keV, and replaced crude estimates adopted by Pronyaev et al [15] by more refined estimates performed by S. Mughabghab for the present project using his latest data published in 2006.

In summary, for ^{56}Fe we adopted BROND/JEFF covariance evaluation with the following modifications:

- (n,el) and (n,γ) uncertainties in the resonance region, $E_n < 850$ keV, were replaced by improved estimates by Mughabghab,

- (n,el) uncertainties in the fast neutron region were increased by a factor of 2, and

- (n,inl) uncertainties were increased by a factor of 2.

2.3.5 Mubars for ^{23}Na and ^{56}Fe

Mubar is defined as the average cosine of elastically scattered neutrons in the laboratory system. In ENDF-6 formatted files this information can be stored in MF1, MT251. As an alternative, it can be obtained from MF4/MT2 which keeps information on angular distribution of elastically scattered neutrons. It can be shown that mubar can be readily computed from the Legendre polynomial representation of angular distribution as

$$\bar{\mu} = A_1/3, \tag{2.2}$$

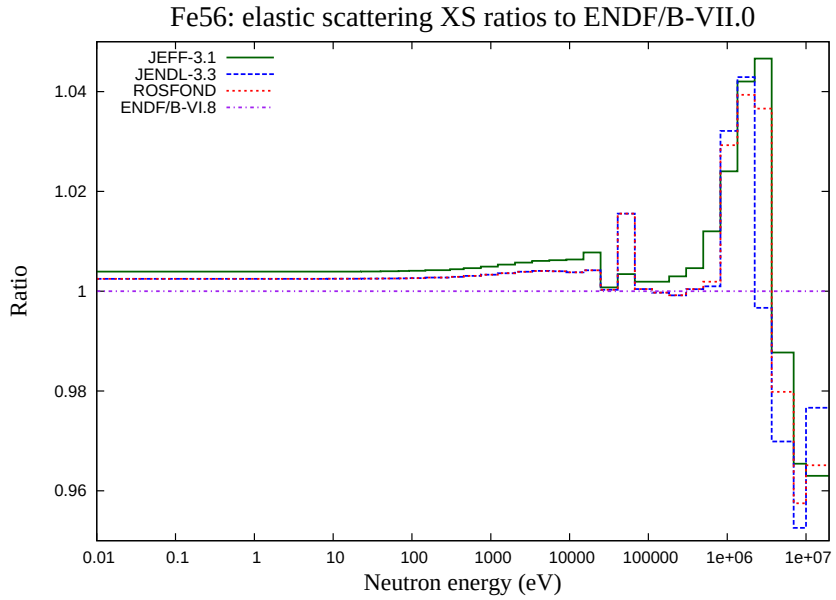

Figure 2.10: Ratios between various evaluations and ENDF/B-VII.0 for ^{56}Fe(n,el). Dispersion of about 3-5% at $E_n > 850$ keV is ruling against adopting 1.5% uncertainties of BROND/JEFF.

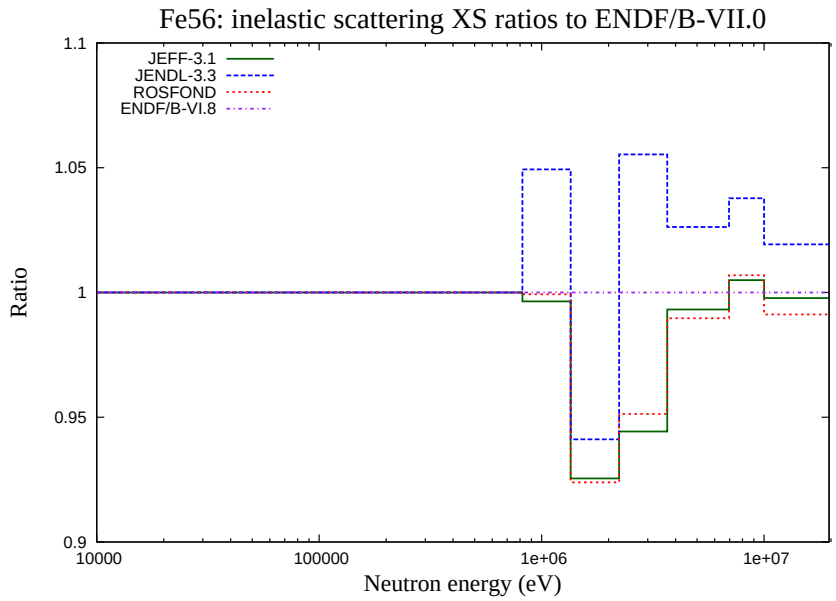

Figure 2.11: Ratios between various evaluations and ENDF/B-VII for ^{56}Fe(n,inl). Dispersion in the first 3 groups above the threshold is about 6%, exceeding by a factor of four the proclaimed uncertainty of 1.5% in BROND/JEFF.

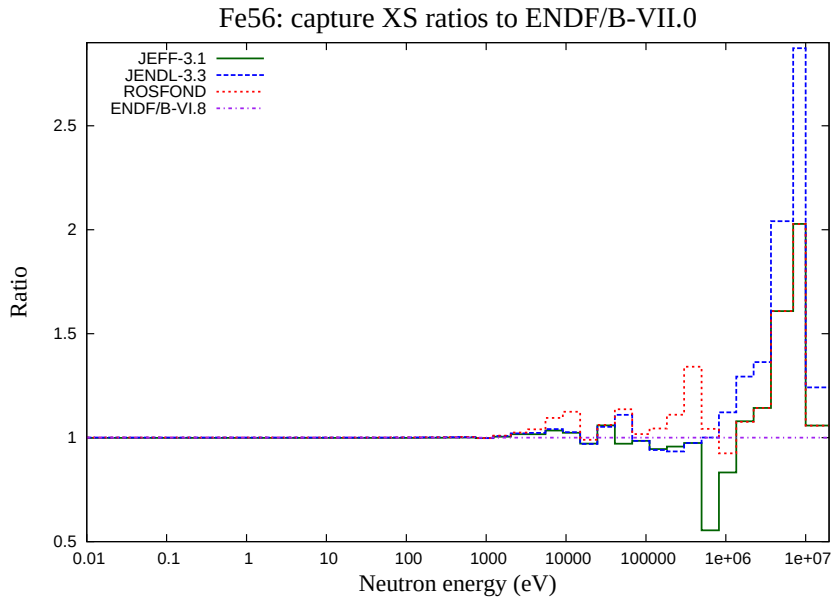

Figure 2.12: Ratios between various evaluations and ENDF/B-VII.0 for ^{56}Fe(n,γ). Considerable dispersion at $E_n > 850$ keV justifies large uncertainties in AFCI-1.2.

where A_1 is the coefficient of the 1st Legendre polynomial. From the physics of elastic scattering one expects that $\bar{\mu}$ values are fairly low at low energies and keep growing with the energy until they ultimately saturate to values close to unity.

While $\bar{\mu}$ may be given explicitly in an evaluated ENDF-6 file, the covariances must instead be computed from MF34, MT2 (covariances of angular distribution of elastically scattered neutrons) by processing with codes such as NJOY.

For the AFCI data adjustment the request for mubar data is limited to four major materials, ^{16}O, ^{23}Na, ^{56}Fe and ^{238}U. Below we describe our estimate for ^{23}Na and ^{56}Fe. It is understood that ^{16}O and ^{238}U should be contributed by LANL at some later point.

Our initial idea was to use optical model calculation with the latest RIPL-3 parametrization along with the latest parameter uncertainties to infer mubars and their covariances. This was done by M. Herman in December 2008, who used the nuclear reaction model code EMPIRE for this purpose. By using the above parametrization and global parameter uncertainties (real volume depth 3%, imaginary volume depth 5% and imaginary surface depth 5%) he obtained mubar values and uncertainties given in Table 2.2.

M. Herman argued that if more refined parametrization is used, the uncertainties would go down by about a factor of 2-3, reaching the level of 2-3% for energies above about 1 MeV. These estimates are close to values produced by other evaluators who used also optical model calculations and ended up with fairly low uncertainties as well. It appears, however, that if

Table 2.2: ^{23}Na and ^{56}Fe mubar values and their uncertainties from the optical model calculations. This was considered to be a conservative estimate, yet the uncertainties appear to be far too low when confronted with experimental data.

^{23}Na			^{56}Fe		
E_n (MeV)	$\bar{\mu}$	Δ (%)	E_n (MeV)	$\bar{\mu}$	Δ (%)
1.0	0.22	11.7	1.0	0.13	6.4
1.5	0.32	7.0	1.5	0.21	3.1
2.0	0.37	4.9	2.0	0.31	4.3
3.0	0.44	4.1	3.0	0.47	5.2
4.0	0.47	4.0	4.0	0.63	5.2
5.0	0.49	4.7	5.0	0.77	2.4

real data are used, the picture is very much different both for ^{23}Na and ^{56}Fe as discussed below.

^{23}Na mubars

Absolute values of $\bar{\mu}$ for ^{23}Na are available in three major evaluated libraries. ENDF/B-VII.0 library took over the 1977 evaluation by D. Larson, ORNL [18] which is based purely on experimental data, both JEFF-3.1 and JENDL-3.3 are based on optical model calculations. As can be seen on Fig. 2.13 there are considerable differences between ENDF/B-VII.0 and the two other libraries. It can be seen that ENDF/B-VII.0 values are considerably higher than optical model predictions at energies from about 700 keV up to about 10 MeV, with strong bump at around 1 MeV and strong fluctuations above 1 MeV. These features reflect the experimental data by Kinney and Perey, ORNL 1976 [19] as shown in Fig. 2.14. These data are in EXFOR, unfortunately, there is virtually no documentation available. It appears that a more recent measurement by S. Kopecky, Geel in 1997 [20] supports fluctuations in Kinney's data, increasing thereby our confidence in the evaluation of Larson in 1997. We note, though, that Kopecky's mubars are about 20-30% lower at 1-2 MeV than Kinney, see Fig. 2.15.

^{23}Na mubar covariances are only available in JENDL-3.3. They can be computed from MF34/MT2. We took this covariance matrix as the basis and applied important modification. In the region of 0.7 MeV - 2 MeV we rescaled JENDL-3.3 uncertainties by a factor of 3 to reflect the differences between basic values of mubars in JENDL-3.3 and ENDF/B-VII.0. With this modification we adopted $\bar{\mu}$ covariances to AFCI-1.2, see Fig. 2.16.

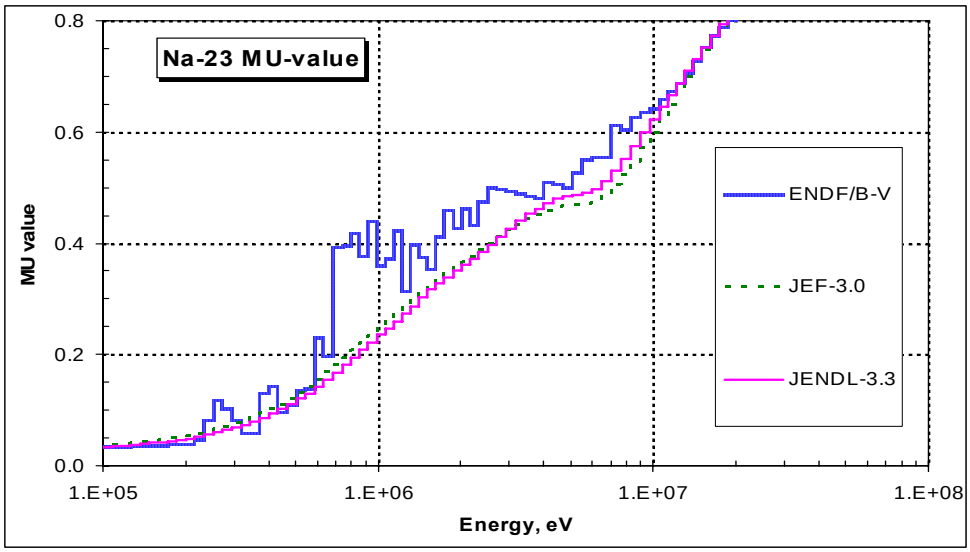

Figure 2.13: Comparison of ^{23}Na $\bar{\mu}$ values in three major libraries up to 20 MeV. ENDF/B-VII, identical with 1977 ENDF/B-V evaluation by ORNL, is based on the experimental data. Both JEFF and JENDL are based on model calculations. Taken from ROSFOND documentation.

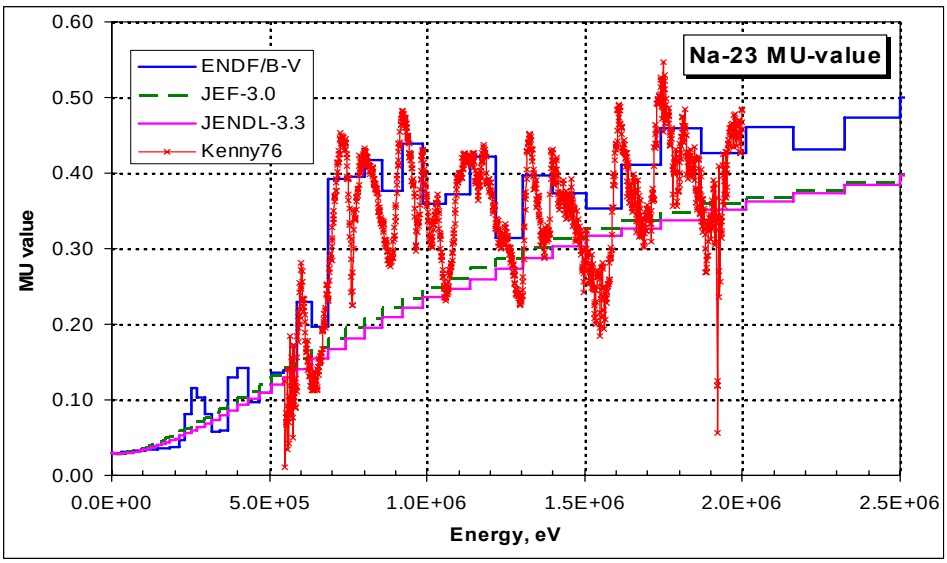

Figure 2.14: Comparison of ^{23}Na $\bar{\mu}$ values in three major libraries up to 2.5 MeV including experimental data of Kinney and Perey [19]. Taken from ROSFOND documentation.

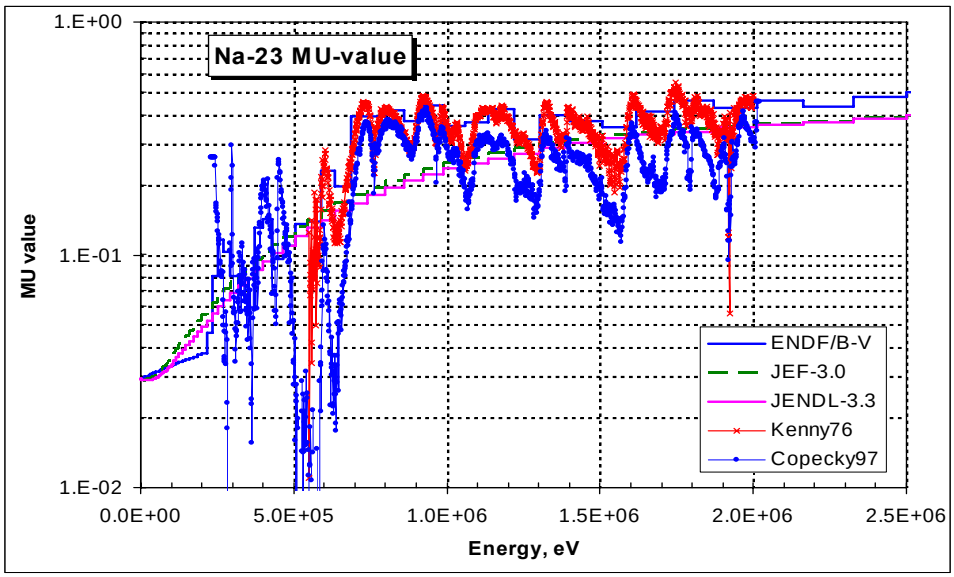

Figure 2.15: As in Fig 2.14, with the experimental data of S. Kopecky [20]. Taken from ROSFOND documentation.

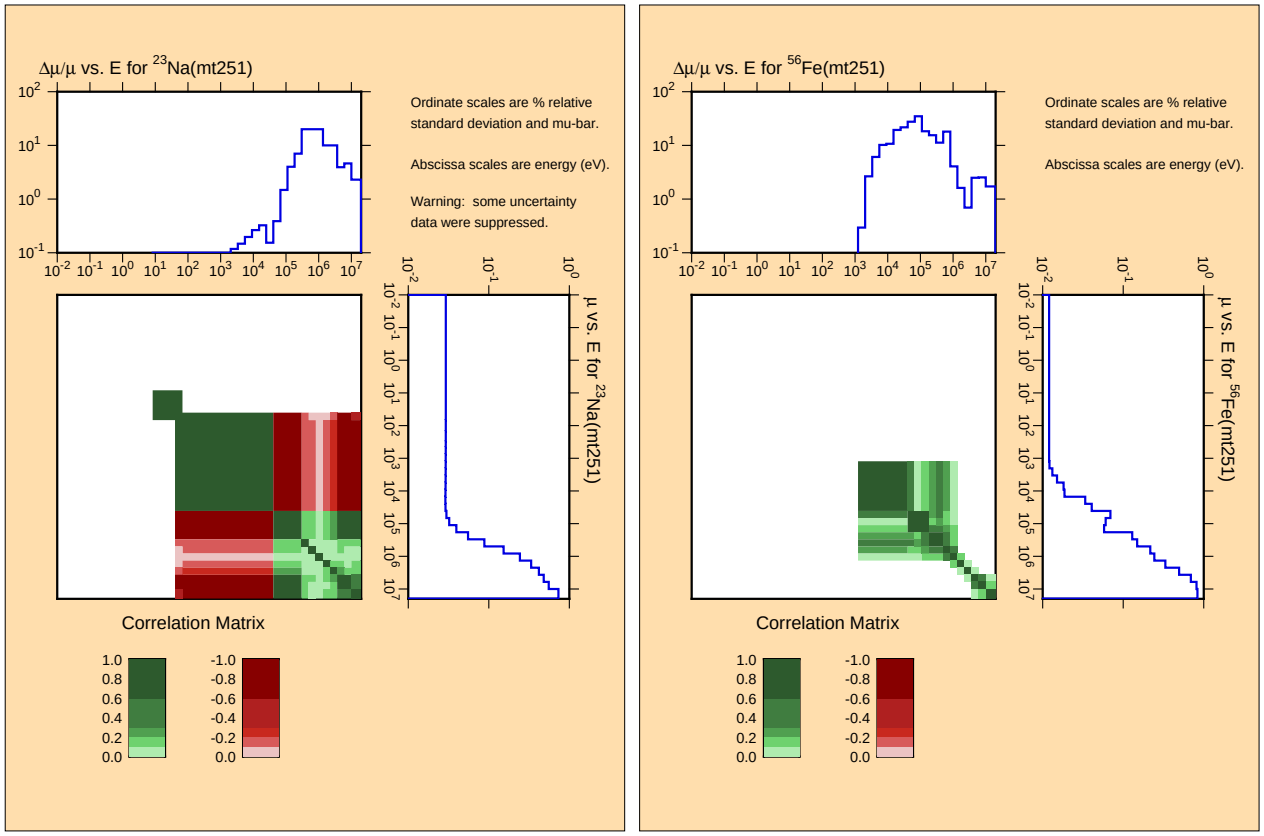

Figure 2.16: ^{23}Na and ^{56}Fe $\bar{\mu}$ covariances adopted by AFCI-1.2.

^{56}Fe mubars

The situation with ^{56}Fe appears to be somewhat less complicated. In this case a fairly robust evaluation of $\bar{\mu}$ is available which is fully based on experimental data. This evaluation was adopted by the recently released Russian library ROSFOND, based on the review of ^{56}Fe evaluations in major libraries performed by V. Pronyaev, Obninsk in 2006. Pronyaev recommended to use the original Russian evaluation developed for BROND-3. This in turn was taken over from the earlier mubar evaluation by Pronyaev-Vonach (1995) [15] and adopted by JEFF-3.1. We reviewed this evaluation and decided to adopt it. The mubar covariances were obtained by processing MF34/MT2 and adopted by AFCI-1.2, see Fig. 2.16.

2.3.6 Other structural materials

Here we briefly describe remaining structural materials including the minor Cr, Fe and Ni isotopes, Zr as well as Pb and Bi isotopes:

- ^{52,53}Cr, ^{54,57}Fe and ^{60}Ni - we reviewed GNEP-1.1 data and made corrections keeping in mind that none of these less abundant isotopes can be better known than the respective leading isotope of ^{56}Fe(92%) and ^{58}Ni(66%).
- ^{90}Zr(51%) and ^{91,92,94}Zr - we first reviewed the leading isotope, ^{90}Zr, and once it was adjusted we proceeded with less abundant istopes following the same principle as above. Radioactive ^{93,95,96}Zr were treated as described under fission products.
- ^{204,206,207,208}Pb and ^{209}Bi - we reviewed GNEP-1.1, took into account that these isotopes have much higher upper end of the resonance region (Pb - between 699 keV and 999 keV; Bi - 264 keV), extended low-fidelity type of estimates to higher energy ranges and fixed capture and elastic accordingly. As above, we took into account the principle of leading isotope in the group, ^{208}Pb(52%) and ^{209}Bi(100%).

2.3.7 Fission products

In the category of fission products we have 40 materials. Except of few materials, such as ^{155,156,157,158,160}Gd which were adopted from the ENDF/B-VII.0 library, virtually all covariances were taken over from the low-fidelity covariance project and included without any change to GNEP-1.0 library. In the process of creating the improved version of the library, AFCI-1.2, fairly extensive review of all fission product files was performed, numerous issues were identified and fixes were made.

Even though all Gd files were taken from ENDF/B-VII.0, rather significant deficiencies were identified in two of them.

- ^{156}Gd
  - (n,γ) uncertainties at low energies exceed 100%, starting with about 75% at thermal energy and displaying several strong peaks at higher energies followed by a

dramatic drop above 5 keV. This behaviour is extremely difficult to explain and was deemed to be unphysical. Much more plausible would be simple low-fidelity estimate of 40% in the thermal region, followed by 15% in the resonance region in compliance with the Atlas of Neutron Resonances. In view of this we adopted the low-fidelity covariances at low energies and retained the fast region.

  - (n,el) deficiencies in uncertainties are similar to (n,γ), but less dramatic at low energies. As a remedy low-fidelity at low energies was adopted and the fast neutron region was retained.

- ^{158}Gd
  - (n,γ) thermal uncertainty was close to 30%, in considerable disagreement with the Atlas value of 9.1%, followed by similar situation in RRR.
  - (n,el) uncertainties as a function of energy in the resonance region show continuous drop, followed by further decrease down to about 0.2%. This would be comparable with the uncertainties for (n,el) standards and deemed entirely unrealistic for the present material. Our fix consisted of changing to 20% for thermal elastic and to 20% for RRR elastic. We adopted low-fidelity covariances for both elastic and capture at low energies and retained the fast region unchaged.

The low-fidelity project adopted a simplified definition of the energy regions, thermal $E_n <$ 0.5 eV, resonance 0.5 eV$< E_n <$5 keV and fast 5 keV$< E_n <$20 MeV. We inspected each low-fidelity file visually and the fixes were made by modifying multigroup uncertainties while leaving correlation matrices unchanged:

- Whenever missing uncertainties were found in GNEP-1.1 they were replaced with simple estimates. This was relevant for many (n,el) cross sections in the resonance region. As a rule for these missing (n,el) uncertainties in the resonance region we adopted $\Delta(n, el) = 20\%$.

- In a few cases also missing capture uncertainties in thermal and/or resonance region were recovered based on the information available in Atlas of Neutron Resonances.

- In several instances we extended the low-fidelity definition of the resonance region to higher and more realistic values. In this way some problematic uncertainties in the fast region were removed. This was the case, for example, for ^{170}Er where 5 keV limit was extended to 24 keV.

- In the fast region the uncertainties for (n,el) were reviewed, two issues were identified and addressed.
  - There are large uncertainty peaks at about 5 keV - 1 MeV which were produced by optical model estimates. These peaks were removed by applying $\Delta(n, el) =$ 20% cut to all of them.
  - Too low uncertainties, again generated by optical model estimates which predict fairly deep minima. These were removed by adopting the rule $\Delta(n, el) \geq 5\%$.

- Uncertainties in inelastic scattering wer also reviewed and unrealistically low values were replaced by adopting the rule $\Delta(n, inl) \geq 5\%$.

2.3.8 Minor actinides

In the category of minor actinides we have 15 materials, of which 14 were handled as described below and #15 (^{246}Cm) was taken from the low-fidelity covariance project.

Covariances for 14 minor actinides (MA) included in AFCI-1.2 were produced and refined in three consecutive steps. In 2007, we produced covariance estimates for WPEC Subgroup 26 activity [21] including minor actinides and these MA covariances have been included in the 15-group covariance library BOLNA. Then, in 2008, the above MA covariances were reviewed by V. Maslov who produced an extensive report and proposed changes, often considerable, in many uncertainties [22, 23]. These modified 15-group estimates have been transformed to GNEP 33-group representation and included in GNEP-1.0 library. In some cases, however, the resulting matrices were not positive-definite and. As a quick remedy, off-diagonal terms for related (n, tot fis) and nubar matrices were removed to achieve positive-definiteness. Finally, in 2009, the NNDC revisited MA covariances in response to ANL-INL request to supply non-diagonal terms of the correlation matrices. In doing so we focused on this and several other issues:

- Fixing covariances at low energies, $E_n < 10$ keV, not addressed by Maslov. This was primarily done by combining information about thermal cross sections and resonance integrals from the Atlas of Neutron Resonances with other sources and inferring uncertainties in the thermal region and the resonance region. These estimates were applied in the low-fidelity style, *i.e.*, simple stepwise function with two values of uncertainties.

- Recovery of missing correlation matrices originally produced for WPEC Subgroup 26 [21]. This was achieved by recovering the original 15-group matrices and converting them into 33-groups.

- Checking text in the original Maslov report against his numerical tables. This revealed several typos in Maslov tables which were corrected.

- Checking uncertainties of fission cross sections and nubars, resulting in a few changes towards more conservative estimates.

- Revisiting uncertainties of elastic cross sections and replacing those judged to be too small by a minimum value of 5%.

- Revisiting uncertainties of inelastic cross sections and replacing those judged to be too small by a minimum value of 15%.

- Revisiting uncertainties of (n,2n) cross sections and replacing those judged to be too small by a minimum value of 20%.

The results can be seen in covariance plots shown in the Appendix.

2.4 LANL covariance work

In FY 2008 LANL completed evaluation of covariance matrices for ^{233,235,2138}U and ^{239}Pu in the fast energy range, while the low-energy part was contributed by ORNL. LANL also evaluated covariances for 16 materials. ^{1}H, ^{6}Li and ^{10}B were obtained by complex R-matrix methodology and covariances, while the remaining materials are simple estimates. Finally, NJOY processing code was upgraded to better handle covariance matrices for very fine energy-group structures. FY2009 contributions are summarized below.

2.4.1 Light nuclei

^{16}O

As shown in recent ANL sensitivity studies, ^{16}O is an important material and a 'good-quality' covariance matrix represents a priority need for the data evaluation work. A full R-matrix analysis for ^{16}O is to be completed shortly, and associated covariance matrices will be released later on.

However, an intermediate result is provided here for $\overline{\mu}$, the mean scattering cosine, uncertainties. The Legendre coefficients were obtained from the fit to the experimental angular distributions and total cross section in the vicinity of the resonance. They are shown in the (relative) ENDF form in the Figure 2.17. Only the first three coefficients (including L=0) are significant in this energy range.

In this form, the first coefficient, c_1, is mu-bar in the c.m. system. Then, propagating the uncertainties of the angular distributions to the Legendre coefficients gave the uncertainties in mu-bar (expressed as %) shown in Fig. 2.18 and summarized in Table 2.3, which depend on the uncertainties of both the (absolute) L=0 and L=1 coefficients. These uncertainties were put into an ENDF-formatted table for energies between 0.3 and 0.6 MeV.

Comments on Current ^{12}C and ^{10}B Covariance Matrix Evaluations

A full R-matrix analysis was performed for ^{10}B, so we expect it to be of good quality, and can be used as such for reactor sensitivity calculations.

On the contrary, the covariance analysis for ^{12}C was performed as part of the 'low-fidelity' project. In this case, only the low-energy part of the covariance matrix was performed in a full R-matrix analysis. At higher energies, the evaluation of uncertainties was performed with less rigorous methods. However a good deal of attention was paid to available experimental data for the cross-sections. Although not as good as a full R-matrix analysis, this work can be considered of relatively good quality.

In summary, the covariance matrix evaluated for ^{10}B should be considered of good quality, and the one for ^{12}C of medium quality. If there is a strong need for improved evaluation of

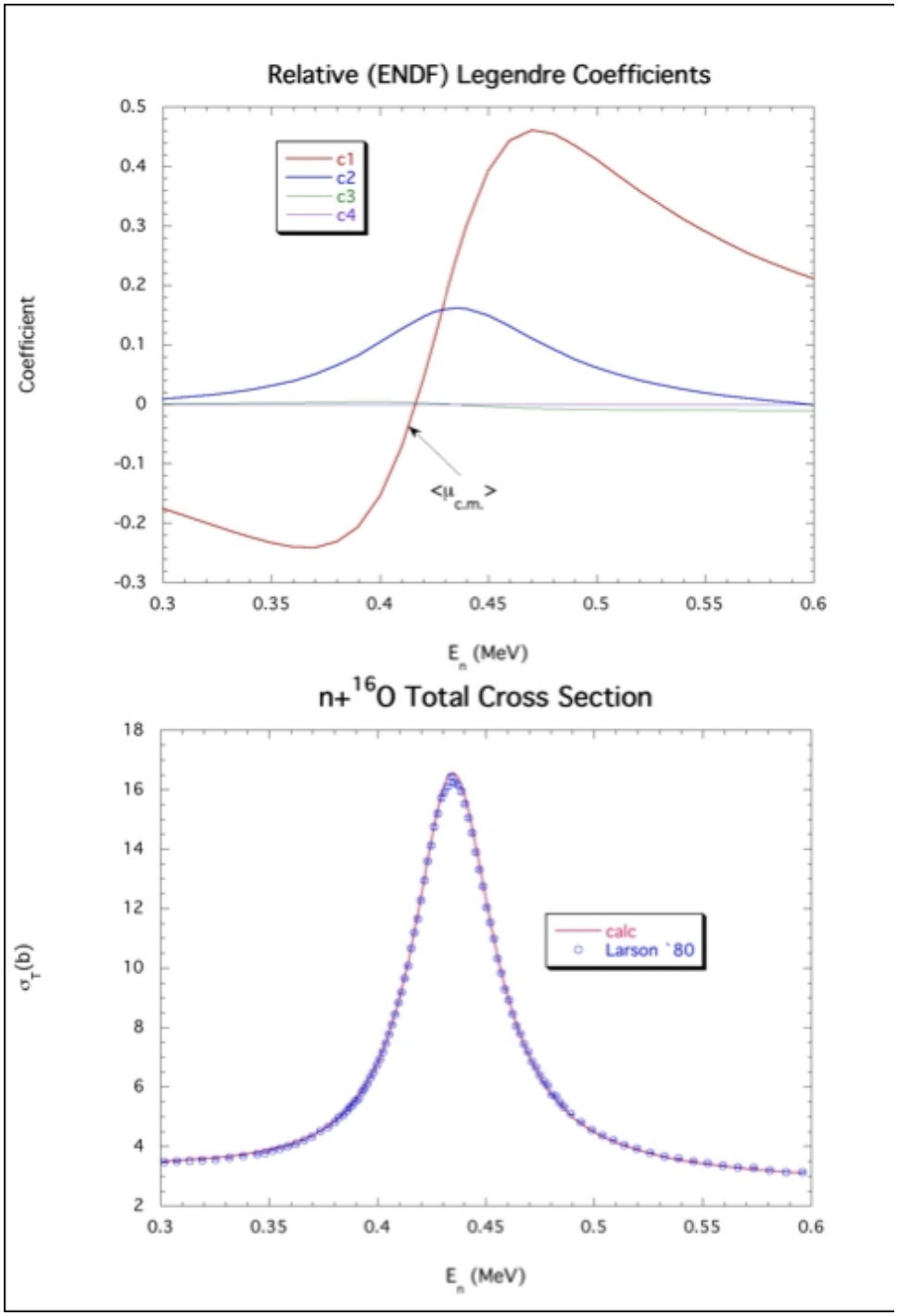

Figure 2.17: Legendre coefficients for ^{16}O obtained from a fit to experimental angular distributions and total cross sections.

Table 2.3: ^{16}O mu-bar uncertainties.

E_n (MeV)	$\overline{\mu}$	d$\overline{\mu}$	(%)
0.30000	-0.17545	0.00061568	0.35091
0.31000	-0.18717	0.00070354	0.37588
0.32000	-0.19924	0.00079271	0.39786
0.33000	-0.21133	0.00088202	0.41736
0.34000	-0.22289	0.00096841	0.43448
0.35000	-0.23293	0.0010454	0.44882
0.36000	-0.23978	0.0011046	0.46068
0.37000	-0.24067	0.0011329	0.47075
0.38000	-0.23125	0.0011112	0.48053
0.39000	-0.20509	0.0010175	0.49611
0.40000	-0.15412	0.00081411	0.52823
0.41000	-0.071188	0.00042476	0.59668
0.42000	0.043668	0.00030095	0.68918
0.42500	0.10927	0.00079699	0.72937
0.43000	0.17638	0.0013378	0.75848
0.43500	0.24134	0.0018748	0.77685
0.44000	0.30068	0.0023748	0.78981
0.45000	0.39265	0.0031553	0.80358
0.46000	0.44400	0.0035717	0.80445
0.47000	0.46089	0.0036477	0.79145
0.48000	0.45482	0.0035039	0.77039
0.49000	0.43599	0.0032600	0.74773
0.50000	0.41134	0.0029878	0.72635
0.51000	0.38491	0.0027193	0.70647
0.52000	0.35888	0.0024674	0.68753
0.53000	0.33426	0.0022388	0.66979
0.54000	0.31146	0.0020380	0.65435
0.55000	0.29057	0.0018686	0.64309
0.56000	0.27153	0.0017284	0.63653
0.57000	0.25418	0.0016080	0.63264
0.58000	0.23836	0.0015017	0.63003
0.59000	0.22390	0.0014064	0.62812
0.60000	0.21066	0.0013202	0.62669

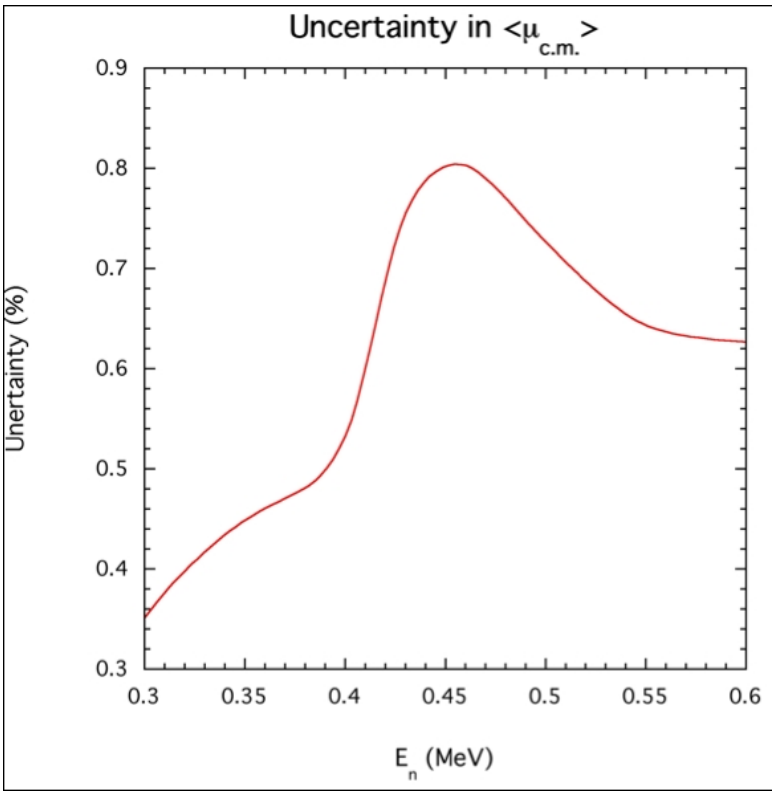

Figure 2.18: Uncertainty in ^{16}O mu-bar.

^{12}C, then it should be made a priority in the near future.

2.4.2 Actinides Improvements

Several improvements were made for ^{233,235,238}U and ^{239}Pu submitted earlier to ENDF/A [12].

^{235}U Capture Cross Section

The covariance matrix for the capture cross-section of n+^{235}U was evaluated back in 2007, using our GNASH+KALMAN methodology. After some feedback from ANL reactor sensitivity calculations, the relatively high standard deviations in the 1-100 keV region were questioned.

First of all, a little background information. In the case of fissile nuclei, the determination of the capture cross-section is very complex, because of the difficulty in distinguishing between gamma rays coming from fission and from capture processes. What is often measured is actually the ratio $\alpha = \sigma_c/\sigma_f$, and not the capture cross-section directly. Figure 2.19 shows the experimental data sets available in the case of n+^{235}U. As can be seen, the spread of data points is quite large in the 1-100 keV region.

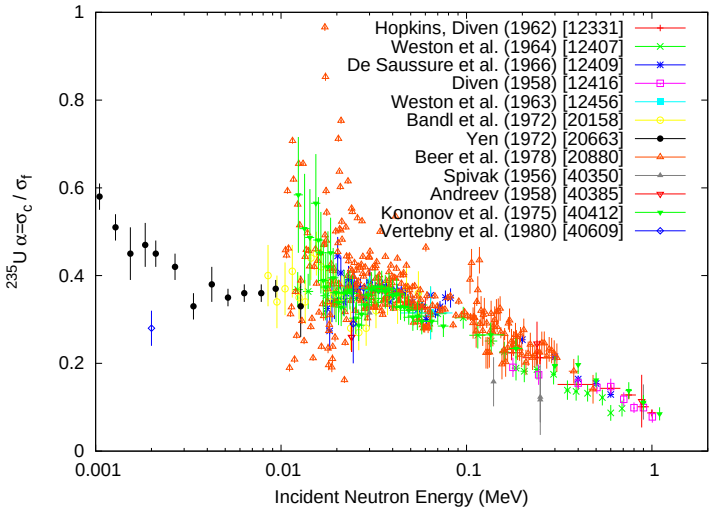

Figure 2.19: Measurements of the capture over fission cross-sections ratio for the n+^{235}U reaction.

Looking at evaluations in Fig. 2.20, the ENDF/B-VII.0 (== ENDF/B-VI) and JENDL-3.3 actually differ by 12% at 100 keV. Of course, comparing two evaluations is not the proper way to estimate an uncertainty, and we should always be cautious to extract too much information from this result alone.

As shown in Fig. 2.21, the ORNL uncertainty evaluation, which goes up to 2.25 keV, shows a large spike close to this energy, and in good agreement with the estimate of 30% from LANLs evaluation at higher energies. Interestingly, this figure also shows that there is almost no reduction of errors going from 618 groups down to 15 groups. It suggests that the systematic errors are an important component of the overall uncertainties.

As explained already in other documents, it is very difficult to estimate properly correlations stemming from experimental measurements, and a wrong estimation can result in quite different final uncertainties.

It is also interesting to compare the results obtained for ^{235}U with the ones for ^{238}U and ^{239}Pu, as the same methodology was used in all three cases. Figure 2.22 shows the results obtained after processing the evaluated covariance matrices, using the NJOY-99.296 code in the AFCI 33-groups structure.

The case of ^{238}U capture cross section is somewhat different as this nucleus is a fertile nucleus, for which the fission cross section is very small up to the MeV region, simplifying significantly capture cross section measurements. ^{239}Pu is more instructive, and it indeed shows that the evaluated uncertainties in the 1-100 keV region are much lower (10%).

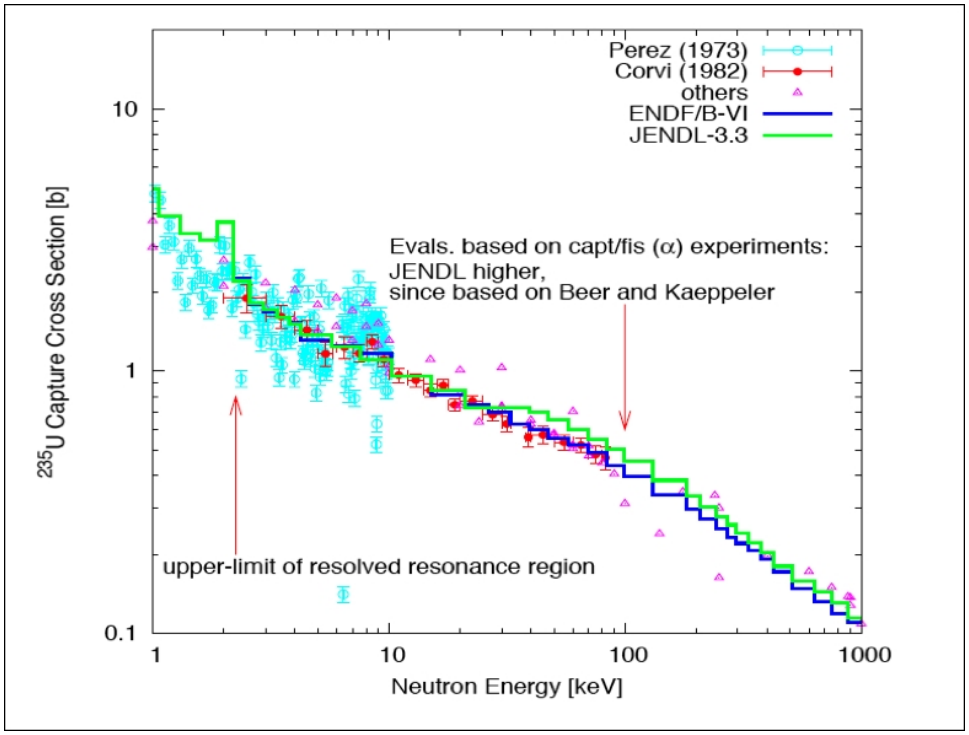

Figure 2.20: Comparisons between ENDF/B-VII (== ENDF/B-VI) and JENDL-3.3 evaluations of ^{235}U capture cross section.

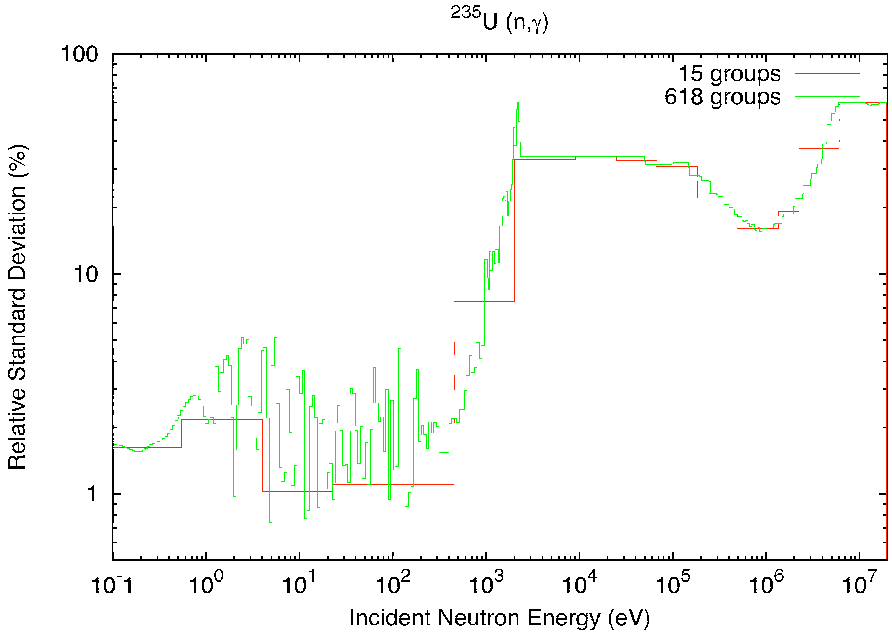

Figure 2.21: Standard deviations (in %) for ^{235}U capture cross section, processed through NJOY in 15 (red curve) and 618 (green curve) groups. For final result see covariance plot in Appendix A.2.3.

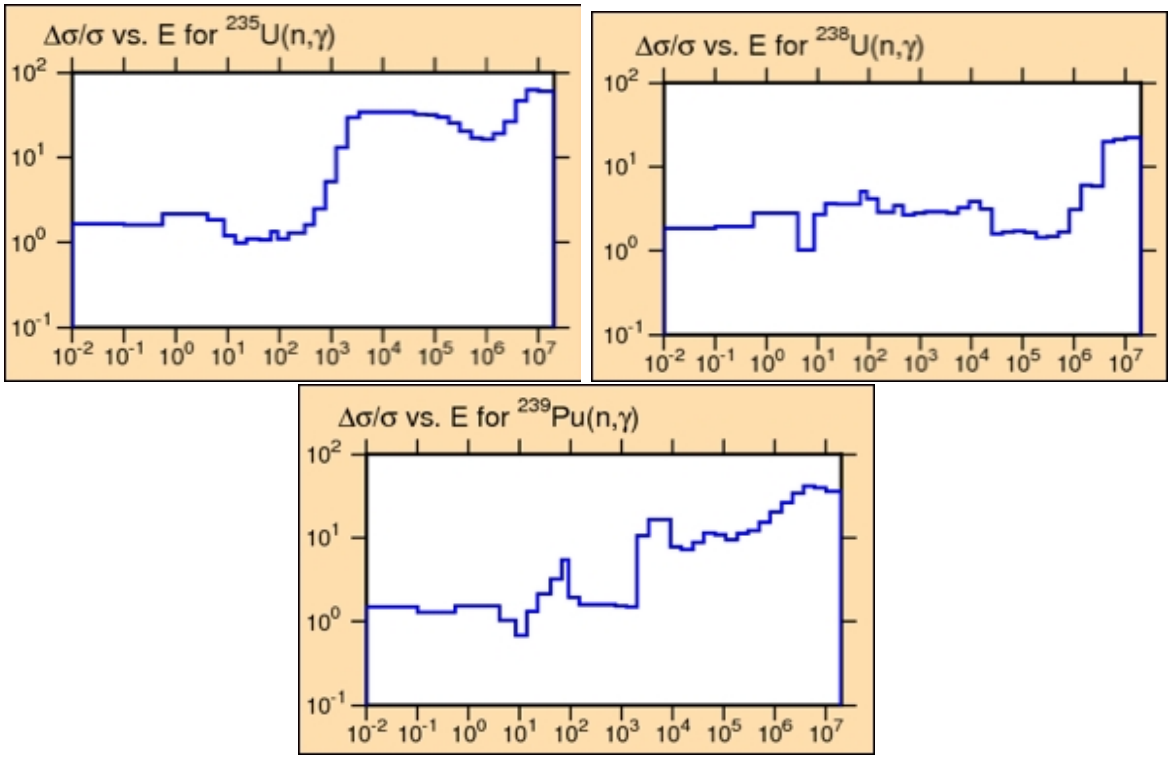

Figure 2.22: Standard deviations obtained for ^{235,238}U and ^{239}Pu(n,γ) reactions. These figures were obtained with NJOY-99.296 in 33-group structure.

Because of the ambiguities mentioned earlier in the estimation of the systematic errors in experimental data sets, and the result for ^{239}Pu capture uncertainties, we decided to adjust the final results obtained for GNEP-1.1 to about 20% in the 1-100 keV range. Note that this is a purely *ad hoc* modification, and a more sound result should be pursued in the future.

A new ENDF file was generated by reducing the standard deviations in this region, and by modifying the off-diagonal elements by keeping the correlation matrix intact. The file was processed with NJOY-99.296 in 33 groups, and the result is shown in Fig. 2.23.

^{239}Pu Neutron Multiplicity Covariance Matrix

In the incident energy range 10^{-5} eV-1.0 keV, the evaluation of nubar is taken directly from ENDF/B-VI.8, based on an evaluation by E.Fort. It was renormalized though to the CSEWG and ENDF/B-VI standard thermal nubar value. No covariance evaluation was made in this energy range.

In the energy region 1 keV-20 MeV, minor modifications were made to the ENDF/B-VI.8 evaluation. The covariance analysis was made with the GLUCS code, which performs a generalized least-square fit to the experimental data. The data sets were renormalized to

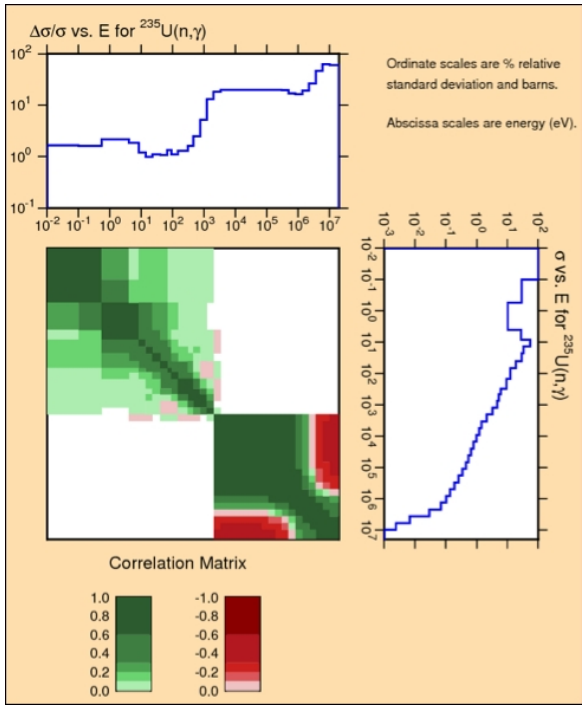

Figure 2.23: New ^{235}U capture covariance matrix (MF33/MT102) processed with NJOY-99.296 in a 33-group structure.

the latest ^{252}Cf (*sf*) nubar standard value. Figure 2.24 shows the standard deviations as a function of incident neutron energy obtained with GLUCS.

Several observations:

- The ENDF/A final evaluation (blue curve) represents a smooth curve fitting the GLUCS results.
- Previous spikes in the evaluated standard deviations (up to 95%) were due to prior values in the Bayesian analysis, which were not removed because of the lack of experimental locally. This has been fixed.
- The local fluctuations observed in the evaluated standard deviations (see Fig. 2.24) are due to smaller or larger uncertainties at specific energy points. These fluctuations are not really physical, and we applied a 5-points smoothing technique to filter them out. The final result is shown as the blue curve in Fig. 2.24.

A final MF31, MT456 ENDF-formatted section has been produced. The exact same results were used for the total $\overline{\nu}$ covariance matrix (MF31, MT452), as the impact of delayed neutrons uncertainties on the final matrix are neglected.

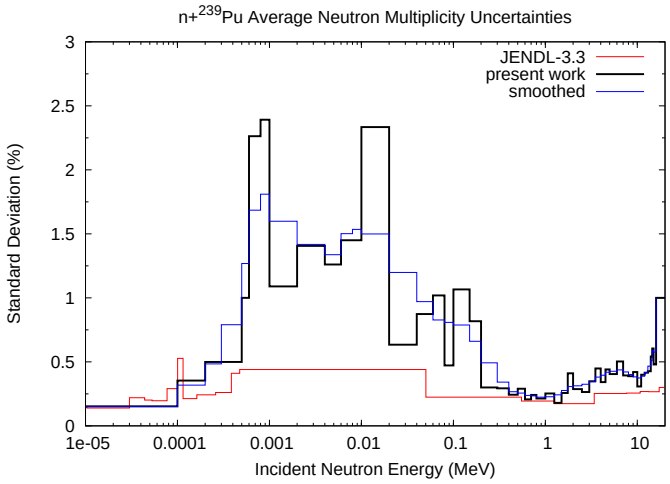

Figure 2.24: Evaluated standard deviations for the average neutron multiplicity of n+^{239}Pu. The black curve represents the GLUCS results, while the blue curve is the final result, which has been smoothed by a 5-points filtering technique. Shown for comparison is JENDL-3.3 as red curve. For final result see covariance plot in Appendix A.2.3.

^{235}U Total Neutron Multiplicity Covariance Matrix

The covariance matrix for the average total number of neutrons was not studied in the previous LANL covariance work. However, because of the small contribution of the delayed neutrons vs. prompt neutrons, it is reasonable to expect that the evaluated covariance matrix for the total should be very similar to the one for the prompt neutrons.

We fixed this issue by copying the exact same covariance matrix for MF31, MT456 (prompt) to MF31, MT452 (total).

2.4.3 Prompt fission neutron spectrum for n(0.5 MeV)+^{239}Pu.

We have evaluated the Prompt Fission Neutron Spectrum (PFNS) covariance matrix for the neutron-induced fission of ^{239}Pu, for 0.5 MeV incident neutron energy. Details of the methodology, experimental database, and model input parameters are described at length in a publication in preparation [24], and will not be repeated here.

Following a methodology similar to what was used for the evaluation of covariance matrices for the neutron-induced reaction cross sections on ^{235,238}U and ^{239}Pu, we have obtained a PFNS covariance matrix that reflects uncertainties originating in experimental data as well as model parameters.

In the case of PFNS calculations, we implemented the so-called Los Alamos or Madland-Nix

model equations [9]. In the present calculation, and since we are only concerned with the first-chance fission, only four parameters (and mainly three) are relevant. They are the: $\langle E_r \rangle$ average energy release; $\langle TKE \rangle$ average total kinetic energy, $\langle a \rangle$ average level density parameter, $\langle B_n \rangle$ average neutron binding energy. These four parameters enter in the equation defining the temperature T of the evaporating compound nucleus:

$$T \propto \sqrt{\frac{\langle E_r \rangle - \langle TKE \rangle}{\langle a \rangle}}. \tag{2.3}$$

We have performed model parameter sensitivity calculations, and relative sensitivity coefficients $(\partial\phi/\phi)/(\partial p/p)$ are shown in Fig. 2.25. Two cases are considered, 5% and 10%, represented by the thick and thin lines respectively, to check if the response of the calculated PFNS is linear with respect to parameters variations. The differences observed show that a linear approximation is rather good, but not completely satisfactory, especially for the two most important parameters $\langle TKE \rangle$ and $\langle E_r \rangle$.

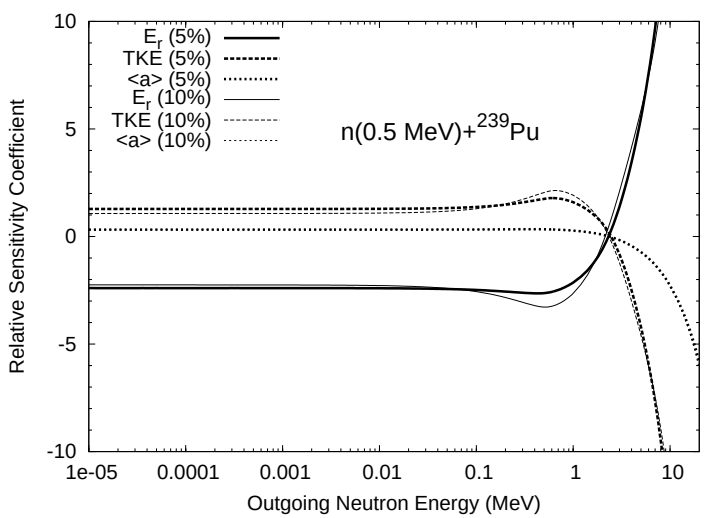

Figure 2.25: Relative sensitivity coefficients calculated for the n (0.5 MeV)+^{239}Pu PFNS using the Los Alamos model parameters.

The most important experimental data sets used for the ENDF/B-VII.0 evaluated spectrum were also used here. They are from Staples [25] and Knitter [26]. Additional experimental data sets were also used, in particular for the low-energy part of the spectrum, but their influence on the final results was rather small.

The final results are summarized in Figs. 2.26- 2.28., which show the PFNS standard deviations (in %), the PFNS correlation matrix, and 100 PFNS samples, respectively. A few remarks are in order: the standard deviations obtained directly from the KALMAN output

were deemed too small, compared to the spread of experimental data. This problem is well-known and appears most strongly when many experimental data points are considered, and systematic uncertainties and correlations are not taken into account properly. To palliate this issue, we decided to renormalize the whole covariance matrix to the better known uncertainty (about 1%) on the average outgoing energy (first moment of the spectrum). A second correction was applied to the KALMAN result: very few experimental data sets exist for low-energy neutrons. In this region (below 500 keV), considerable differences exist in the scarce available data. While Los Alamos model predictions lie right in the middle of experimental values, the calculated uncertainties were also deemed to be too optimistic. An additional contribution to the covariance matrix was added below 500 keV to take into account unknown limitations of the model itself (not model parameters!). A possible explanation for the discrepancies between Los Alamos model calculations and several data sets could be due to the contribution of neutrons emitted before the full acceleration of the fragments. Such neutron source is not considered in the Los Alamos model. However, at this stage, it is still too early to conclude on this question.

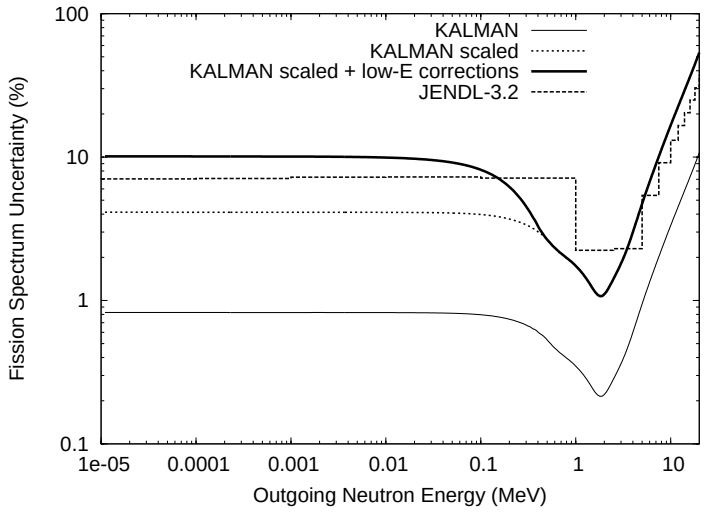

Figure 2.26: Calculated standard deviations for the evaluated PFNS of n(0.5 MeV)+^{239}Pu.

Finally, the evaluated covariance matrix was saved in an ENDF section MF=35, MT=18, and processed successfully through the latest release of NJOY-99.296 into 33 and 590 groups. Results are shown in Figs. 2.29 and 2.30.

2.4.4 n+^{240}Pu

A completely new evaluation was performed on neutron-induced reactions on ^{240}Pu. In this section, we will only mention the uncertainty quantification piece of the evaluation work,

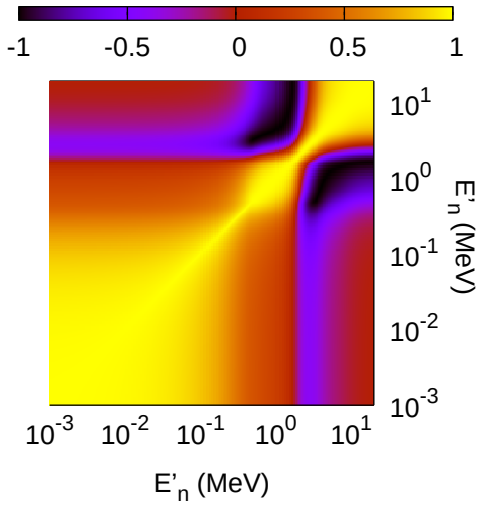

Figure 2.27: PFNS correlation matrix for n(0.5 MeV)+^{239}Pu.

while other details on the evaluation itself are gathered in Appendix B.

Following the same methodology as for other actinides studied at LANL, several codes were used to produce covariance matrices; they are: GNASH, statistical Hauser-Feshbach nuclear reaction code; SOK and GLUCS, two generalized least-squares fitting programs to compute experimental covariance matrices; and KALMAN a Bayesian statistical tool to combine experimental and model parameters uncertainties.

GNASH sensitivity calculations were performed varying the following set of model parameters: (E_A, E_B, $\hbar\omega_A$, $\hbar\omega_B$, ρ_A, ρ_B) for the 1st, 2nd and 3rd compound nuclei formed in the n+^{240}Pu reaction. These are the fission barrier heights, barrier widths and collective enhancement factors on top of the barriers, respectively. Were also varied the level density parameters, pairing energies, pre-equilibrium constants and experimental γ-ray strength function.

Many experimental data sets were considered (see Appendix...) and analyzed with the GLUCS and SOK codes. In particular, recent LANSCE measurements of the (n,fission) and (n,capture) reaction cross sections were used in this work. However, no measurement exist for the inelastic, (n,2n) and (n,3n) cross sections. In those cases, dummy experimental data sets were used (following GNASH results) and prior uncertainties were only guessed. In

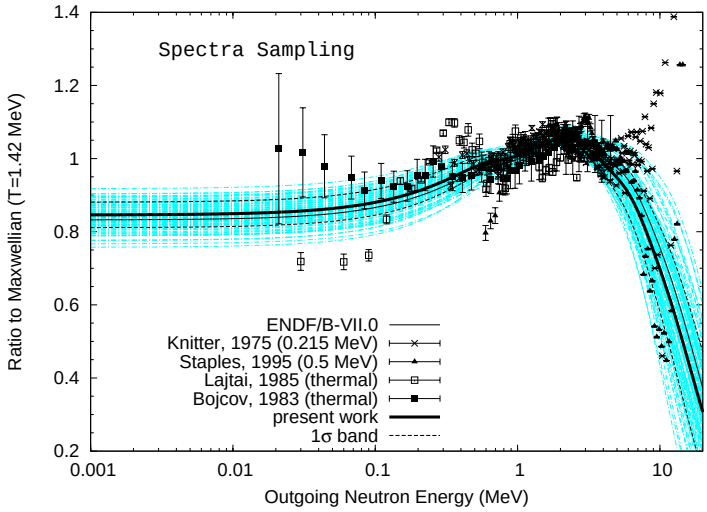

Figure 2.28: Monte Carlo samples of the PFNS for n(0.5 MeV)+^{239}Pu, obtained by sampling the spectrum covariance matrix.

particular, a comparison with other existing evaluations was used as a guide.

The KALMAN code was then used to combine model parameter sensitivity calculations and experimental uncertainties. The results are summarized in Figure 2.31, which shows the calculated standard deviations for the fission, capture, inelastic, (n,2n) and (n,3n) reaction cross sections.

A few comments are important to make:

- An additional contribution of 0.3% was added to the uncertainties obtained for the fission cross-section; the same correction was done for the ^{235}U (n,f) cross section uncertainties, from which the present ones are obtained;
- The capture standard deviations were renormalized to get a standard deviation of about 3% around 100 keV. The raw KALMAN result gave about 1.5% at that point;
- The capture uncertainties become very large beyond 1 MeV, where the capture cross-section becomes very small. A cut-off uncertainty of 100% was used there;
- Uncertainties for the (n,2n) and (n,3n) cross sections were obtained by assuming dummy experimental data sets following GNASH calculations, for which uncertainties and correlations were assumed;
- Standard deviations for the inelastic cross section in the 100 keV region drop to below 10%. Since only GNASH (and no ECIS) model parameters were varied in the present sensitivity study, uncertainties on the direct component of the inelastic scattering cross

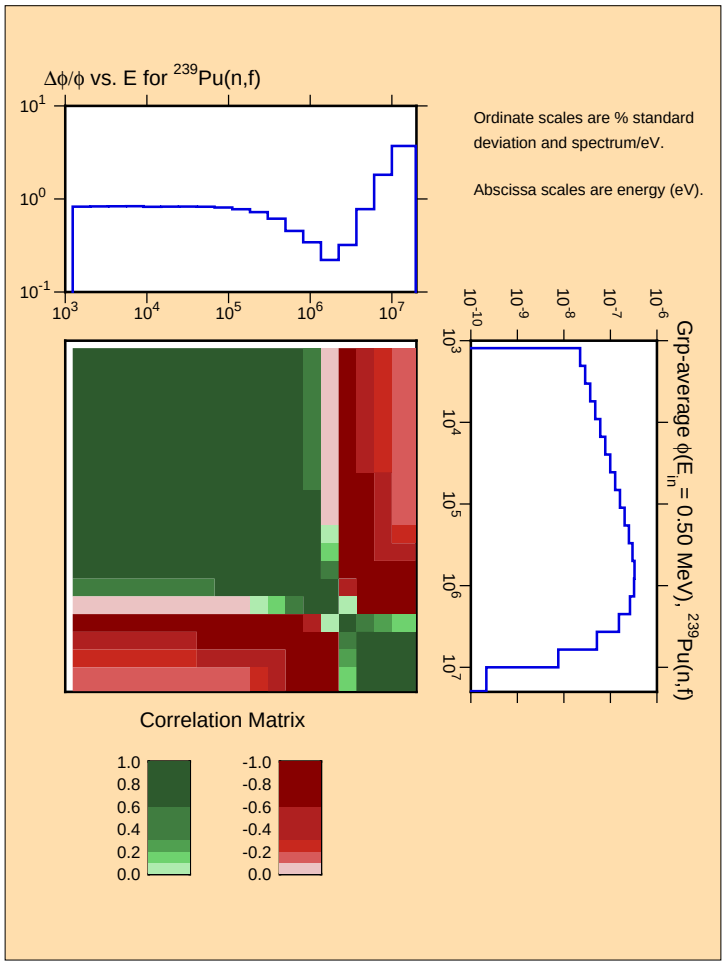

Figure 2.29: Result of processing the MF35, MT18 section of the final ENDF-formatted file in a 33-group energy structure used at ANL for GEN-IV reactor sensitivity calculations. The processing was performed with the NJOY code, version 99.296.

section are missing. A correction was made in the final ENDF file to account for this contribution (only approximately, though).

The correlation matrices for the evaluated fission and capture cross-section uncertainties are shown in Figs. 2.32 and 2.33, respectively. As expected, the capture correlation matrix displays very strong off-diagonal elements.

The average neutron multiplicity $\overline{\nu}(E_n)$ was obtained through a GLUCS analysis of experimental data sets. It served as a basis for prompt fission neutron spectrum (PFNS) calculations using the Los Alamos model. Figure 2.34 shows the result of the GLUCS analysis and calculations performed within the Los Alamos model, and compared with experimental data sets and evaluations.

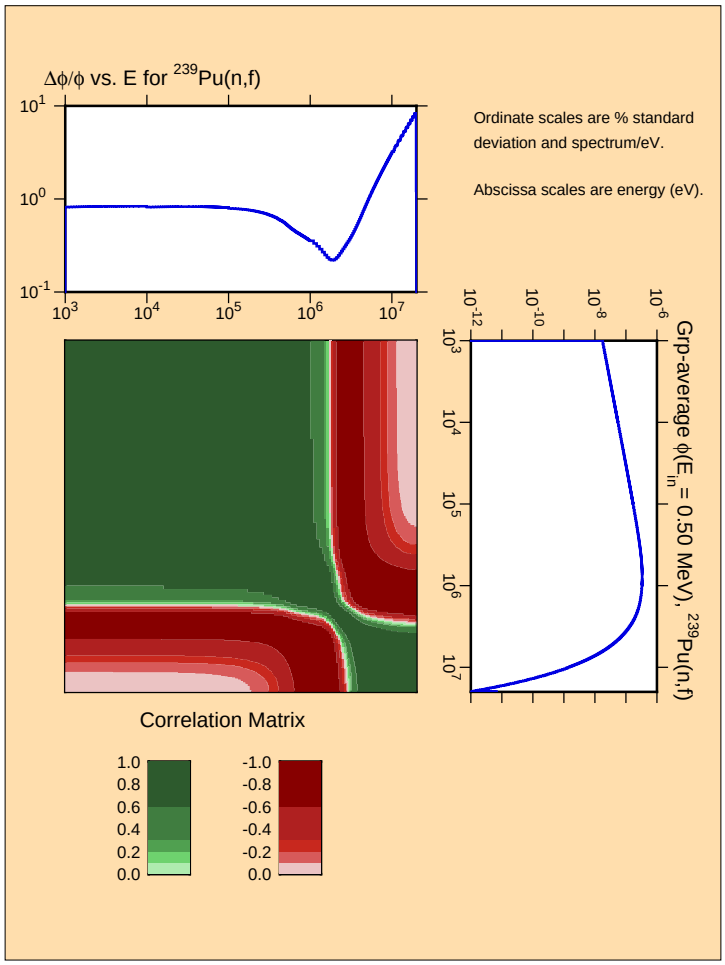

Figure 2.30: Same as in Fig. 2.29 but with a 590-groups energy grid.

An uncertainty quantification of the PFNS (at 0.5 MeV incident neutron energy) was also performed, following our work on ^{239}Pu. However, in the case of ^{240}Pu, no experimental data exist for the PFNS and one had to assume some uncertainties at specific outgoing energy points. More details can be found in the Appendix... Figures 2.35 and 2.36 show the final results for the fission spectrum standard deviations and correlation matrix.

All UQ results for n+^{240}Pu reaction cross sections (MF=33, MT=1,2,4,16,17,18,102), average prompt neutron multiplicity (MF=31,MT=456) and prompt fission neutron spectrum (MF=35,MT=18) were processed successfully through NJOY-99.296 into the ANL 33-group structure.

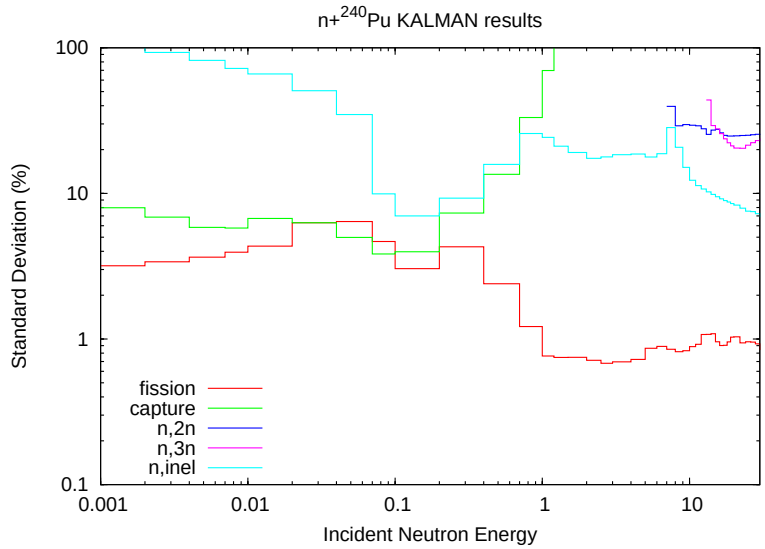

Figure 2.31: Results of the KALMAN code for selected reactions following n+^{240}Pu.

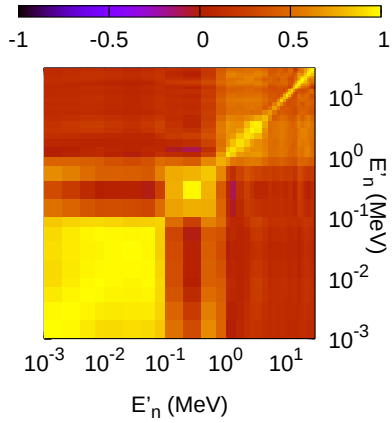

Figure 2.32: ^{240}Pu neutron-induced fission cross-section correlation matrix.

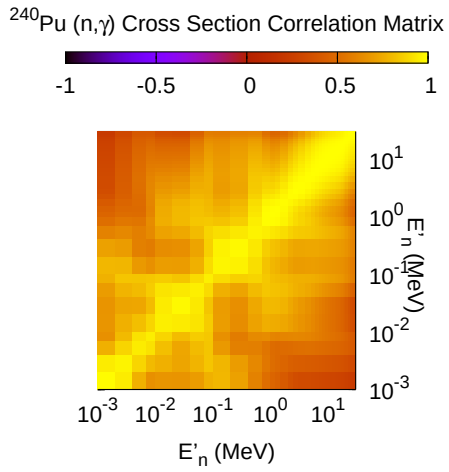

Figure 2.33: ^{240}Pu neutron-induced capture cross-section correlation matrix.

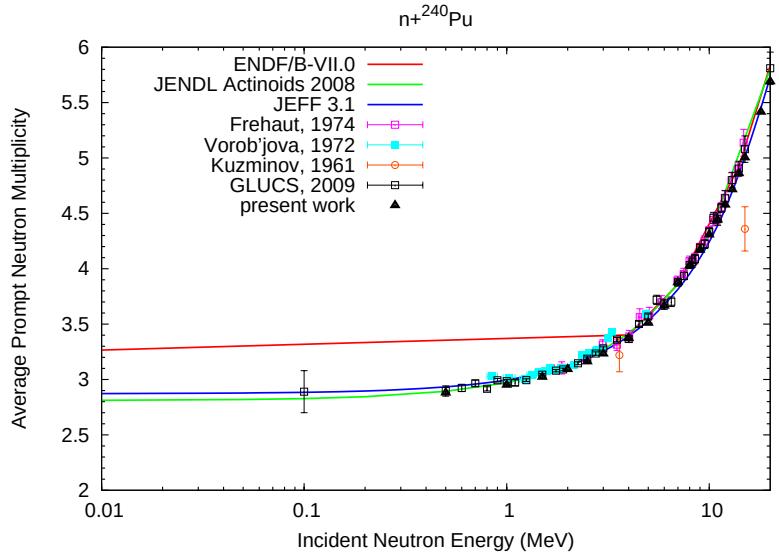

Figure 2.34: ^{240}Pu average prompt neutron multiplicity. The values obtained with Madland-Nix model calculations are shown as black triangles. The GLUCS covariance analysis results are shown as black empty squares.

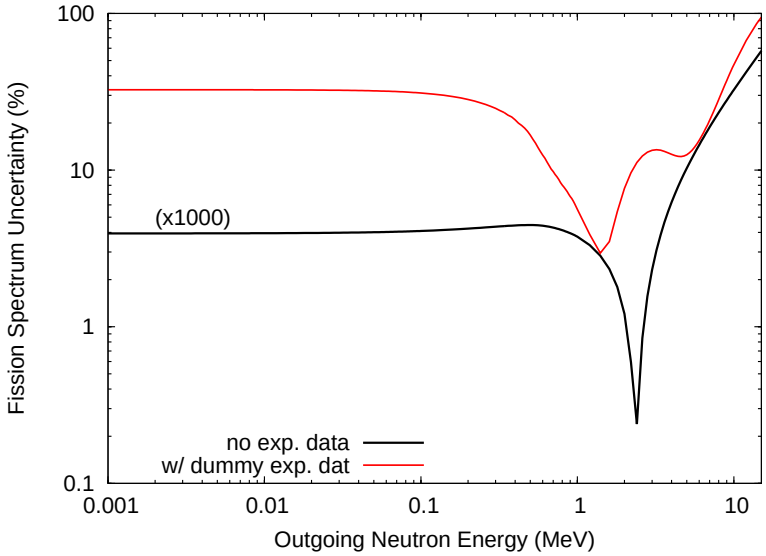

Figure 2.35: ^{240}Pu PFNS standard deviations.

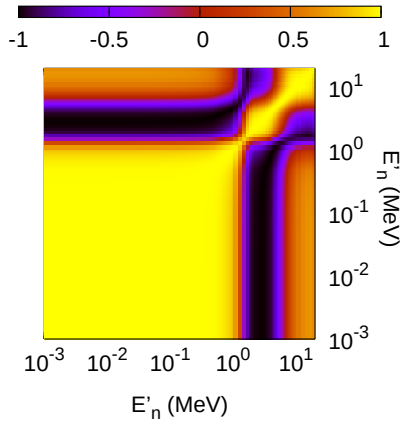

Figure 2.36: ^{240}Pu PFNS correlation matrix.

Chapter 3

AFCI-1.2 covariance library

3.1 Creation of library

The AFCI-1.2 covariance library was created in three steps. First, in FY2008 we produced the initial version of the library with starter files for 108 materials. Even though our M2 milestone was restricted to 64 priority materials [1] this initial library already contained virtually all materials on the AFCI list. This was made possible by adopting as many as 75 covariance files from the recently completed Low-Fidelity Covariance project funded by the US Nuclear Criticality Safety Program. This GNEP-1.0 library was released to ANL-INL users in October 2008.

Then, in April 2009 we improved 11 materials and provided mubars for two of them, which formed new version of the library, GNEP-1.1. These modifications and additions addressed most pressing issues and user feedback on GNEP-1.0.

Finally, in July 2009 we assembled the improved version of the library including the full list of 110 materials. Virtually no file was adopted for this improved library before performing its critical review. As a consequence, numerous changes in most of the files were implemented. The assembled library was subjected to considerably extended QA procedure as described in the following two sections. Once this QA process was completed, the library was named AFCI-1.2 and released to ANL and INL users, in August 2009.

In many cases uncertainties in the AFCI-1.2 library were changed, after processing with NJOY was completed. These changes primarily included increasing low uncertainties, and removing uncertainty peaks (see Sections 2.3.2 and 2.3.3 for examples). These changes were made on the multigroup level mainly due to the time constraints of the AFCI project. The point is that it is much easier to modify multigroup data than to achieve the same effect by modifying ENDF-6 formatted data. As a consequence it is important to recognize that, due to these multigroup interventions, files in the AFCI-1.2 covariance library in general do not represent the contents of processed ENDF-6 formatted files.

3.2 Quality assurance

3.2.1 Data checking

Once the library was assembled, careful checking of data was done with the dedicated code, followed by visual inspection of covariance plots.

Checking with the unCor code

All numerical files were checked by the newly developed BNL code 'unCor' designed for the specific purpose of checking processed, multigroup uncertainties and correlations. The unCor code is written in python, and depends on 'numpy', a module for handling numeric arrays, and on the 'empy' module now distributed along with EMPIRE. It identifies unphysical values of uncertainties and correlation coefficients, surprising peaks or jumps in uncertainties, etc. and issues warnings to the reviewer and/or evaluator. Criteria defined below are based on considerable feedback from ANL-INL users to earlier versions of the library and on our extensive experience with covariance evaluations, covariance methodology and creation of covariance libraries.

Current checks for unphysical uncertainties and correlation coefficients:

1. Uncertainties too high. Rationale: uncertainties should not exceed one hundred percent. Even though the 100% upper limit is debatable it appears that the AFCI users prefer this convention rather than the pain of introducing asymmetric uncertainties into their application codes. We thus strictly require that

   - $\Delta \leq 100\%$ for any type of data.

2. Uncertainties too low. Rationale: low uncertainty often indicates unrealistic assessment on the part of evaluator. The deeper reason behind it might be the use of "rigorous" methods that are known to produce very small uncertainties if systematic uncertainties were not properly included in the evaluation. At the moment warning is issued if

   - $\Delta < 1\%$,

   but more refined criteria should be used in the future

   - $\Delta(n, tot) < 1\%$
   - $\Delta(n, el) < 2\%$
   - $\Delta(n, \gamma) < 2\%$
   - $\Delta(n, inl) < 3\%$
   - $\Delta(n, 2n) < 3\%$
   - $\Delta(n, chp) < 3\%$
   - $\Delta(n, fis) < 0.7\%$
   - $\Delta(\bar{\nu}) < 0.7\%$

3. Uncertainties $\neq 0\%$ except below thresholds. Rationale: for non-zero cross sections the undertainties must always exceed zero. We thus strictly require that

   - $\Delta > 0\%$ if $\sigma > 0$ barns.

4. Improper correlation matrix. Rationale: improper properties such as asymmetry, correlation coefficients out of range and lack of unitarity along diagonal are in violation with the basic properties of a correlation matrix. We strictly require that the matrices are symmetric and coefficients are within the range (unitarity will be addressed later),

   - $\text{corr}_{ii} = 1$ for $E_n > E_{threshold}$
   - $-1 \leq \text{corr}_{ij} \leq 1$
   - $\text{corr}_{ij} = \text{corr}_{ji}$.

Sudden discontinuities and peaks in uncertainty

5. Uncertainties exhibit strong discontinuity. Rationale: sudden changes in uncertainties as a function of energy are unlikely and often reflect evaluation issues rather than genuine discontinuities in data. A typical reason is disconnect between two parts of evaluation, one at low energies and another one in the fast neutron region. Currently a warning is issued if uncertainties in two neighboring groups differ by more than a factor of 10,

   - $\Delta_i < 0.1\ \Delta_{i+1}$ or
   - $\Delta_i > 10\ \Delta_{i+1}$.

6. Strong peaks in uncertainties. Rationale: sharp peaks in uncertainties are unlikely except for the resonance region, in the fast neutron energy region such peaks usually indicate an evaluation problem. A warning is issued if the uncertainty increases by a factor of 5 or more, then decreases also by a factor of 5 or more within 3 bins.

   - $\Delta_{i+1} > 5\ \Delta_i$ and $\Delta_{j+1} < 0.2\ \Delta_j$, where $j - i < 3$

Future checks that should be implemented in unCor code:

1. Positive-definiteness. Rationale: correlation matrices must be positive-definite so that inverse matrices can be produced. At this stage this criterion is not applied since the issue has not been raised by the users. Ultimately, as soon the covariance library reaches its mature stage, it will be applied and strictly required,

   - λ_i (eigenvalues of $corr$) ≥ 0, $\det(corr) > 0$.

2. Rows/columns sum to zero for spectra covariance matrices (MF35). Rationale: MF35 contains covariances of prompt fission neutron spectra and it is required that the zero sum-rule is duly observed for the summation of every column and every row of correlation coefficients. We thus strictly require that

   - $\Sigma_i(\text{cov}_{ij}) = 0.0$ for any j and

- $\Sigma_j(\mathrm{cov}_{ij}) = 0.0$ for any i in MF35 matrices.

We note that this sum rule is not upheld in the AFCI-1.2 release.

3. Decline of uncertainties for non-threshold reactions. Rationale: this is specific issue mostly related to MF32 where such decline usually indicates lack of correlations among resonances. This effect may be particularly strong at the end of the resolved resonance region where many resonances can fall into a single energy group. Due to statistical averaging the uncertainty drop would be proportional to square root of the number of resonances, $\sqrt{N}$. A warning would be issued if there is continuous drop of uncertainties in three consecutive energy groups, perhaps also linked to the energy of the upper cutoff of the resolved resonance region,

   - $\Delta_i > \Delta_{i+1} > \Delta_{i+2} > \Delta_{i+3}$.

Unlikely uncertainties

4. Uncertainties too high. Rationale: high uncertainties may indicate a problem for some reactions. For instance, total cross sections are deemed to be known to relatively high precision and too high uncertainty may suggest that the assessment of evaluator is not realistic. Warning would be issued if

   - $\Delta(n, tot) > 20\%$.

Unlikely uncertainties for rare materials and low cross sections

5. Low uncertainties not plausible for materials with low abundance and short half-lives. Rationale: covariances for materials and reactions that are difficult to measure should be more conservative than for materials where experimental data are available. This applies to isotopes which have low natural abundance (abd) or that are radioactive. A warning would be issued if

   - Δ(low abd)$<$ 2 Δ(high abd), where low abundance is defined as abd $< 3\%$ or radioactive; for actinides abd $< 0.5\%$ or $T_{1/2} < 100$ y. We note that as many as 25 out of 110 materials fall into this category, though some of them might not qualify for this test such as ^{2}H and ^{99}Tc where many measurements are available.

6. Uncertainties not plausible due to low cross sections. Rationale: it is unlikely that low cross sections are determined to very high precision. One should develop adequate test to check this relationship which should be of the type

   - Δ large if σ small.

   One could adopt some earlier recipes developed along this line in the past. Thus, in 1991, Hetrick et al [14] used the assignments for uncertainties of model-based cross sections given in Table 3.1. JAERI, in 1997, pursued similar though somewhat more optimistic approach as seen in Table 3.2.

Table 3.1: Assigned uncertainties for calculated cross sections by ORNL, 1991 [14].

σ (mb)	Δ (%)
$\sigma > 500$	10
$100 < \sigma < 500$	15
$30 < \sigma < 100$	20
$\sigma < 30$	30

Table 3.2: Assigned uncertainties for calculated cross sections by JAERI, 1997 [16].

σ (mb)	Δ (%)
$\sigma > 500$	5
$100 < \sigma < 500$	10
$1 < \sigma < 100$	15
$\sigma < 1$	> 25

With some limitations the AFCI-1.2 library was subjected to data checking as described above. The code unCor produced a number of warnings, see Table 3.3. All of them were examined, but only some were fixed due to limited time available. It should be made very clear that even though unCor would issue warnings, it is up to evaluator to assess all evidence and available data and come up with final answer.

Visual inspection of covariance plots

The second part of data checking involved visual inspection of covariance plots (uncertainties and correlation matrices). Considerable attention was given to uncertainty trends (shapes of uncertainty curves/histograms) and their relationship to absolute values of cross sections since small cross sections should likely have large uncertainties and vice versa; uncertainties might fluctuate if cross section fluctuate, while they would be smooth if cross sections are smooth. In order to enhance a chance to catch as many deficiencies as possible the covariance plots should be produced in three different ways.

- Unprocessed MF33 files visualized by the NNDC retrieval and plotting system Sigma. These plots would reveal all details in MF33, such as unrealistic peaks in uncertainties, that might be easily overlooked if plots in broad energy groups would be inspected.
- Covariances produced by processing with NJOY in fine group structure, usually 187- or 618-energy groups. Such NJOY plots would be fairly detailed and might reveal deficiencies primarily in MF32 which cannot be currently visualized by Sigma.
- Covariances produced by processing with NJOY in 33-groups. This is AFCI user group structure in which covariances must ultimately be inspected before the library is released.

Table 3.3: Summary of warnings raised by checking code UnCor when checking the AFCI-1.2 library. Also shown are checks not yet adopted.

No.	Name of the check	Warnings	Comment
1	Δ >100%	none	Strictly required
2	$\Delta < 1\%$	55	Uniformaly applied
3	$\Delta = 0$ if $\sigma > 0$	none	Strictly required
4	corr_{ij} unphysical	none	Strictly required
5	Δ discontinuity	3	Factor of 10 applied
6	Δ peak	5	Factor of 5 up/down applied
1	corr_{ij} positive-definite	n/a	Not yet adopted
2	MF35 sum-rule	n/a	Not yet adopted
3	Δ decline in RRR	n/a	Not yet adopted
4	Δ too high	n/a	Not yet adopted
5	rare material	n/a	Not yet adopted
6	small cross section	n/a	Not yet adopted

3.2.2 Data testing

Data testing was conducted only partly since the related tools are still under development. Our intention is to develop a set of comparisons capable of checking basic plausibility of covariances.

To achieve this goal we intend to analyze integral cross sections as well as multigroup cross sections. These should be compared to data whenever possible. They should also be compared to other evaluated libraries including ENDF/B-VII.0 (2006), JEFF-3.1 (2005), JENDL-3.3 (2002) and ROSFOND (2008). The idea is to use data whenever available, but look also into dispersion between evaluated libraries to judge the quality of covariances.

Even though this method has inherent limitations it is expected that in many cases it would help to identify unrealistically low uncertainties. This is the issue of considerable importance. For example, for structural materials such as ^{52}Cr, ^{56}Fe and ^{58}Ni, evaluations done with rigorous methods are available and we adopted some of them. However, these evaluations claim extremely low uncertainties that do not look plausible for AFCI users. Therefore, an effort has been initiated to find out whether such low uncertainties would survive the dispersion test outlined here.

Integral cross sections

Integral cross sections characterize data over broader portions of neutron energies and are often viewed as quantities of basic interest to users. These quantities include thermal cross sections, resonance integrals (RI), averages over 30-keV Maxwellian spectrum (MACS) and averages over ^{252}Cf fission spectrum. For some of these quantities experimental data are

available which make this comparison more powerful:

- capture - thermal (Atlas), RI (Atlas), MACS (KADoNiS - Karlsruhe Astrophysical Database of Nucleosynthesis in Stars)
- elastic - thermal (Atlas)
- fission - thermal (Atlas), RI (Atlas)
- $\bar{\nu}$ - thermal (Atlas), RI (Atlas).

As an example of integral cross sections we show ^{23}Na(n,γ) and ^{56}Fe(n,γ) in Fig. 3.1. One can see the integral values relative to ENDF/B-VII.0 and also MACS value with uncertainty from KADoNiS. In future the data from Atlas will also be shown along with the values computed from the AFCI covariance library. This last step, however, would need creation of ENDF-6 formatted files first.

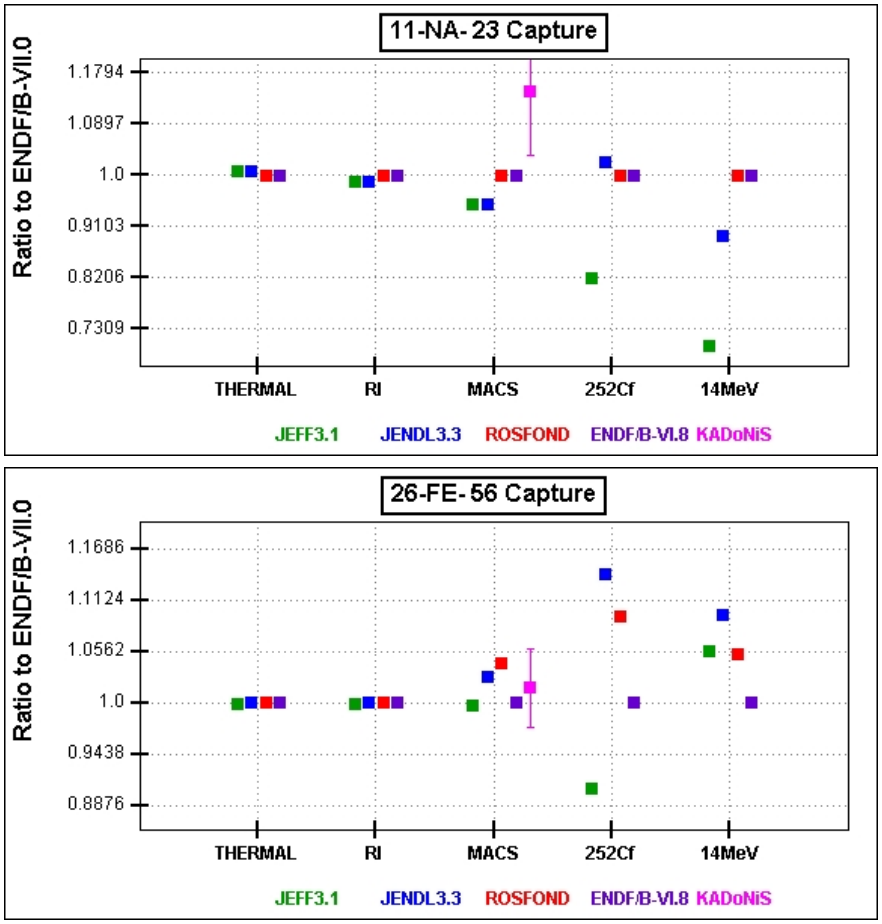

Figure 3.1: Integral quantities for ^{23}Na and ^{56}Fe(n,γ) in various evaluations relative to ENDF/B-VII.0.

Ratios of multigroup cross sections

Processed cross sections in 33-group representation can be readily produced for all major libraries and ratios to ENDF/B-VII.0 values can be computed. The resulting plots showing these ratios can be used to identify dispersion of the libraries in order to judge plausibility of uncertainties in AFCI-1.2 library.

As an example we discuss ^{56}Fe(n,inl). In April 2009, we adopted covariances from the Vienna-Obninsk collaboration of H. Vonach, V. Pronyaev et al produced in 1992 [27] and updated in 1995 [15]. These data, adopted by JEFF-3.1 and also by a more recent BROND-3 library, represent the best evaluation available. It used carefully analyzed experimental data, followed by the Bayesian least squares fitting and update with the code GLUCS. The resulting uncertainties for (n,inl), however, were small, often less than 1.5%.

ANL-INL users felt uncomfortable with such high precision and demanded review on our part. This become possible once we developed a set of comparative plots in 33-group representation. As already discussed in Chapter 2, see Fig. 2.11, differences between ENDF/B-VII.0 in the several initial groups above the threshold considerably exceed 1.5% precision of BROND/JEFF and would suggest increasing these uncertainties by a factor of 3-4, bringing it to much more plausible values of about 5%.

3.2.3 Some issues identified by QA

To illustrate some of the issues identified by the above QA procedure we discuss a couple of prominent cases. Except for ^{156,158}Gd, however, no changes to AFCI-1.2 were introduced since they would require more work and time than currently available. Below we briefly describe these cases, followed by figures in support of our findings.

1. ^{156,158}Gd: ^{156}Gd(n,γ) has large uncertainties ($>$ 100%) and strong peaks in RRR; ^{158}Gd(n,el) displays strong decline in RRR, very small uncertainties at ≈1-10 keV, followed by a jump showing disconnect between evaluation in low energy and fast energy regions.

2. ^{232}Th: ^{232}Th(n,γ) has uncertainty dip down to $\Delta \approx 1\%$ at ≈10 keV-1 MeV which implies better precision than for ^{197}Au(n,γ) standard; ^{232}Th(n,el) suffers from the uncertainty dip with $\Delta < 1\%$ at ≈5-100 keV which would put it on the level of (n,el) standard; there is discontinuity between RRR-URR-fast uncertainties, each of them being evaluated by different party.

3. ^{233}U: ^{233}U(n,el) shows strong decline in RRR, followed by strong dip of uncertainties down to ≈0.2% at URR energy of 0.6 keV-40 keV. These very small uncertainties are suspect, as they would make this cross section as precise as the ^{1}H(n,el) standard; ^{233}U(n,f) also suffers from an uncertainty jump at URR indicating disconnect in evaluation by two different parties, which propagate into (n,el) URR dip.

4. ^{235}U: ^{235}U(n,fis) has a strong uncertainty peak at about 1-3 keV that is missing in the evaluation of standards cross sections. This issue should be clarified and requires discussion between LANL-ORNL evaluators and standards evaluators.

5. ^{241}Pu: $\bar{\nu}$ has unrealistically low uncertainties of 0.3-0.5%, which are better or comparable to $\bar{\nu}$ of ^{239}Pu.

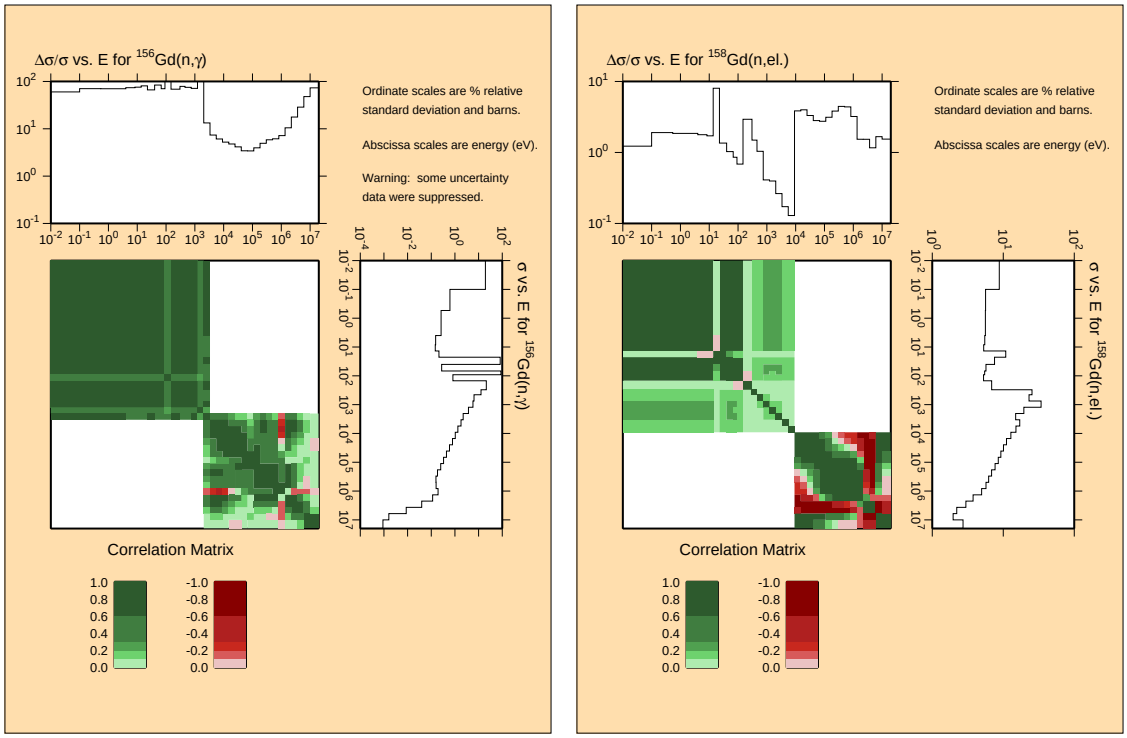

Figure 3.2: Trouble in ^{156}Gd(n,γ) and ^{158}Gd(n,el). See text for explanation.

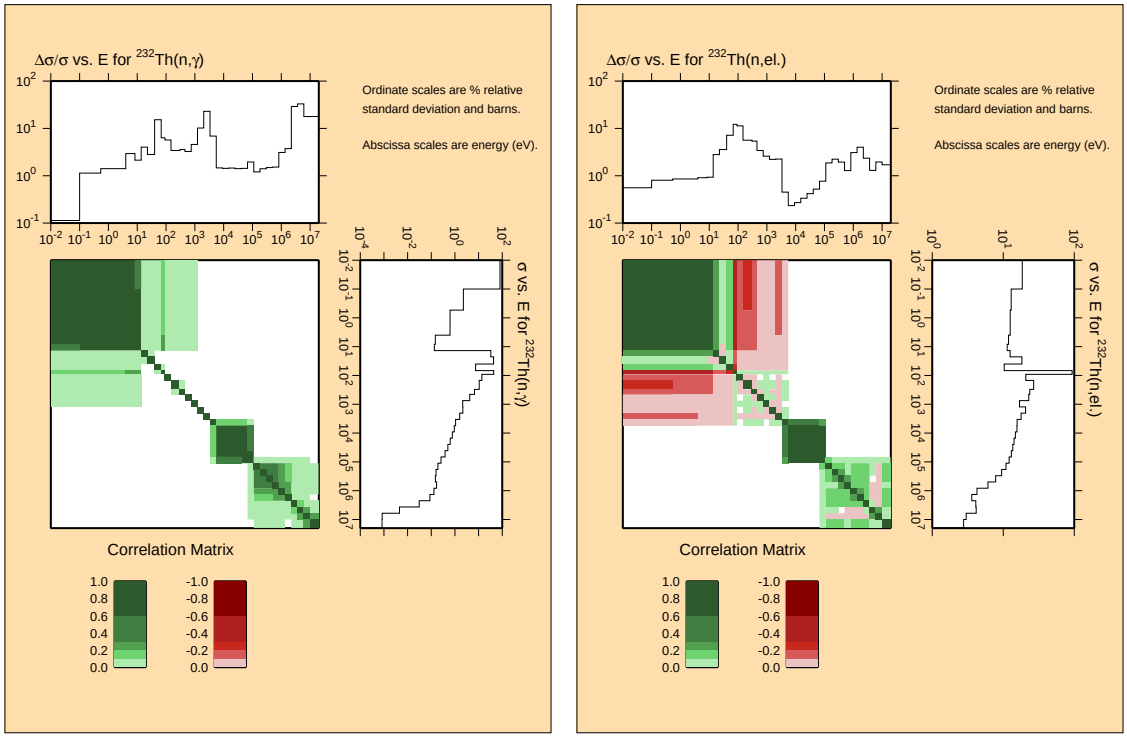

Figure 3.3: Trouble in ^{232}Th(n,γ) and (n,el). See text for explanation.

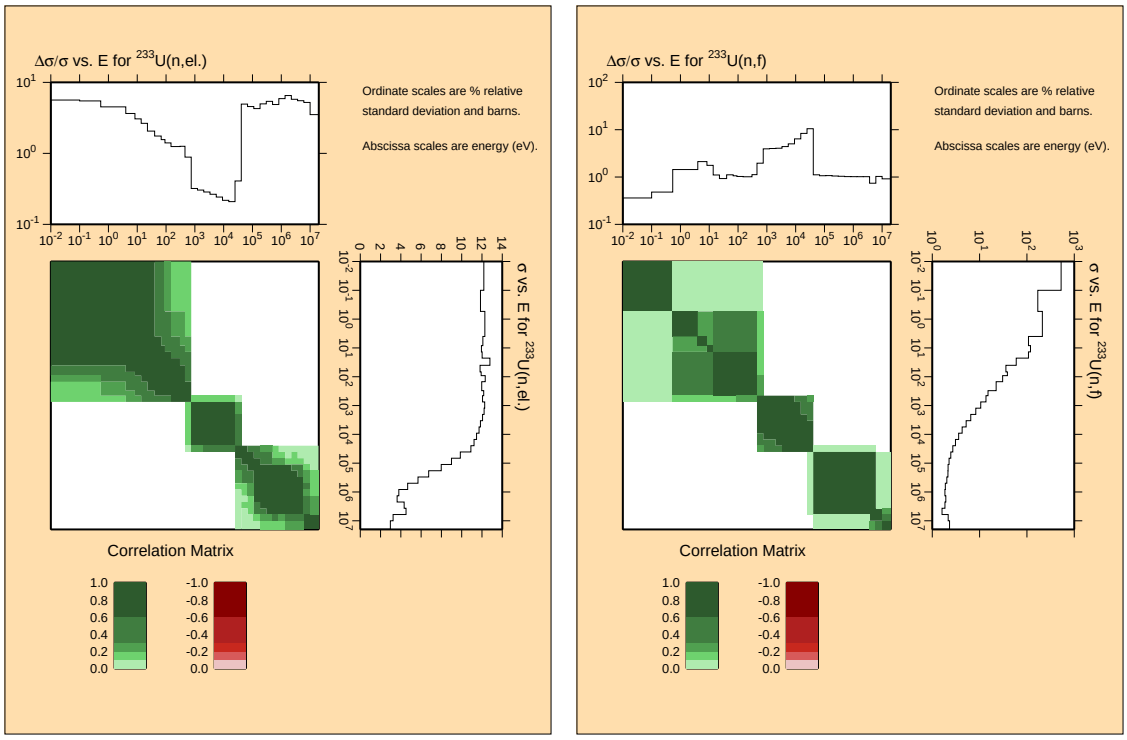

Figure 3.4: Trouble in ^{233}U(n,el) and (n,fis). See text for explanation.

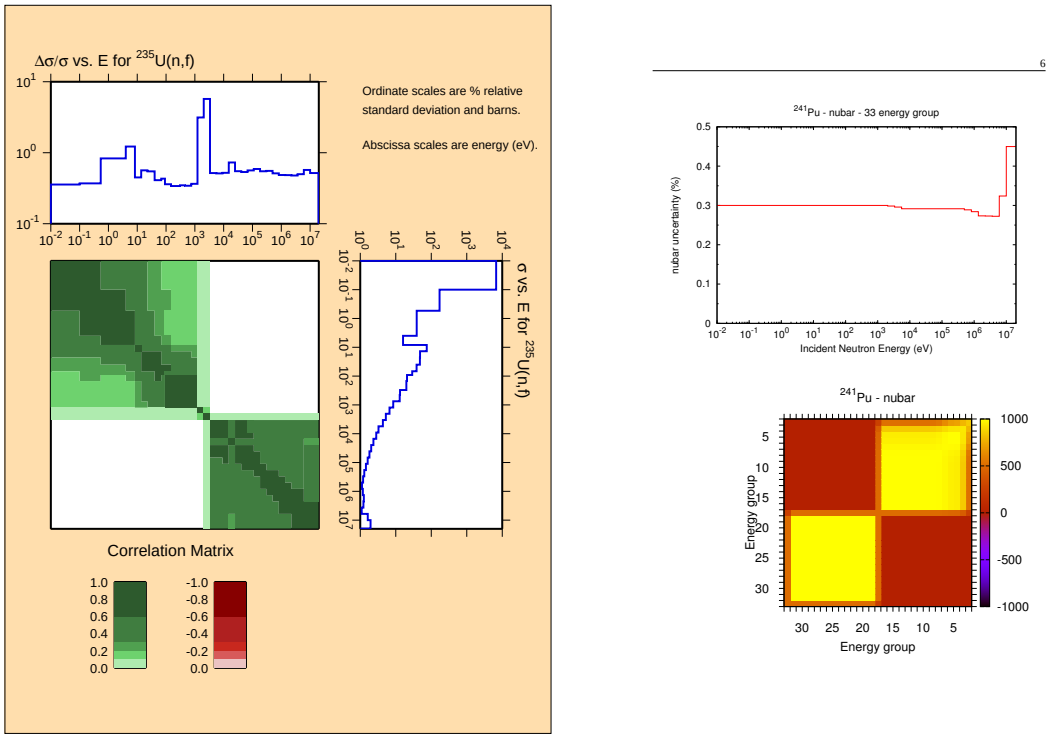

Figure 3.5: Trouble in ^{235}U(n,fis) and ^{241}Pu $\bar{\nu}$. See text for explanation.

Chapter 4

Conclusions

The AFCI-1.2 covariance library contains much improved data compared to the initial set of starter files collected in FY2008. This library represents a solid step towards producing robust covariance information for AFCI applications.

One of the most important issues that needs to be addressed is the quality of covariance data. Development of adequate QA procedures and tools is an issue of key importance. This development has already started as described in the present report, but more needs to be done in the future.

Anticipated goal for FY2010 is to produce AFCI-2 covariance library that would represent the final product of the current effort. A more specific to-do-list for FY2010 includes the following tasks:

BNL

- BNL intends to develop robust QA system. Such a system would include checking code to identify deficiencies in the 33-group library, visual inspection of covariance files (plots) and cross comparison with other sources of information.
- We further plan to perform careful review priority structural materials (Cr, Fe and Ni isotopes). Once the review would be completed we will proceed with addressing the deficiencies and producing more robust and consistent set of covariances for these materials.
- Finally we intend to produce improved data for other structural materials and fission products. To this end we would use refined methodlogy procedures as built-in in the latest version of the covariance module in Empire.

LANL

- In FY2010, LANL will focus on developing more robust and faithful uncertainty quantification tools, which will be integrated seamlessly in the LANL evaluation toolkit. This task is very important to assess realistic uncertainties and correlations associated to evaluated data libraries. The quality of the resulting covariance matrices will be

tested through relatively simple transport simulations to ensure consistency with clean integral measurements.

- LANL will also develop UQ methods to evaluate uncertainties for the average prompt fission neutron multiplicity and spectrum simultaneously. It is of particular importance in the case only one type of data is available (e.g., ^{240}Pu). Some preliminary work to assess more representative experimental data covariance matrices will be performed.

- This work will be extend to other actinides and light nuclei, which are of priority to the AFCI program.

Bibliography

[1] P. Obložinský et al., "Covariance Nuclear Data for 65 Priority Materials (M2 FY2008 Report for GNEP)," Tech. Rep. unpublished, BNL-LANL, 2008.

[2] M. Herman et al., "Development of Covariance Capabilities in EMPIRE code," Nuclear Data Sheets, vol. 109, p. 2752, 2008.

[3] M. Herman et al., "Covariance Evaluation Methodology for Cross Sections," Tech. Rep. BNL-81623-2008, Brookhaven National Laboratory, 2008.

[4] M. Herman et al., "Nuclear Reaction Model Code System for Data Evaluation," Nuclear Data Sheets, vol. 108, p. 2655, 2007.

[5] S. Mughabghab, Atlas of Neutron Resonances. Elsevier, Amsterdam, 2006.

[6] T. Kawano, "KALMAN code." in Japanese, unpublished, 1997.

[7] R. Arcilla et al., "Processing Neutron Cross Section Covariances using NJOY-99 and PUFF-IV," Nuclear Data Sheets, vol. 109, p. 2910, 2008.

[8] T. Kawano et al., "Evaluation Covariances for Actinides and Light Elements at LANL," Nuclear Data Sheets, vol. 109, p. 2858, 2008.

[9] D. Madland and J. Nix Nucl. Sci. Eng., vol. 81, pp. 213–271, 1982.

[10] R. Capote et al., "RIPL - Reference Input Parameter Library for Calculation of Nuclear Reactions and Nuclear Data Evaluations," Nuclear Data Sheets, vol. 110, pp. in–print, 2009.

[11] H. Derrien et al., "Evaluation of ^{23}Na in the resonance region," tech. rep., International Conference on the Physics of Reactors, Interlaken, Switzerland, 2008.

[12] CSEWG, "ENDF/A - Depository of Candidate Evaluations for the ENDF/B-VII.1 Library." www.nndc.bnl.gov/endfa, 2009.

[13] C. Fu and D. Hetrick, "Update of ENDF/B-V Mod-3 Iron," Tech. Rep. ORNL/TM-9964, Oak Ridge National Laboratory, 1986.

[14] D. Hetrick, D. Larson, and C. Fu, "Generation of Covariance Files for the Isotopes of Cr, Fe, Ni, Cu and Pb in ENDF/B-VI," Tech. Rep. ORNL/TM-11763, Oak Ridge National Laboratory, 1991.

[15] V. Pronyaev, S. Tagesen, H. Vonach, and S. Badikov, "Evaluation of the fast neutron cross sections of ^{52}Cr and ^{56}Fe including complete covariance information," Tech. Rep. Fachinformationszentrum Karlsruhe No.13-8, 1995.

[16] K. Shibata, Y. Nakajima, T. Kawano, S.-Y. Oh, H. Matsunobu, and T. Murata, "Estimation of Covariances for ^{16}O, ^{23}Na, Fe, ^{238}U and ^{239}Pu Neutron Nuclear Data in JENDL-3.2," Tech. Rep. JAERI-Research 97-074, Japan Atomic Energy Research Institute, 1997.

[17] V. Pronyaev, "Assessment of ^{56}Fe evaluation for ROSFOND," Tech. Rep. unpublished, IPPE Obninsk, 2006.

[18] D. Larson et al., "Evaluation of 23Na," tech. rep., Oak Ridge National Laboratory, 1977.

[19] Kenney and Perey, "mubar measurements of 23Na," Tech. Rep. EXFOR entry, Oak Ridge National Laboratory, 1976.

[20] S. Kopecky et al., "Measurements of 23Na(n,el)," Tech. Rep. EXFOR entry, Geel, 1997.

[21] D. Rochman, M. Herman, P. Obložinský, and S. Mughabghab, "Preliminary cross-section covariances for WPEC Subgroup 26," Tech. Rep. BNL-77407-2007-IR, Brookhaven National Laboratory, 2007.

[22] V. Maslov, P. Obložinský, and M. Herman, "Review and Assessment of Neutron Cross Section and Nubar Covariances for Advanced Reactor Systems," Tech. Rep. BNL-81884-2008-IR, Brookhaven National Laboratory, December 2008.

[23] V. Maslov, "Current Inconsistencies in ^{238}Pu, ^{241,243}Am and ^{242}Cm Evaluations and their Impact on Uncertainties," Nuclear Data Sheets, vol. 109, p. 2846, 2008.

[24] P. Talou et al. to be submitted.

[25] P. Staples et al. Nucl. Phys., vol. A591, pp. 46–60, 1995.

[26] Knitter Atomenergie, vol. 26, p. 76, 1975.

[27] H. Vonach, S. Tagesen, M. Wagner, and V. Pronyaev, "Evaluation of the fast neutron cross sections of ^{56}Fe including complete covariance information," Tech. Rep. Fachinformationszentrum Karlsruhe No.13-7, 1992.

Appendix A

AFCI-1.2 covariances

A.1 Contents of the library

The AFCI-1.2 covariance library contains data for the quantities summarized in Table A.1 which are supplied in the 33-energy group representation defined in Table A.2. In terms of ENDF-6 format nomenclature basic covariance data refer to MT = 102, 2, 4, 16 and are given for all materials. Light nuclei may also include charged particle emission such as MT = 22 (nn'α), 24 (n2nα), 103 (np), 104 (nd), 105 (nt), 107 (nα), while actinides always include total fission (MT18) and $\bar{\nu}$ (MT452). The library also includes covariances of the average scattering cosine ($\bar{\mu}$, MT251) and prompt neutron fission spectra.

Table A.1: Covariance data in AFCI-1.2 library for 110 materials, nγ denotes the radiative capture.

Type of materials	Amount	Basic data	Other data
Light nuclei	12	nγ, el, inl, n2n, nchp	
Structural and FPs	78	nγ, el, inl, n2n	$\bar{\mu}$ - ^{23}Na, ^{56}Fe
Actinides	20	nγ, el, inl, n2n, fis, $\bar{\nu}$	fis spectra - ^{239}Pu

Full list of 110 materials can be found in four subsequent tables, with Table A.3 showing 12 light nuclei, Table A.4 and A.5 78 structural materials and fission products, and Table A.6 20 actinides.

Table A.2: 33-energy group structure with bound energies given in eV.

Group	Upper bound	Lower bound	Group	Upper bound	Lower bound
1	1.96E+07	1.00E+07	18	3.35E+03	2.03E+03
2	1.00E+07	6.06E+06	19	2.03E+03	1.23E+03
3	6.06E+06	3.67E+06	20	1.23E+03	7.48E+02
4	3.67E+06	2.23E+06	21	7.48E+02	4.54E+02
5	2.23E+06	1.35E+06	22	4.54E+02	3.04E+02
6	1.35E+06	8.20E+05	23	3.04E+02	1.48E+02
7	8.20E+05	4.97E+05	24	1.48E+02	9.16E+01
8	4.97E+05	3.01E+05	25	9.16E+01	6.79E+01
9	3.01E+05	1.83E+05	26	6.79E+01	4.01E+01
10	1.83E+05	1.11E+05	27	4.01E+01	2.26E+01
11	1.11E+05	6.73E+04	28	2.26E+01	1.37E+01
12	6.73E+04	4.08E+04	29	1.37E+01	8.31E+00
13	4.08E+04	2.47E+04	30	8.31E+00	4.00E+00
14	2.47E+04	1.50E+04	31	4.00E+00	5.40E-01
15	1.50E+04	9.11E+03	32	5.40E-01	1.00E-01
16	9.11E+03	5.53E+03	33	1.00E-01	1.00E-05
17	5.53E+03	3.35E+03			

Table A.3: List of 12 light nuclei, highlighted by red are priority materials. Two materials have natural abundance $< 3\%$.

No.	No.	Z	Isotope	Abundance	Source of covariances
1	1	1	^{1}H	99.99%	R-matrix, LANL 2008
2	2		^{2}H	0.01%	Estimate, LANL
3	3	2	^{4}He	100%	Estimate, LANL
4	4	3	^{6}Li	7.6%	R-matrix, LANL 2008
5	5		^{7}Li	92.4%	ENDF/B-VII.0, R-matrix
6	6	4	^{9}Be	100%	Estimate, LANL
7	7	5	^{10}B	19.8%	R-matrix, LANL 2008
8	8		^{11}B	80.2%	Estimate, LANL
9	9	6	^{12}C	99.9%	Estimate, LANL
10	10	7	^{15}N	0.4%	Estimate, LANL
11	11	8	^{16}O	99.9%	R-matrix, LANL, under completion
12	12	9	^{19}F	100%	Estimate, LANL

Table A.4: List of the first part of 78 structural materials and fission products, highlighted by red are priority materials. Nine materials have natural abundance < 3% or are radioactive.

No.	No.	Z	Isotope	Abundance	Source of covariances
13	1	11	^{23}Na	100%	Estimate, BNL, new eval underway
14	2	12	^{24}Mg	79%	Estimate, BNL, revisited 2009
15	3		^{25}Mg	10%	Estimate, BNL, revisited 2009
16	4		^{26}Mg	11%	Estimate, BNL, revisited 2009
17	5	13	^{27}Al	100%	Estimate, BNL, revisited 2009
18	6	14	^{28}Si	92%	Estimate, BNL, revisited 2009
19	7		^{29}Si	4.7%	Estimate, BNL, revisited 2009
20	8		^{30}Si	3.1%	Estimate, BNL, revisited 2009
21	9	24	^{50}Cr	4.3%	Estimate, BNL modified
22	10		^{52}Cr	84%	Estimate, BNL modified
23	11		^{53}Cr	9.5%	Estimate, BNL modified
24	12	25	^{55}Mn	100%	Estimate, BNL, eval underway
25	13	26	^{54}Fe	5.8%	Estimate, BNL modified
26	14		^{56}Fe	92%	BROND-3, BNL modified
27	15		^{57}Fe	2.1%	Estimate, BNL modified
28	16	28	^{58}Ni	66%	Estimate, BNL modified
29	17		^{60}Ni	26%	Estimate, BNL modified
30	18	40	^{90}Zr	51%	Estimate, BNL, revisited 2009
31	19		^{91}Zr	11%	Estimate, BNL, revisited 2009
32	20		^{92}Zr	17%	Estimate, BNL, revisited 2009
33	21		^{93}Zr	1.5x10^{6}y	Estimate, BNL, revisited 2009
34	22		^{94}Zr	17%	Estimate, BNL, revisited 2009
35	23		^{95}Zr	64 d	Estimate, BNL, revisited 2009
36	24		^{96}Zr	2.8%	Estimate, BNL, revisited 2009
37	25	41	^{95}Nb	35 d	Estimate, BNL, revisited 2009
38	26	42	^{92}Mo	15%	Estimate, BNL, revisited 2009
39	27		^{94}Mo	9.2%	Estimate, BNL, revisited 2009
40	28		^{95}Mo	16%	Estimate, BNL, revisited 2009
41	29		^{96}Mo	17%	Estimate, BNL, revisited 2009
42	30		^{97}Mo	9.6%	Estimate, BNL, revisited 2009
43	31		^{98}Mo	24%	Estimate, BNL, revisited 2009
44	32		^{100}Mo	9.6%	Estimate, BNL, revisited 2009
45	33	43	^{99}Tc	2.1x10^{5}y	ENDF/B-VII.0, BNL
46	34	44	^{101}Ru	17%	Estimate, BNL, revisited 2009
47	35		^{102}Ru	32%	Estimate, BNL, revisited 2009
48	36		^{103}Ru	39 d	Estimate, BNL, revisited 2009
49	37		^{104}Ru	19%	Estimate, BNL, revisited 2009
50	38		^{106}Ru	373 d	Estimate, BNL, revisited 2009

Table A.5: List of remaining structural materials and fission products, highlighted by red are priority materials. Eight materials have natural abundance < 3% or are radioactive.

No.	No.	Z	Isotope	Abundance	Source of covariances
51	39	45	^{103}Rh	100%	Estimate, BNL, revisited 2009
52	40	46	^{105}Pd	22%	Estimate, BNL, revisited 2009
53	41		^{106}Pd	27%	Estimate, BNL, revisited 2009
54	42		^{107}Pd	6.5x10^{5}y	Estimate, BNL, revisited 2009
55	43		^{108}Pd	26%	Estimate, BNL, revisited 2009
56	44	47	^{109}Ag	48%	Estimate, BNL, revisited 2009
57	45	53	^{127}I	100%	Estimate, BNL, revisited 2009
58	46		^{129}I	1.6x10^{7}y	Estimate, BNL, revisited 2009
59	47	54	^{131}Xe	21%	Estimate, BNL, revisited 2009
60	48		^{132}Xe	27%	Estimate, BNL, revisited 2009
61	49		^{134}Xe	10%	Estimate, BNL, revisited 2009
62	50	55	^{133}Cs	100%	Estimate, BNL, revisited 2009
63	51		^{135}Cs	2.1 y	Estimate, BNL, revisited 2009
64	52	57	^{139}La	100%	Estimate, BNL, revisited 2009
65	53	58	^{141}Ce	32 d	Estimate, BNL, revisited 2009
66	54	59	^{141}Pr	100%	Estimate, BNL, revisited 2009
67	55	60	^{143}Nd	12%	Estimate, BNL, revisited 2009
68	56		^{145}Nd	8.3%	Estimate, BNL, revisited 2009
69	57		^{146}Nd	17%	Estimate, BNL, revisited 2009
70	58		^{148}Nd	5.7%	Estimate, BNL, revisited 2009
71	59	61	^{147}Pm	2.6 y	Estimate, BNL, revisited 2009
72	60	62	^{149}Sm	14%	Estimate, BNL, revisited 2009
73	61		^{151}Sm	90 y	Estimate, BNL, revisited 2009
74	62		^{152}Sm	27%	Estimate, BNL, revisited 2009
75	63	63	^{153}Eu	52%	Estimate, BNL, revisited 2009
76	64		^{155}Eu	4.7 y	Estimate, BNL, revisited 2009
77	65	64	^{155}Gd	15%	Estimate, BNL, revisited 2009
78	66		^{156}Gd	20%	Estimate, BNL, revisited 2009
79	67		^{157}Gd	16%	Estimate, BNL, revisited 2009
80	68		^{158}Gd	25%	Estimate, BNL, revisited 2009
81	69		^{160}Gd	22%	Estimate, BNL, revisited 2009
82	70	68	^{166}Er	34%	Estimate, BNL, revisited 2009
83	71		^{167}Er	23%	Estimate, BNL, revisited 2009
84	72		^{168}Er	27%	Estimate, BNL, revisited 2009
85	73		^{170}Er	15%	Estimate, BNL, revisited 2009
86	74	82	^{204}Pb	1.4%	Estimate
87	75		^{206}Pb	24%	Estimate
88	76		^{207}Pb	22%	Estimate
89	77		^{208}Pb	52%	Estimate
90	78	83	^{209}Bi	100%	Estimate

Table A.6: List of 20 actinides, highlighted by red are priority materials. Six actinides have natural abundance $< 0.5\%$ or $T_{1/2}$ <100 y.

No.	No.	Z	Isotope	Abundance	Source of covariances
91	1	90	^{232}Th	100%	ENDF/B-VII.0
92	2	92	^{233}U	1.6x10^{6}y	ENDF/A, LANL-ORNL 2008
93	3		^{234}U	0.0054%	BNL-Maslov, revisited 2009
94	4		^{235}U	0.72%	ENDF/A, LANL-ORNL 2008, updated 2009
95	5		^{236}U	2.3x10^{7}y	BNL-Maslov, revisited 2009
96	6		^{238}U	99.27%	ENDF/A, LANL-ORNL 2008
97	7	93	^{237}Np	2.1x10^{7}y	BNL- Maslov, revisited 2009
98	8	94	^{238}Pu	87.7 y	BNL- Maslov, revisited 2009
99	9		^{239}Pu	2.4x10^{4}y	ENDF/A, LANL-ORNL 2008, updated 2009
100	10		^{240}Pu	6.5x10^{3}y	BNL-Maslov, revisited 2009
101	11		^{241}Pu	14 y	BNL-Maslov, revisited 2009
102	12		^{242}Pu	3.7x10^{5}y	BNL-Maslov, revisited 2009
103	13	95	^{241}Am	432 y	BNL-Maslov, revisited 2009
104	14		^{242m}Am	141 y	BNL-Maslov, revisited 2009
105	15		^{243}Am	7.4x10^{3}y	BNL-Maslov, revisited 2009
106	16	96	^{242}Cm	163 d	BNL-Maslov, revisited 2009
107	17		^{243}Cm	29 y	BNL-Maslov, revisited 2009
108	18		^{244}Cm	18 y	BNL-Maslov, revisited 2009
109	19		^{245}Cm	8.5x10^{3}y	BNL-Maslov, revisited 2009
110	20		^{246}Cm	4.8x10^{3}y	ENDF/B-VII.0

A.2 Covariance plots

In the following pages we show a complete set of covariance plots for 110 materials in 33-energy group representation. These plots were generated by the processing code NJOY, except for 14 minor actinides which were handled by another software. The NJOY plots always display uncertainties in %, relative correlation matrices normalized to unity, and also absolute values of cross sections and nubars. These latter quantities were, however, not produced for the minor actinides.

The plots are grouped by isotopes with increasing atomic number Z following the list of materials found in Tables A.3, A.4, A.5 and A.6. In most cases, only the four reaction channels (n,elastic), (n,inelastic), (n,2n) and (n,γ) are shown. Covariances for (n,total fission) and $\bar{\nu}$ (average neutrons emitted per fission) are also given for the actinides. Extra reaction channels may be presented in some cases for light nuclei and for major actinides.

A.2.1 Light nuclei

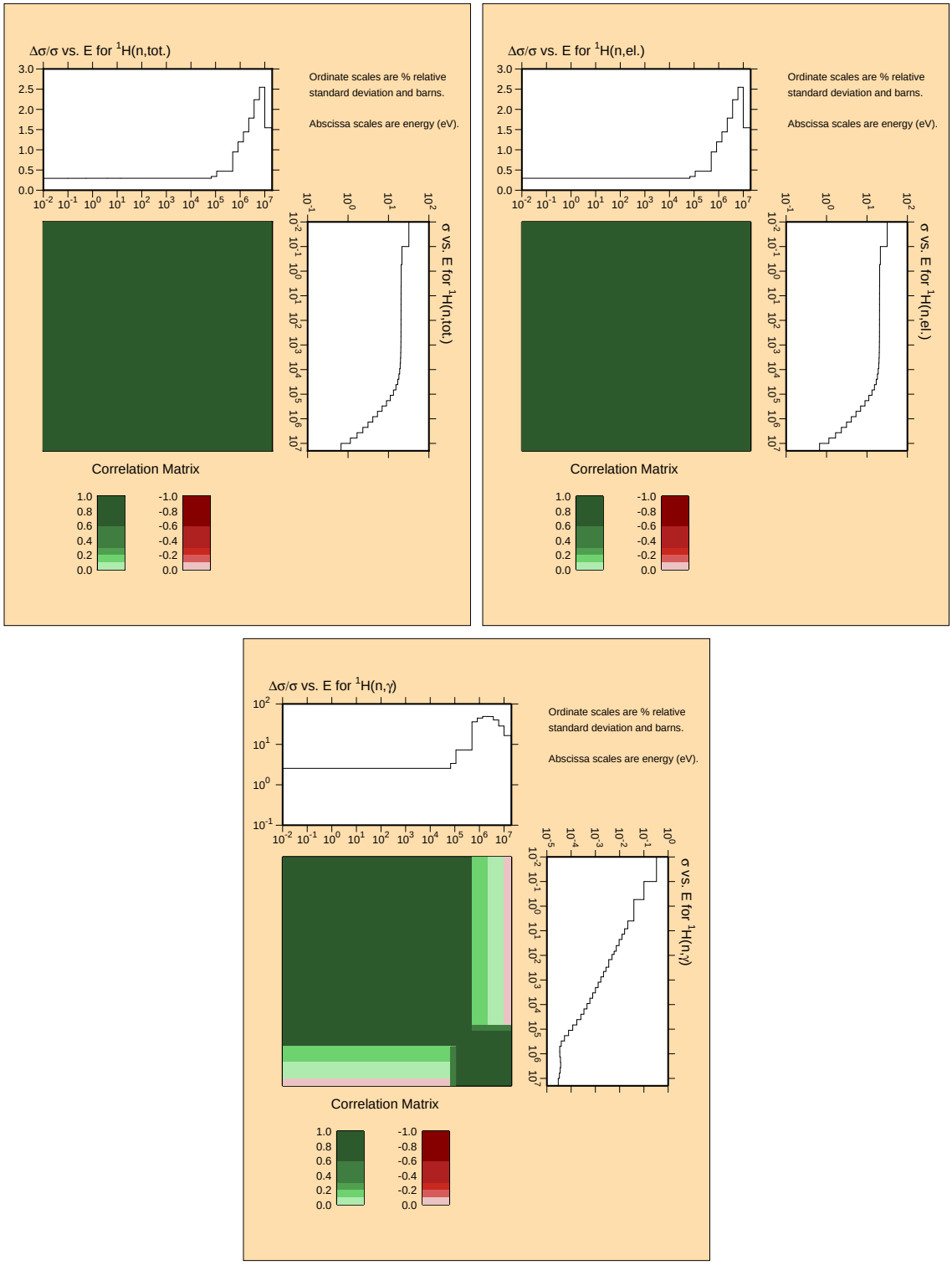

Figure A.1: Covariances for light nucleus ^{1}H

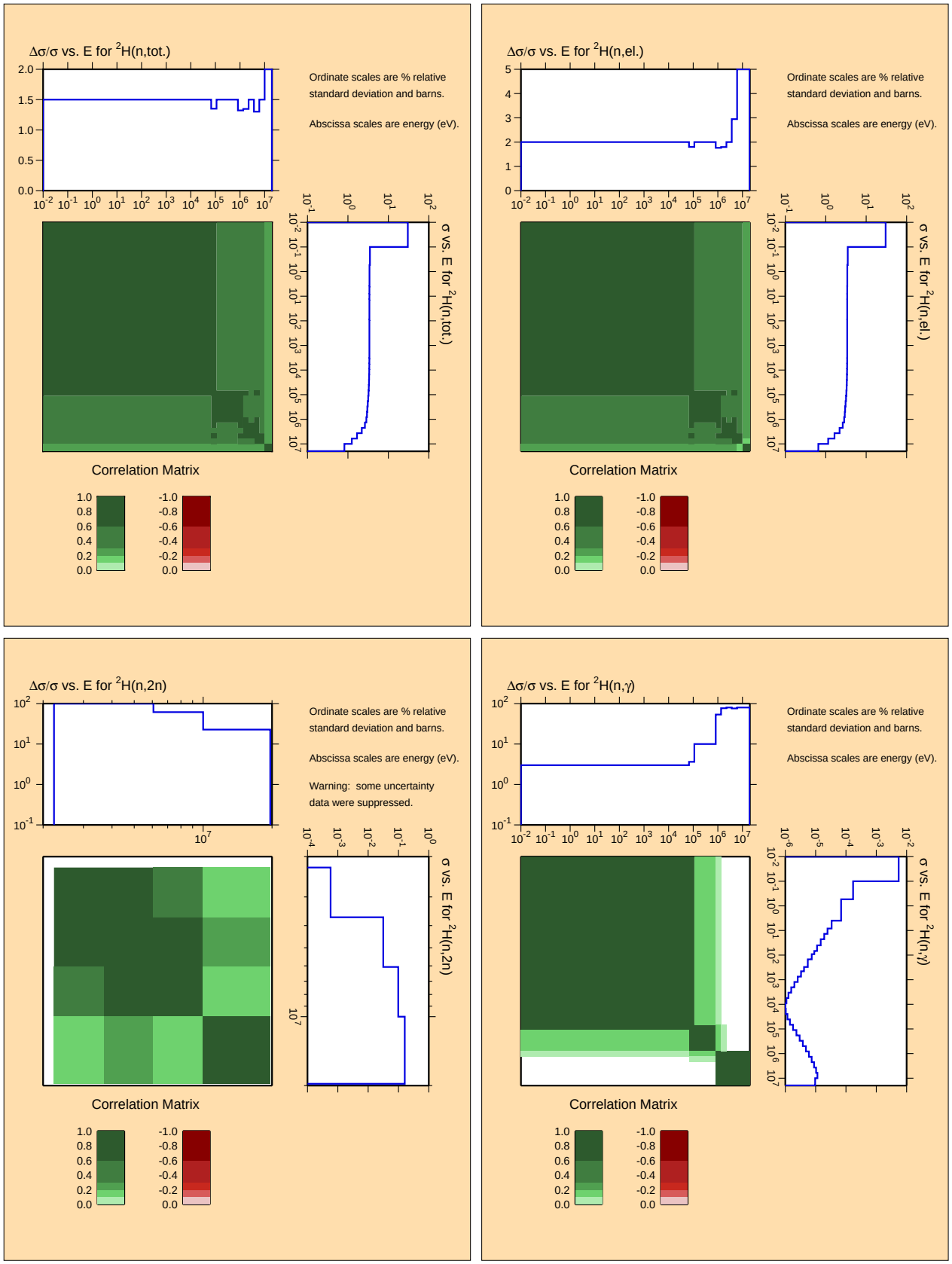

Figure A.2: Covariances for light nucleus ^{2}H.

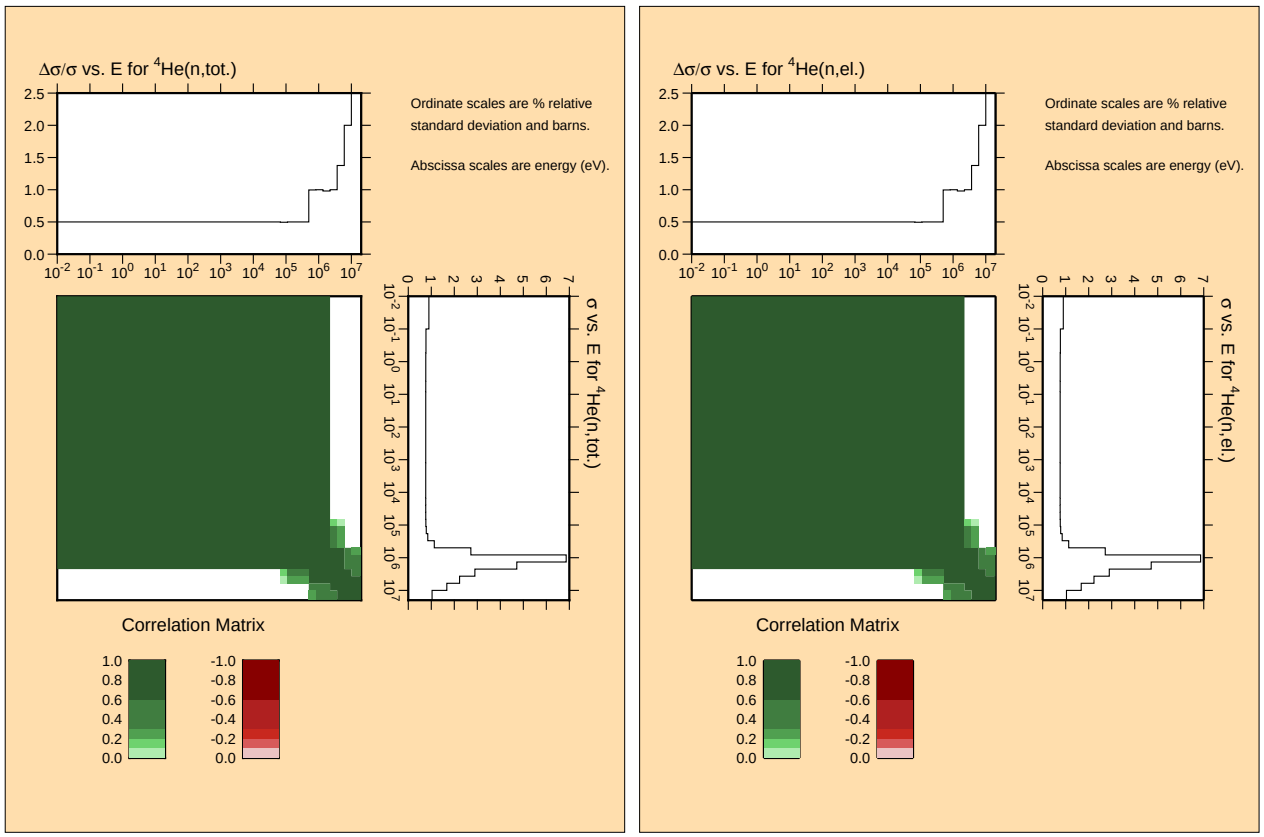

Figure A.3: Covariances for light nucleus ^{4}He.

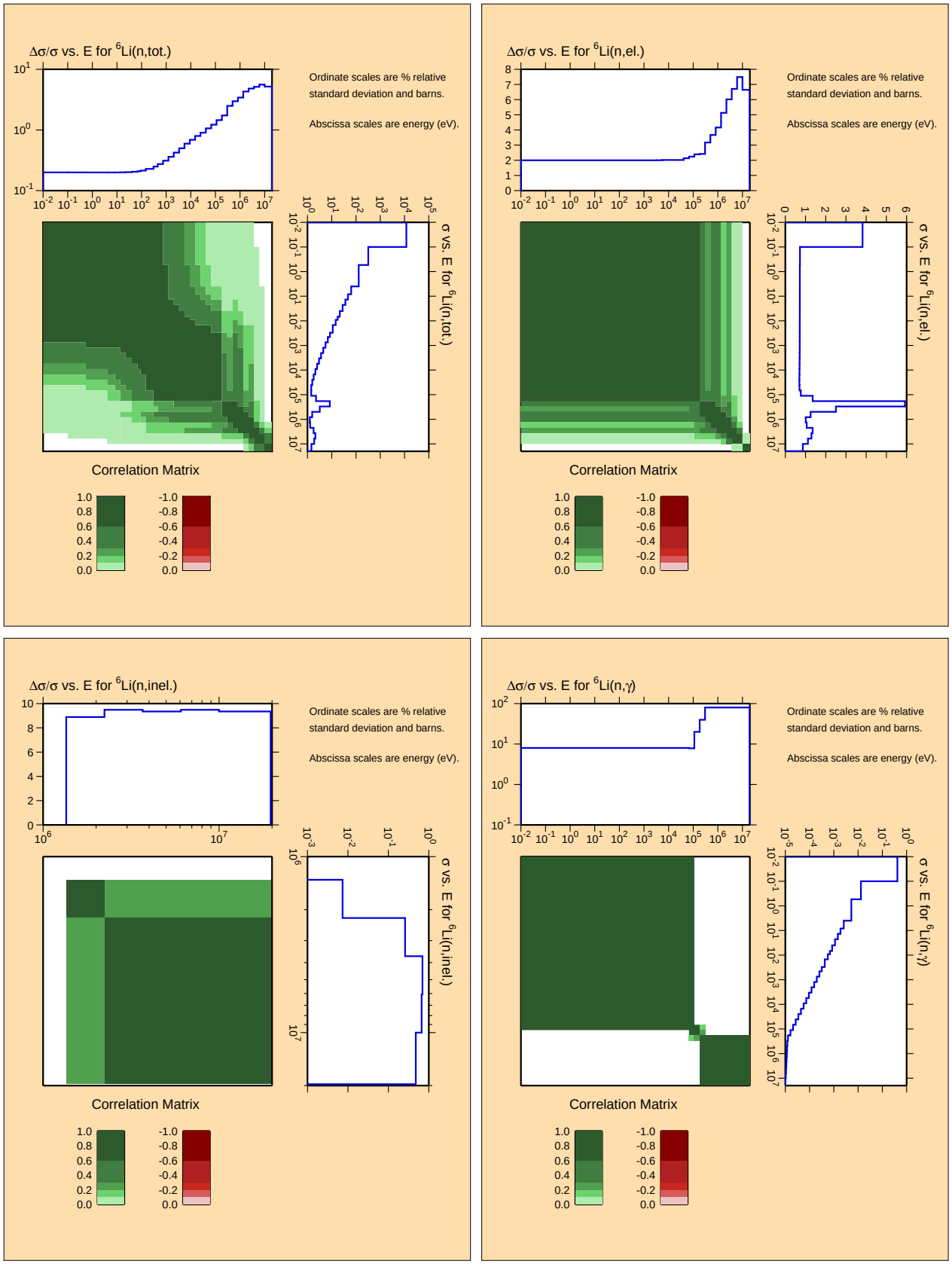

Figure A.4: Covariances for light nucleus ^{6}Li.

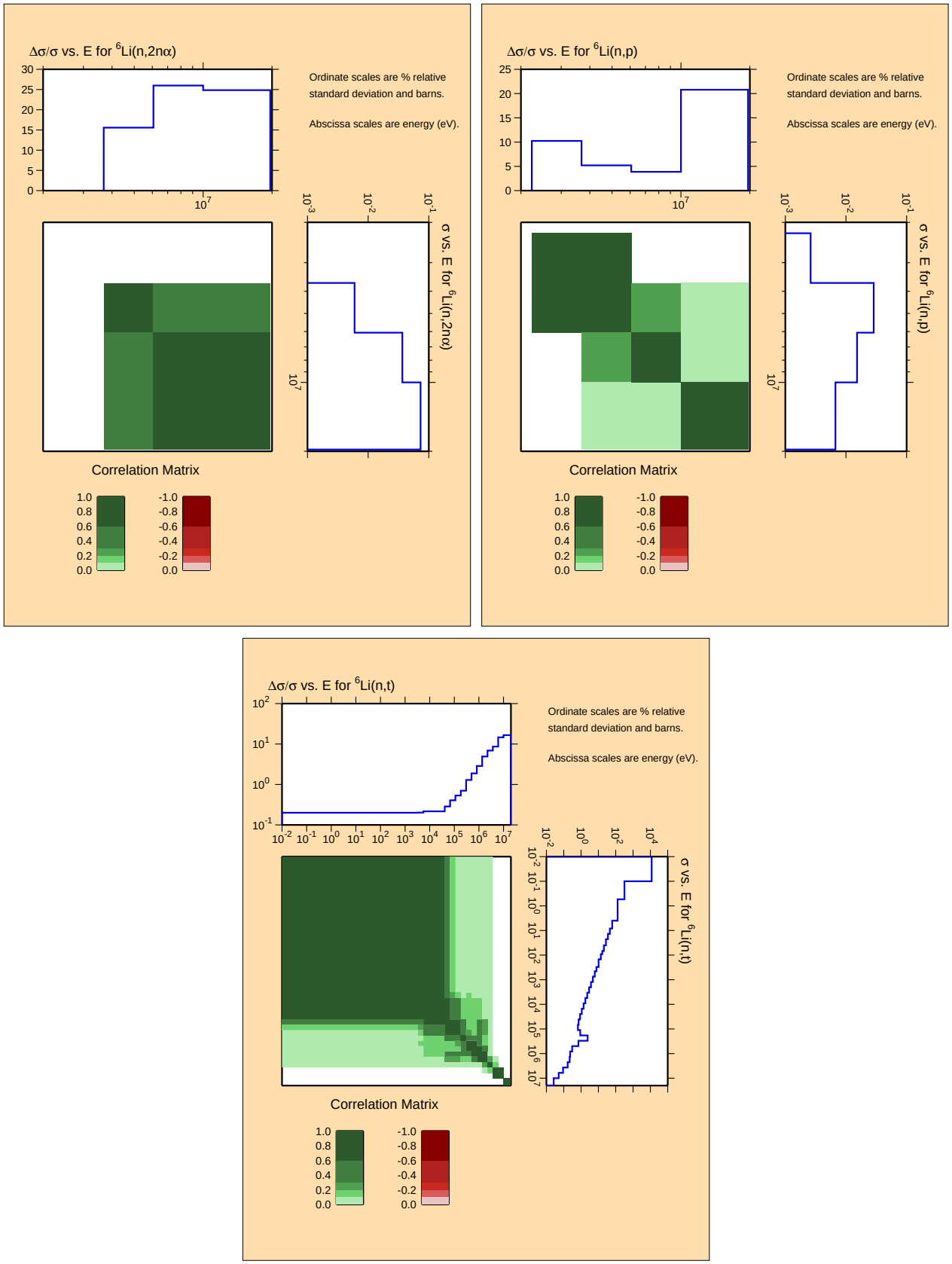

Figure A.4: Covariances for light nucleus ^{6}Li (continued)

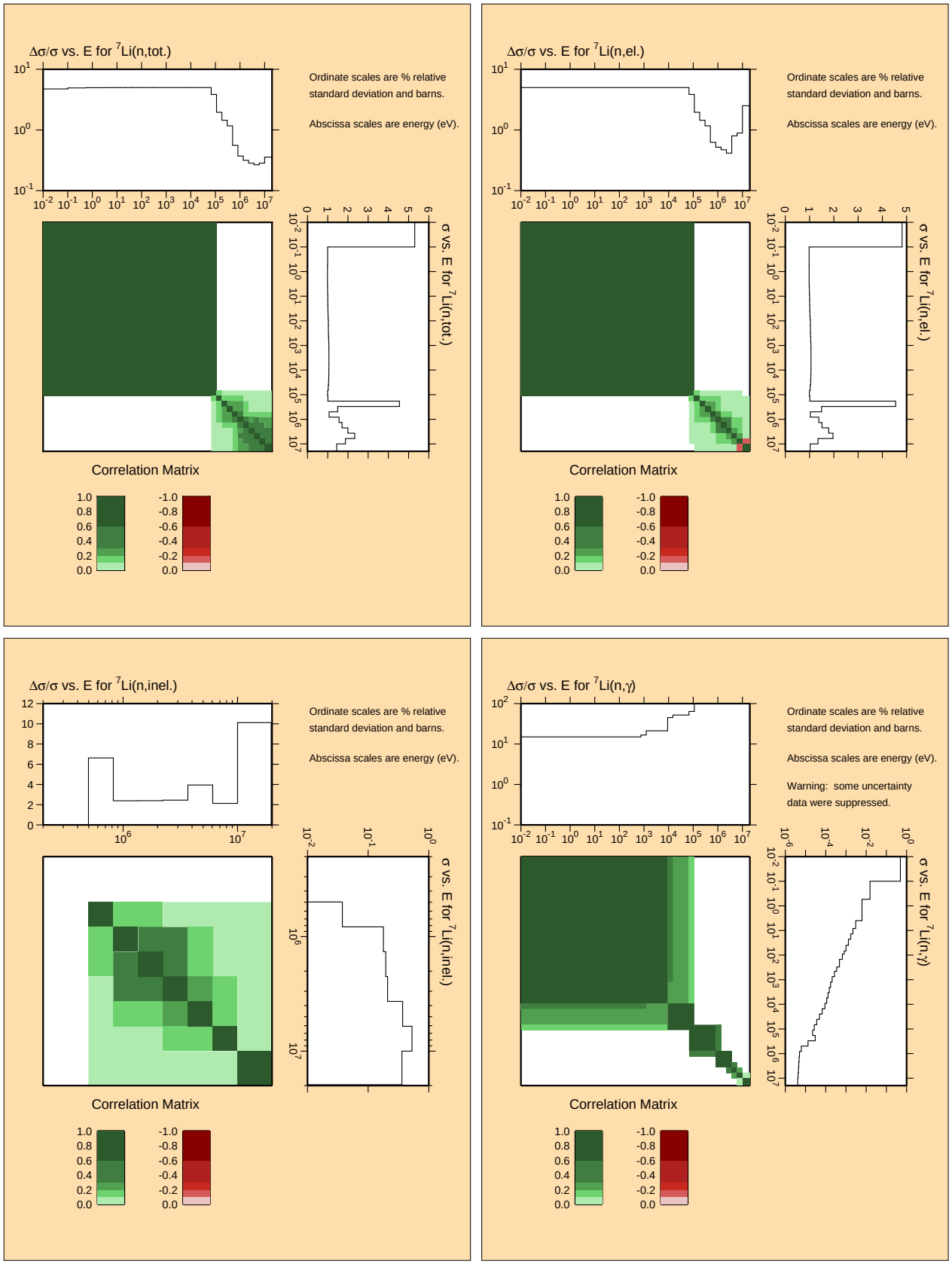

Figure A.5: Covariances for light nucleus ^{7}Li.

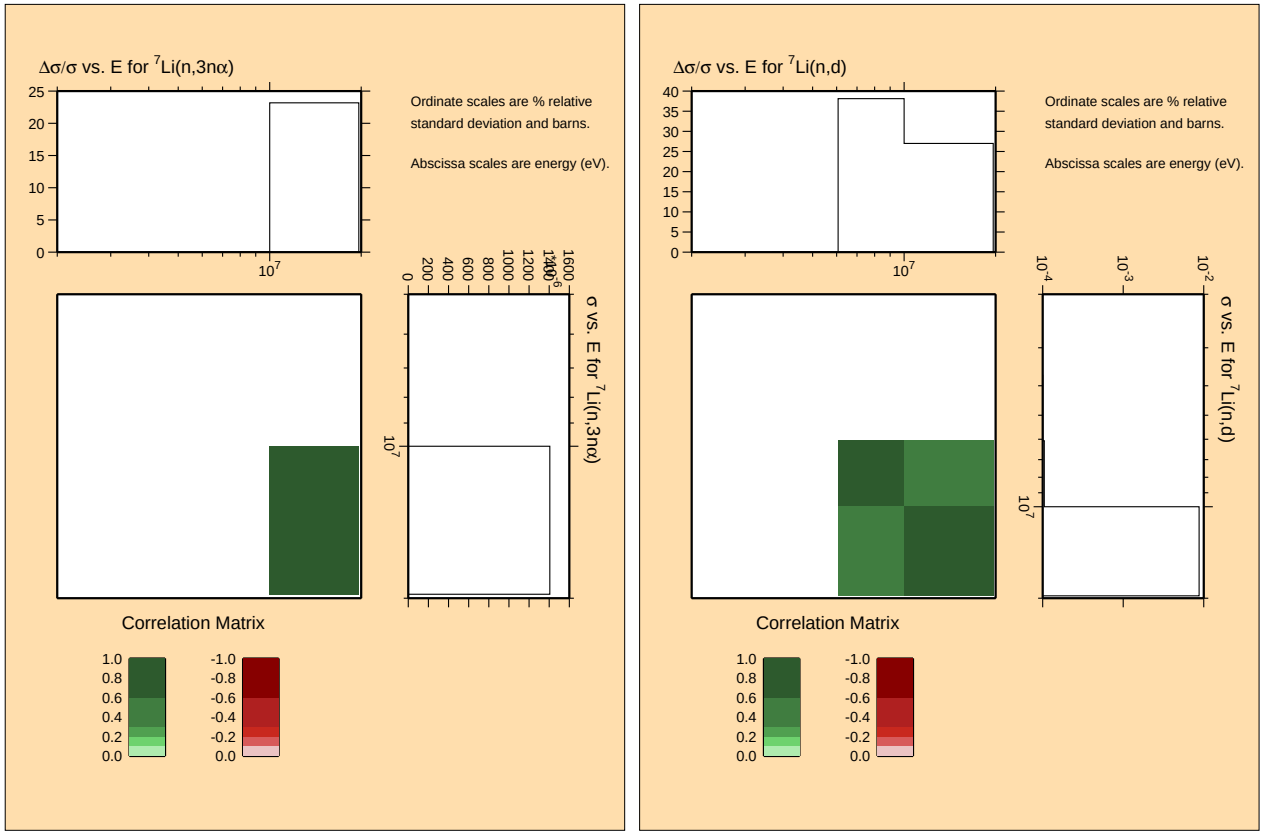

Figure A.5: Covariances for light nucleus ^{7}Li (continued)

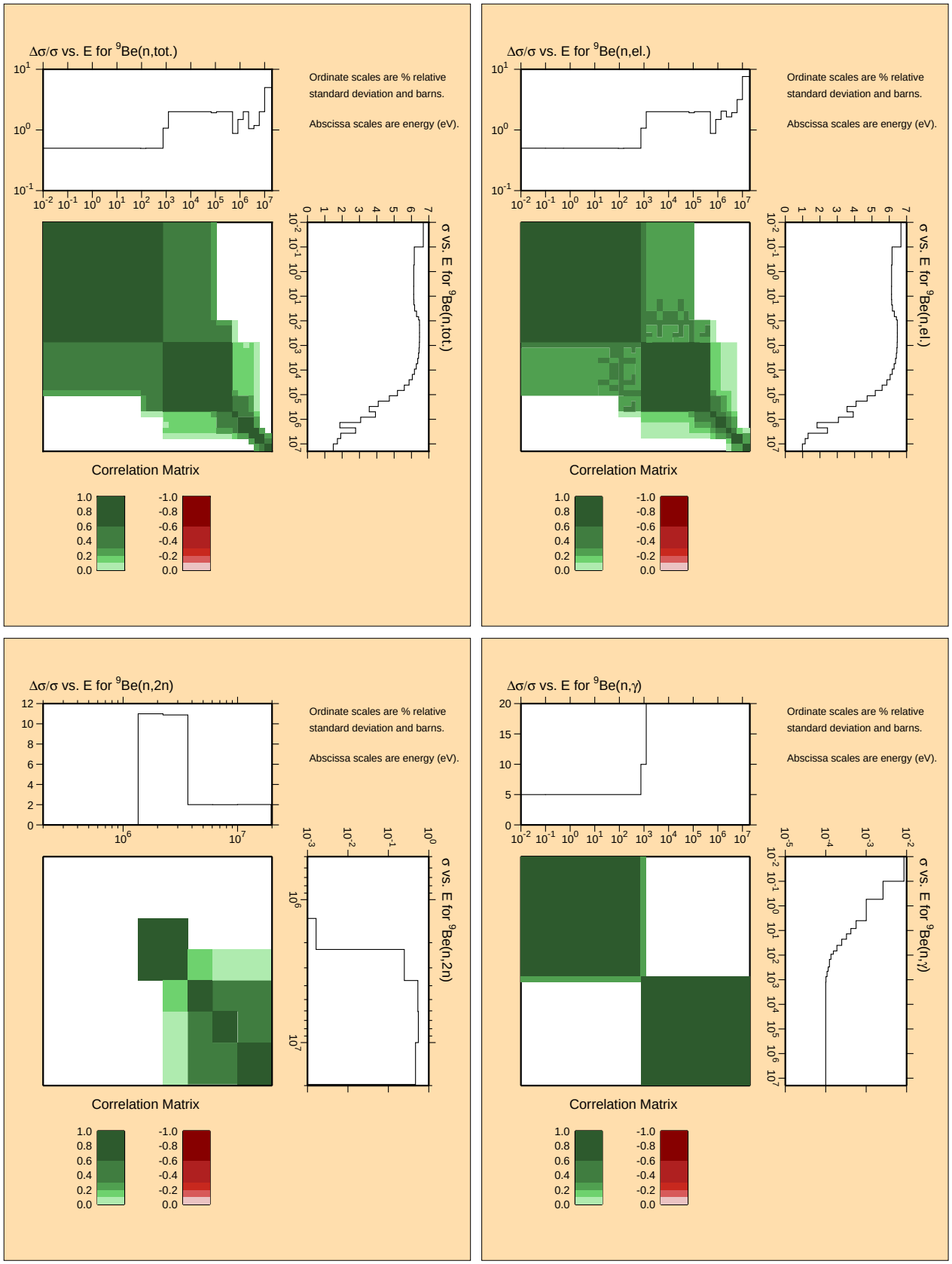

Figure A.6: Covariances for light nucleus ^{9}Be.

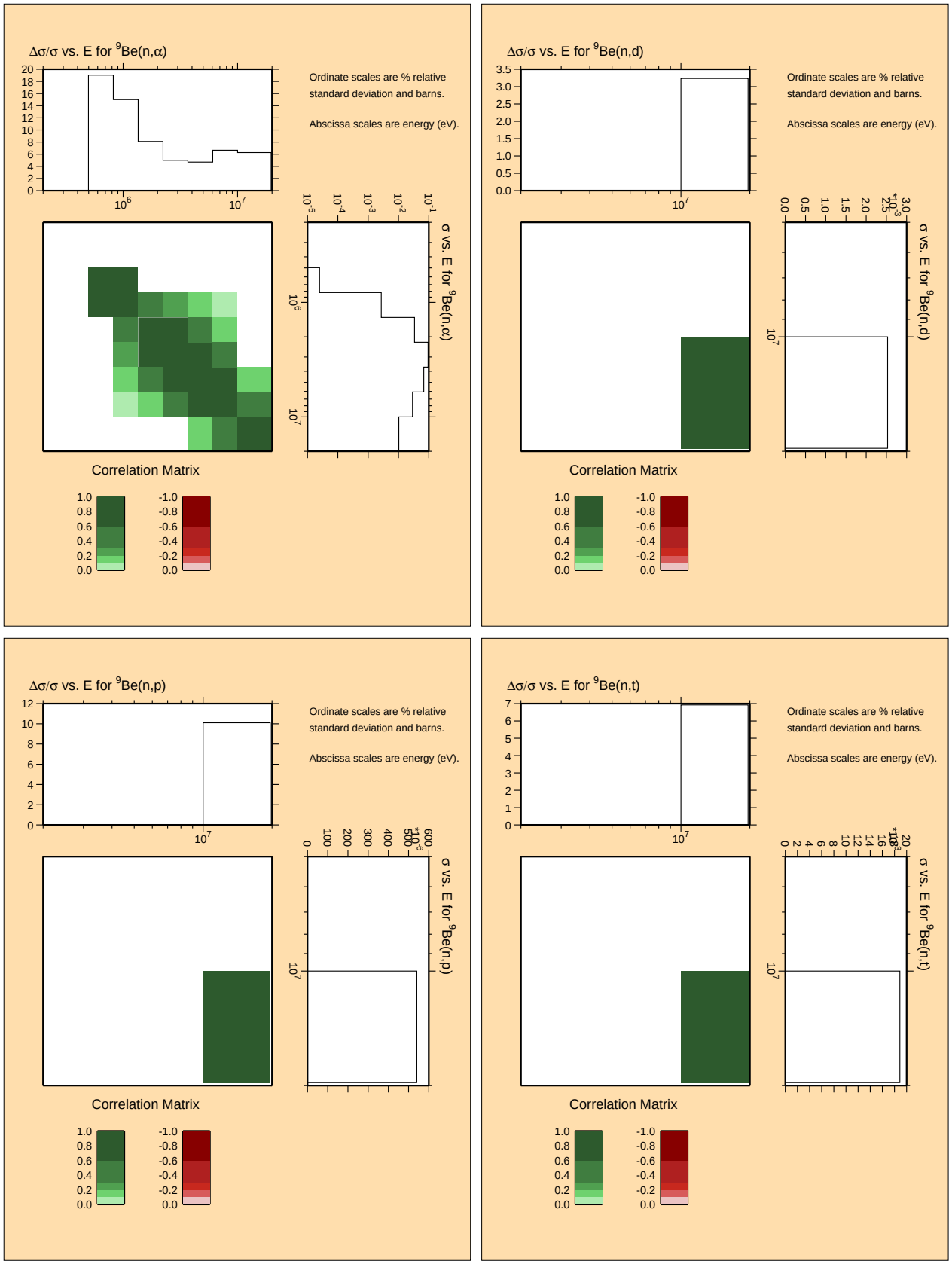

Figure A.6: Covariances for light nucleus ^{9}Be (continued)

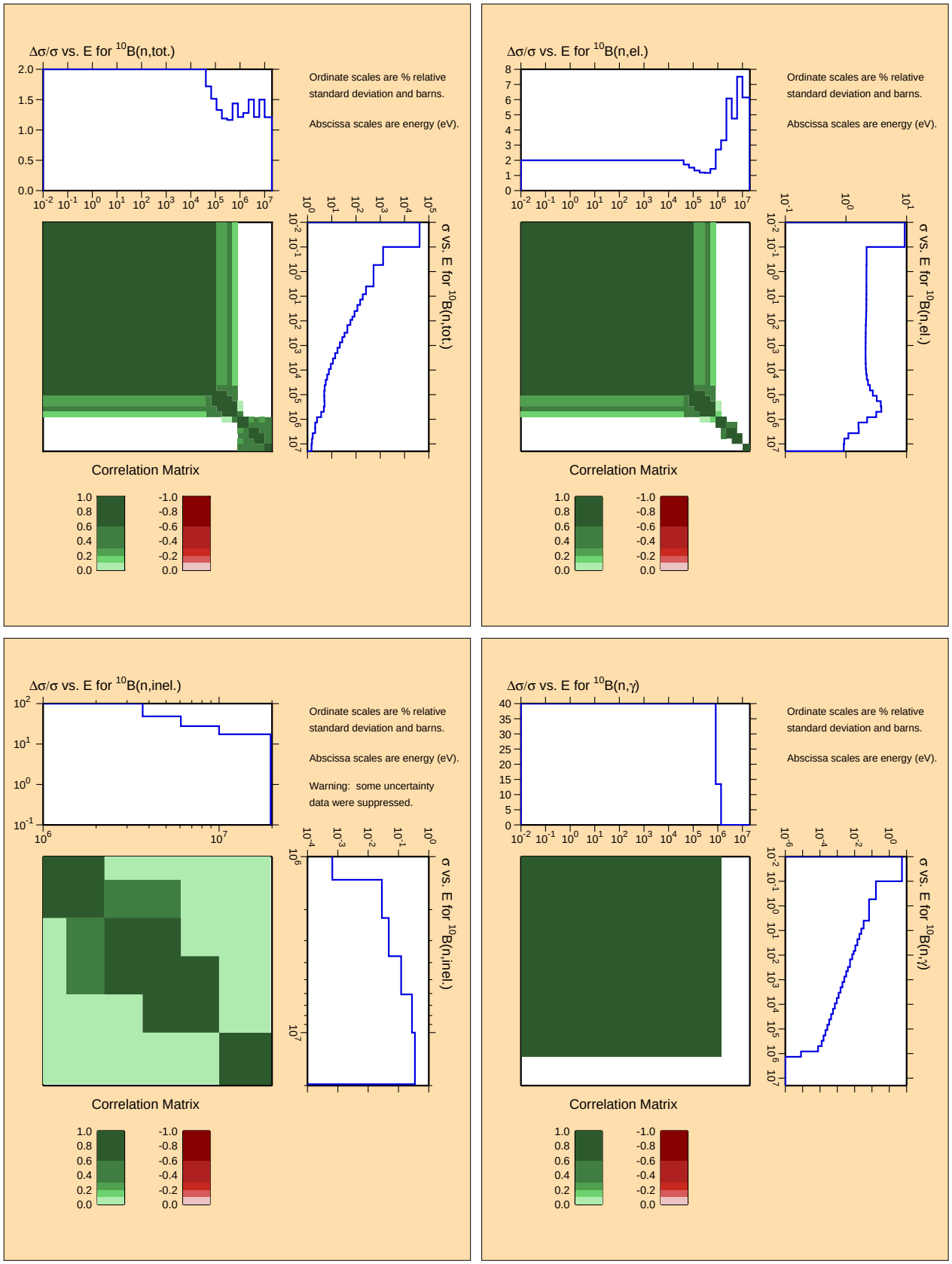

Figure A.7: Covariances for light nucleus ^{10}B.

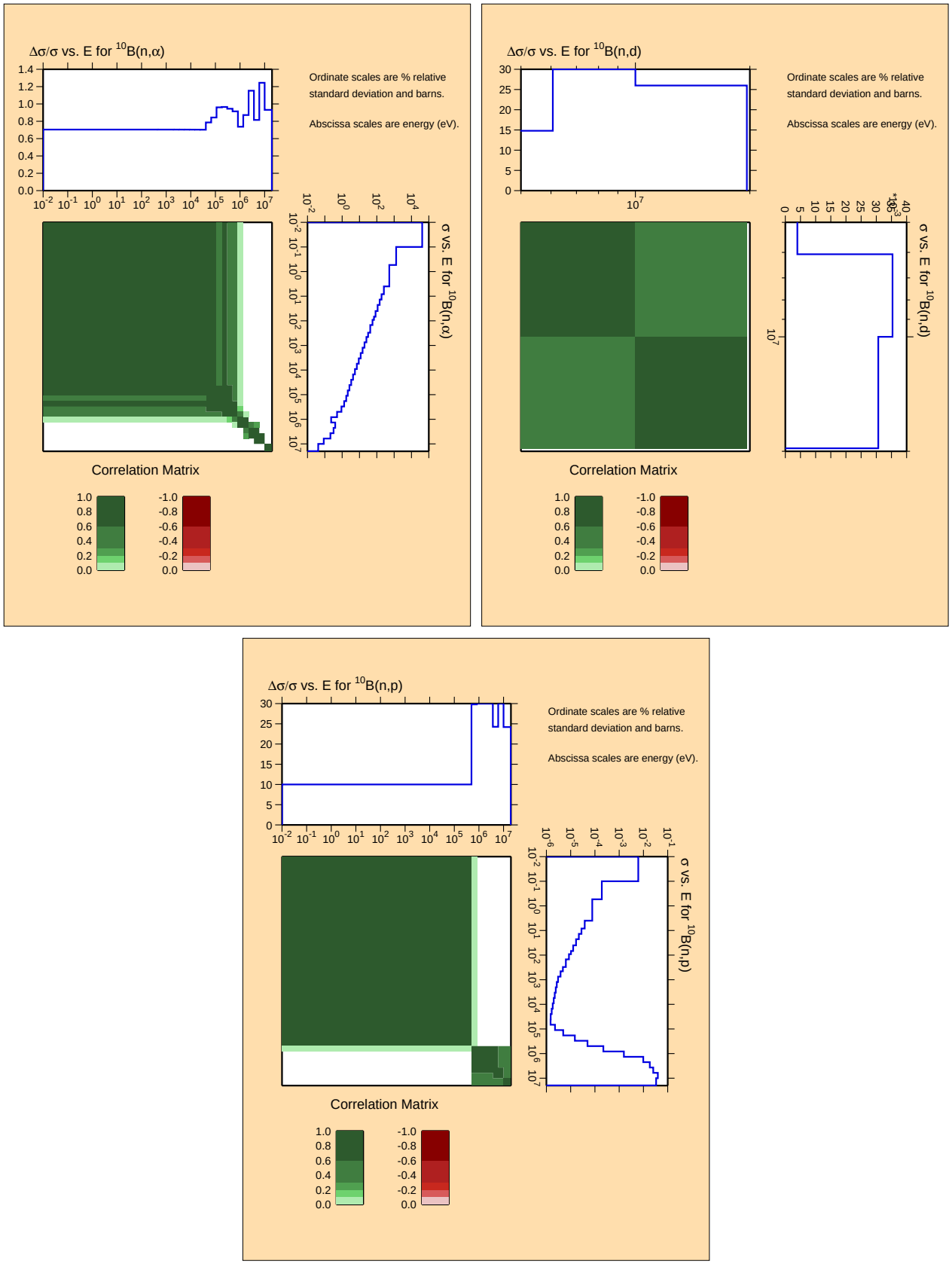

Figure A.7: Covariances for light nucleus ^{10}B (continued)

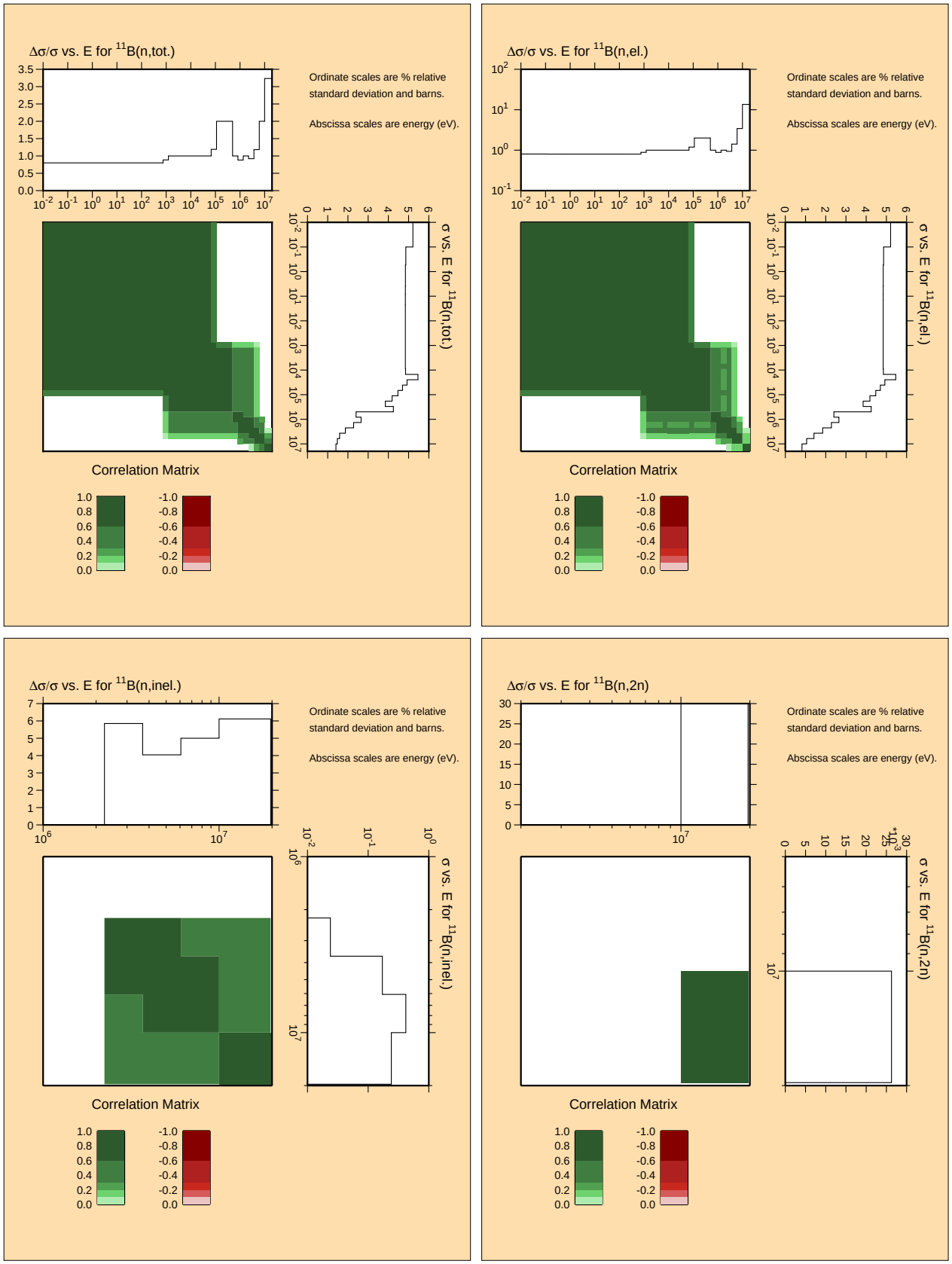

Figure A.8: Covariances for light nucleus ^{11}B.

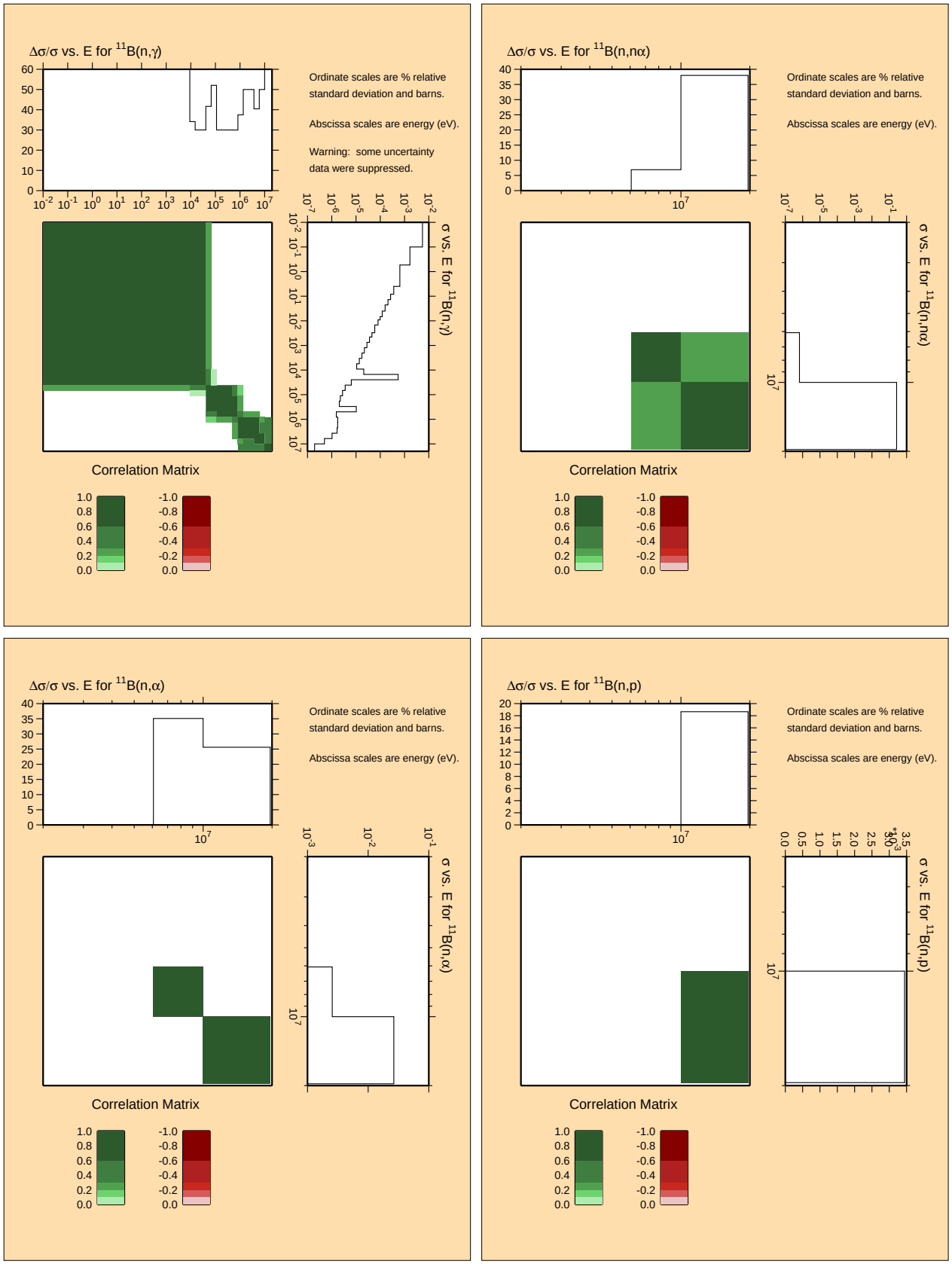

Figure A.8: Covariances for light nucleus ^{11}B (continued)

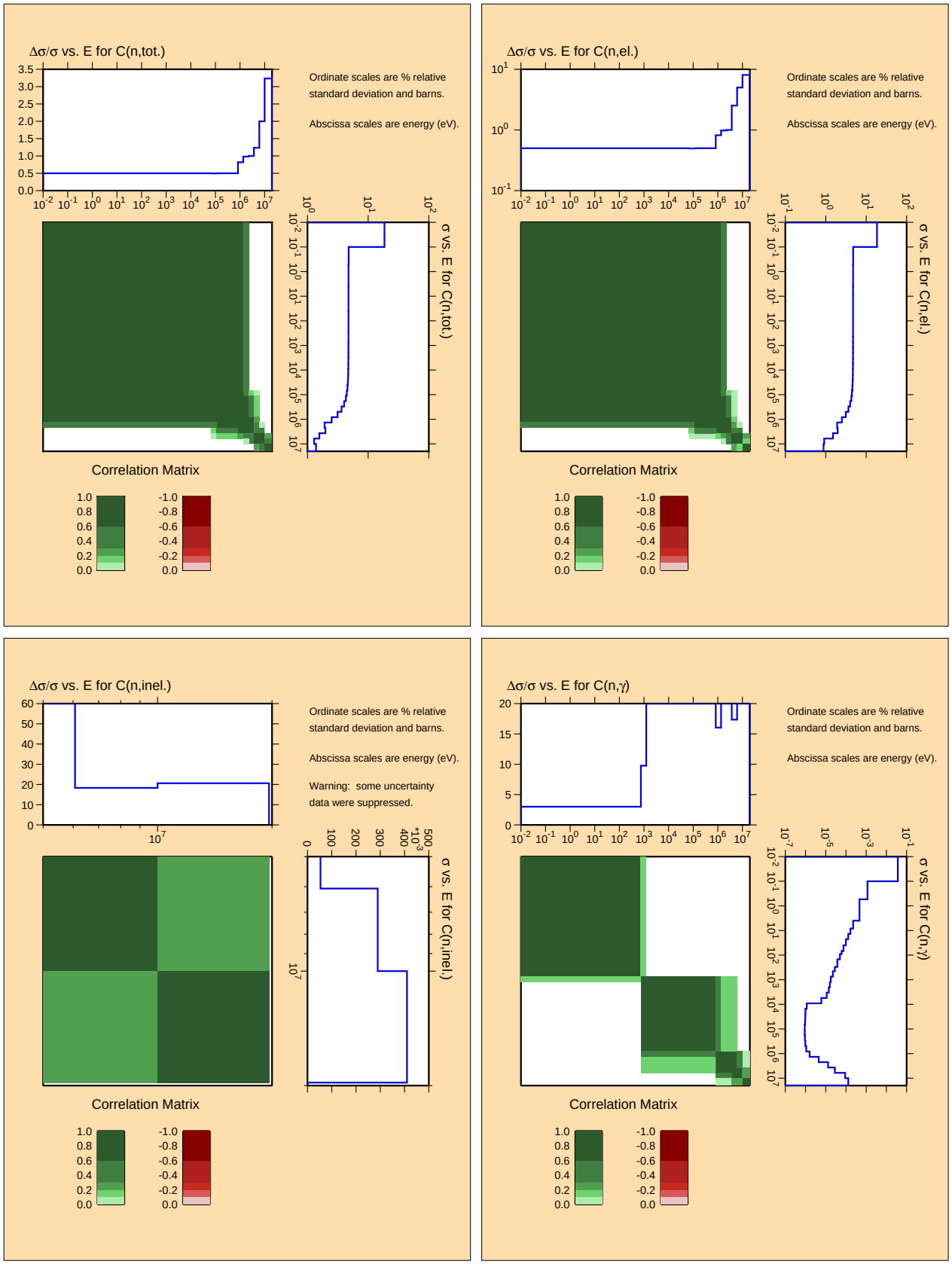

Figure A.9: Covariances for light nucleus ^{12}C.

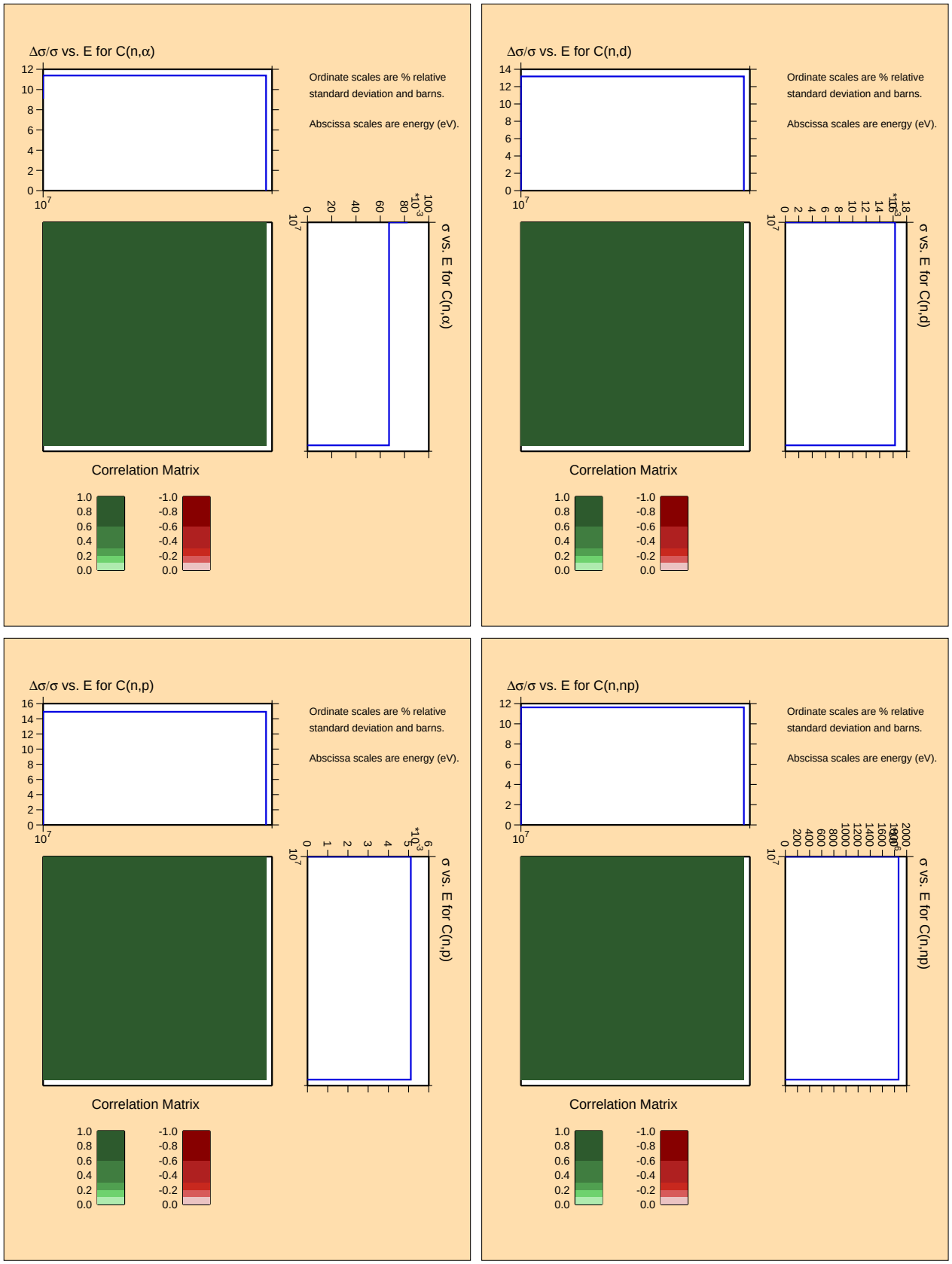

Figure A.9: Covariances for light nucleus ^{12}C (continued)

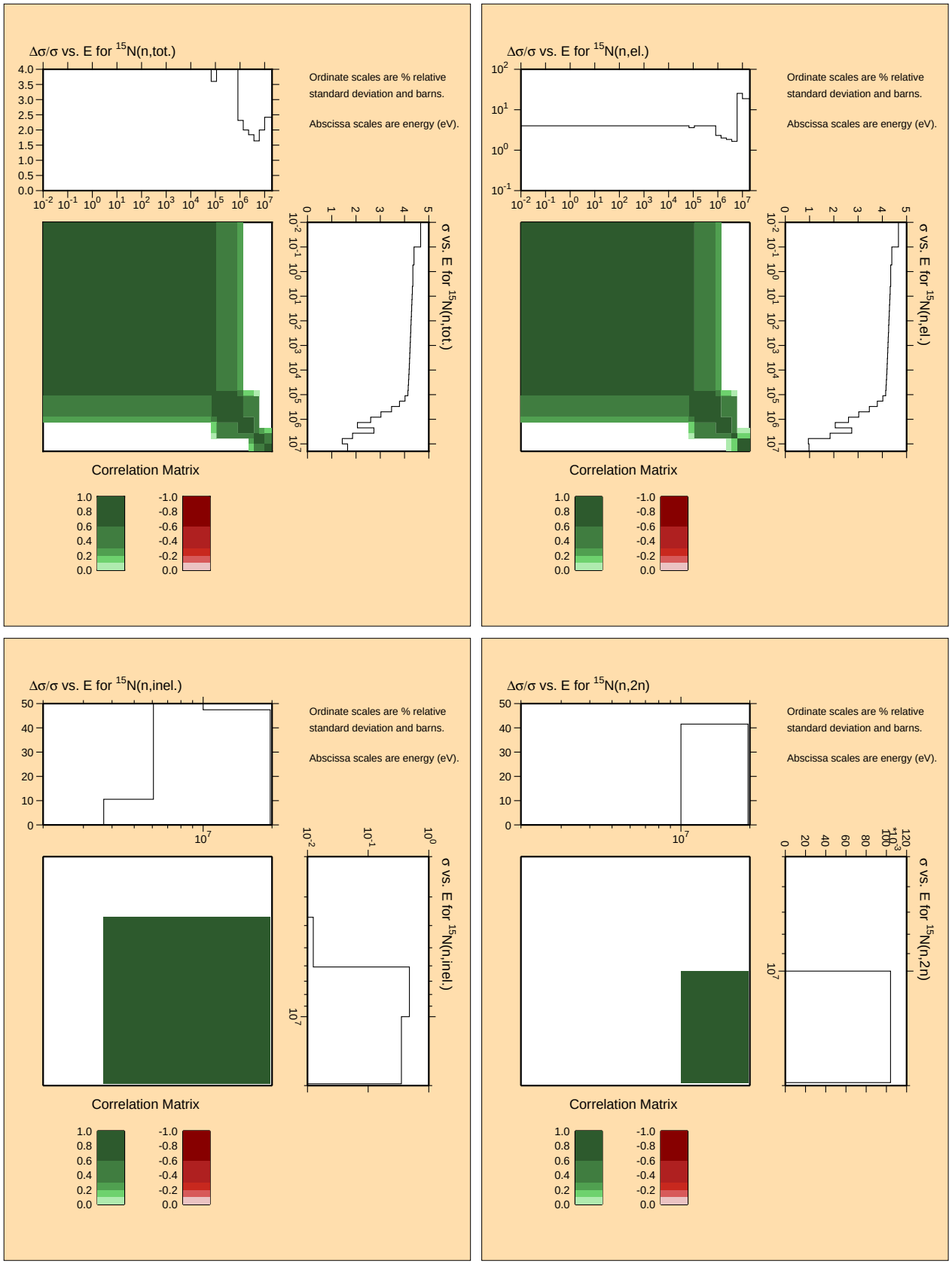

Figure A.10: Covariances for light nucleus ^{15}N.

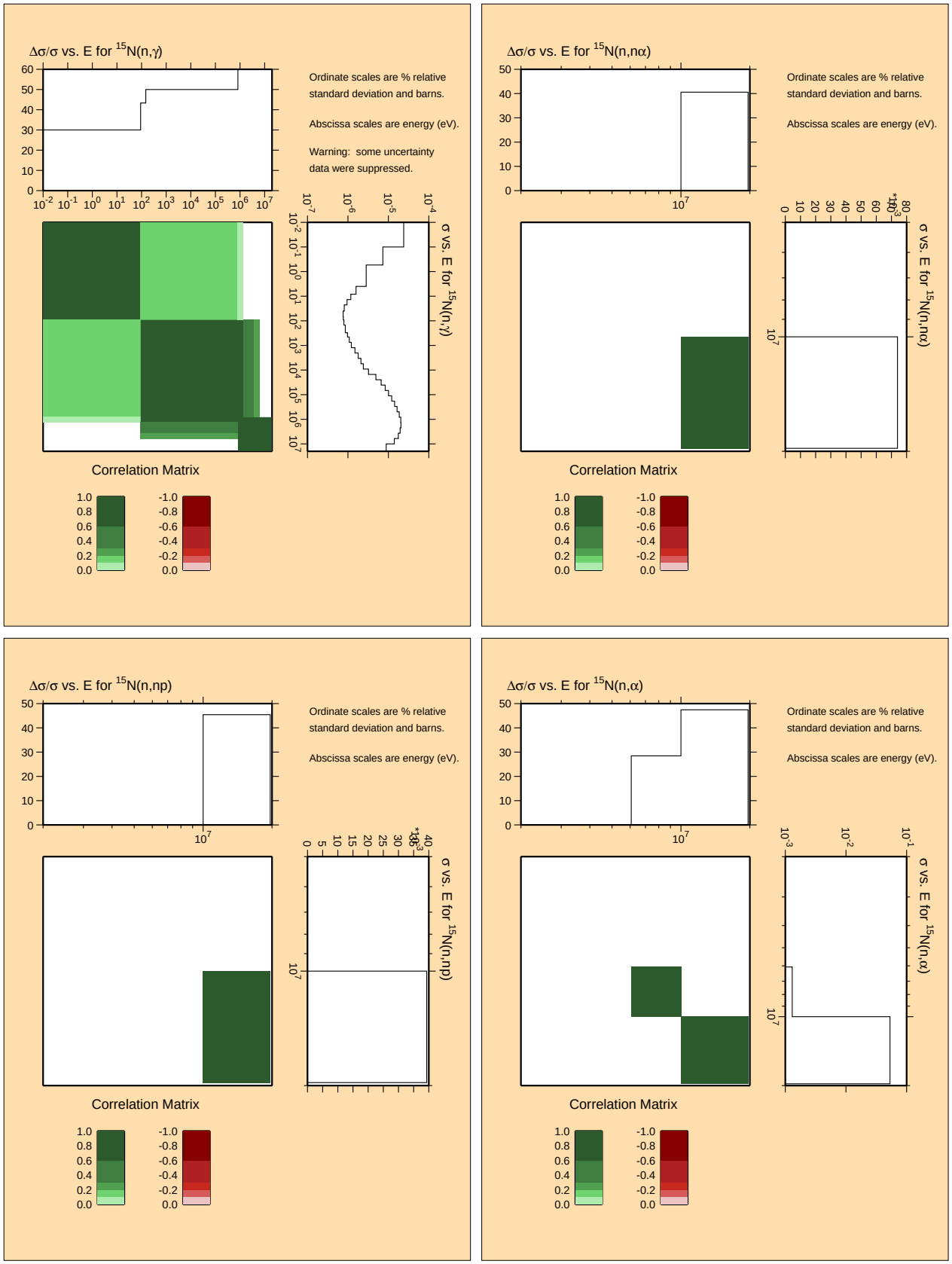

Figure A.10: Covariances for light nucleus ^{15}N (continued)

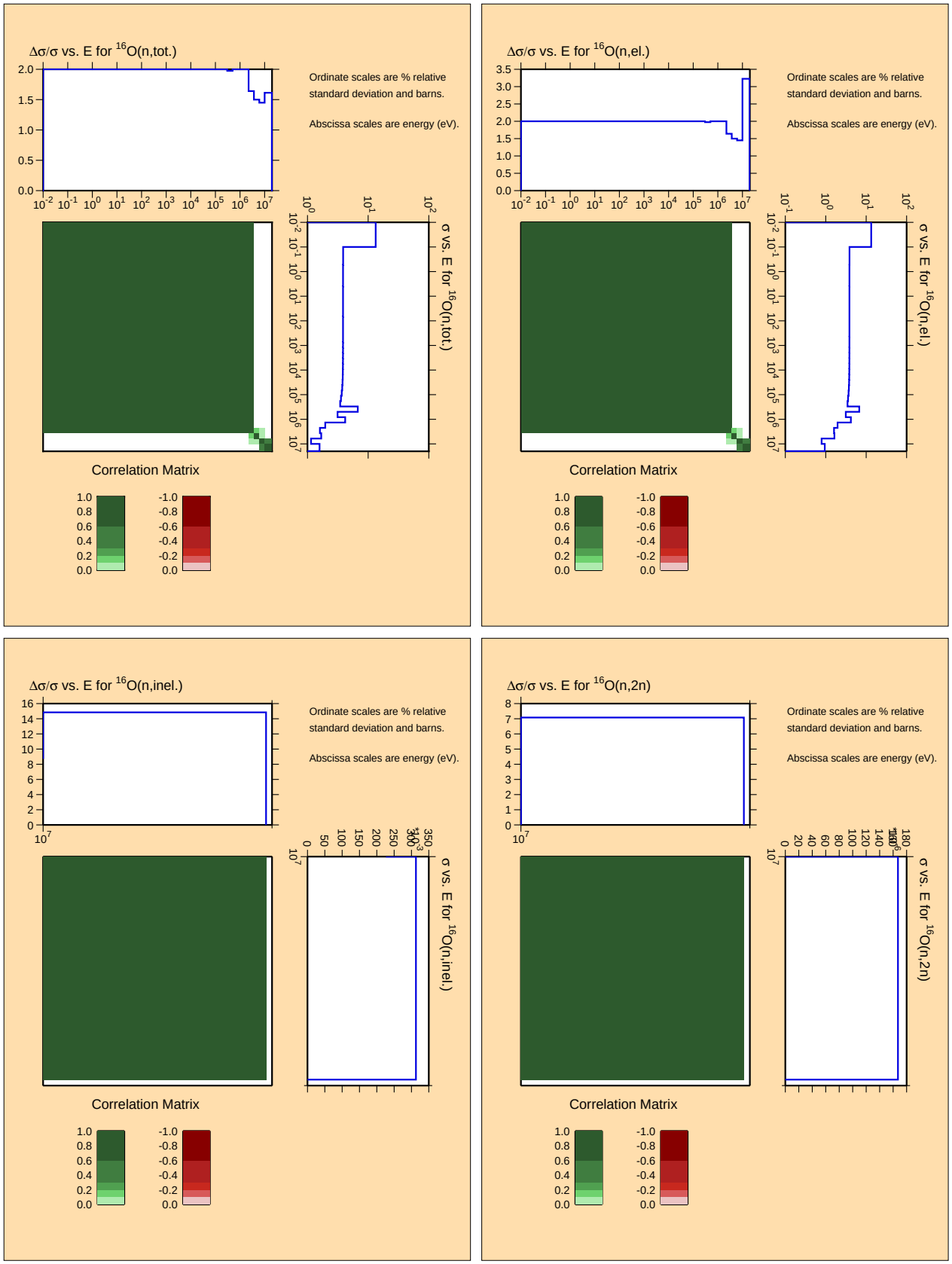

Figure A.11: Covariances for light nucleus ^{16}O.

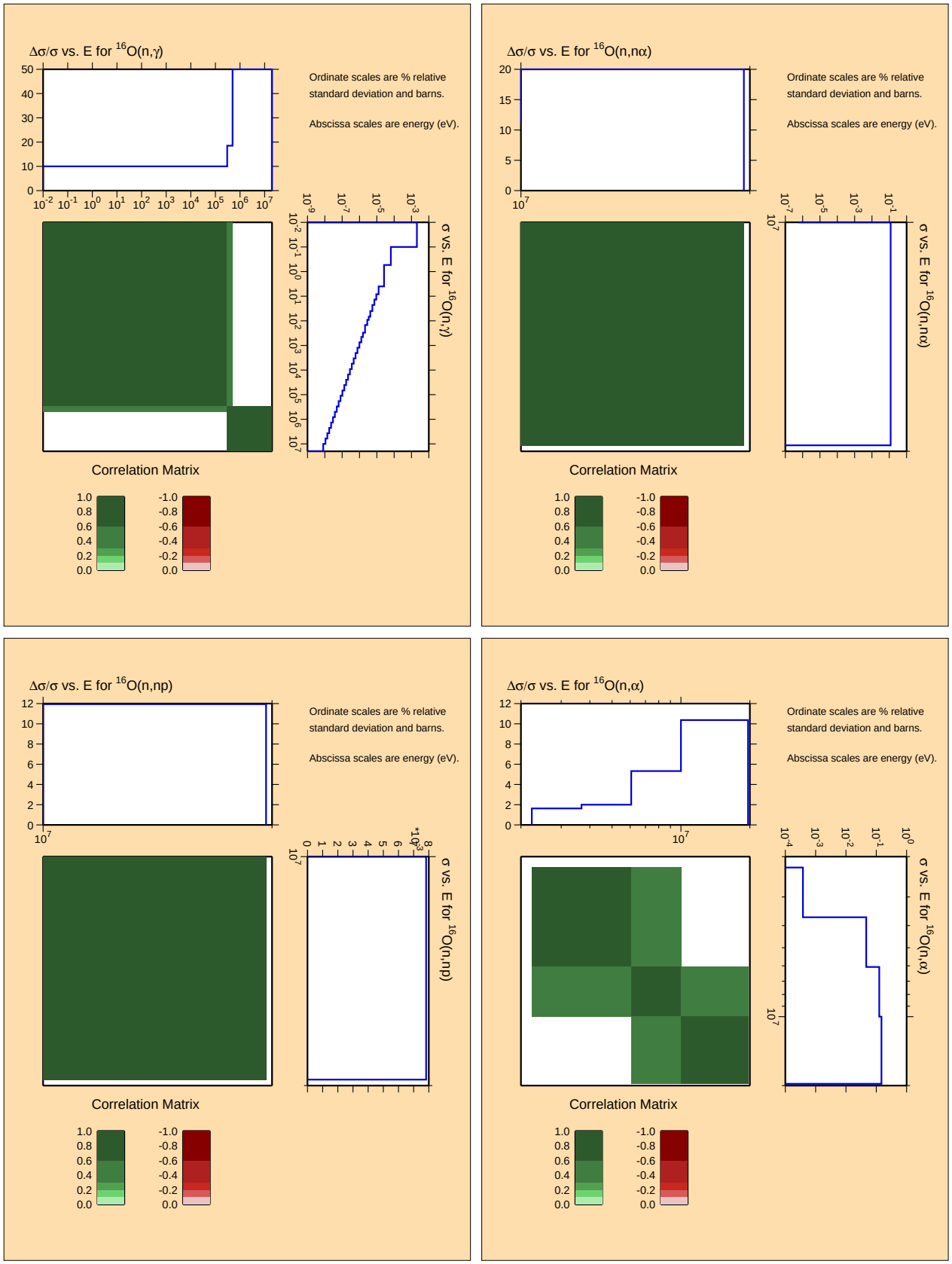

Figure A.11: Covariances for light nucleus ^{16}O (continued)

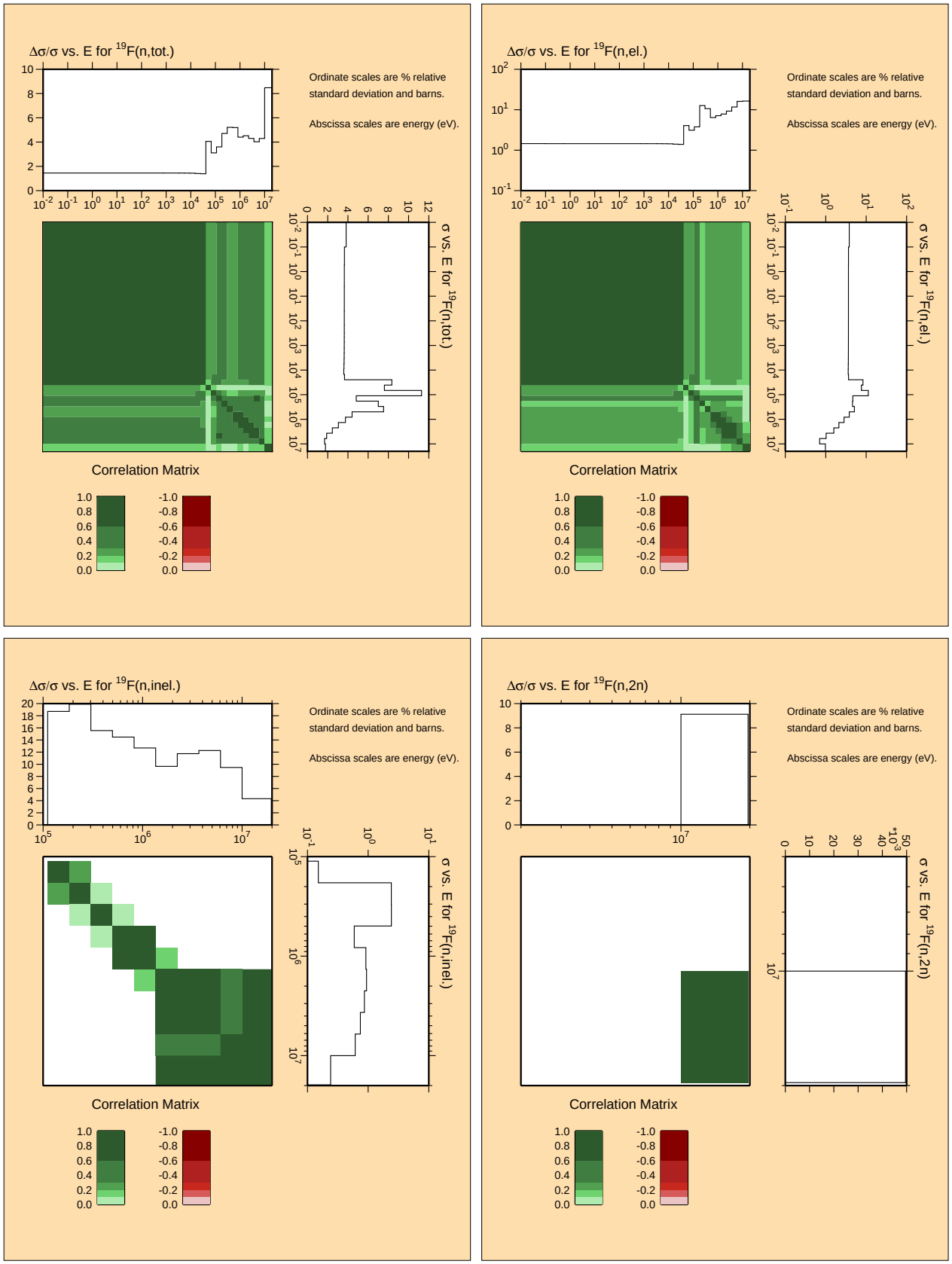

Figure A.12: Covariances for light nucleus ^{19}F.

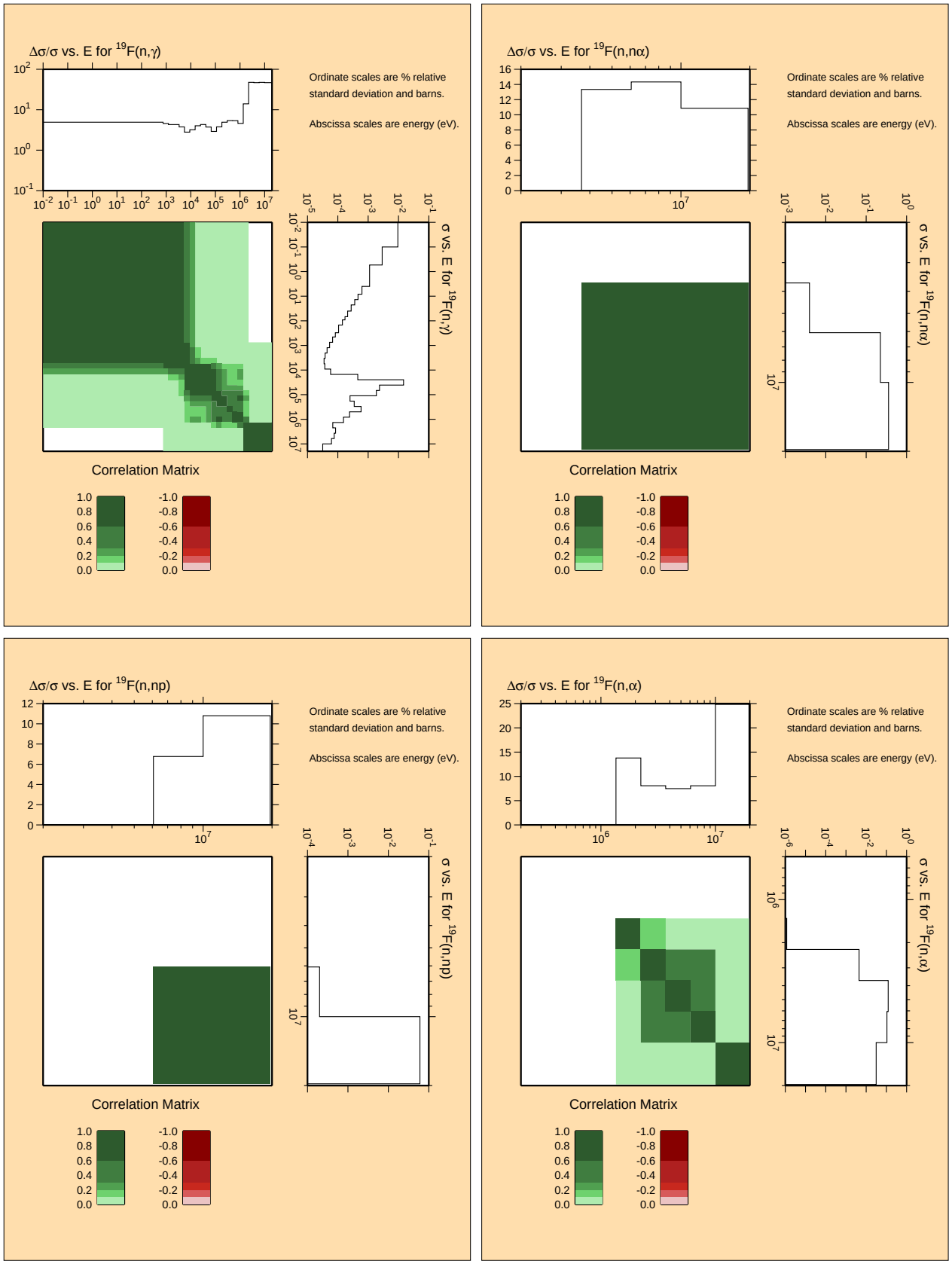

Figure A.12: Covariances for light nucleus ^{19}F (continued)

A.2.2 Structural materials and fission products

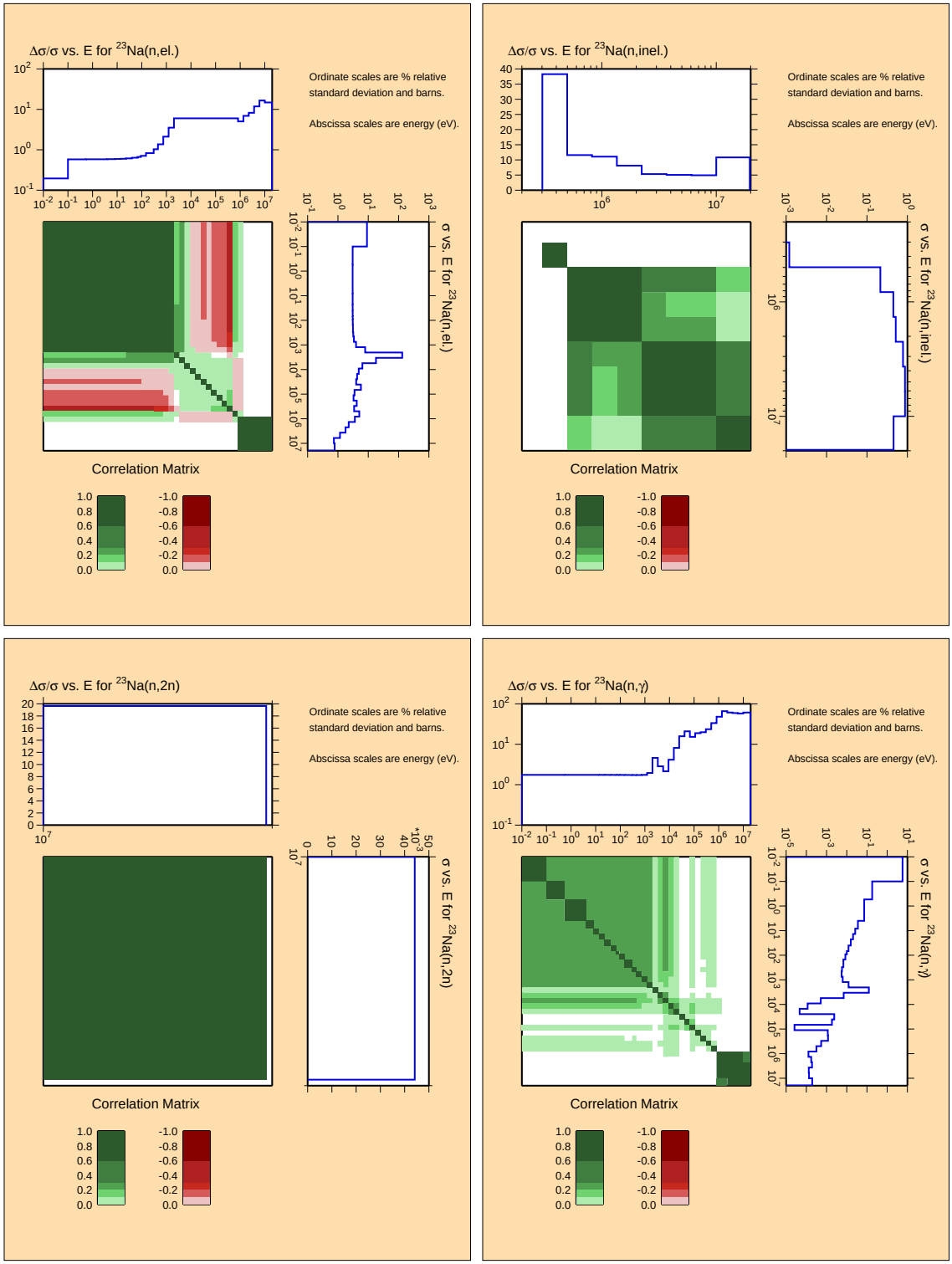

Figure A.13: Covariances for coolant ^{23}Na

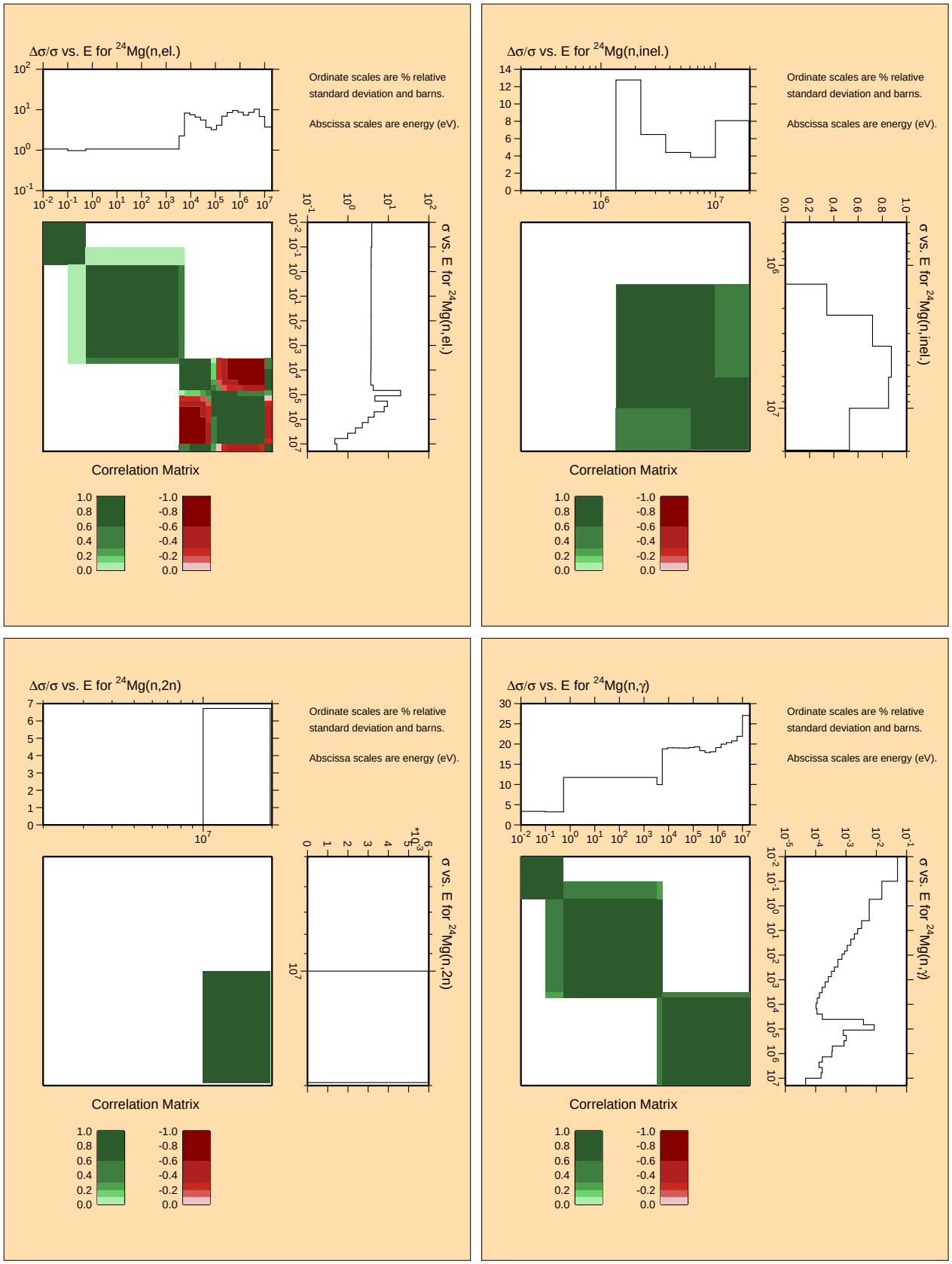

Figure A.14: Covariances for structural material ^{24}Mg.

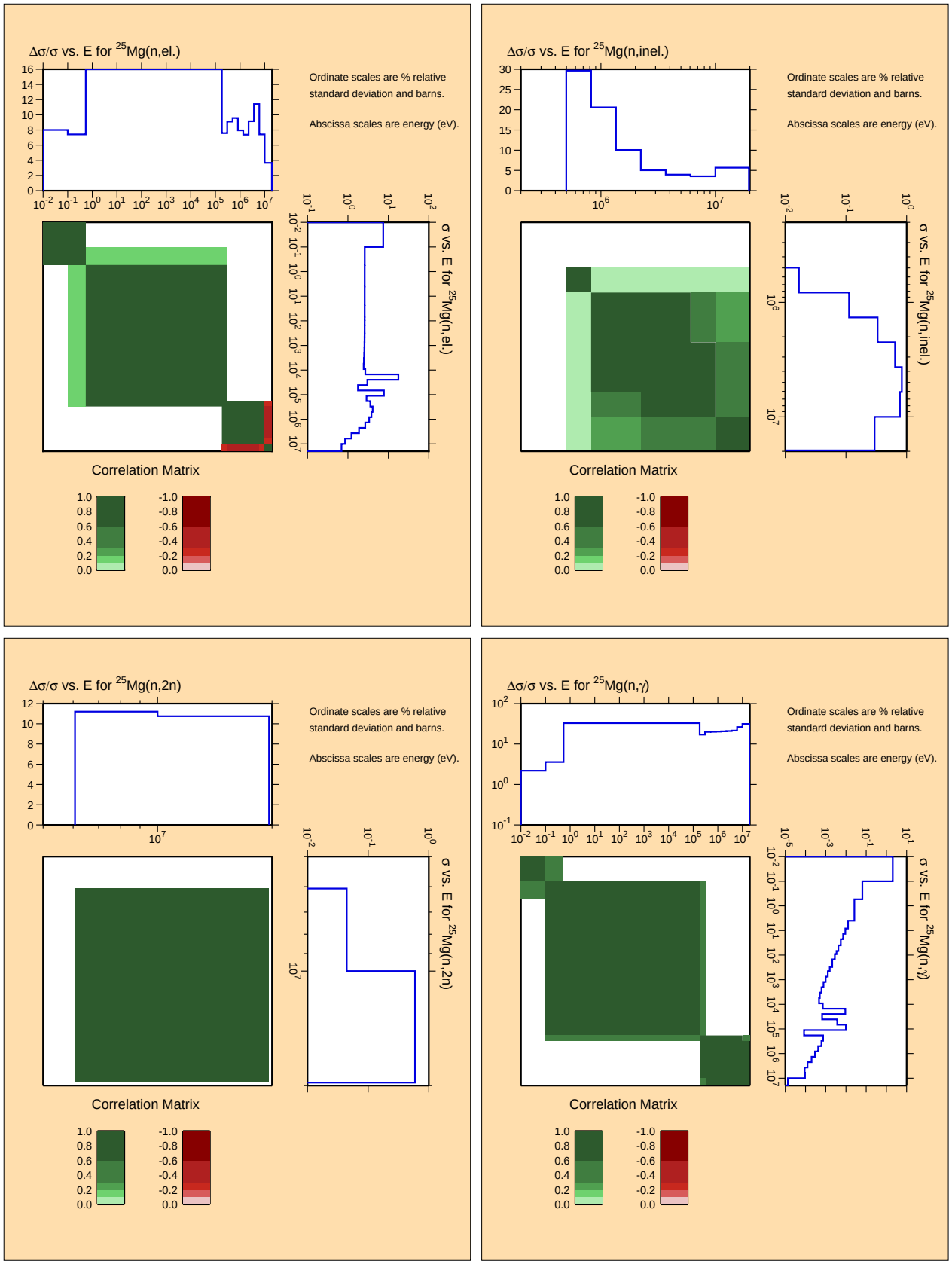

Figure A.15: Covariances for structural material ^{25}Mg.

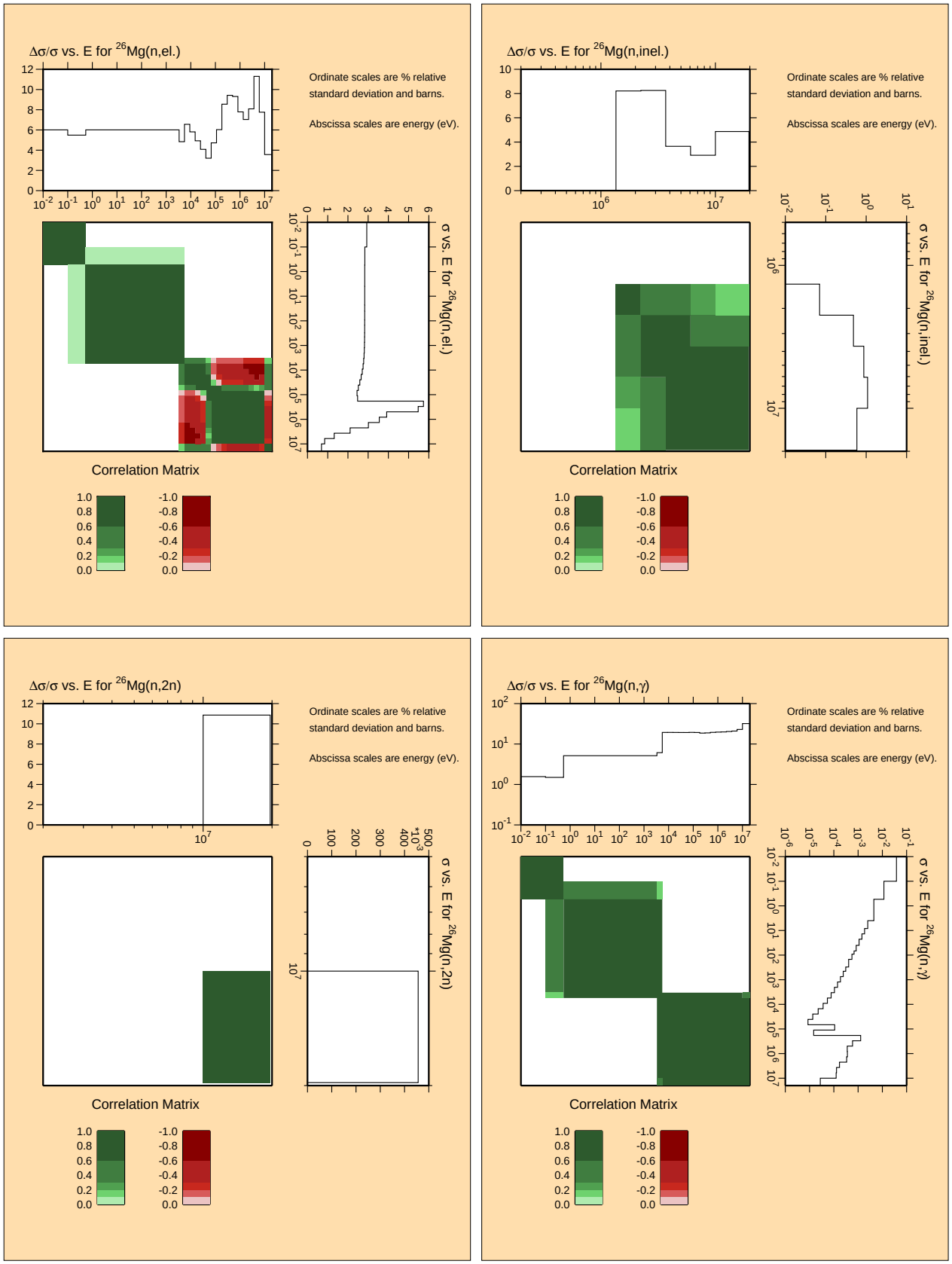

Figure A.16: Covariances for structural material ^{26}Mg.

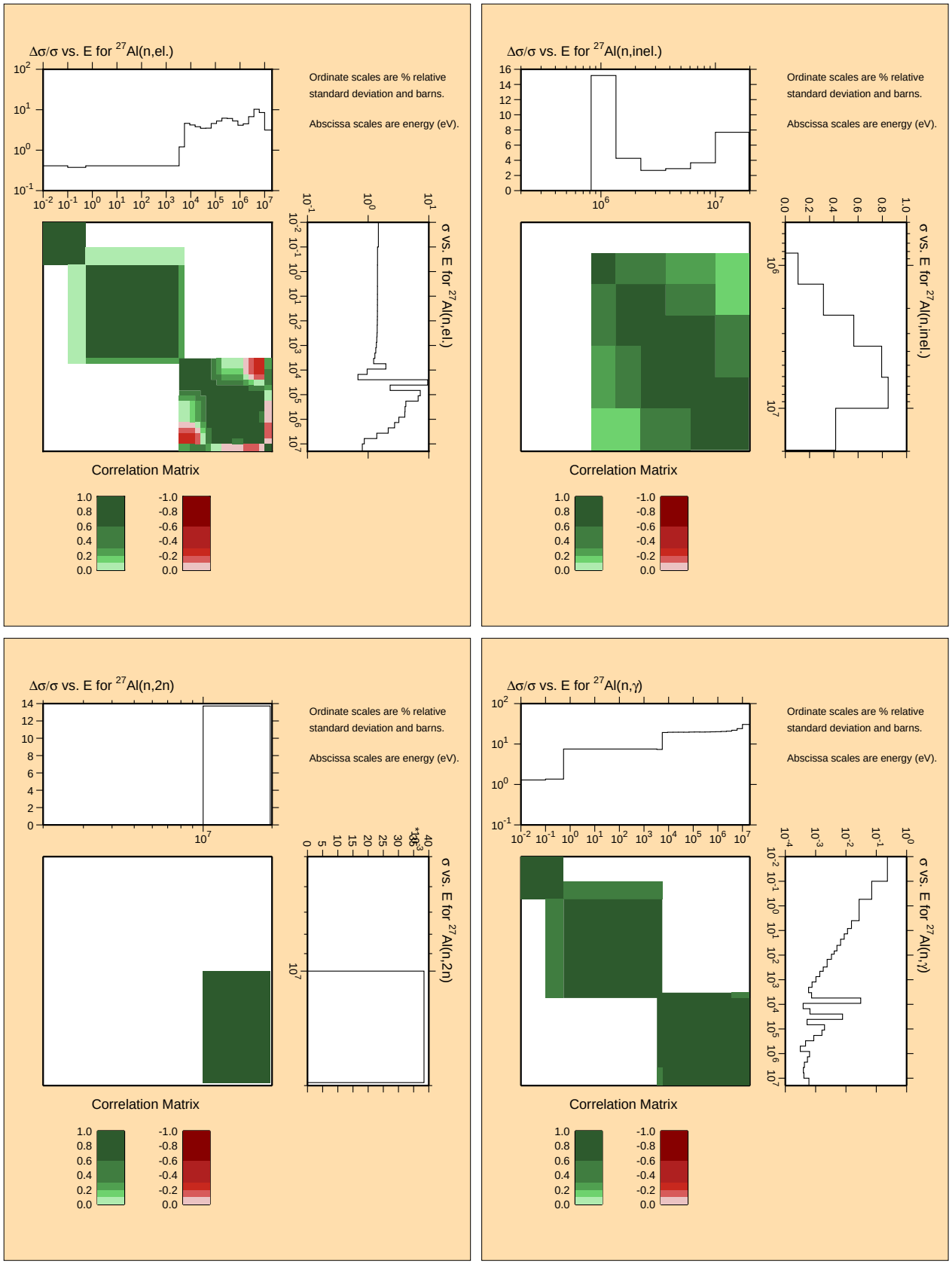

Figure A.17: Covariances for structural material ^{27}Al.

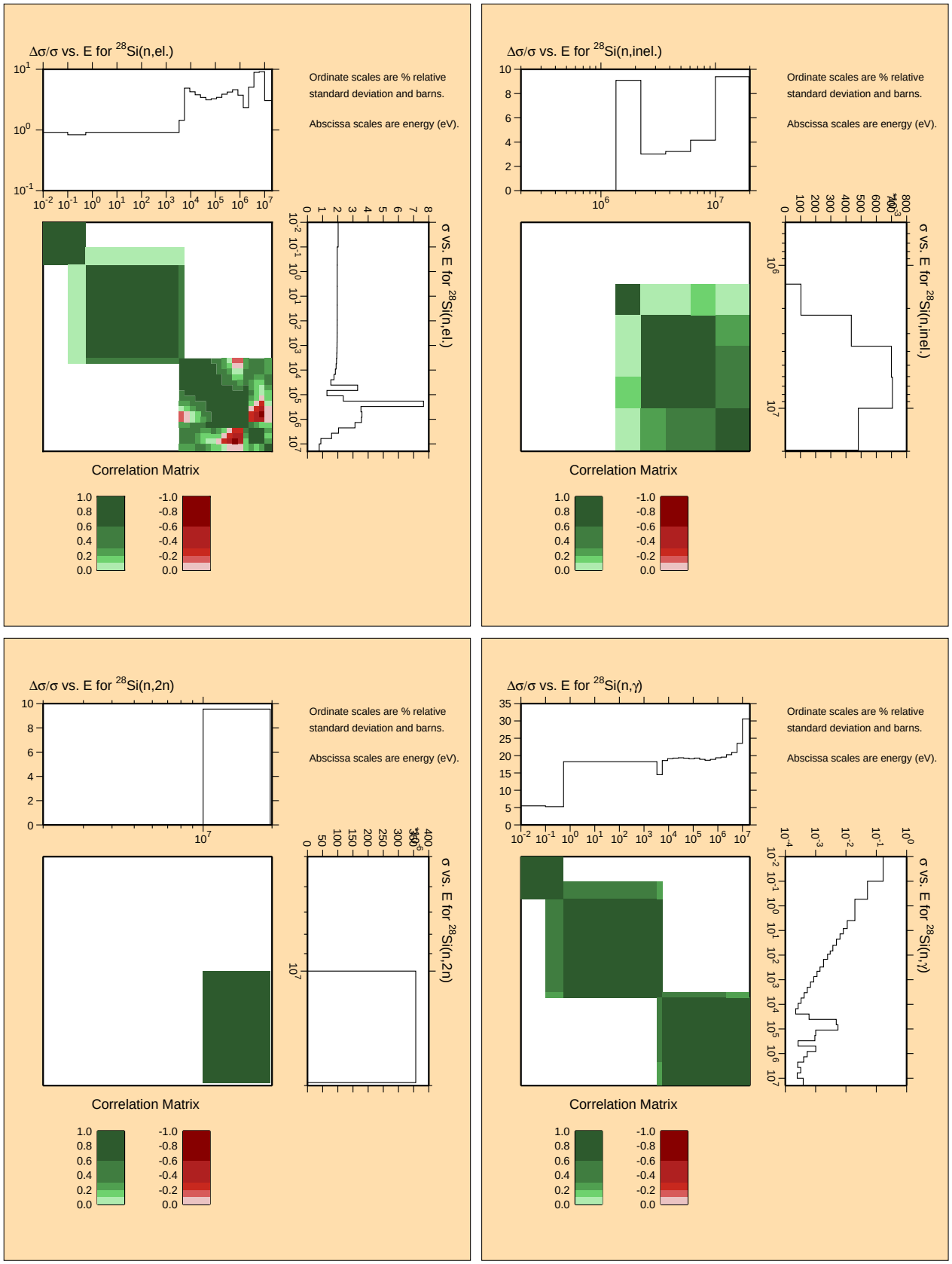

Figure A.18: Covariances for structural material ^{28}Si.

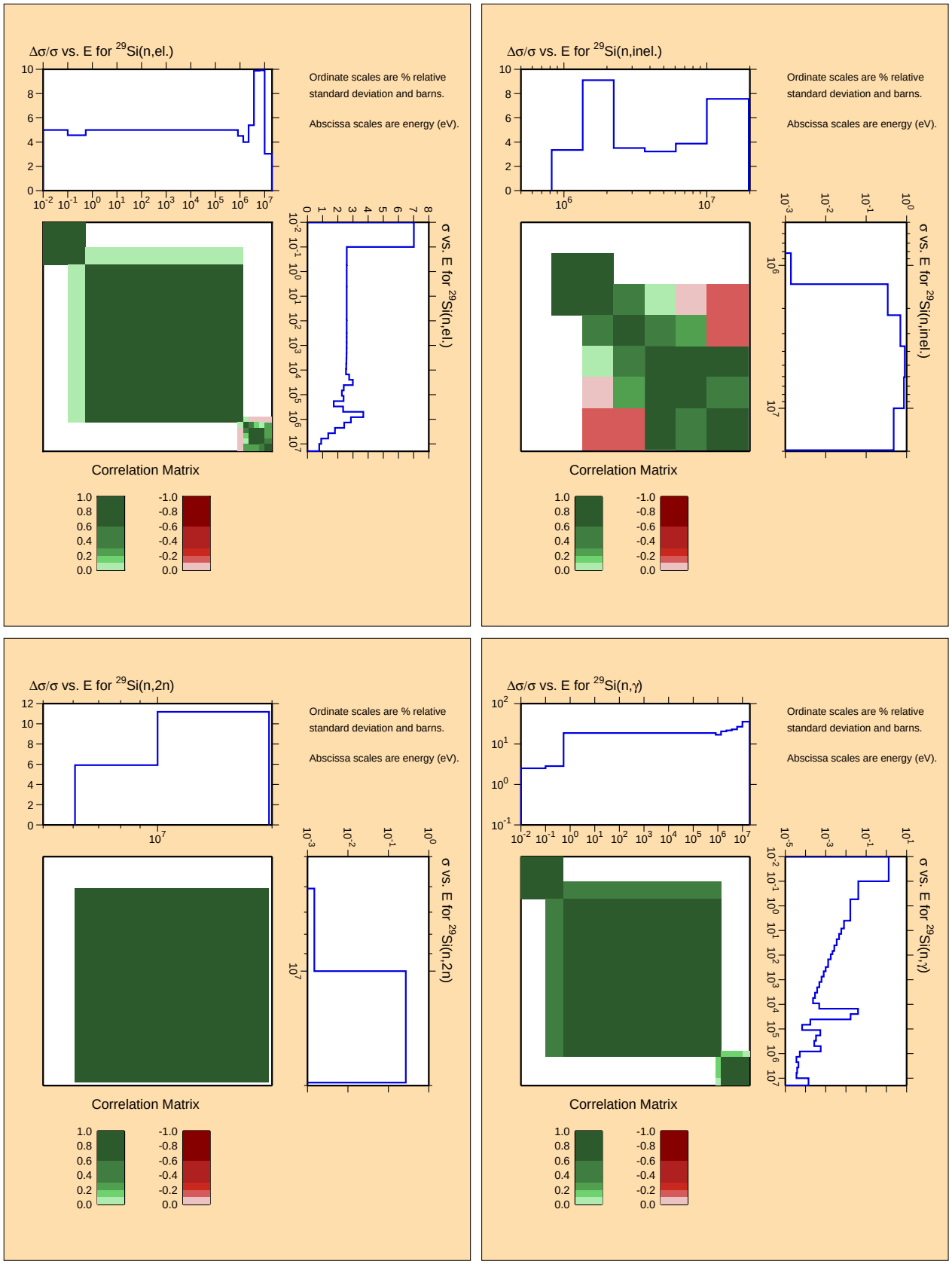

Figure A.19: Covariances for structural material ^{29}Si.

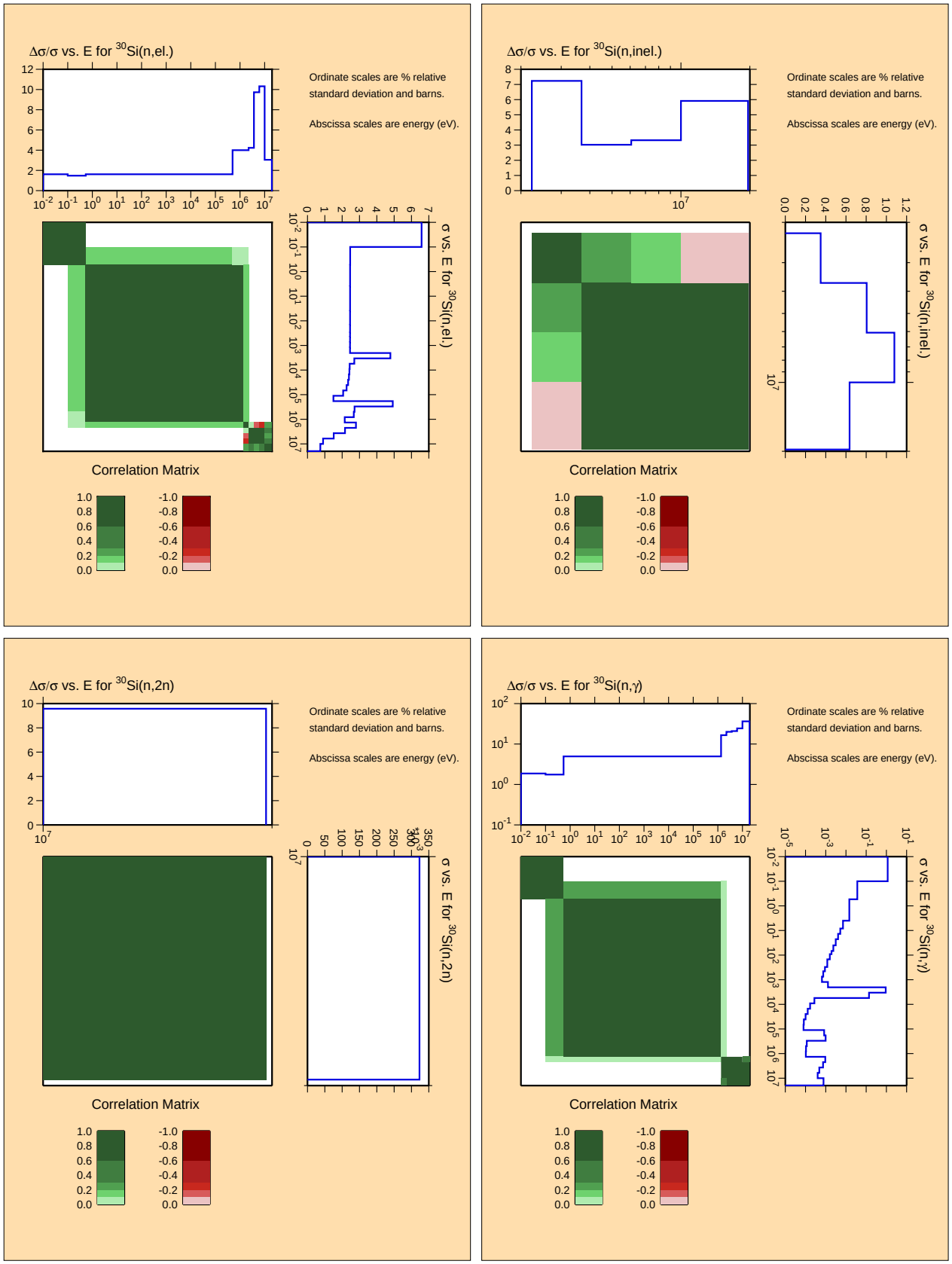

Figure A.20: Covariances for structural material ^{30}Si.

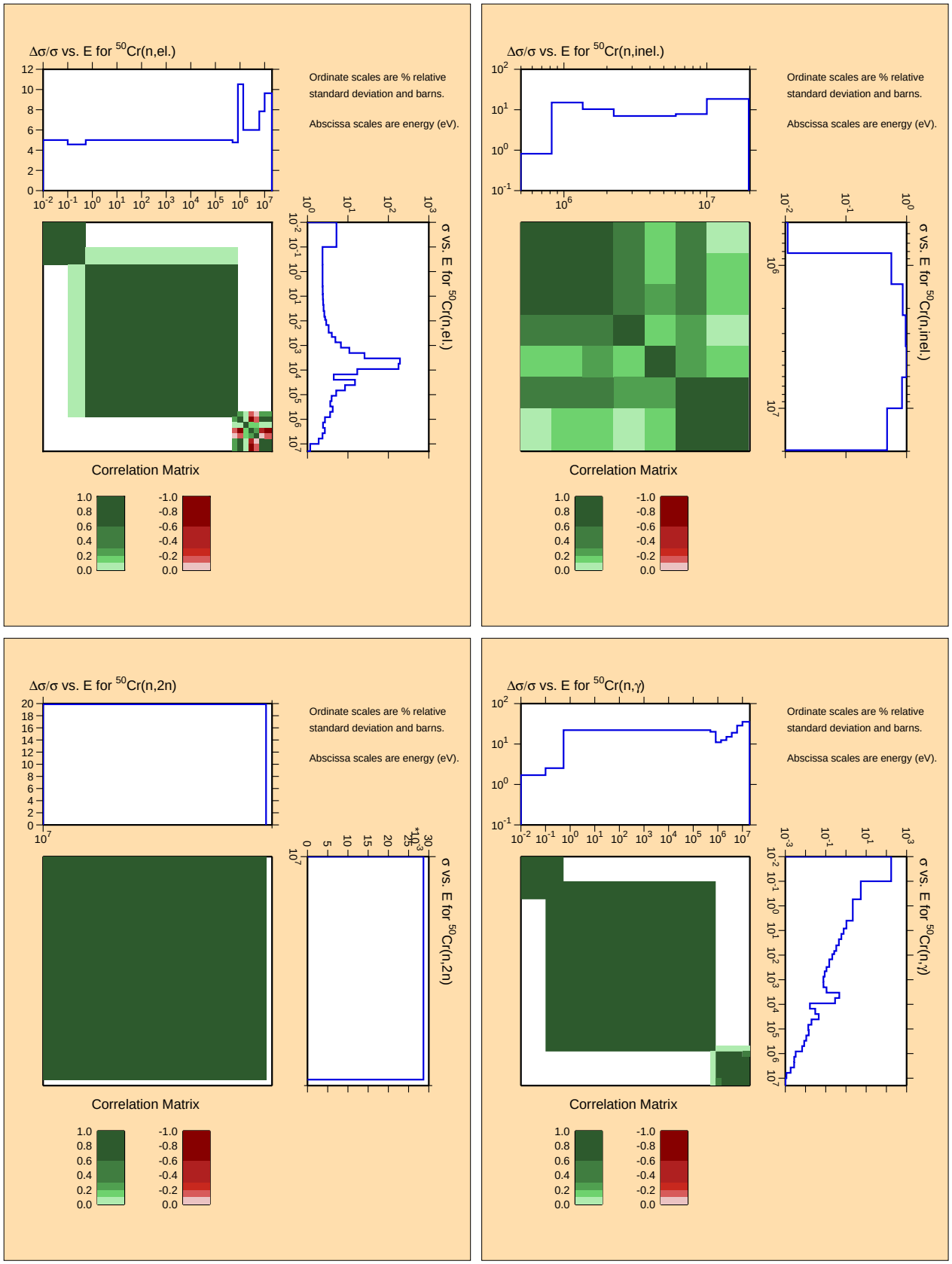

Figure A.21: Covariances for structural material ^{50}Cr.

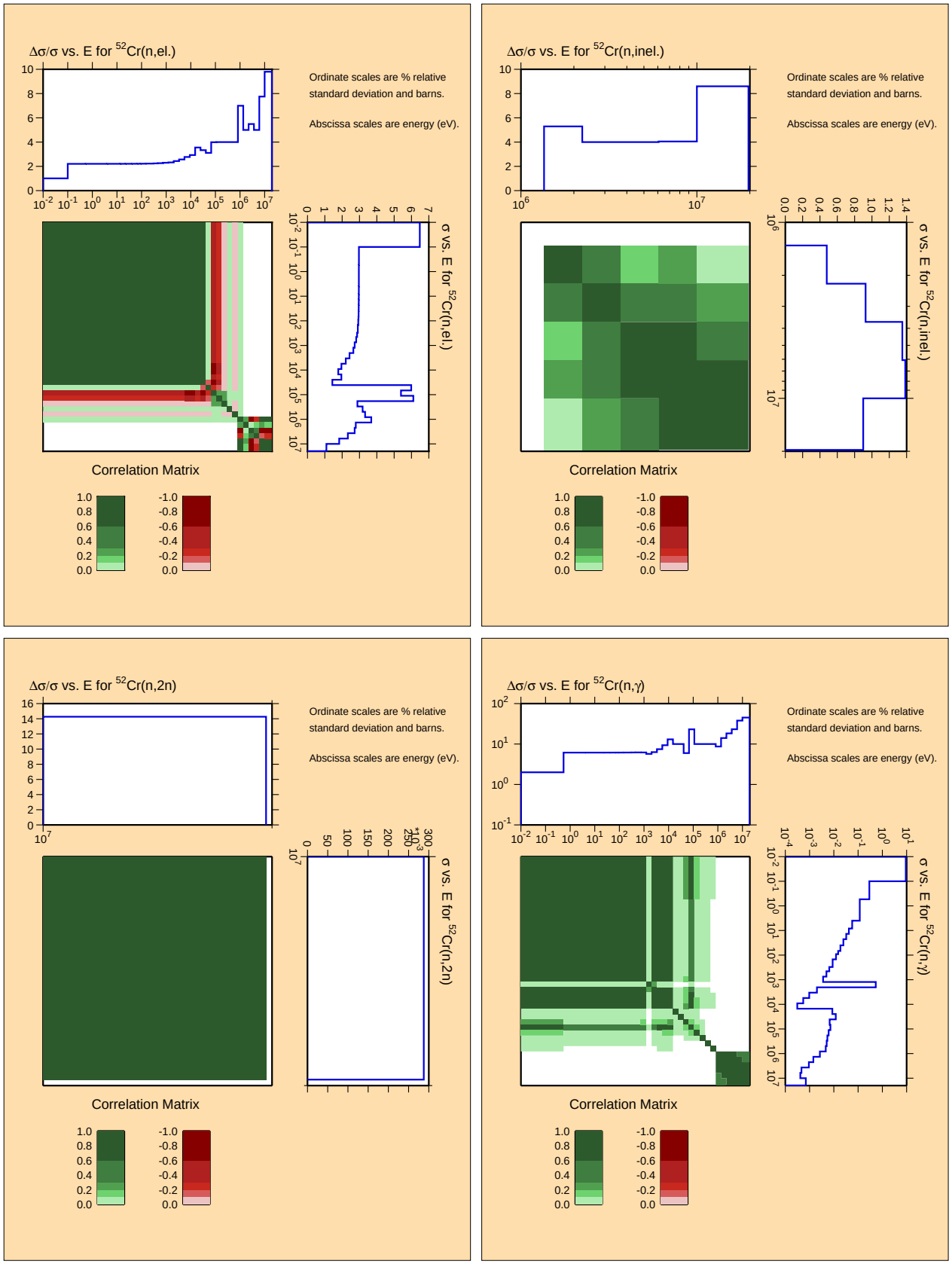

Figure A.22: Covariances for structural material ^{52}Cr.

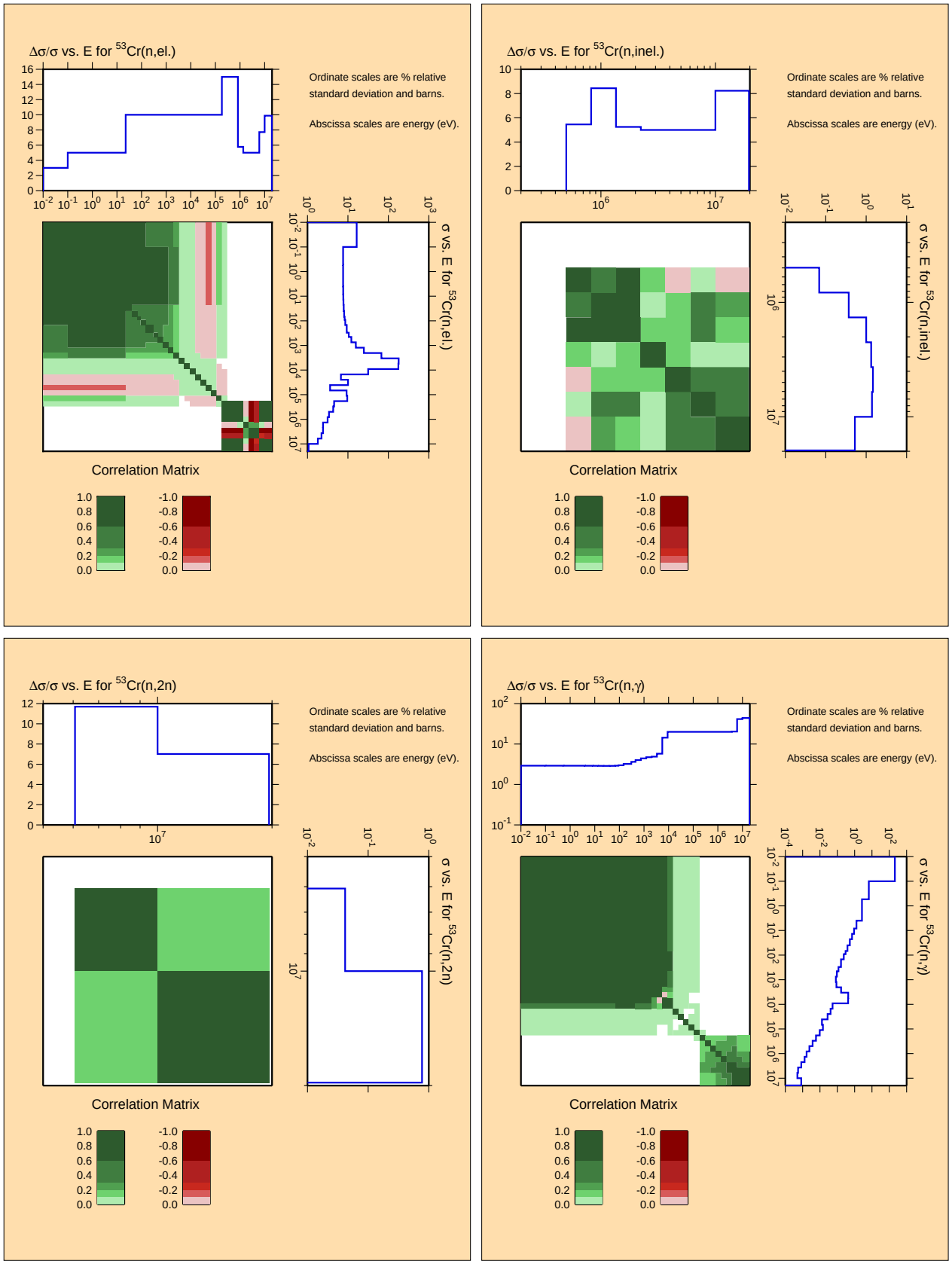

Figure A.23: Covariances for structural material ^{53}Cr.

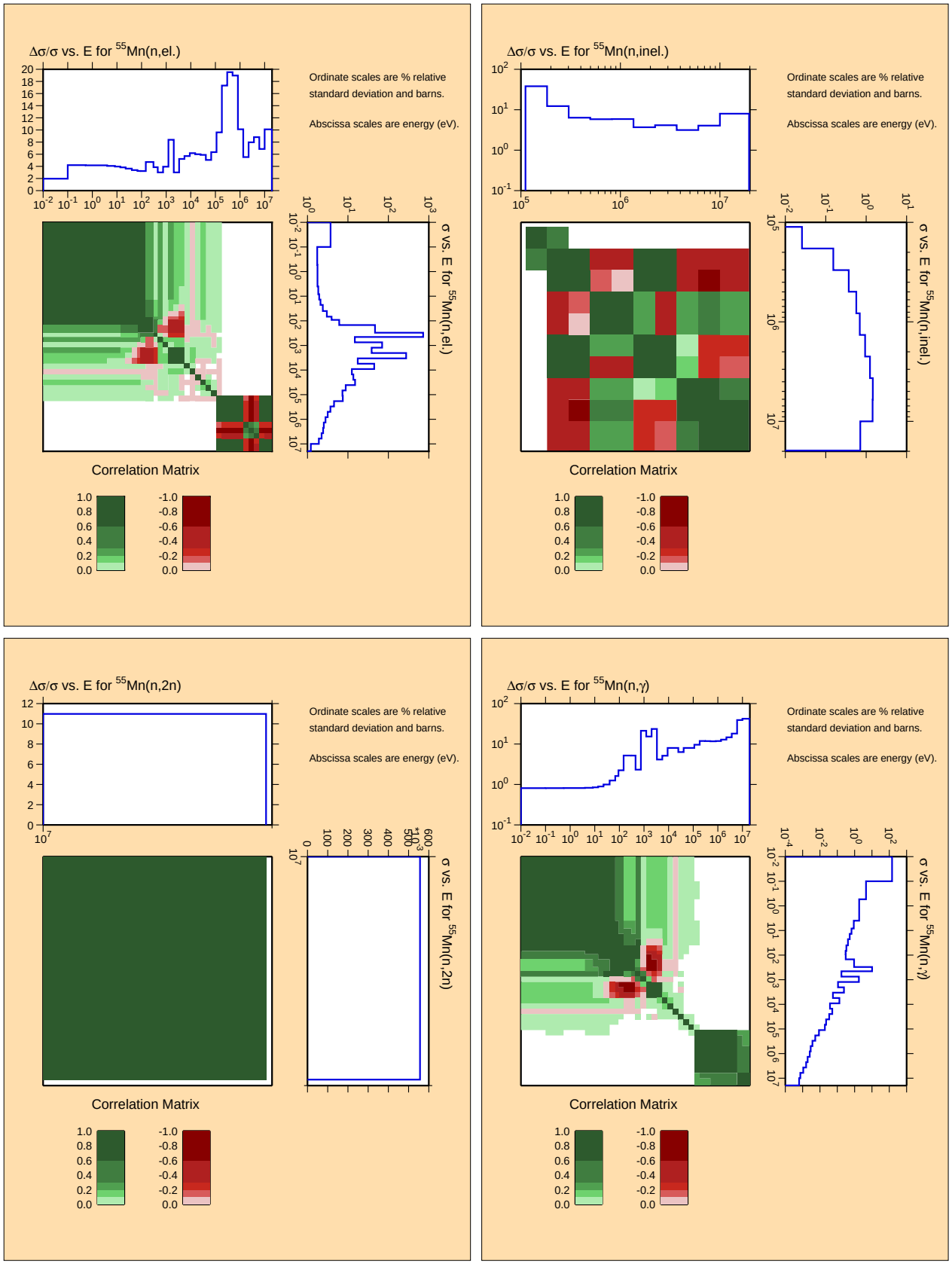

Figure A.24: Covariances for structural material ^{55}Mn.

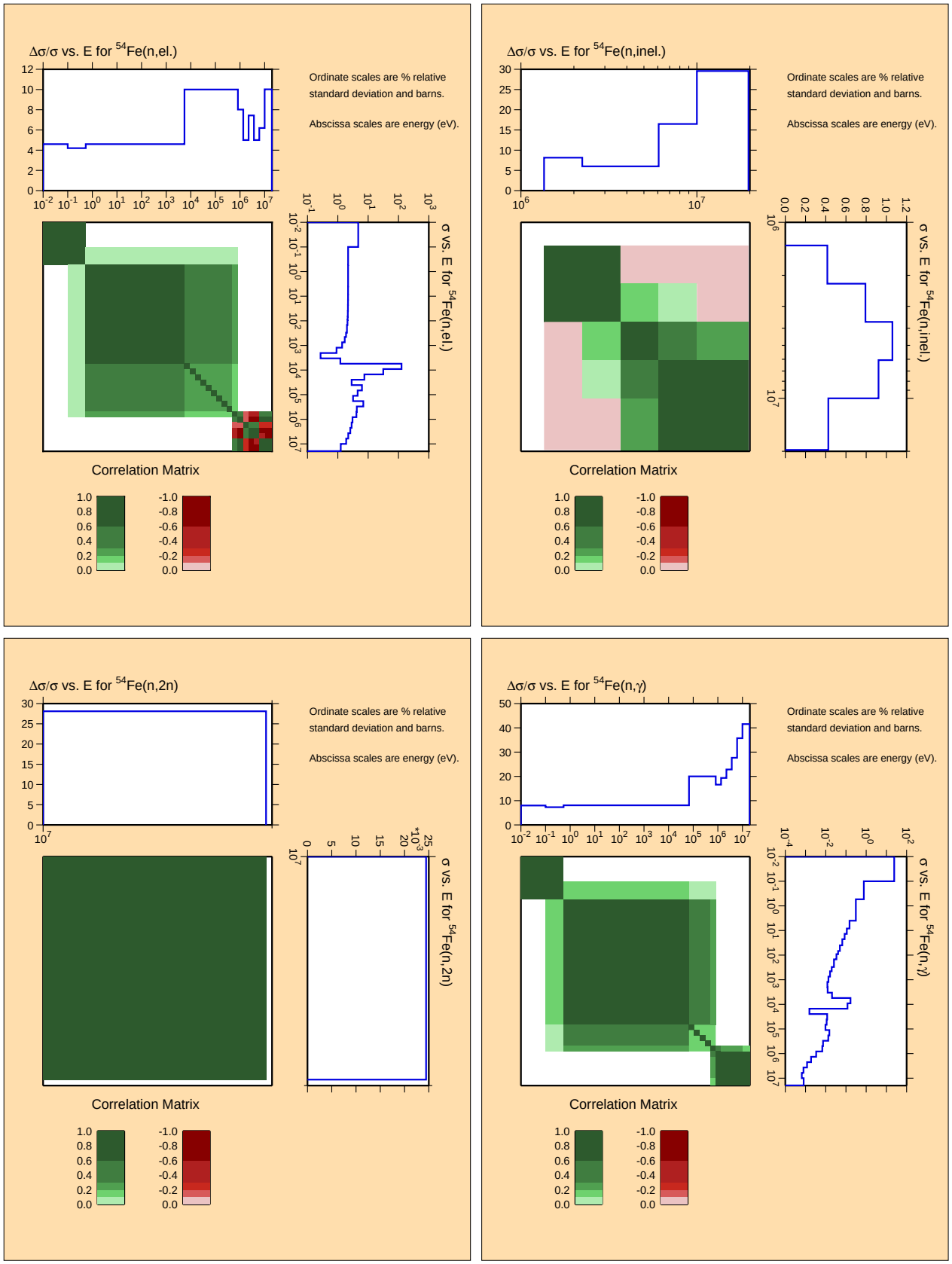

Figure A.25: Covariances for structural material ^{54}Fe.

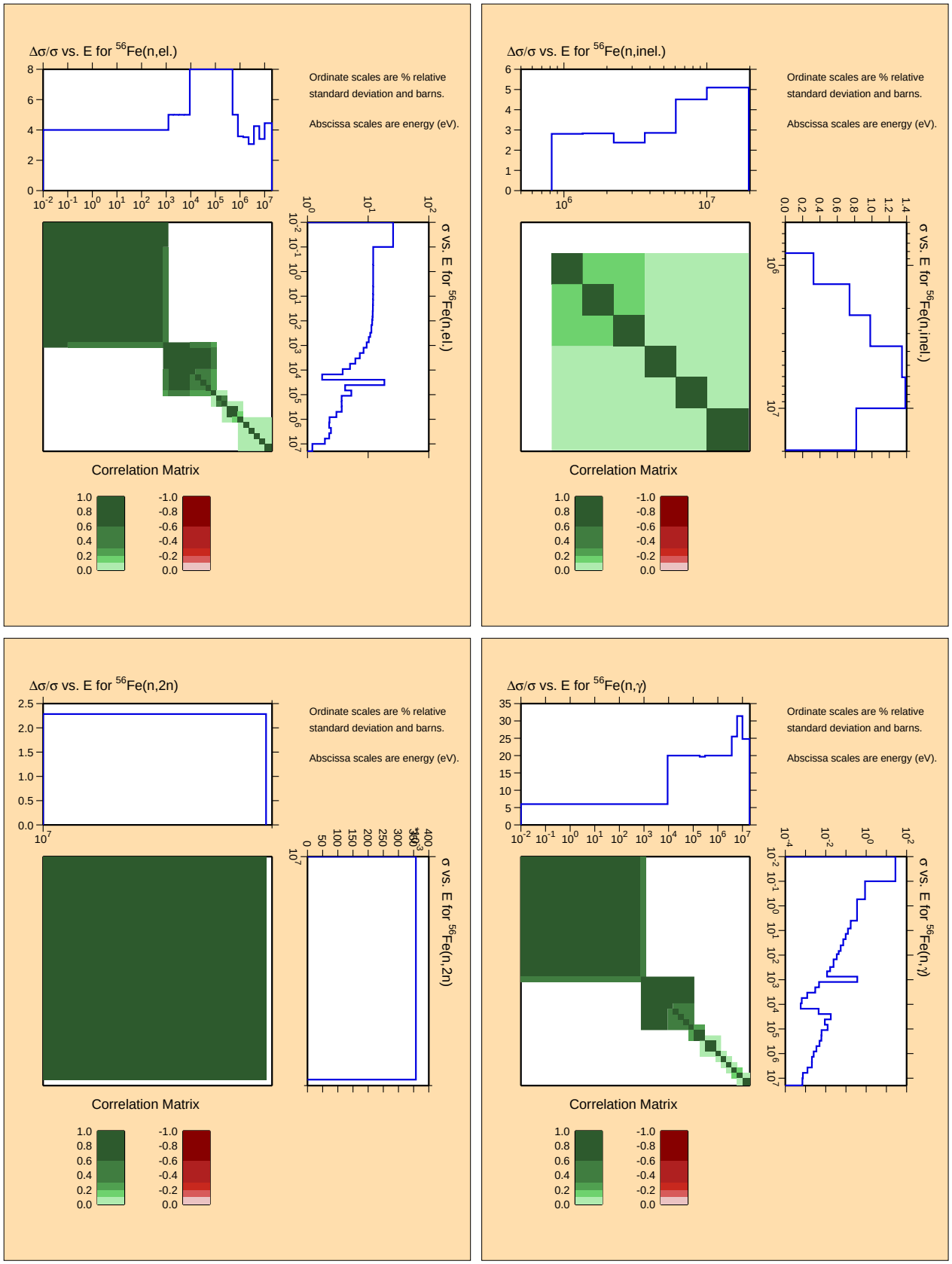

Figure A.26: Covariances for structural material ^{56}Fe.

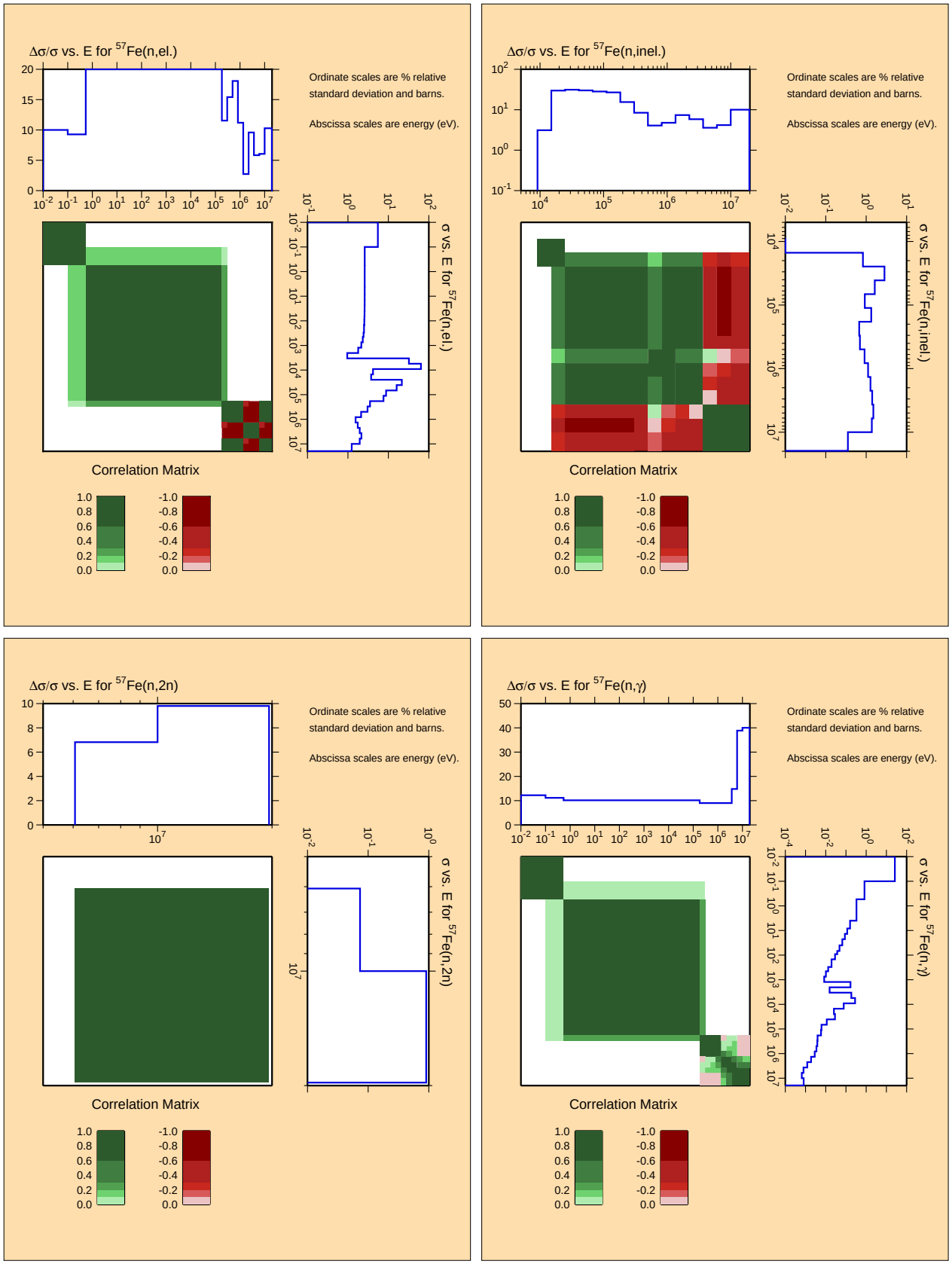

Figure A.27: Covariances for structural material ^{57}Fe.

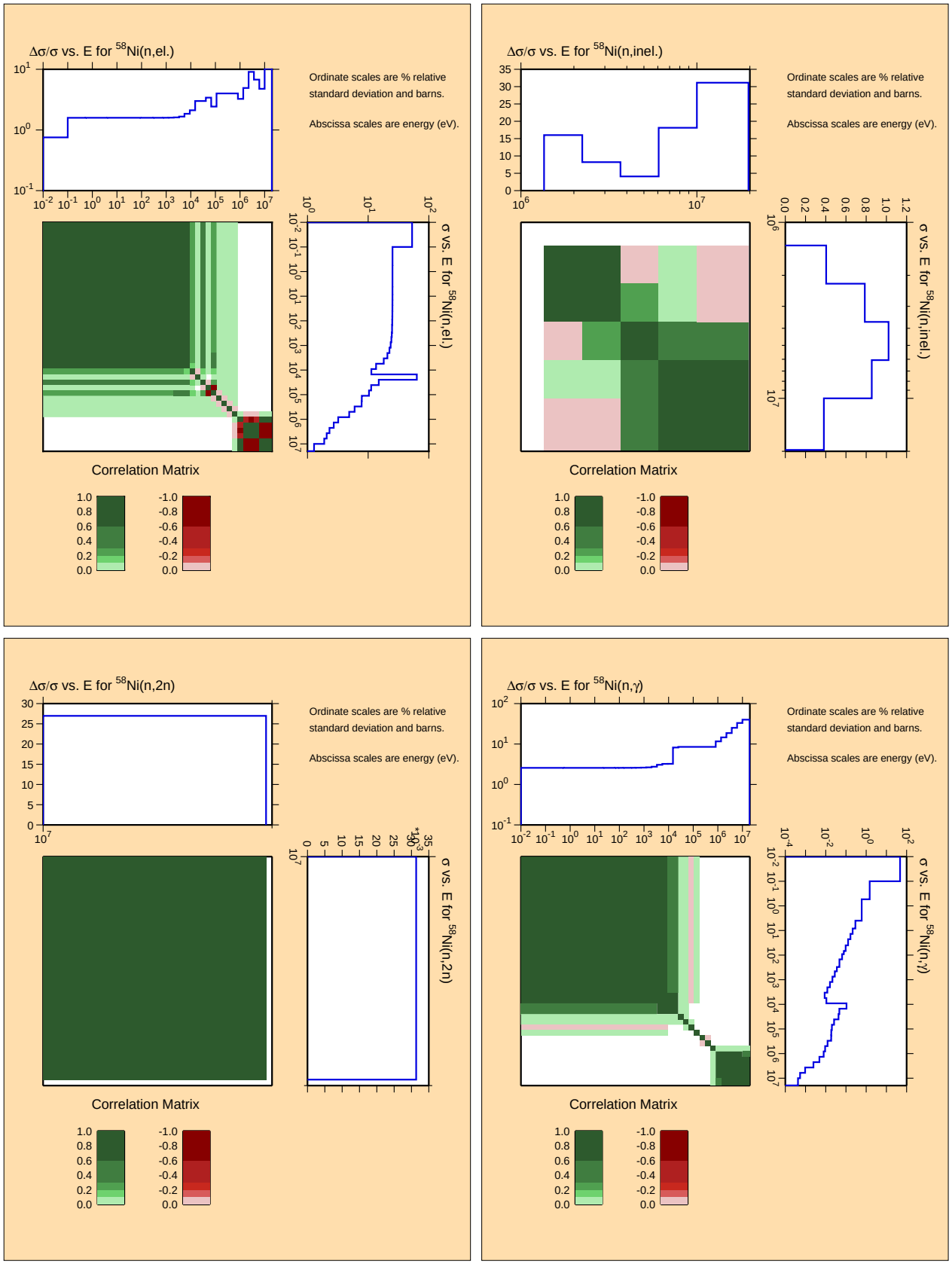

Figure A.28: Covariances for structural material ^{58}Ni.

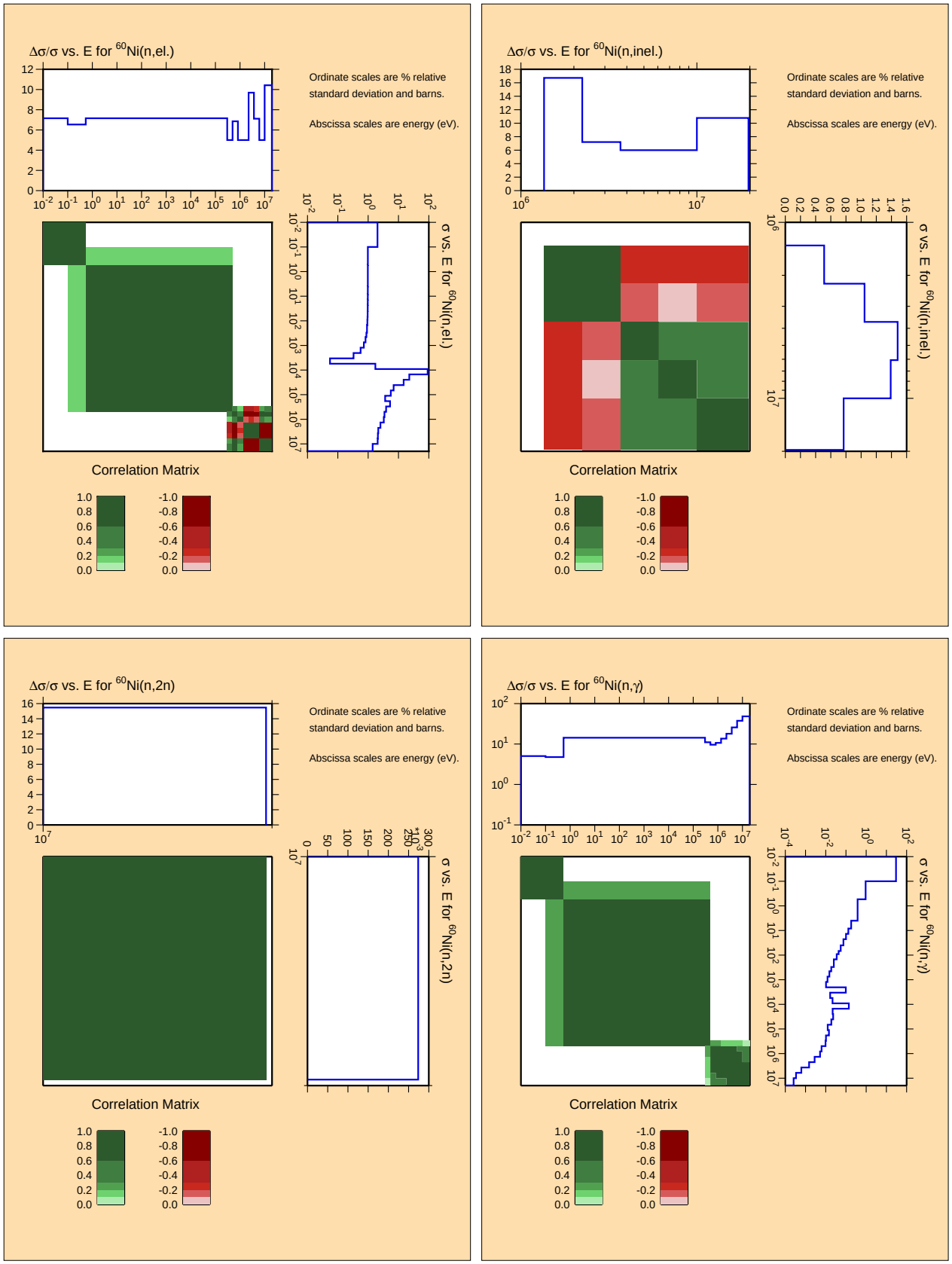

Figure A.29: Covariances for structural material ^{60}Ni.

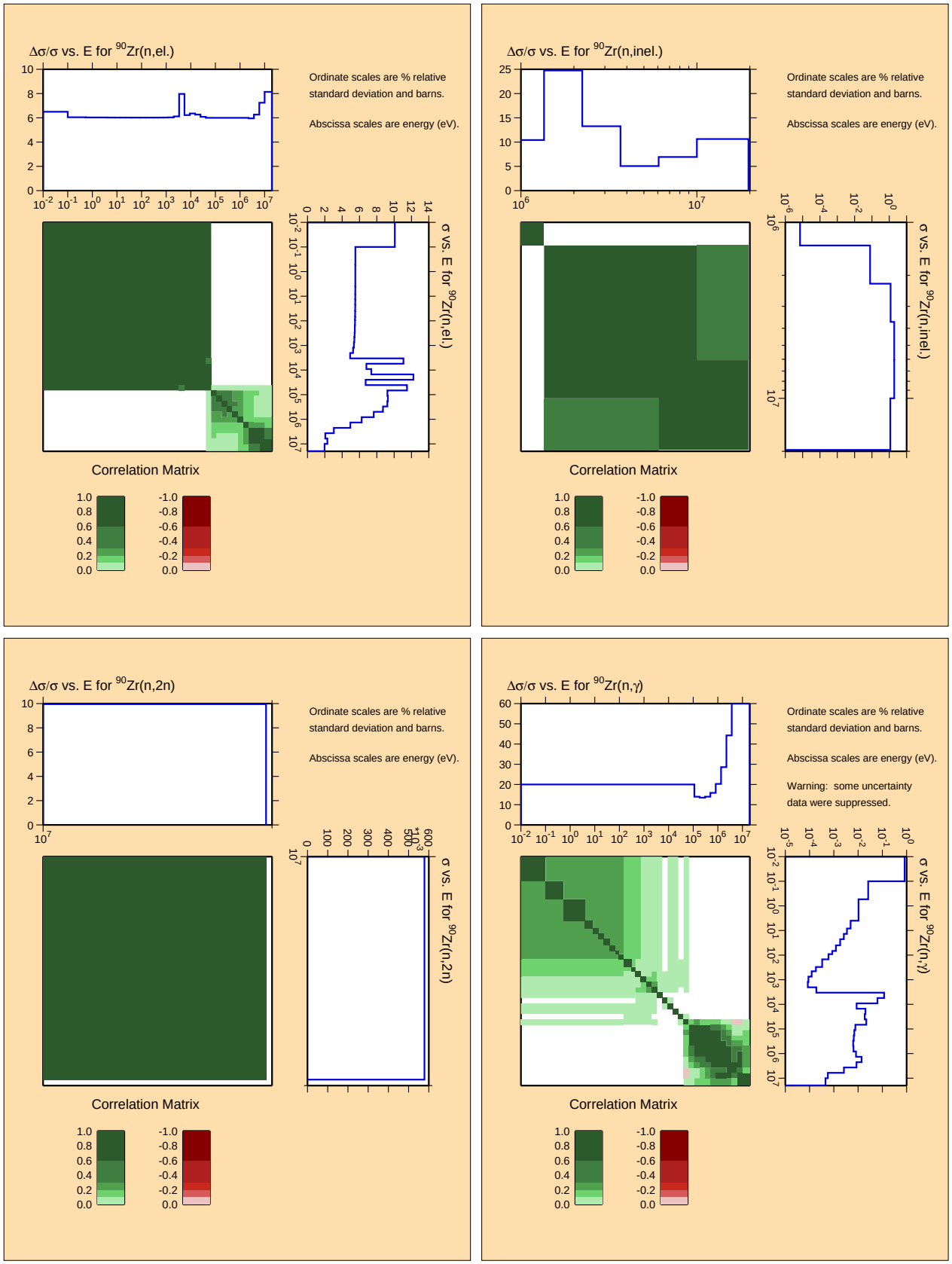

Figure A.30: Covariances for structural material ^{90}Zr.

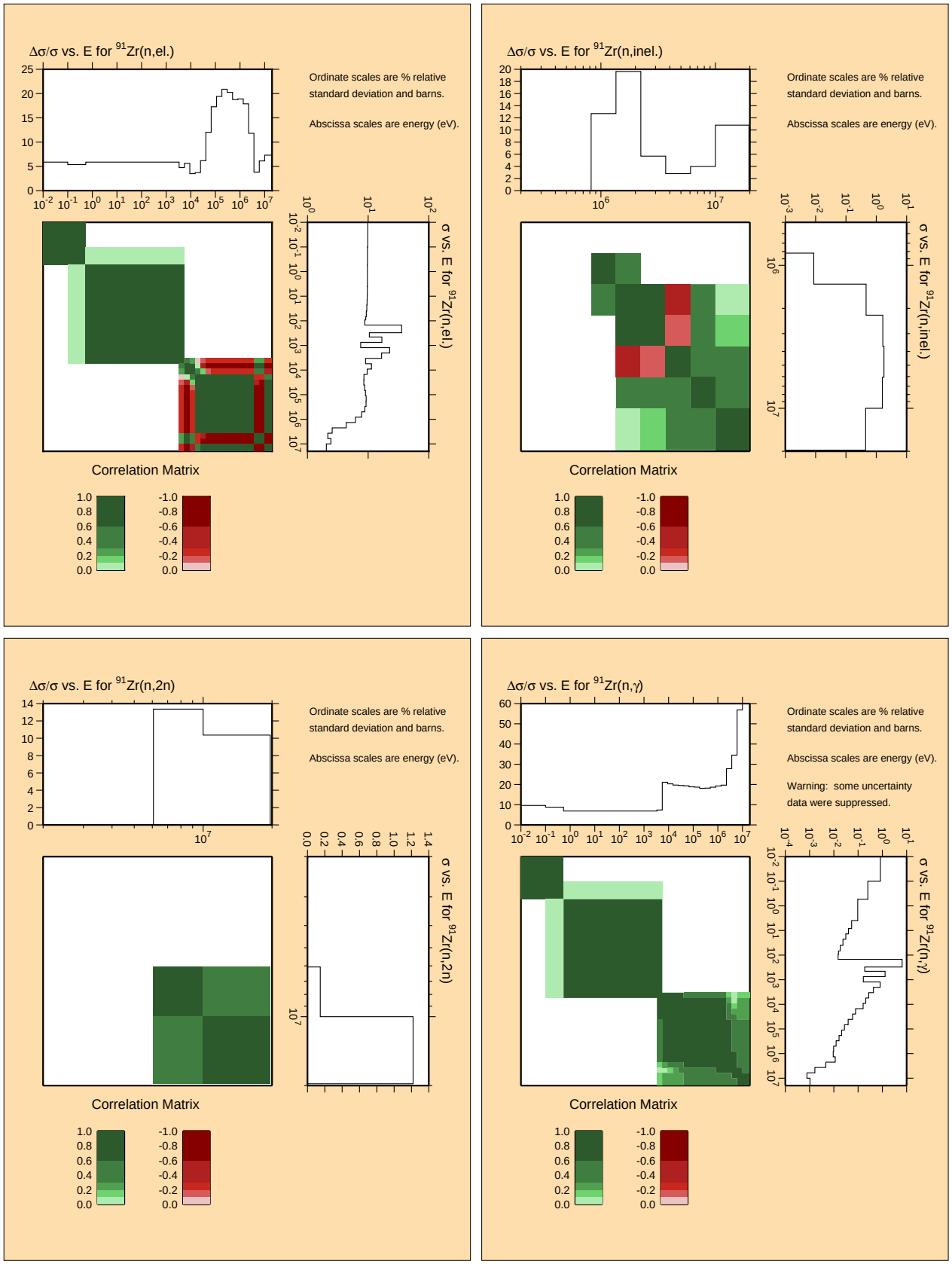

Figure A.31: Covariances for structural material ^{91}Zr.

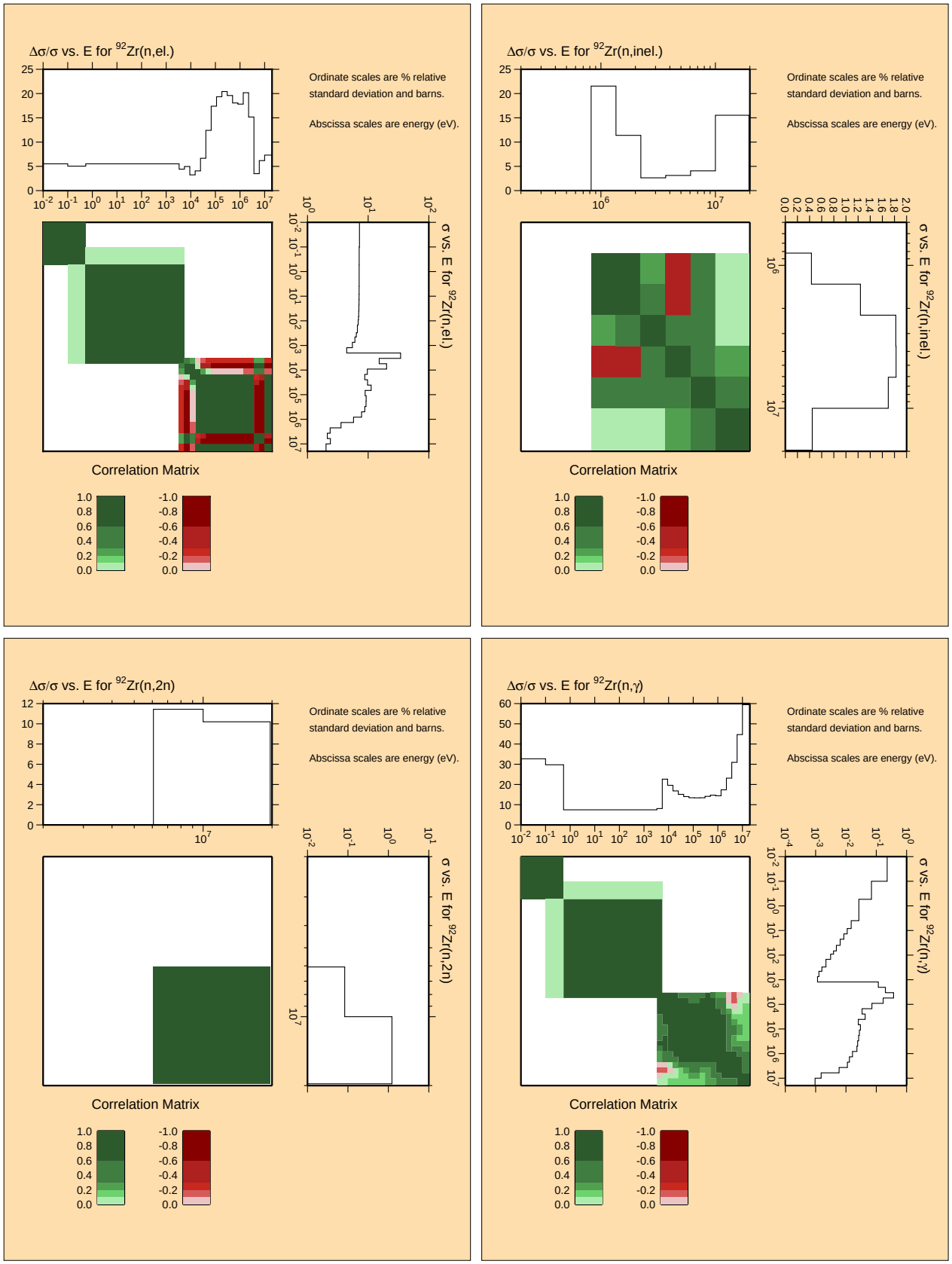

Figure A.32: Covariances for structural material ^{92}Zr.

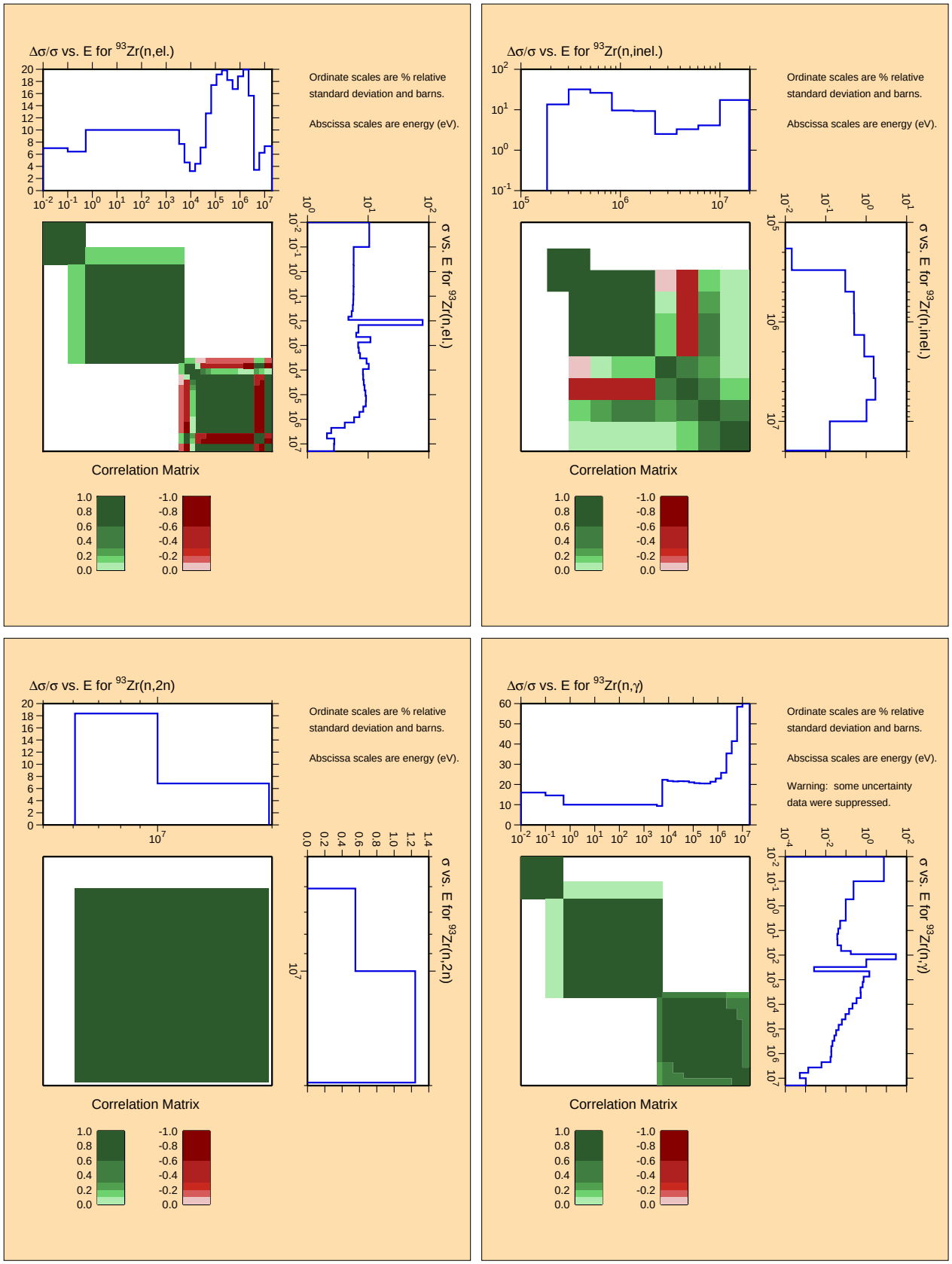

Figure A.33: Covariances for structural material ^{93}Zr.

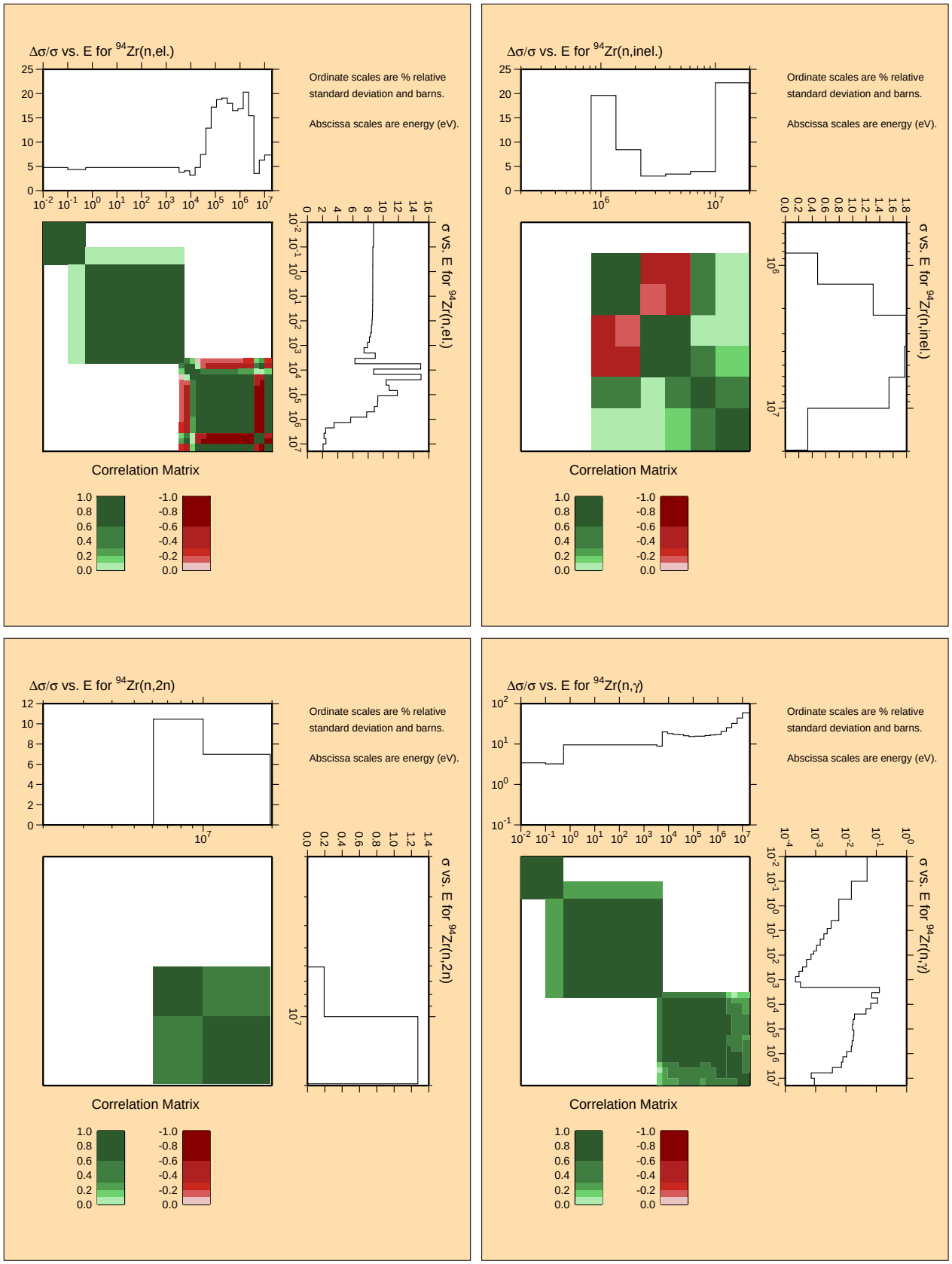

Figure A.34: Covariances for structural material ^{94}Zr.

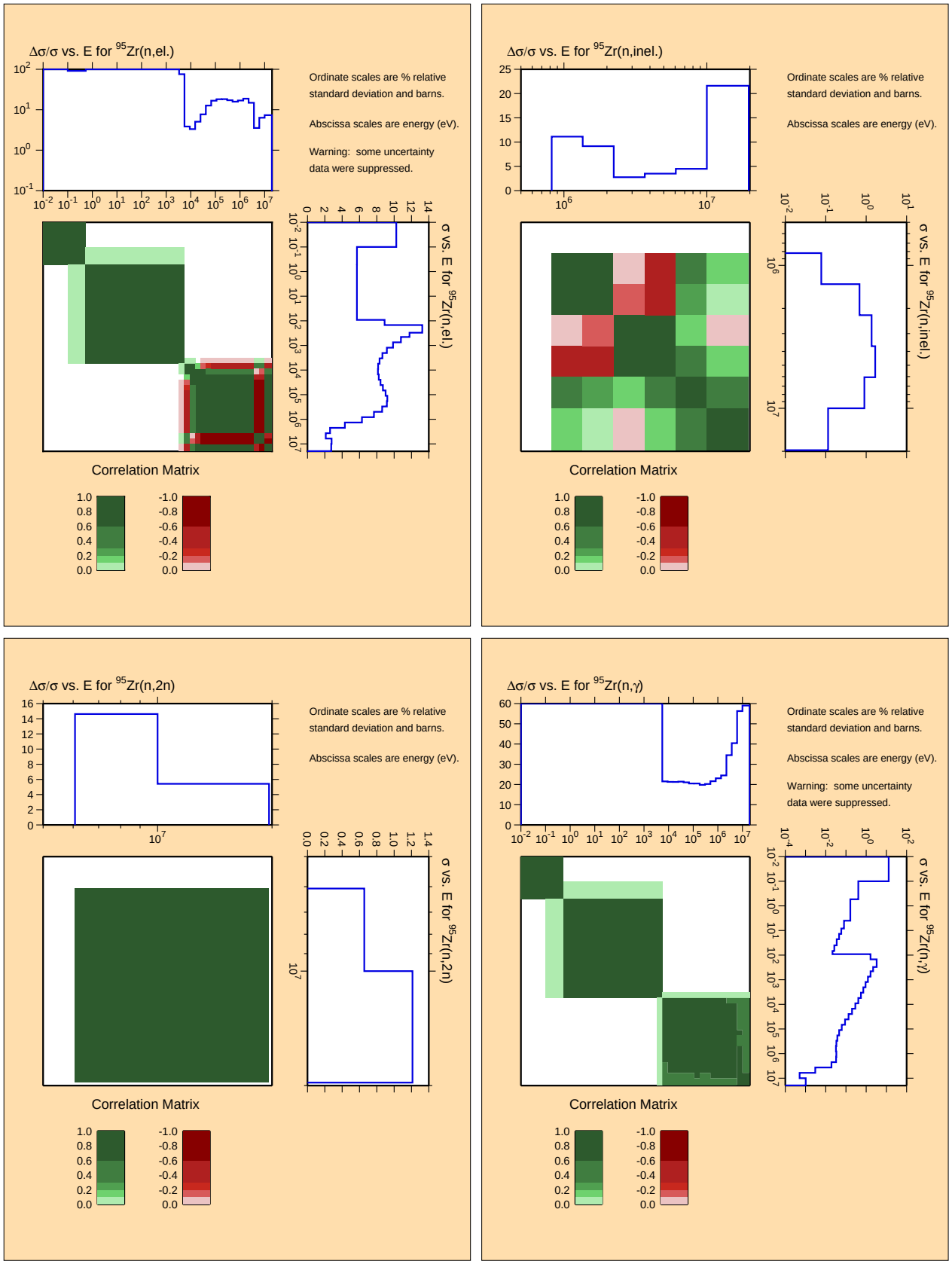

Figure A.35: Covariances for fission product ^{95}Zr.

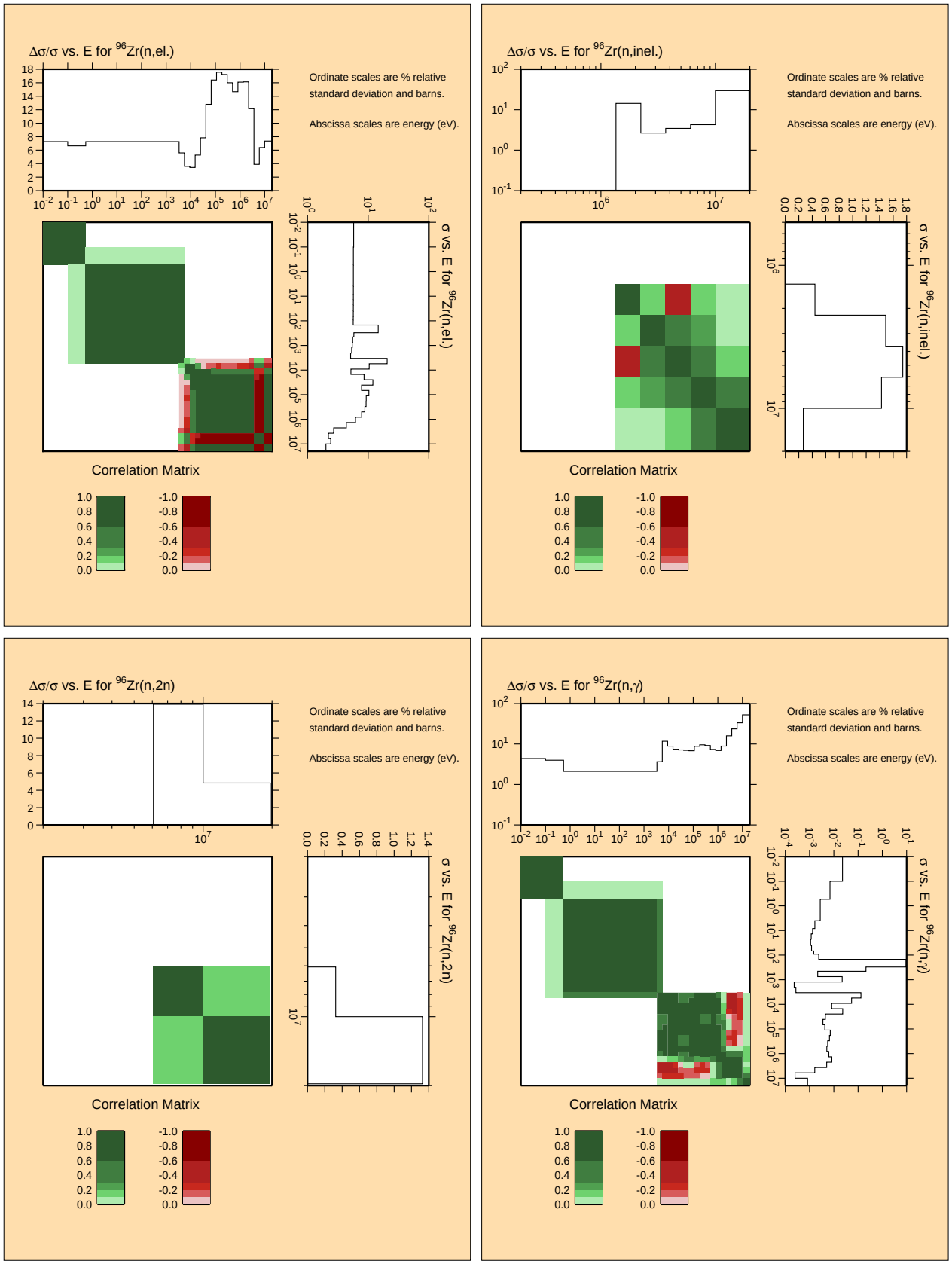

Figure A.36: Covariances for fission product ^{96}Zr.

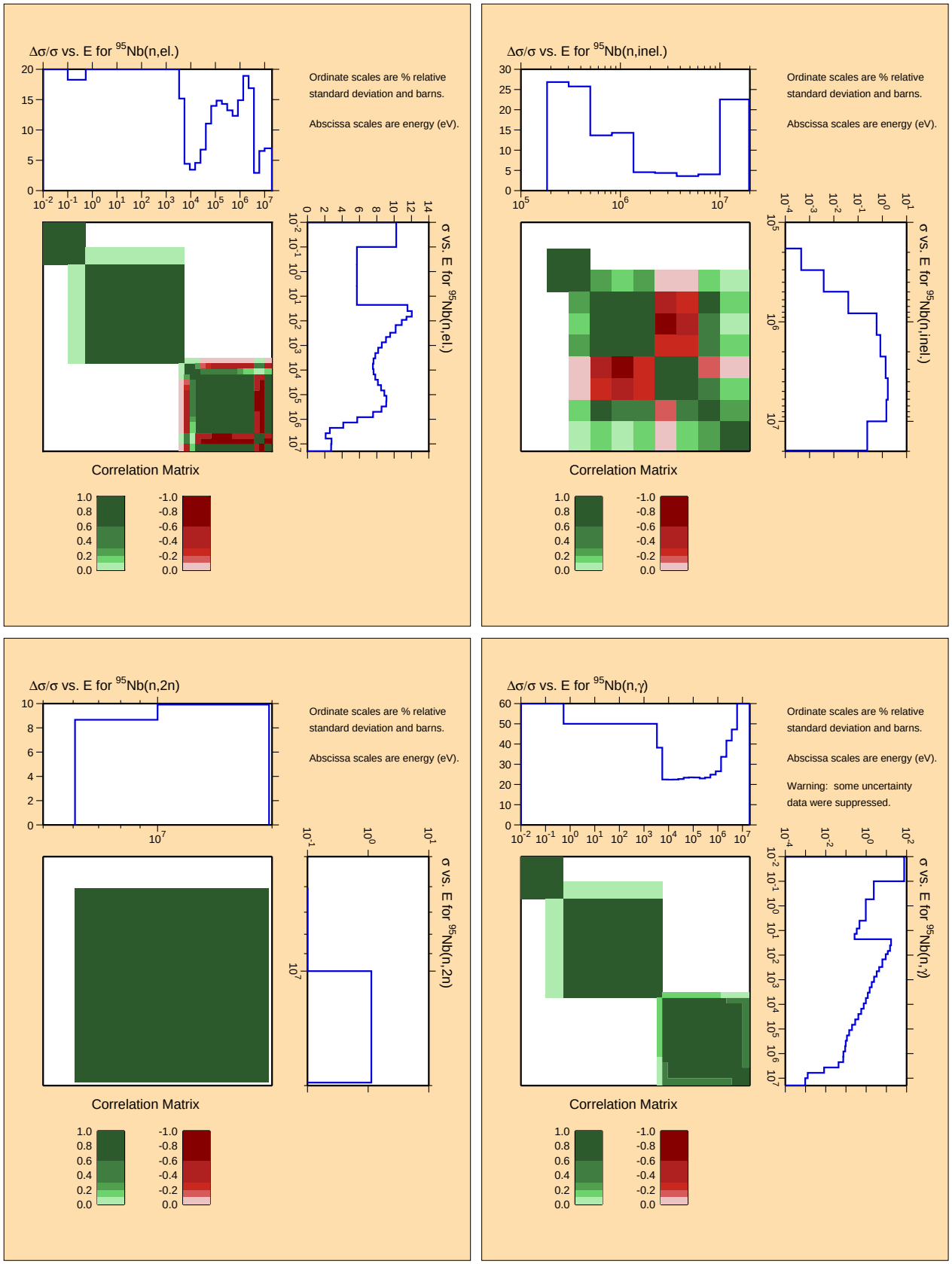

Figure A.37: Covariances for fission product ^{95}Nb.

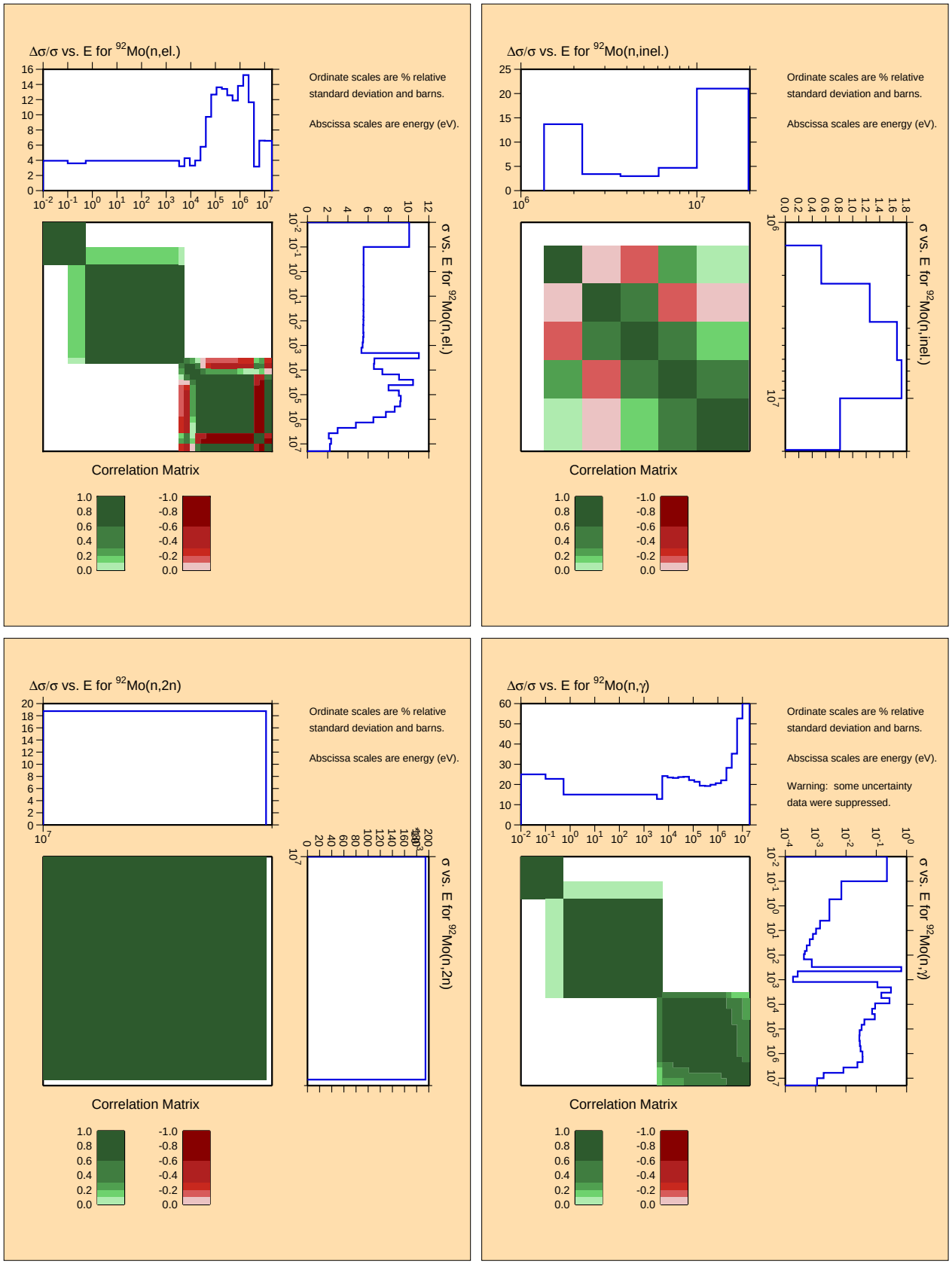

Figure A.38: Covariances for structural material ^{92}Mo.

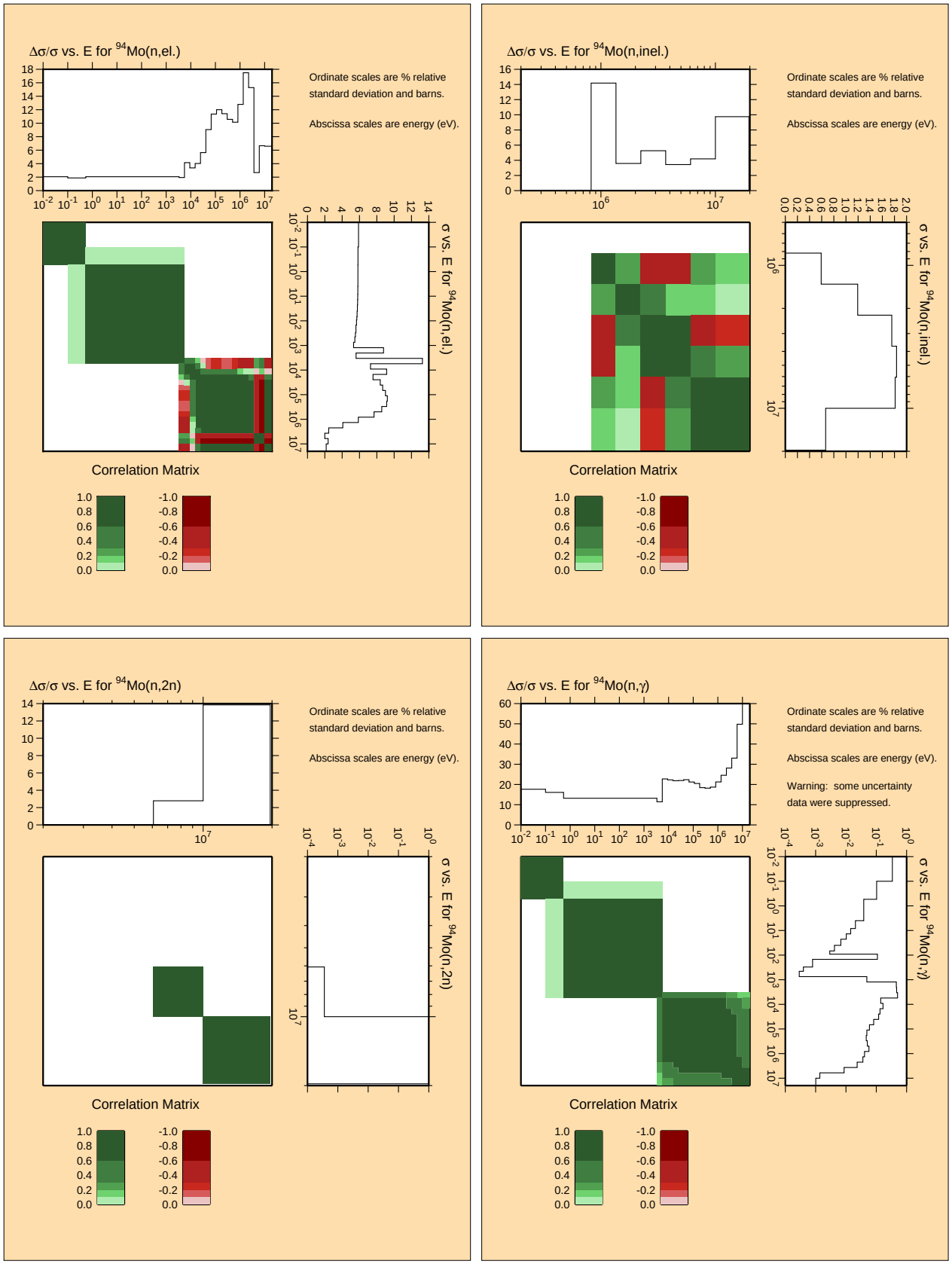

Figure A.39: Covariances for structural material ^{94}Mo.

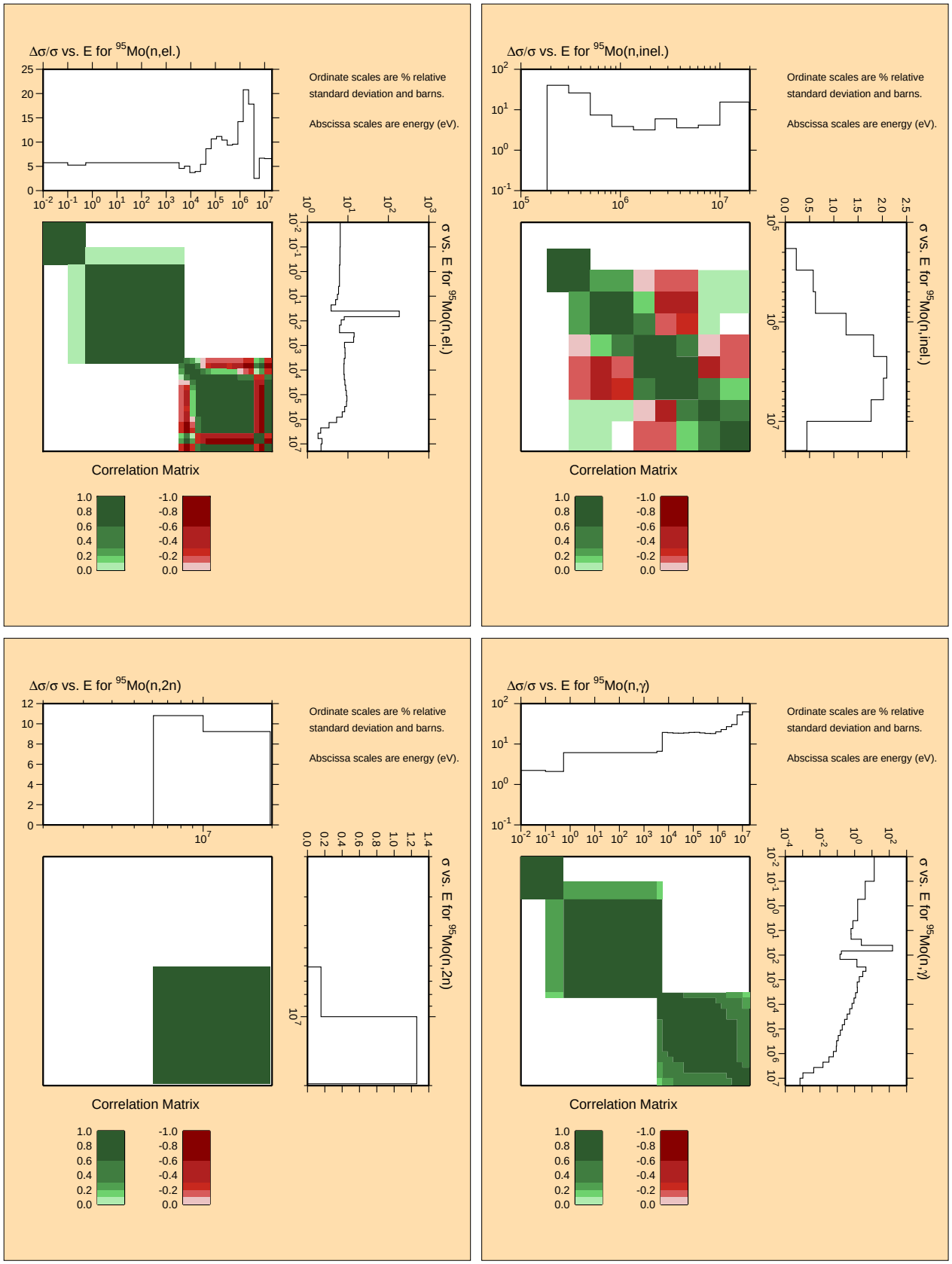

Figure A.40: Covariances for structural material ^{95}Mo.

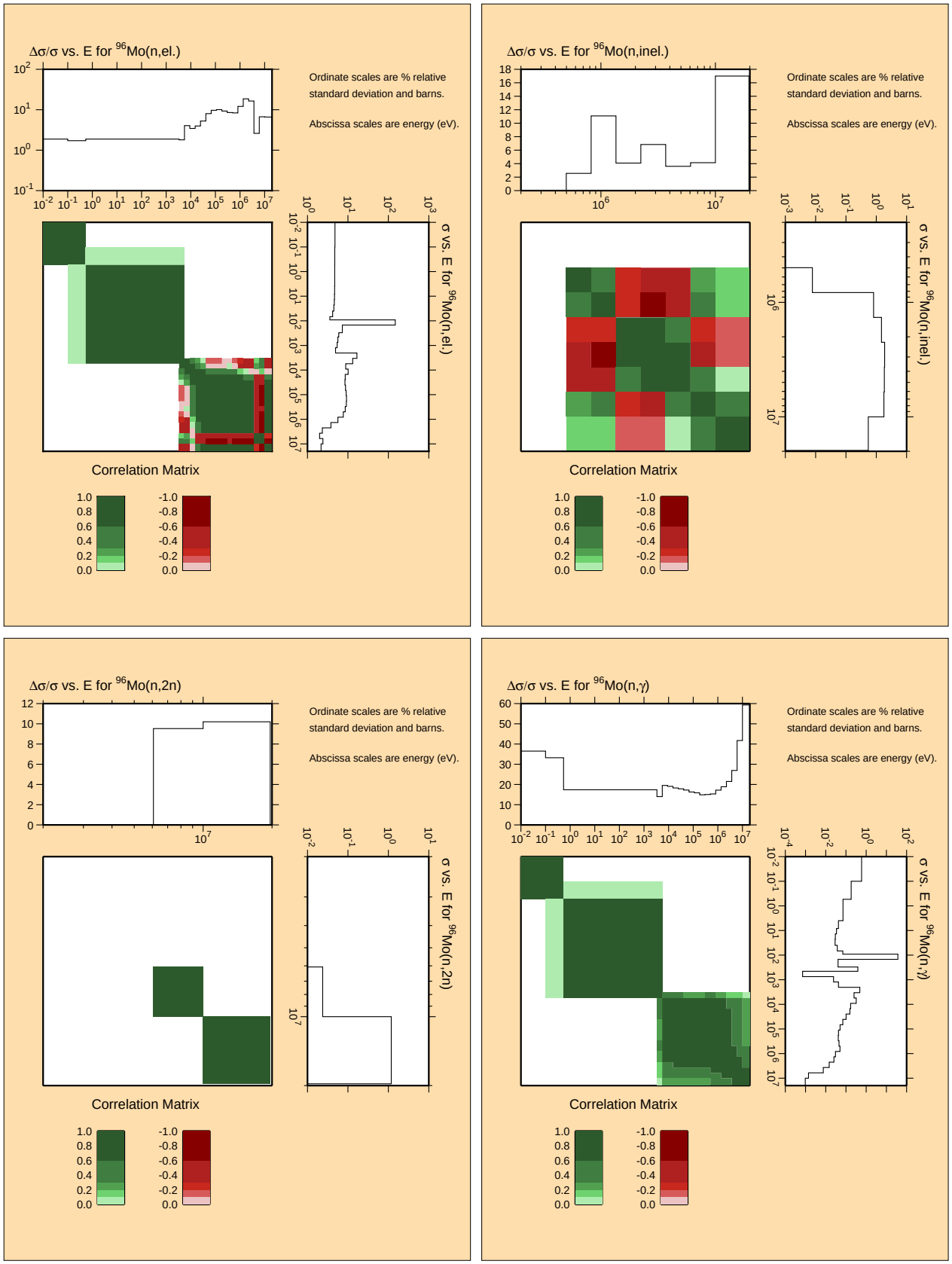

Figure A.41: Covariances for structural material ^{96}Mo.

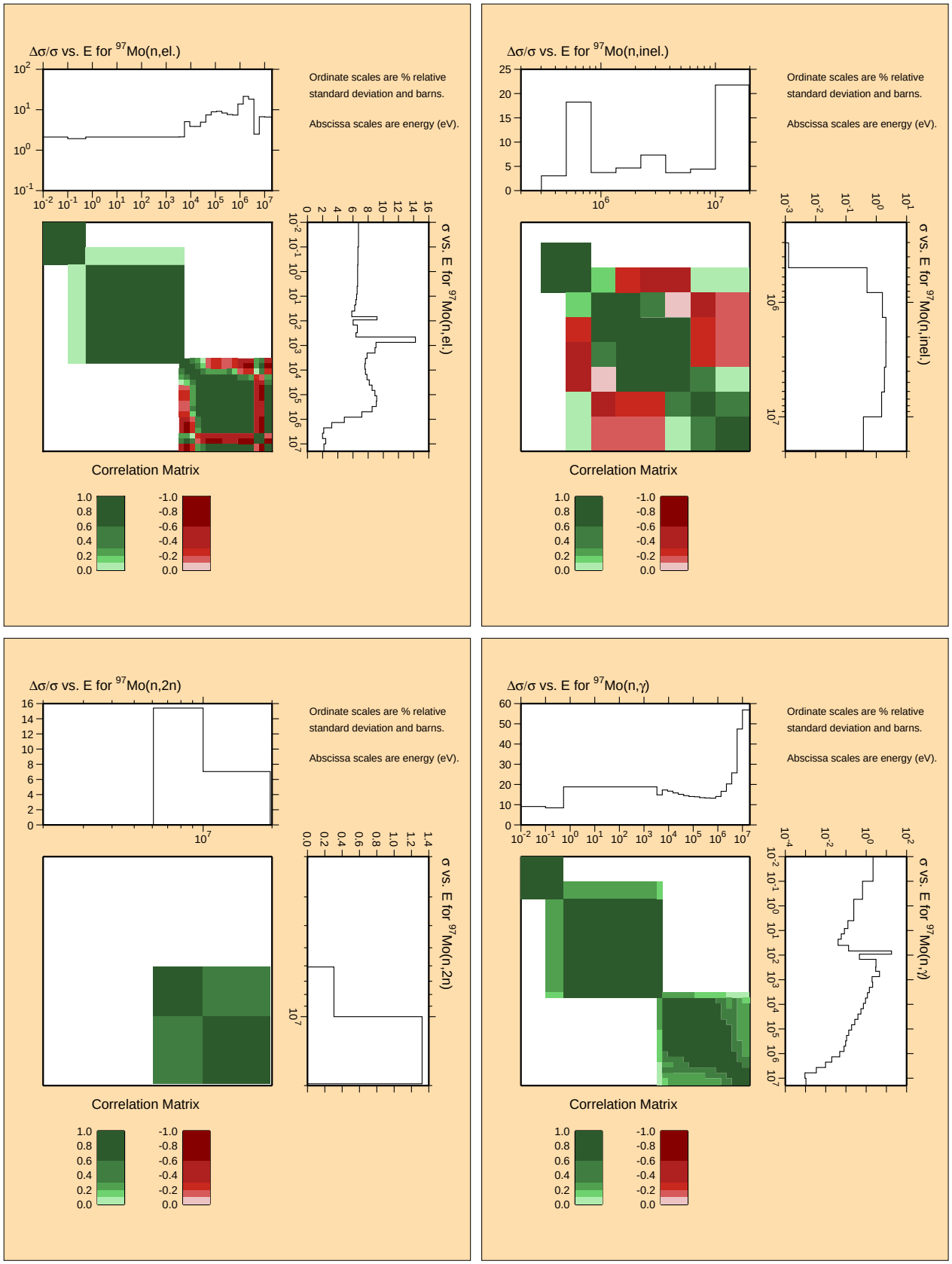

Figure A.42: Covariances for structural material ^{97}Mo.

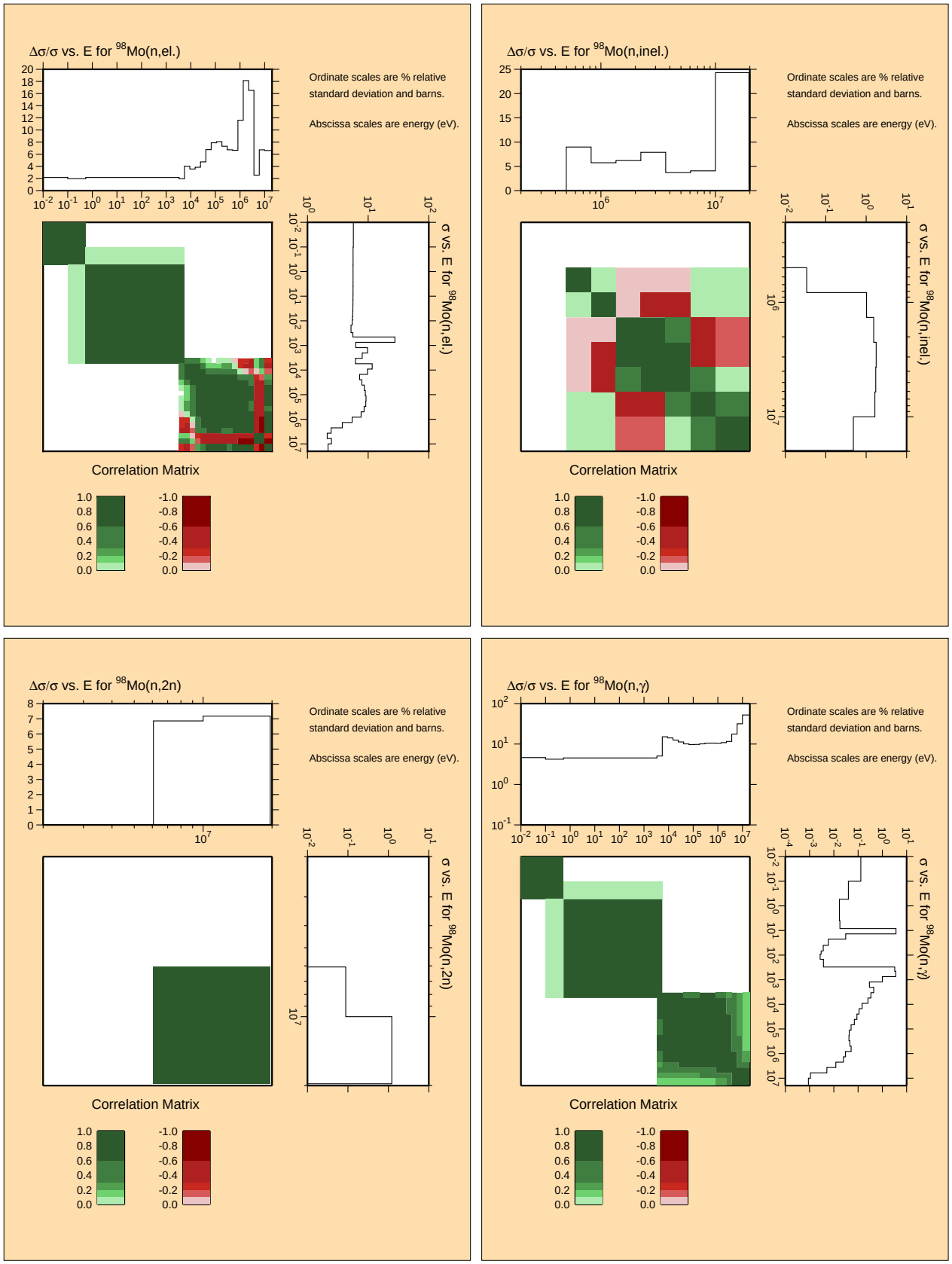

Figure A.43: Covariances for structural material ^{98}Mo.

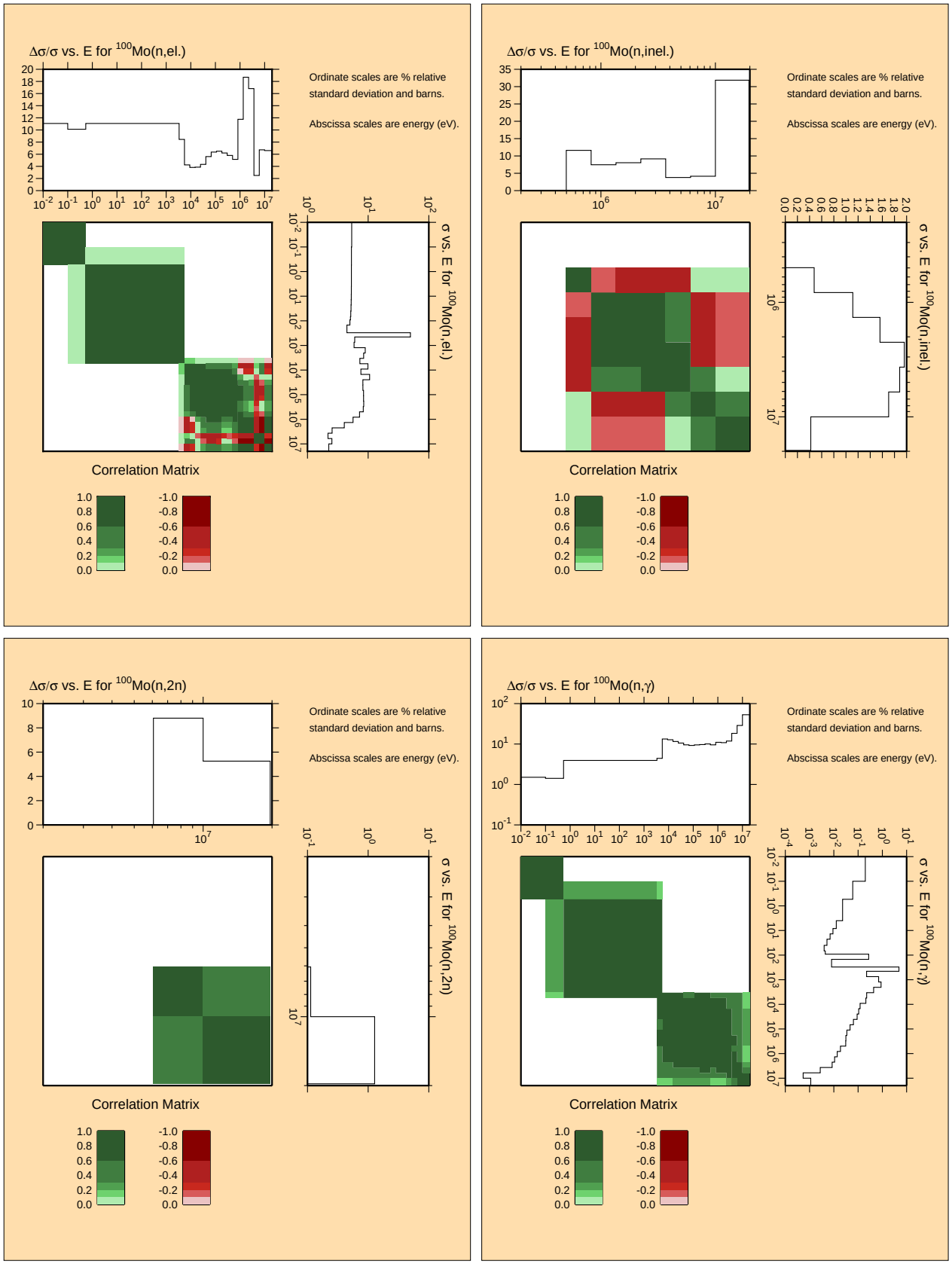

Figure A.44: Covariances for structural material ^{100}Mo.

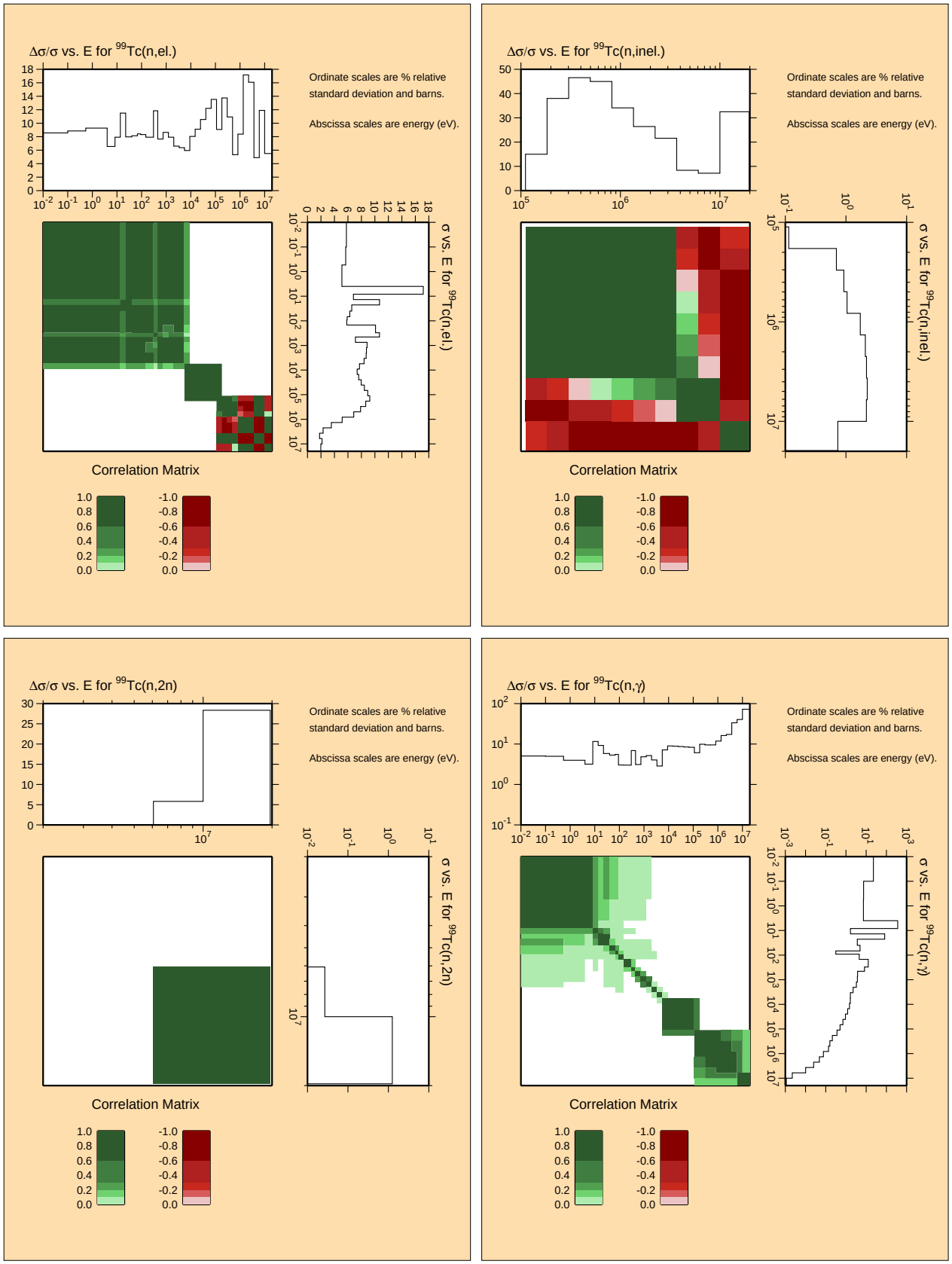

Figure A.45: Covariances for fission product ^{99}Tc.

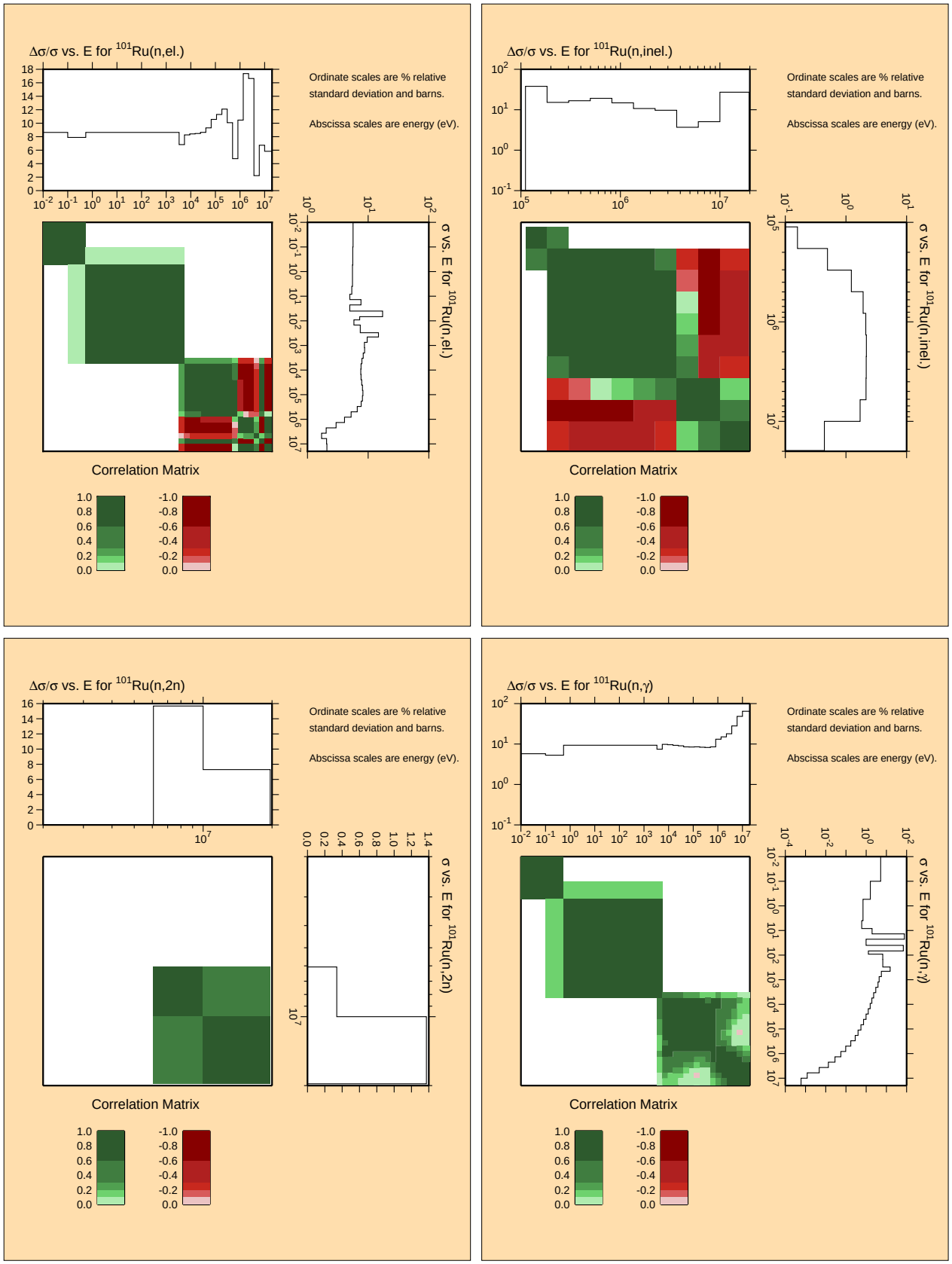

Figure A.46: Covariances for fission product ^{101}Ru.

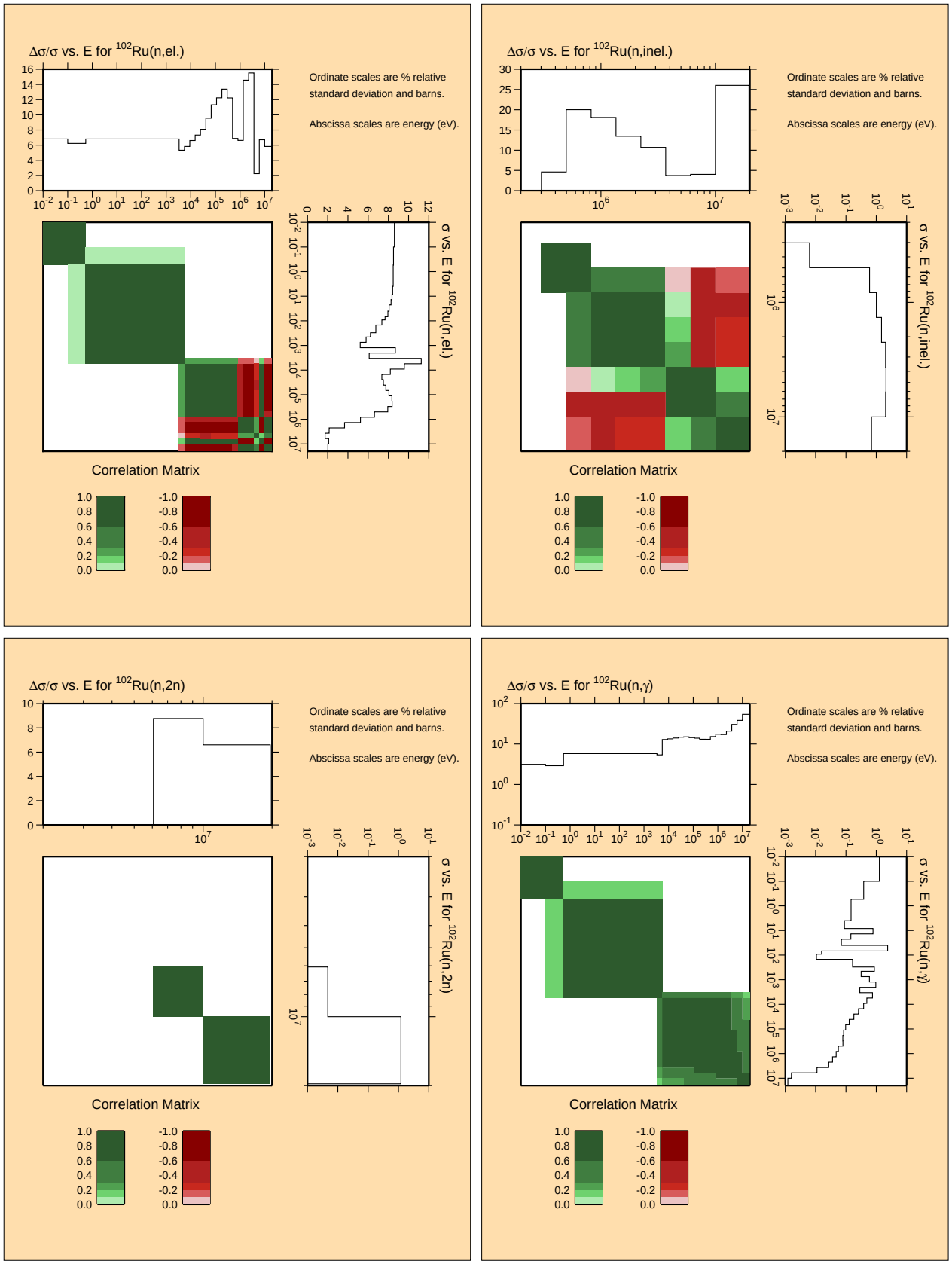

Figure A.47: Covariances for fission product ^{102}Ru.

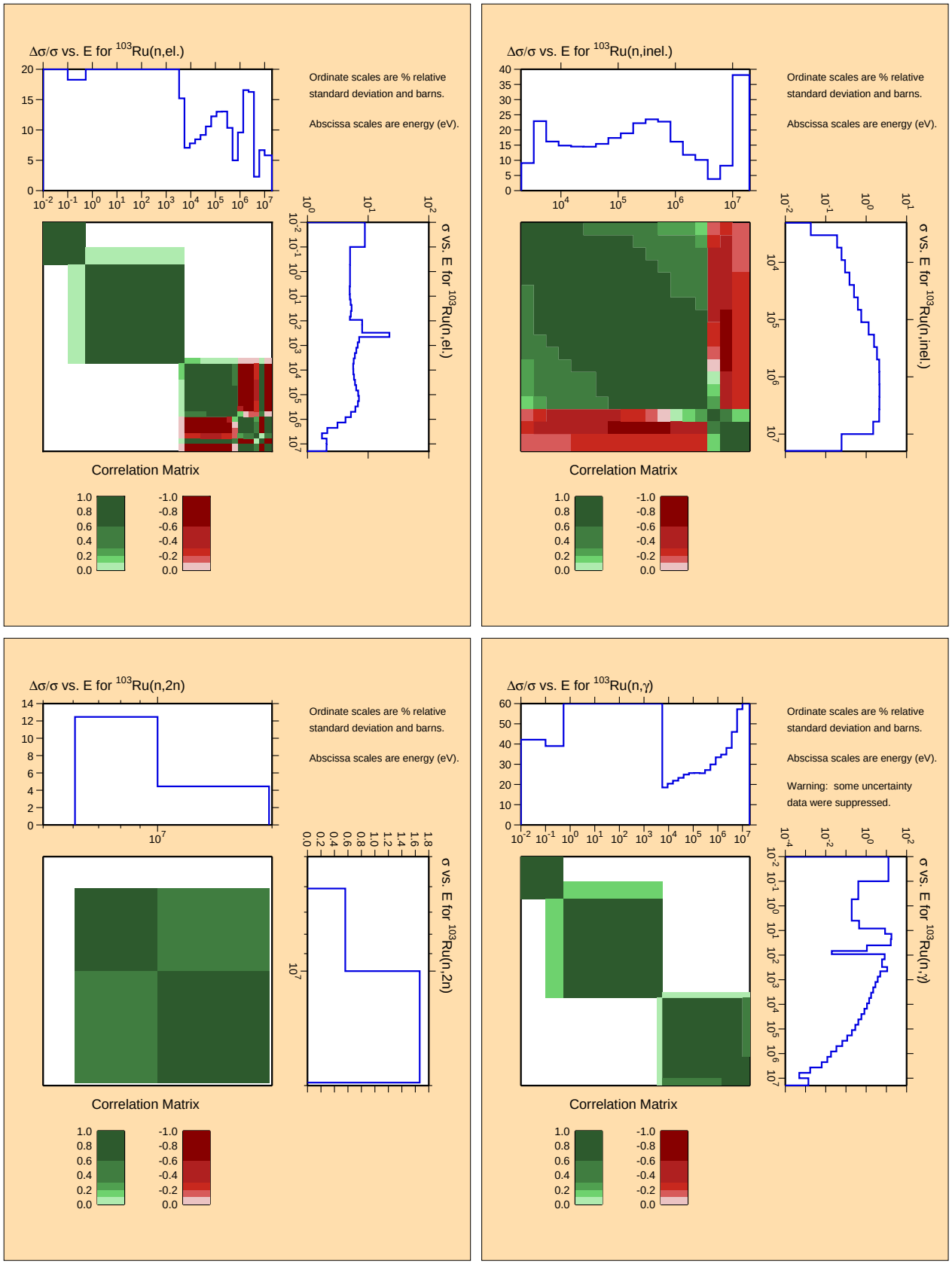

Figure A.48: Covariances for fission product ^{103}Ru.

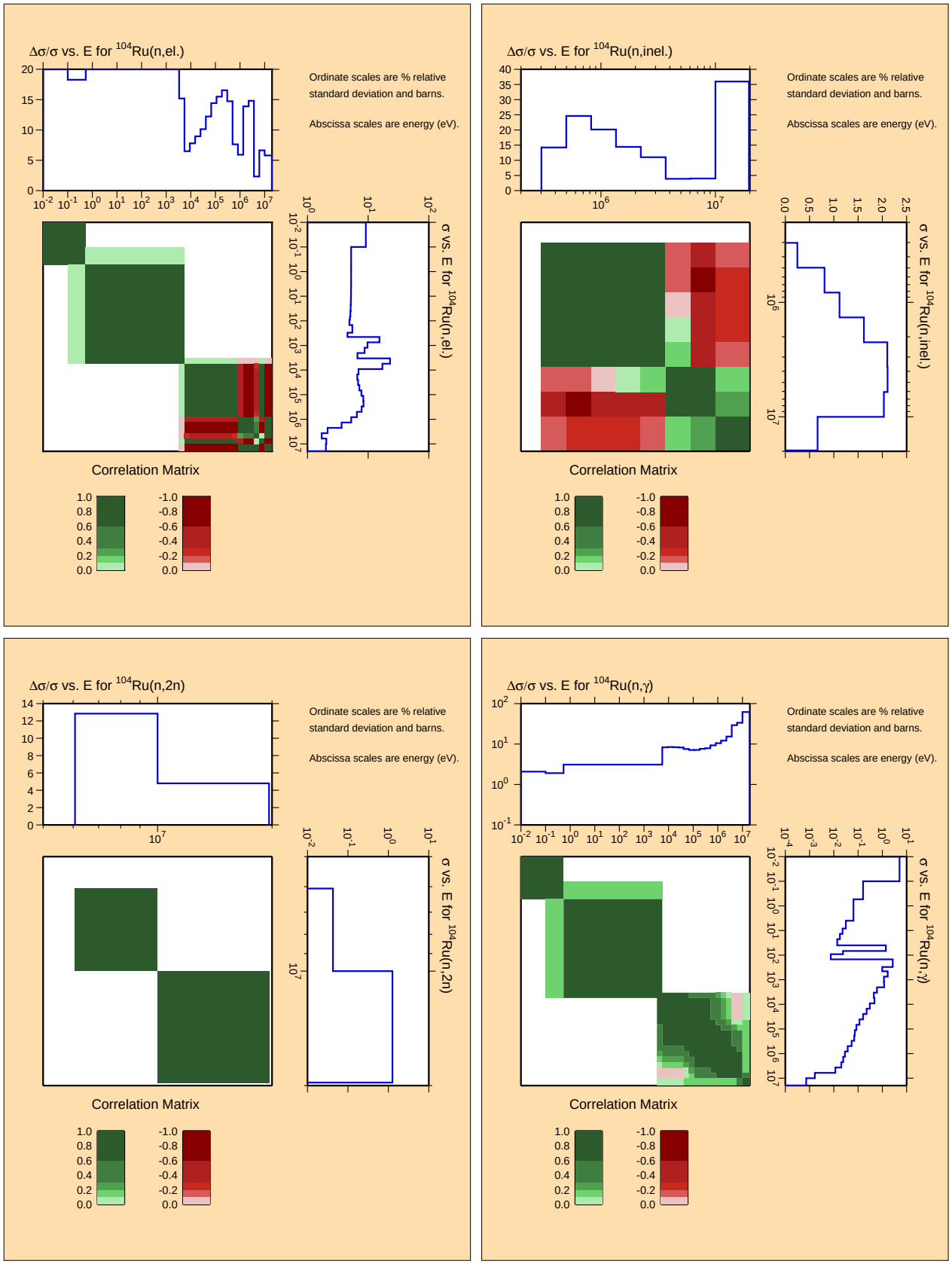

Figure A.49: Covariances for fission product ^{104}Ru.

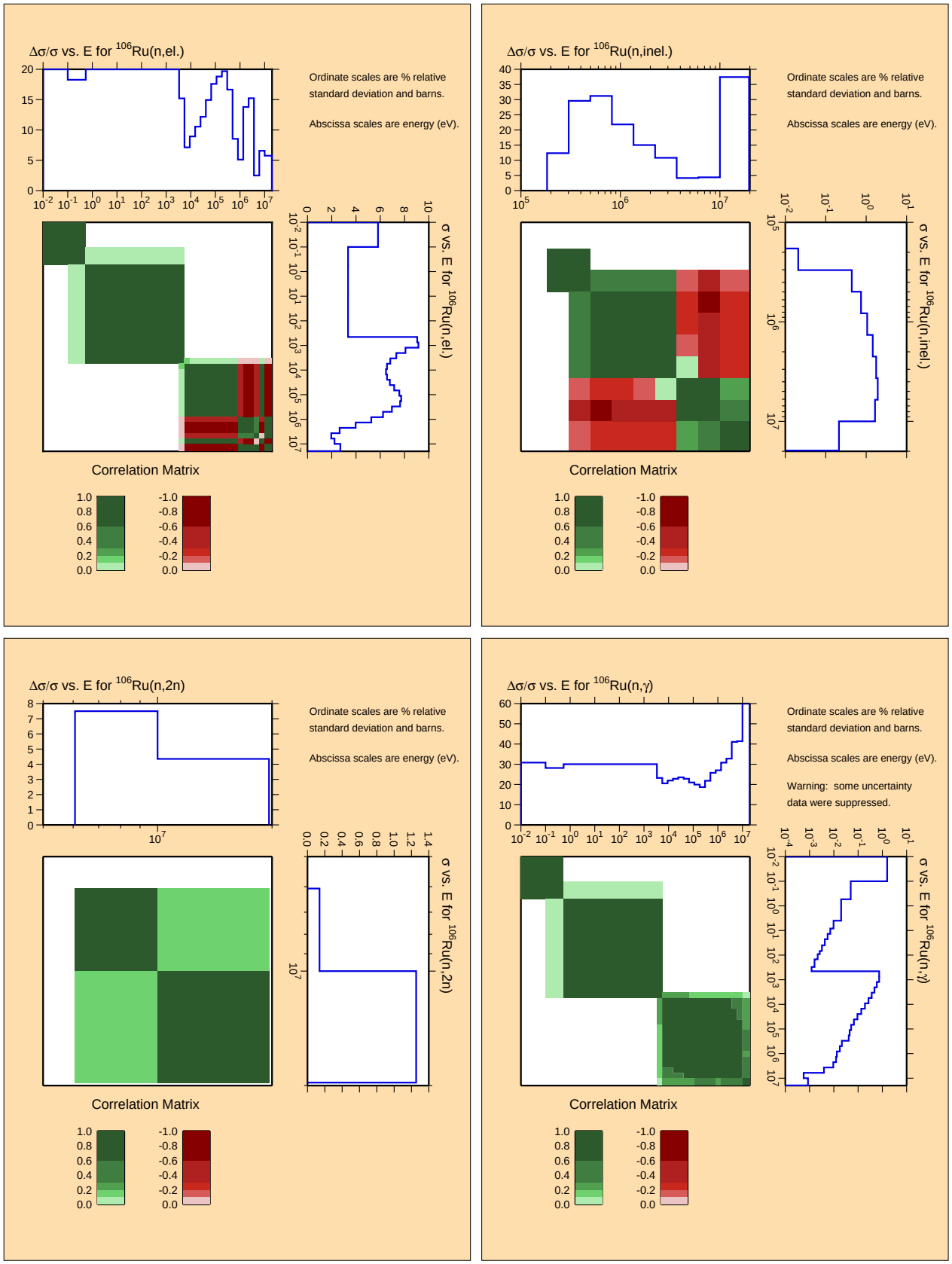

Figure A.50: Covariances for fission product ^{106}Ru.

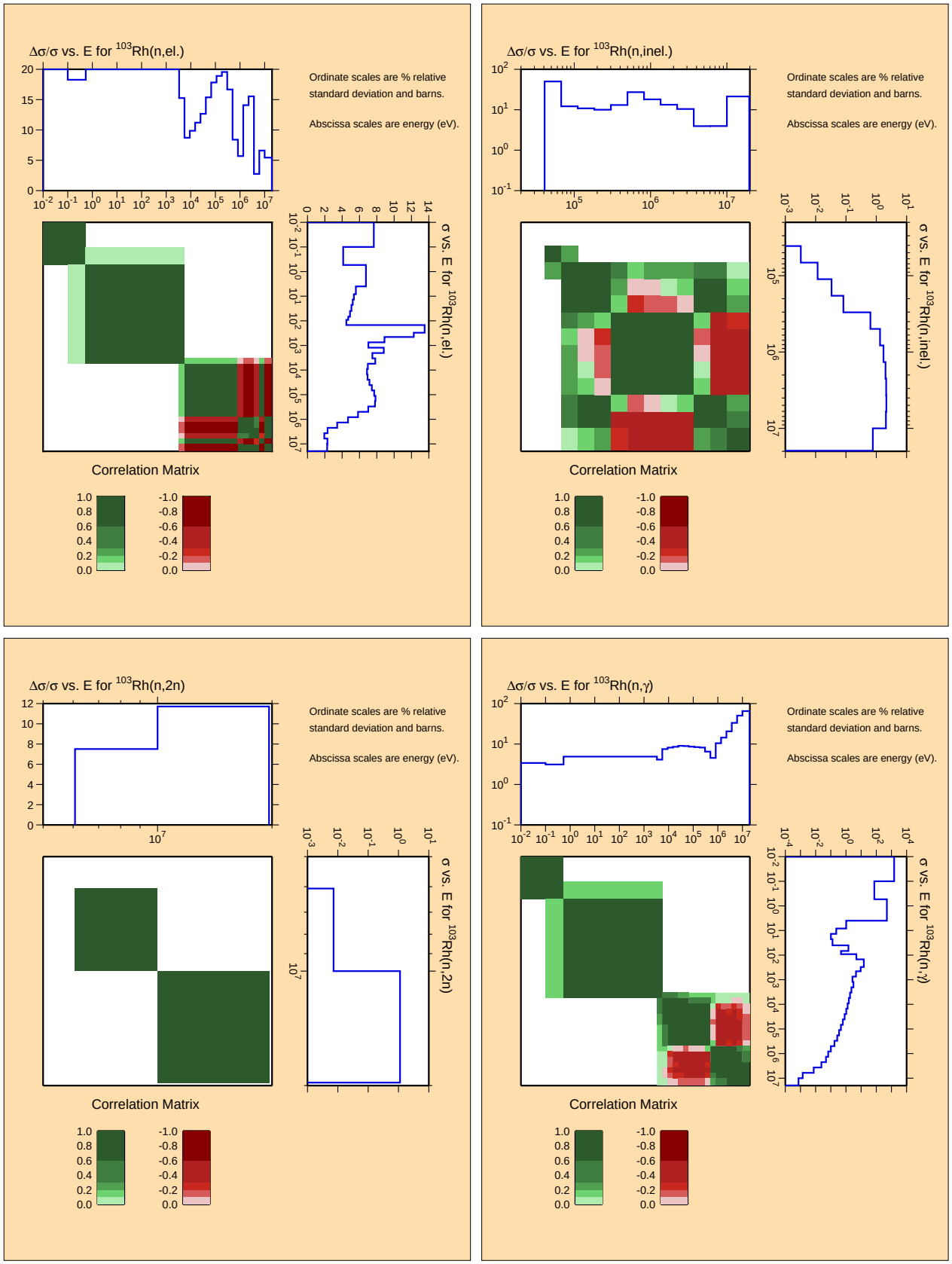

Figure A.51: Covariances for fission product ^{103}Rh.

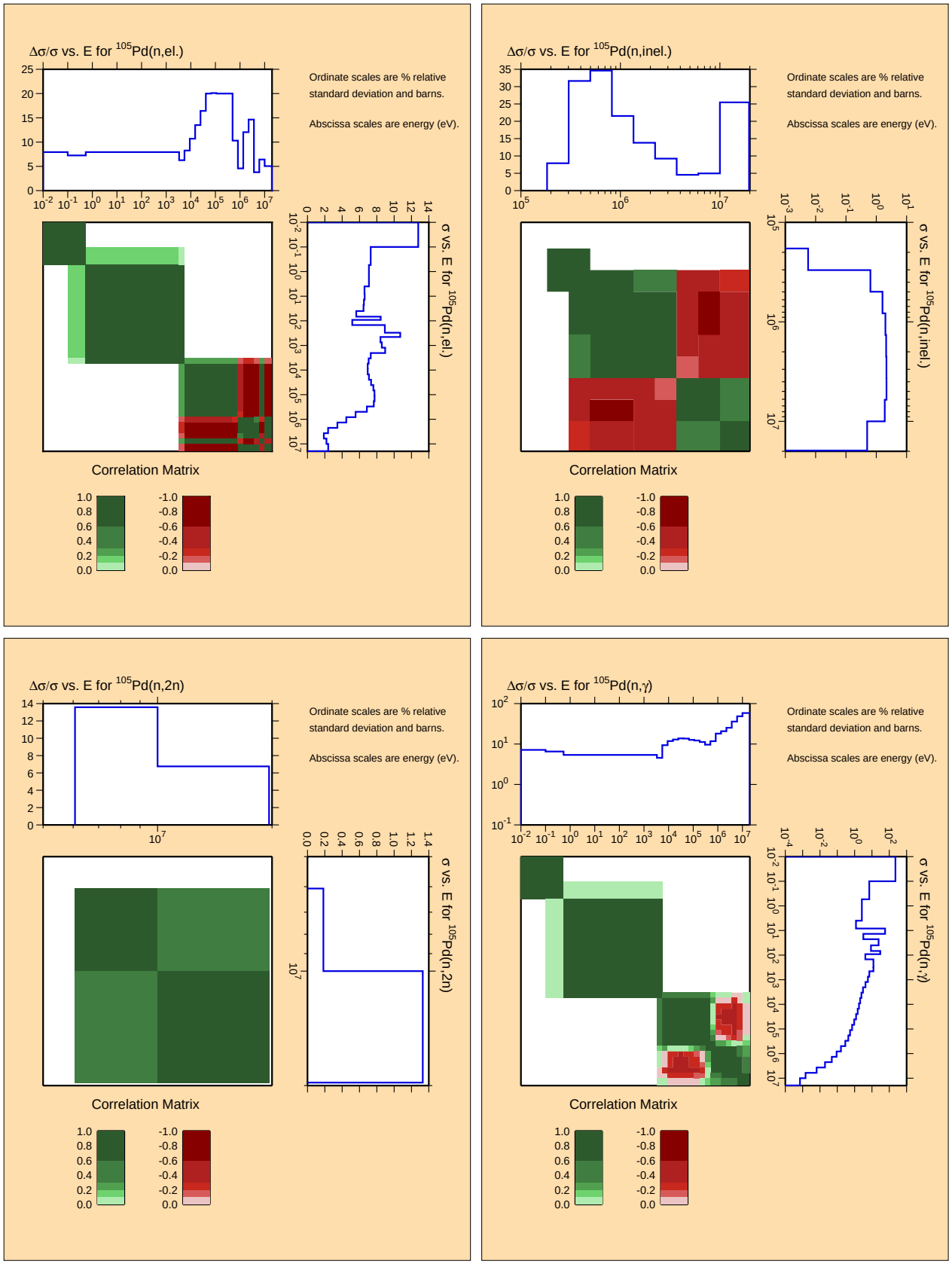

Figure A.52: Covariances for fission product ^{105}Pd.

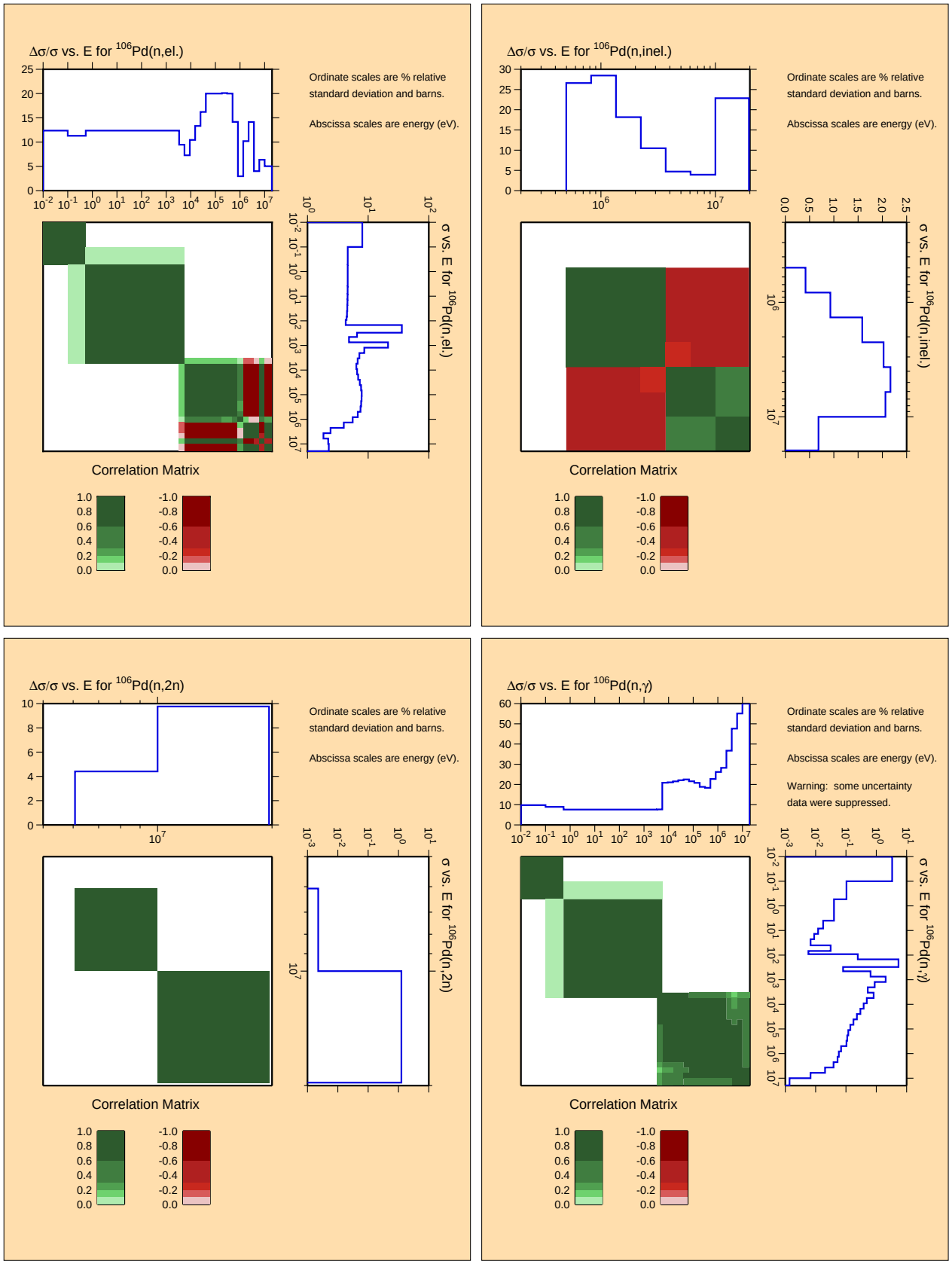

Figure A.53: Covariances for fission product ^{106}Pd.

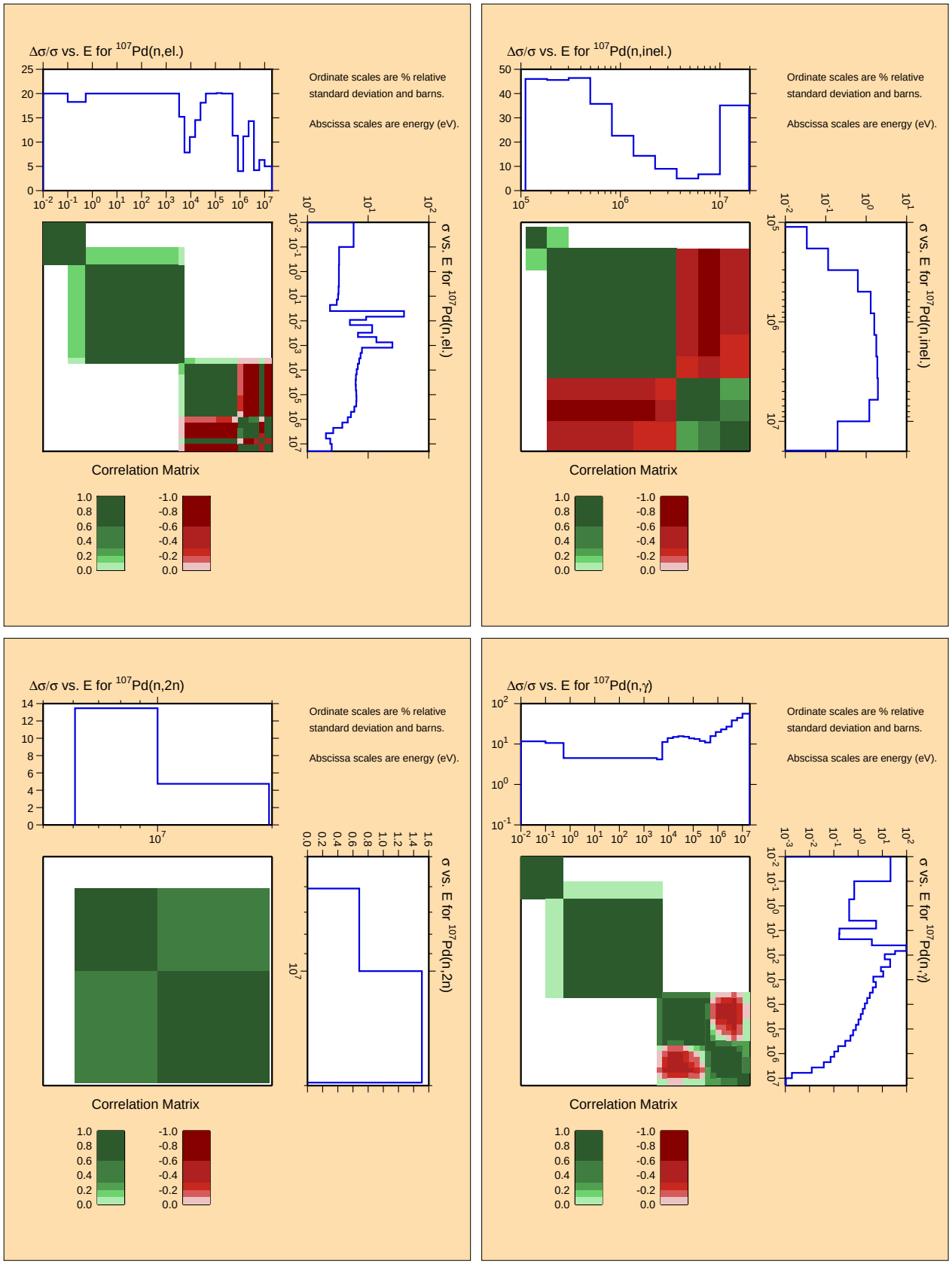

Figure A.54: Covariances for fission product ^{107}Pd.

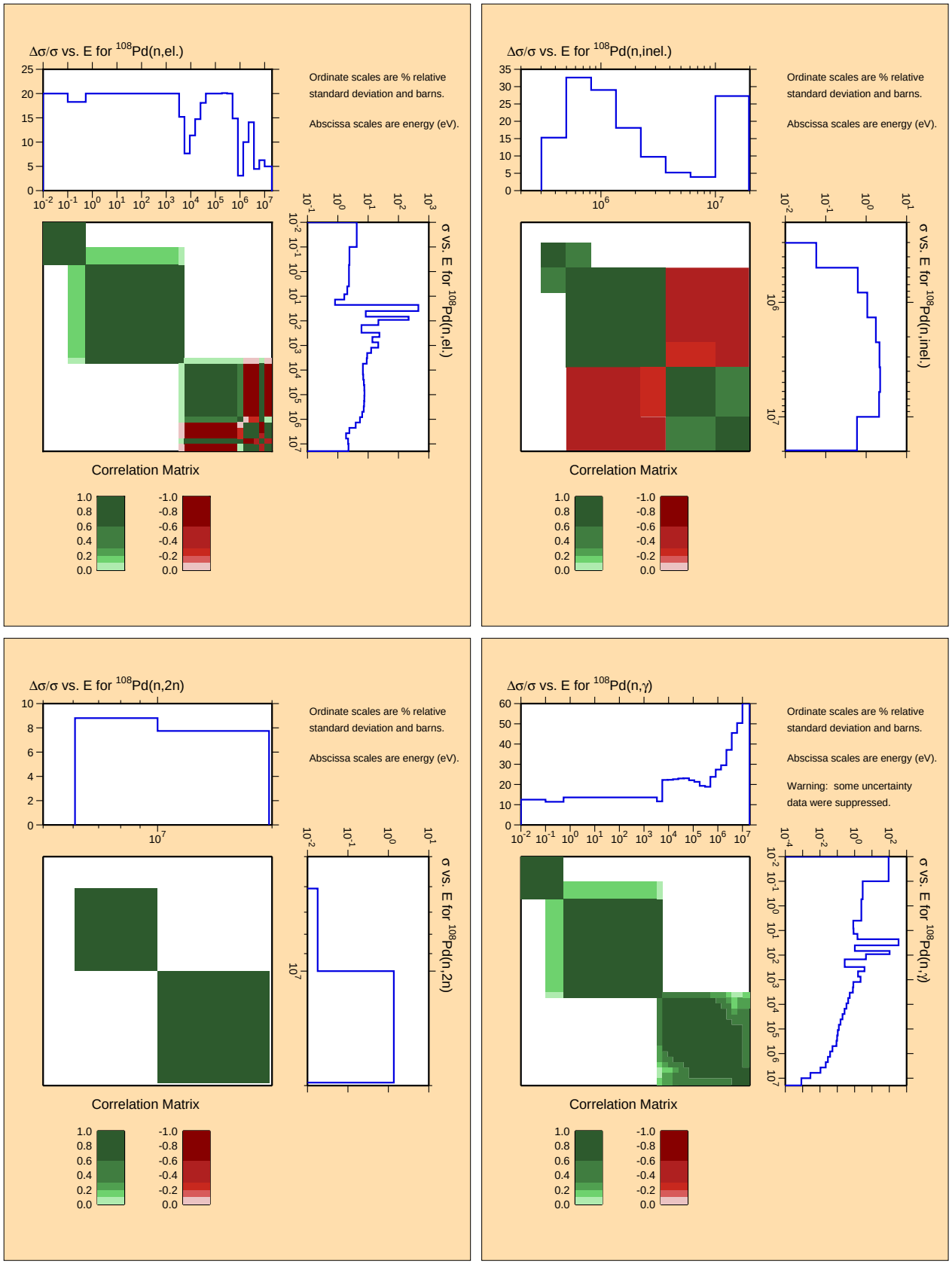

Figure A.55: Covariances for fission product ^{108}Pd.

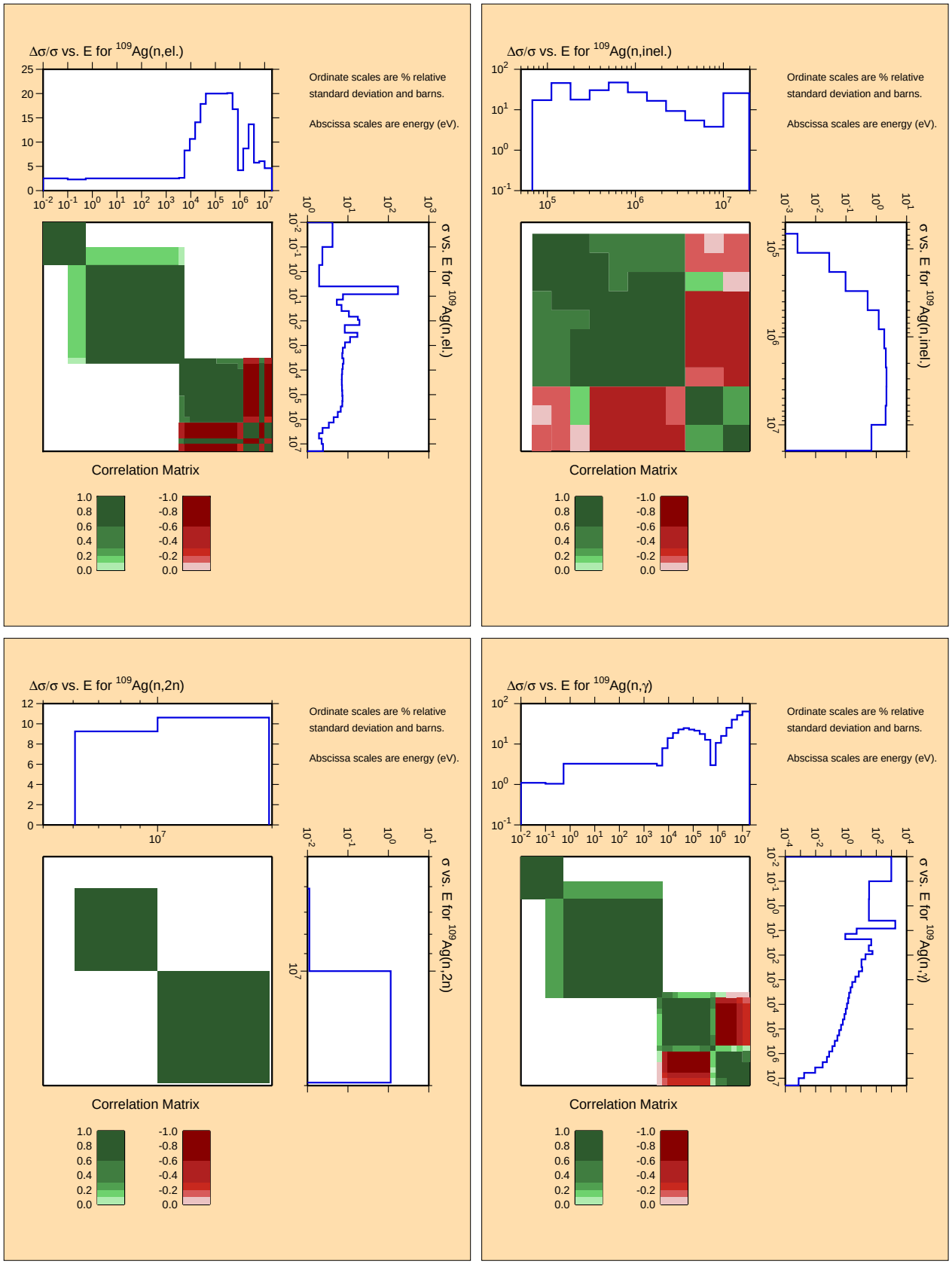

Figure A.56: Covariances for fission product ^{109}Ag.

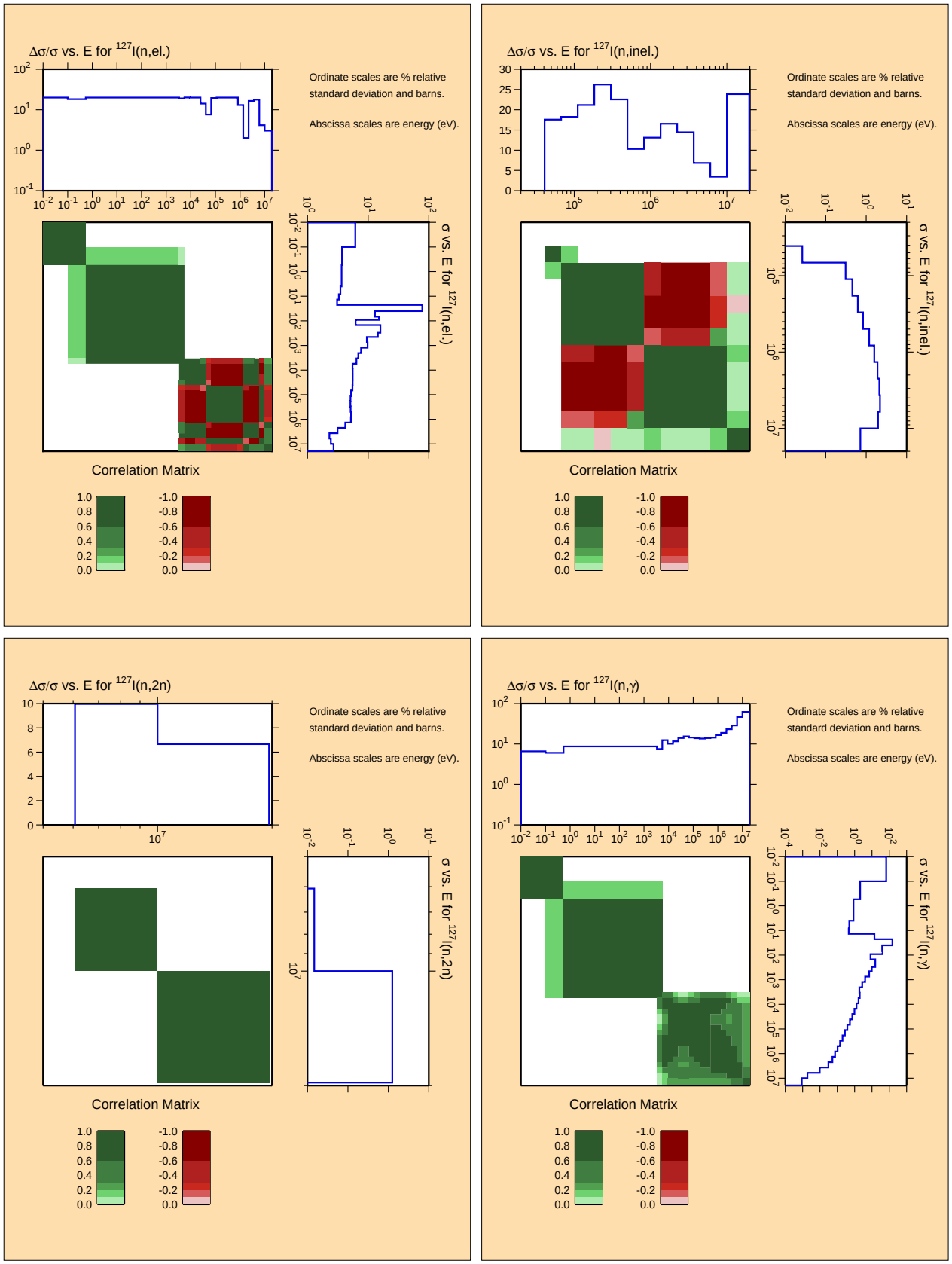

Figure A.57: Covariances for fission product ^{127}I.

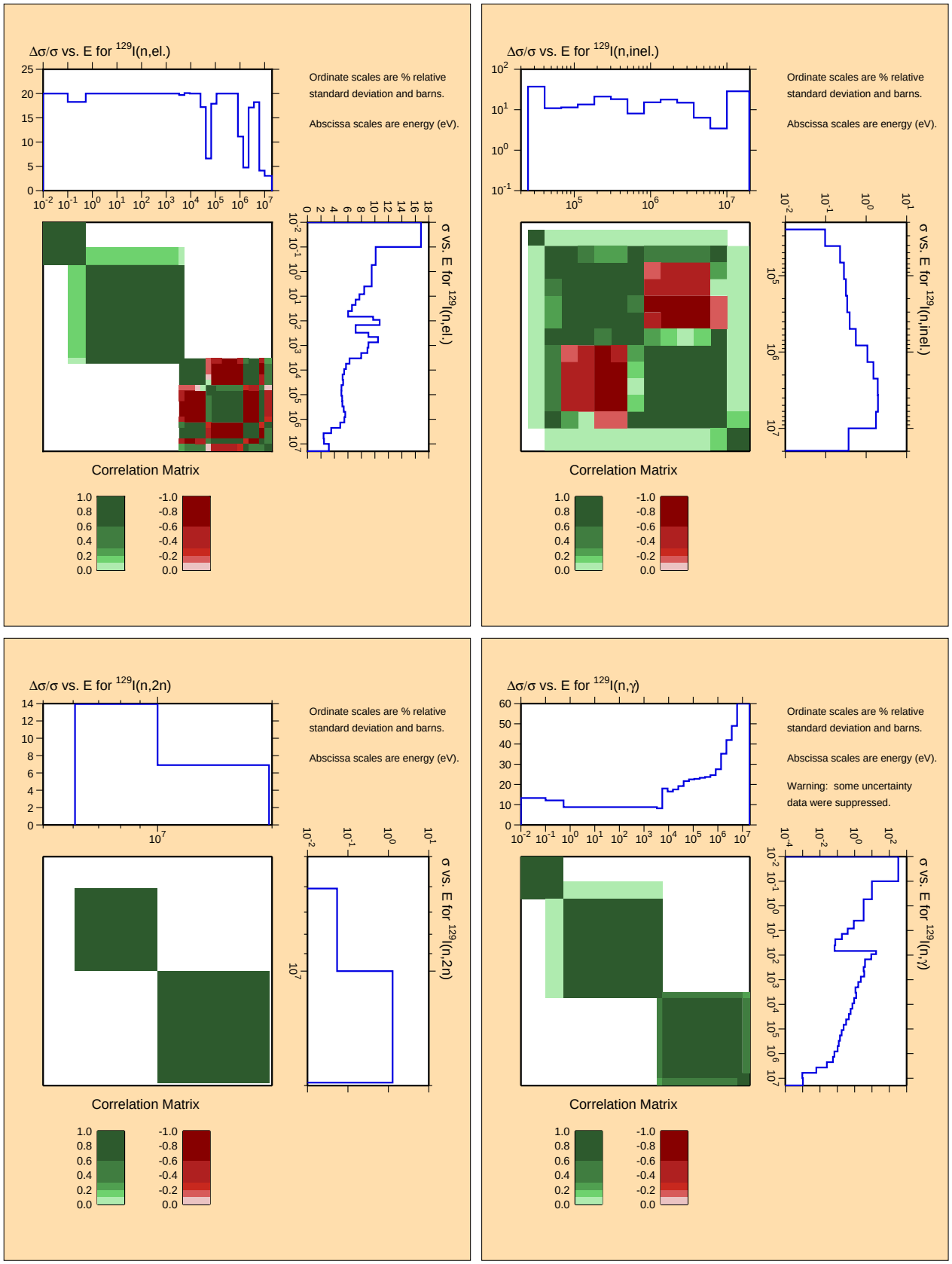

Figure A.58: Covariances for fission product ^{129}I.

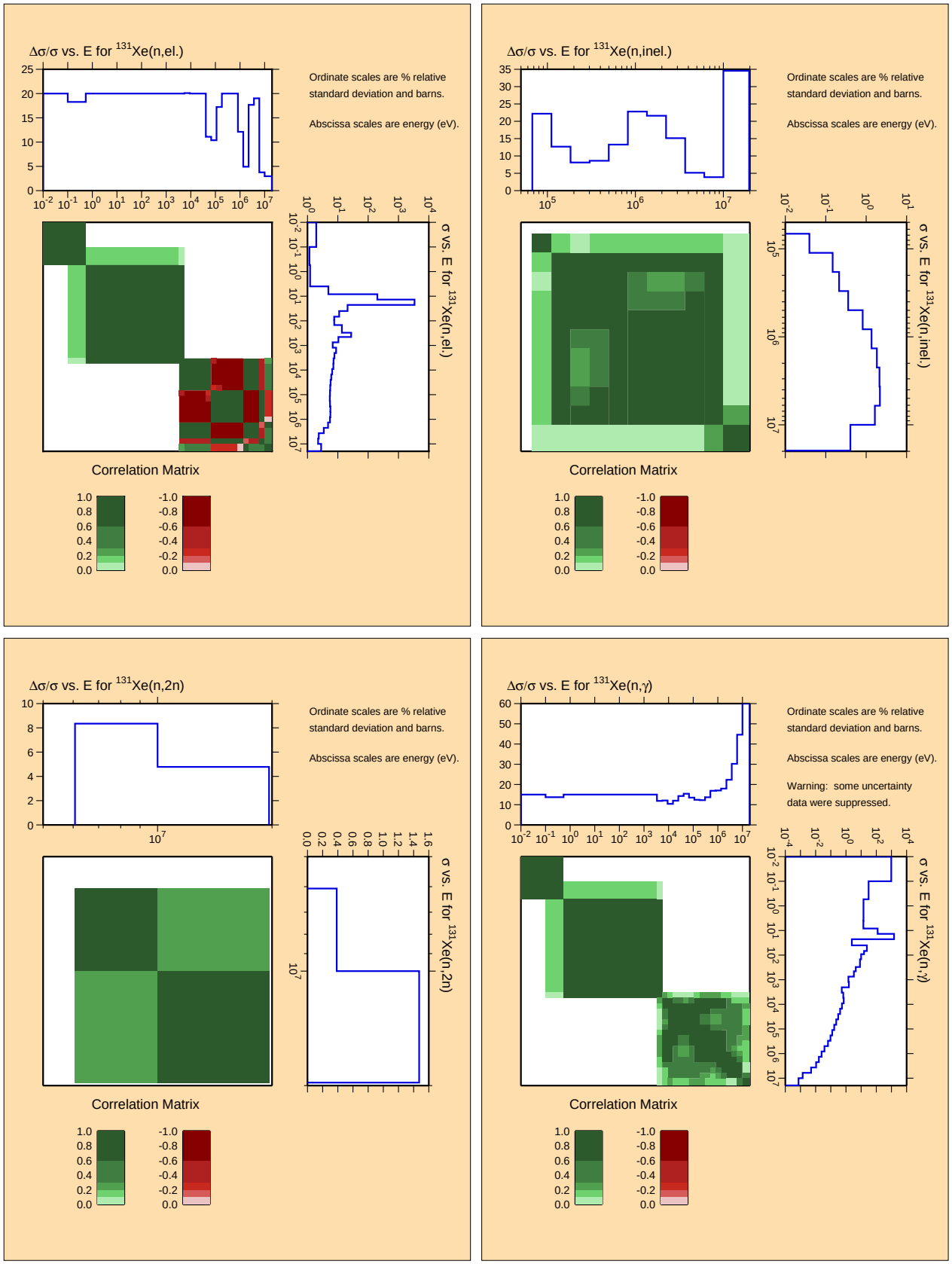

Figure A.59: Covariances for fission product ^{131}Xe.

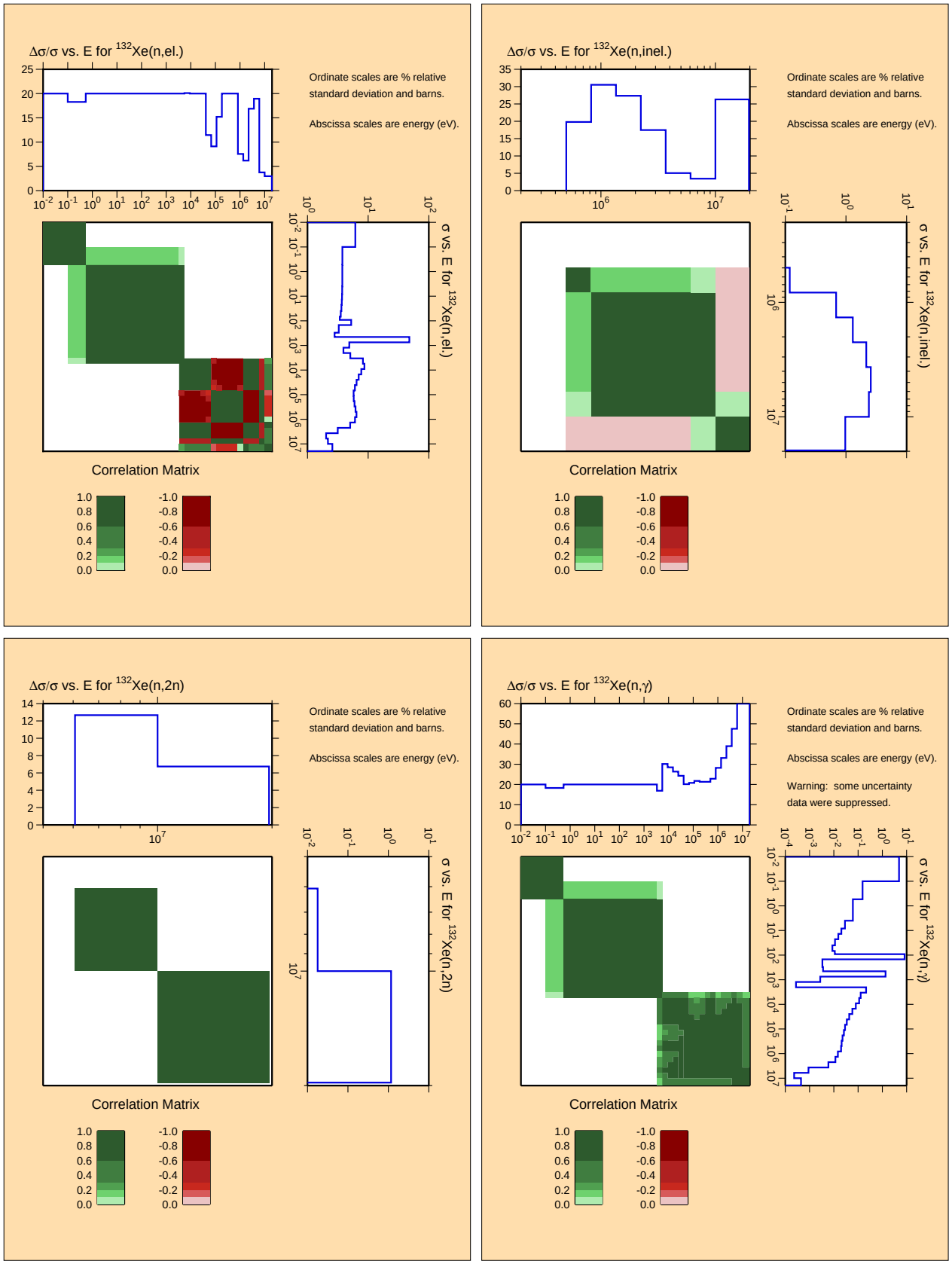

Figure A.60: Covariances for fission product ^{132}Xe.

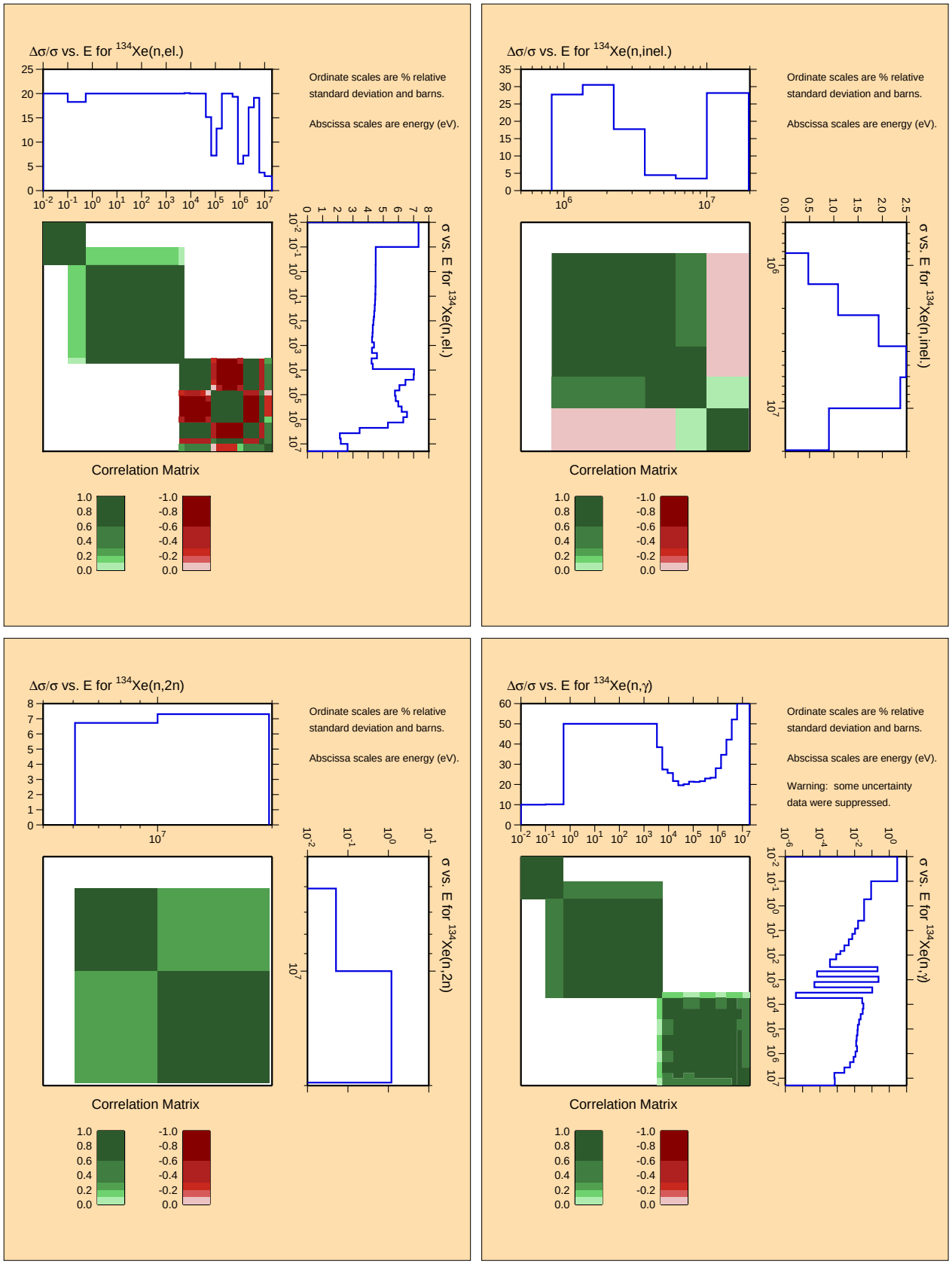

Figure A.61: Covariances for fission product ^{134}Xe.

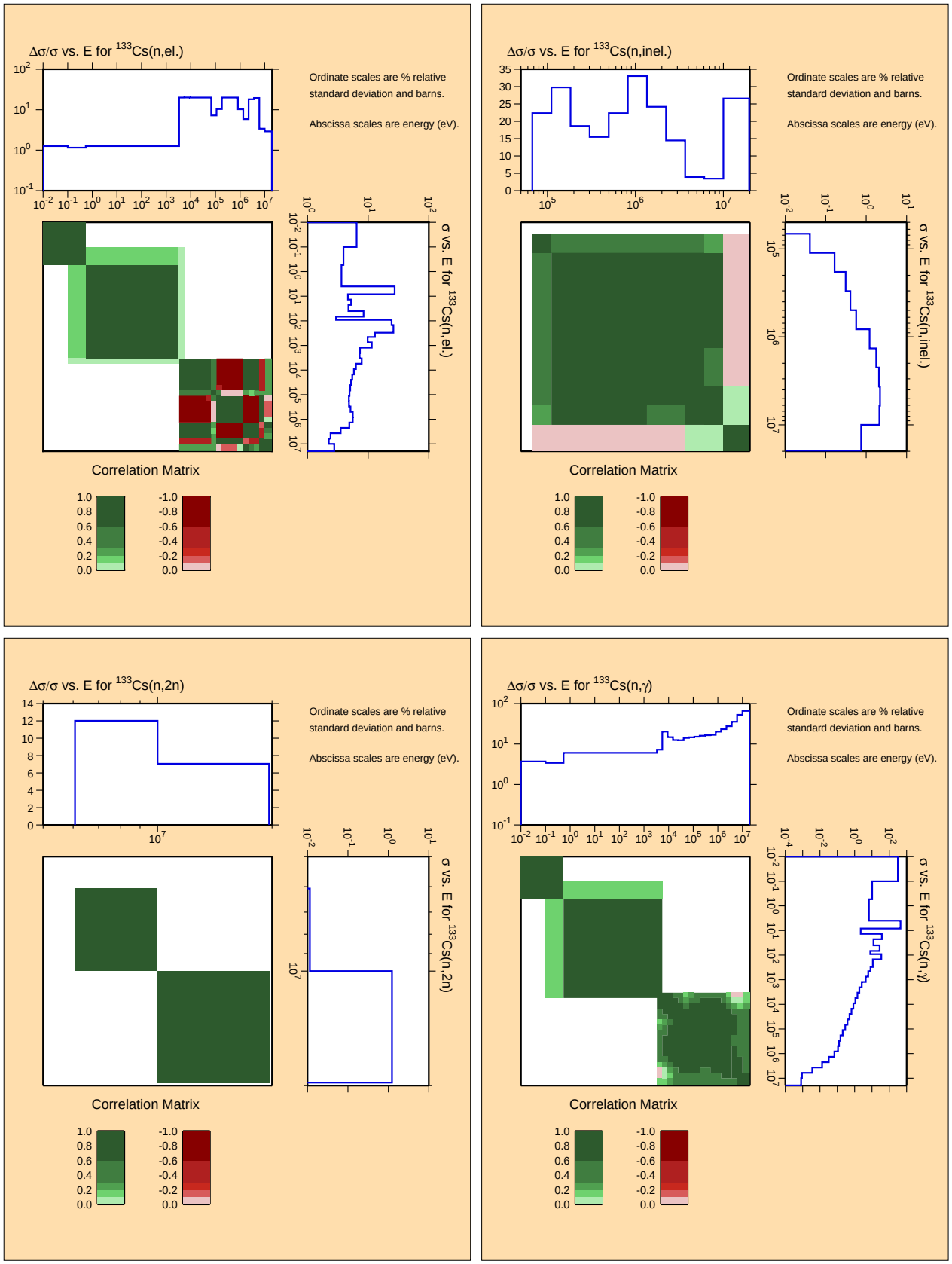

Figure A.62: Covariances for fission product ^{133}Cs.

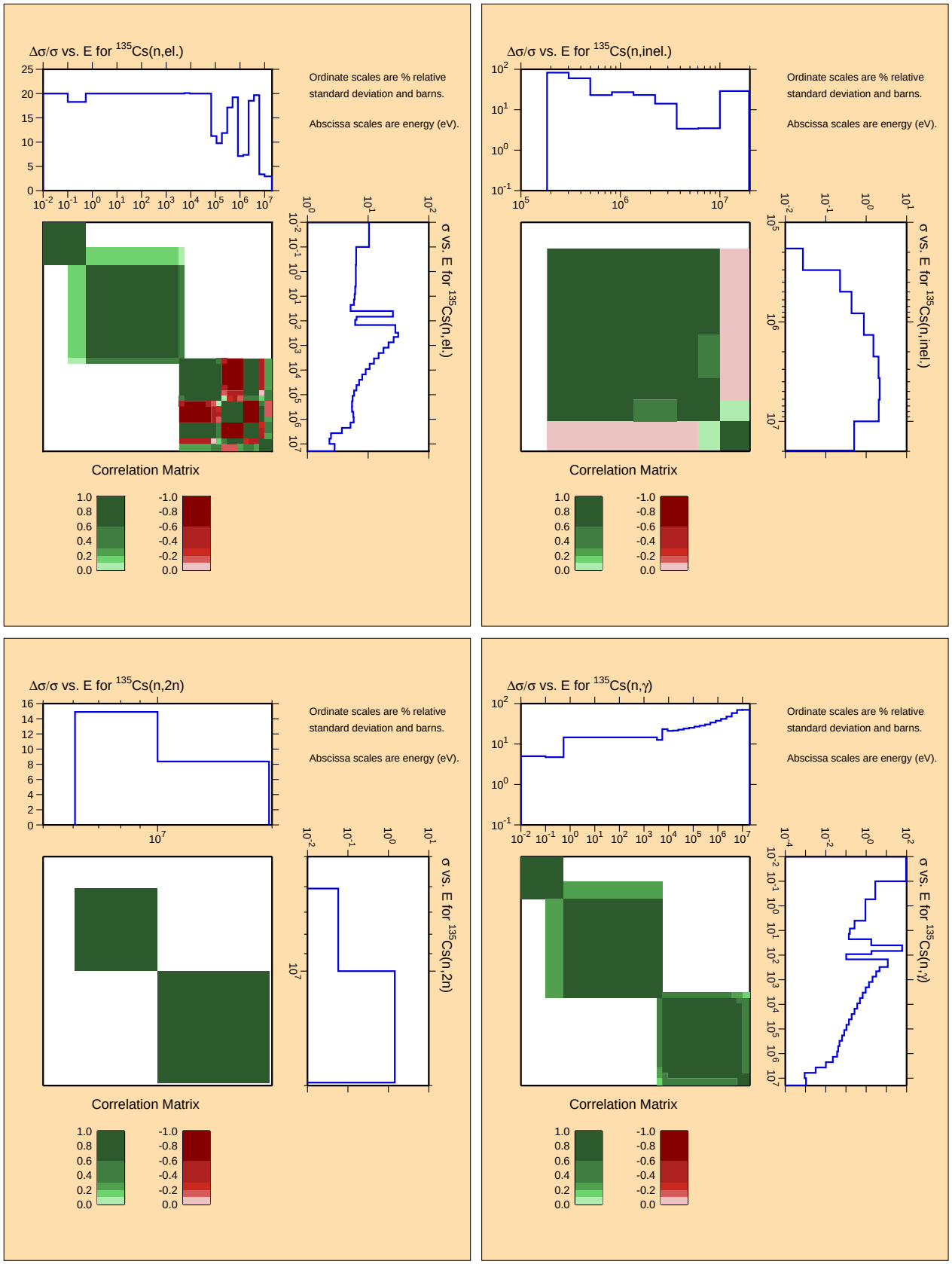

Figure A.63: Covariances for fission product ^{135}Cs.

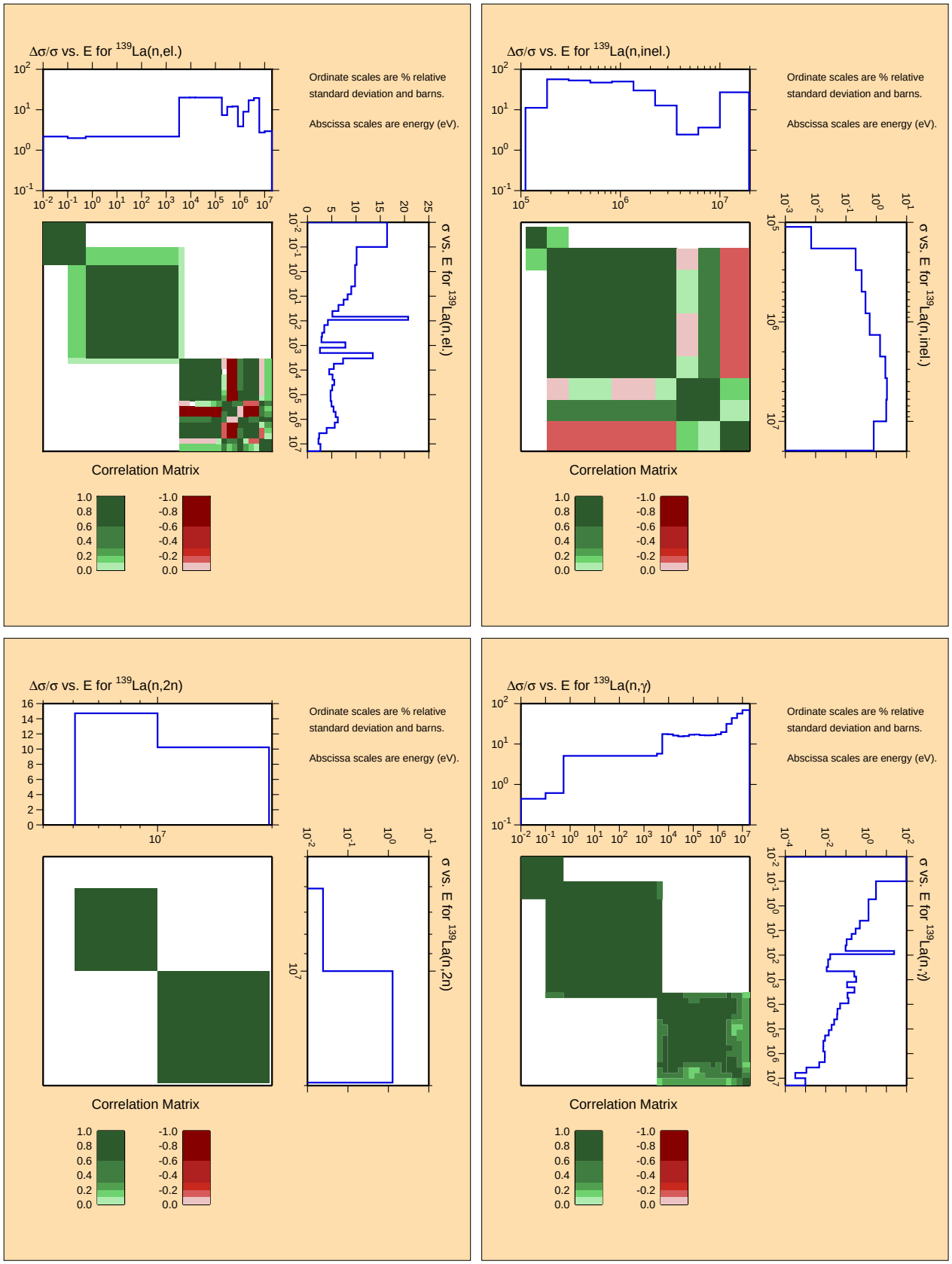

Figure A.64: Covariances for fission product ^{139}La.

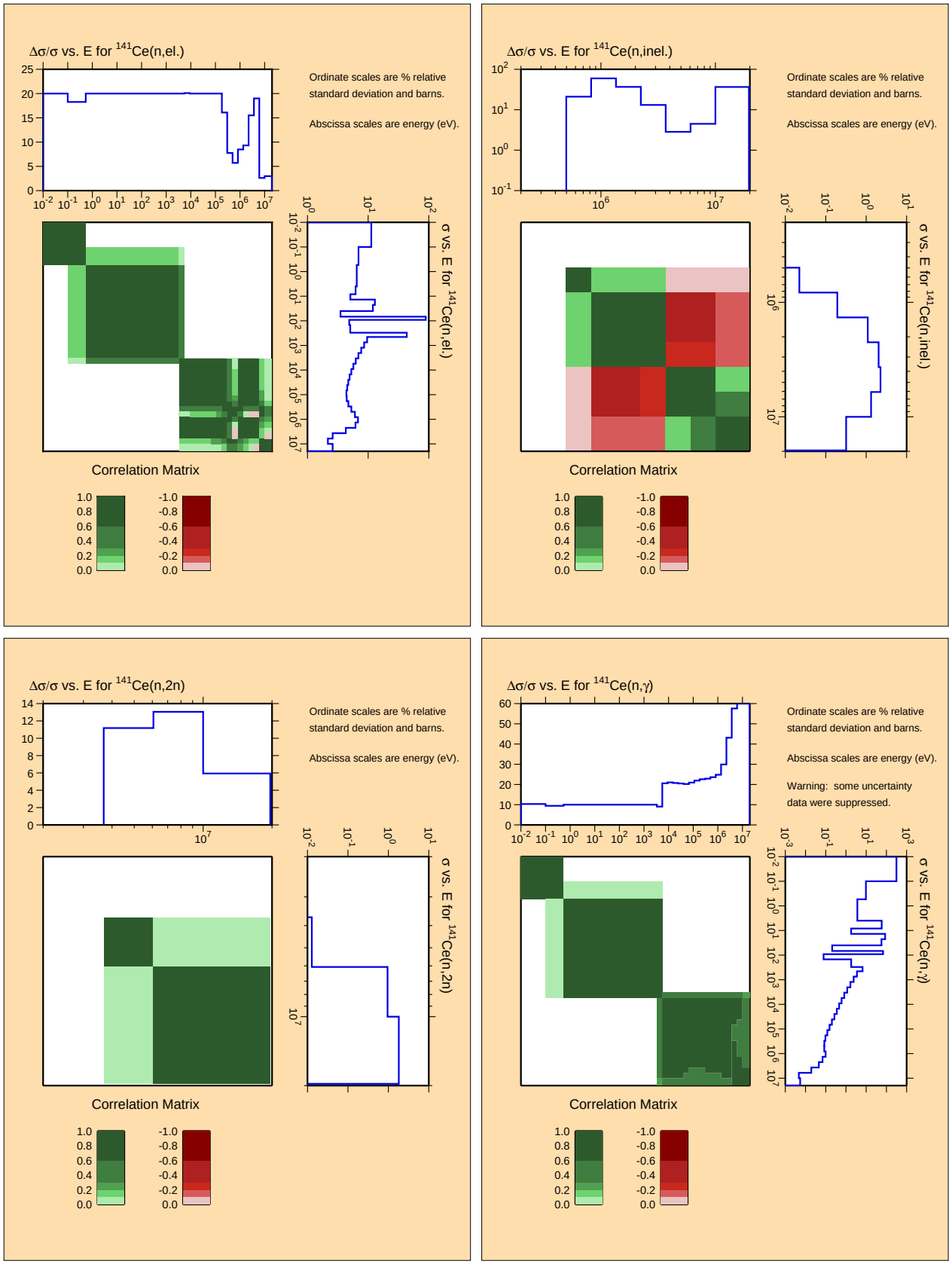

Figure A.65: Covariances for fission product ^{141}Ce.

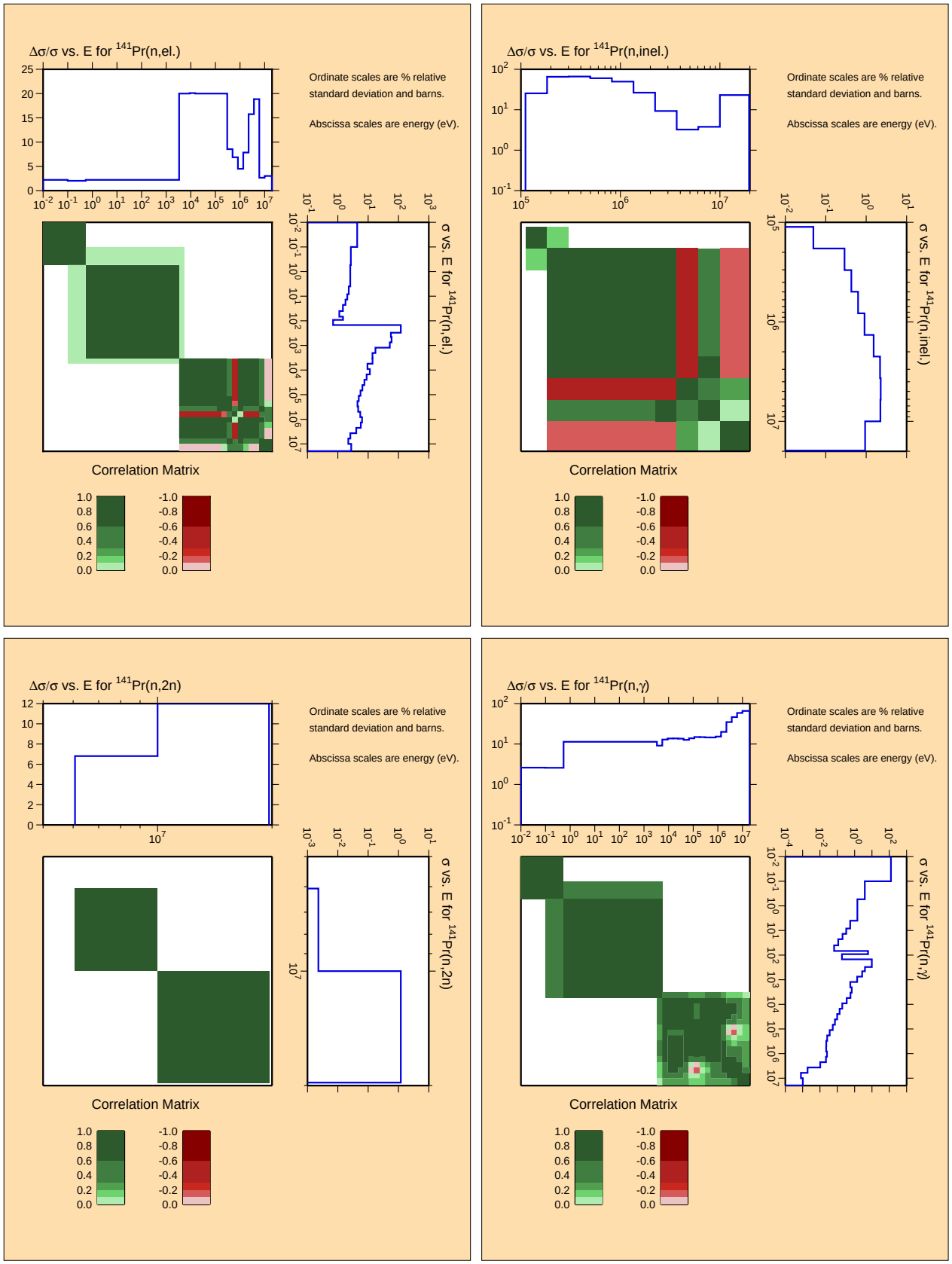

Figure A.66: Covariances for fission product ^{141}Pr.

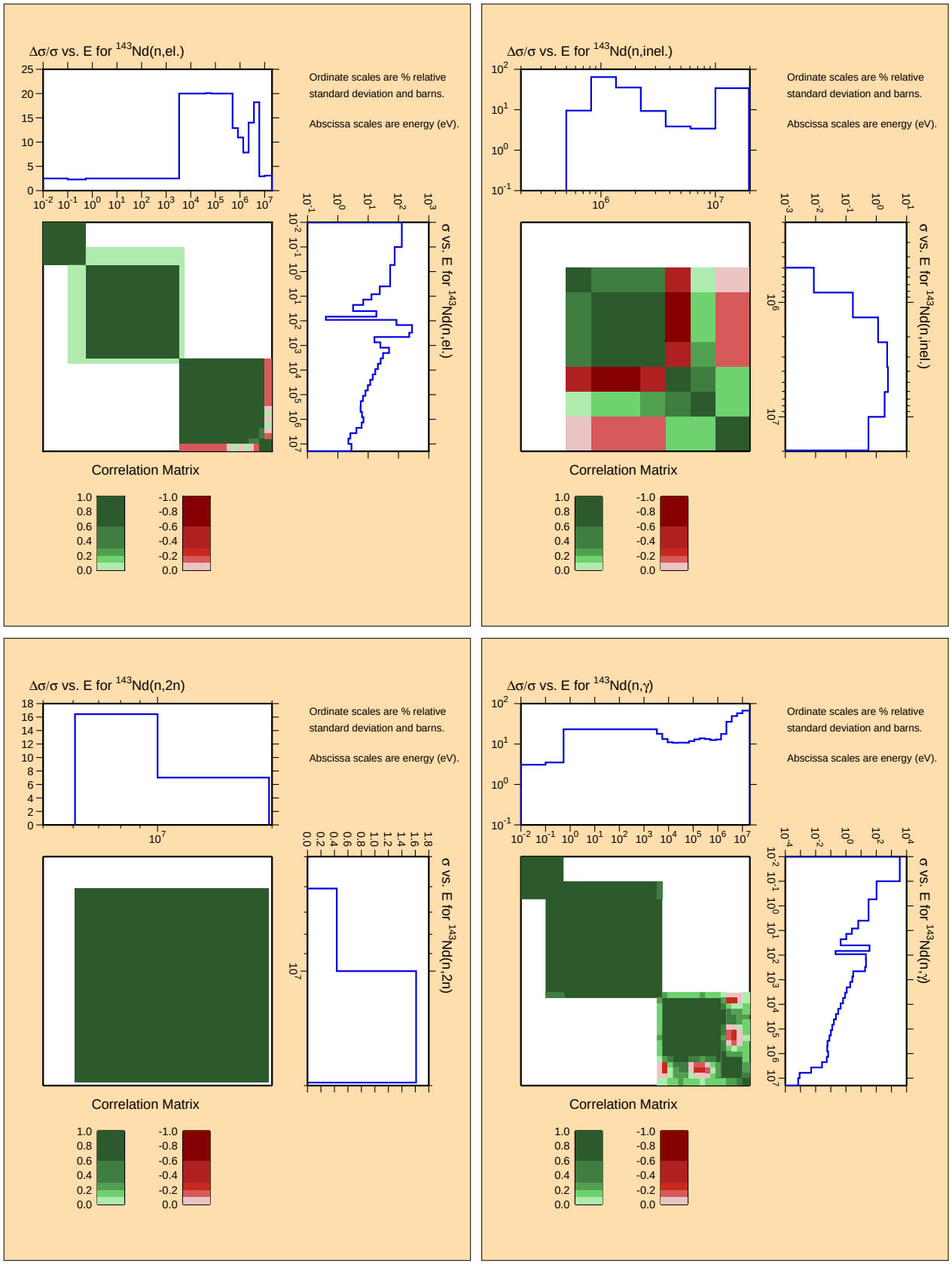

Figure A.67: Covariances for fission product ^{143}Nd.

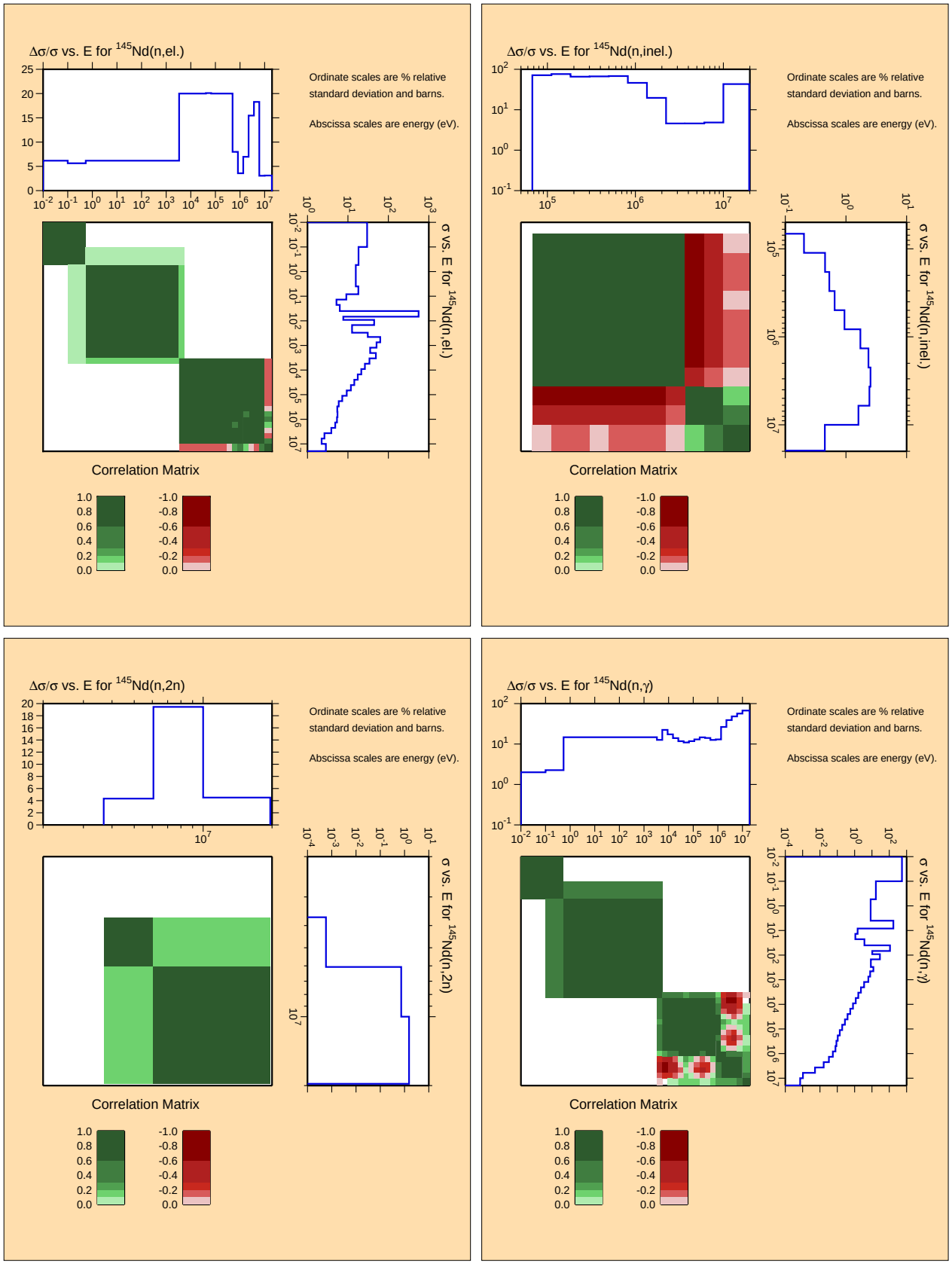

Figure A.68: Covariances for fission product ^{145}Nd.

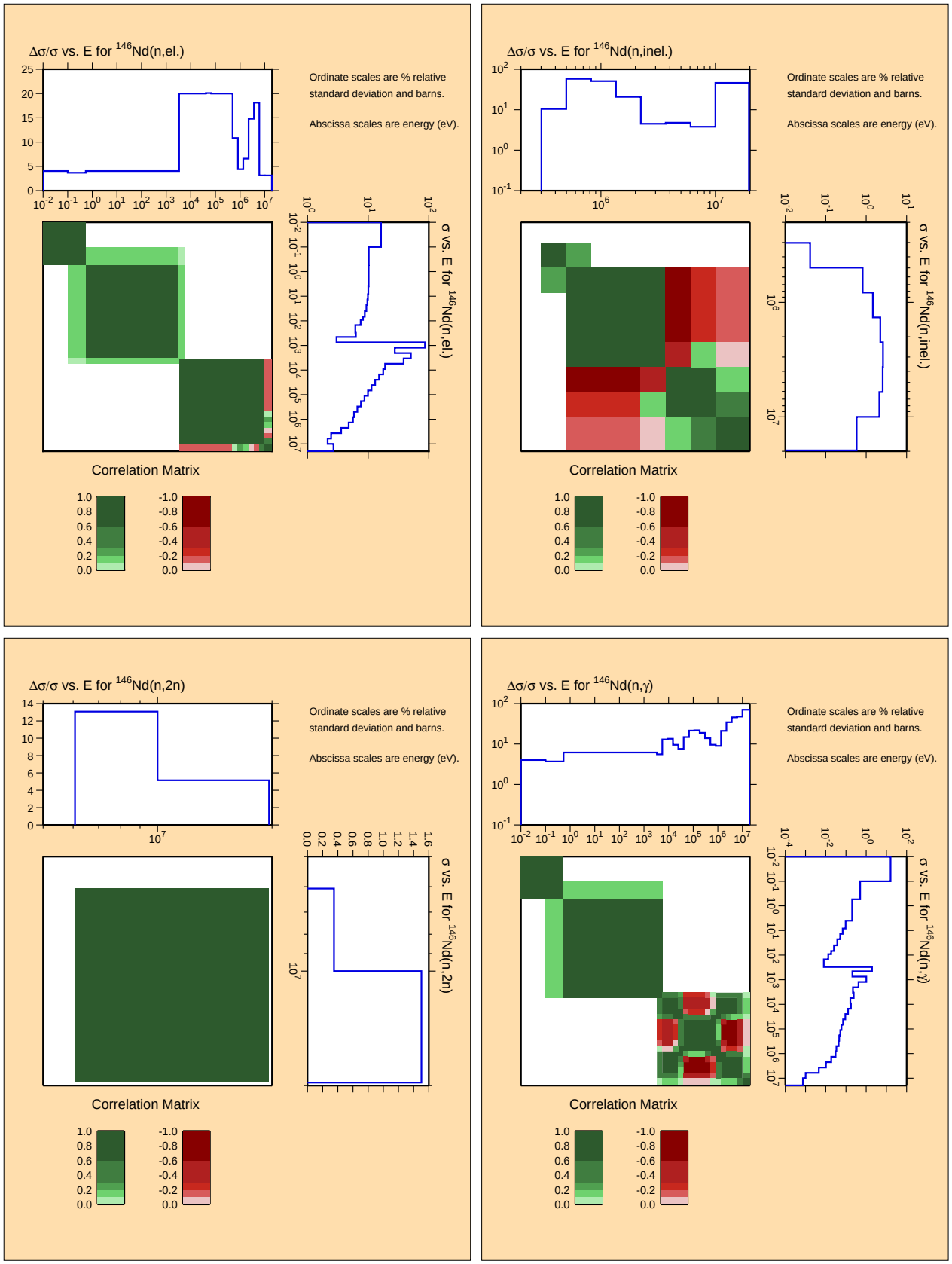

Figure A.69: Covariances for fission product ^{146}Nd.

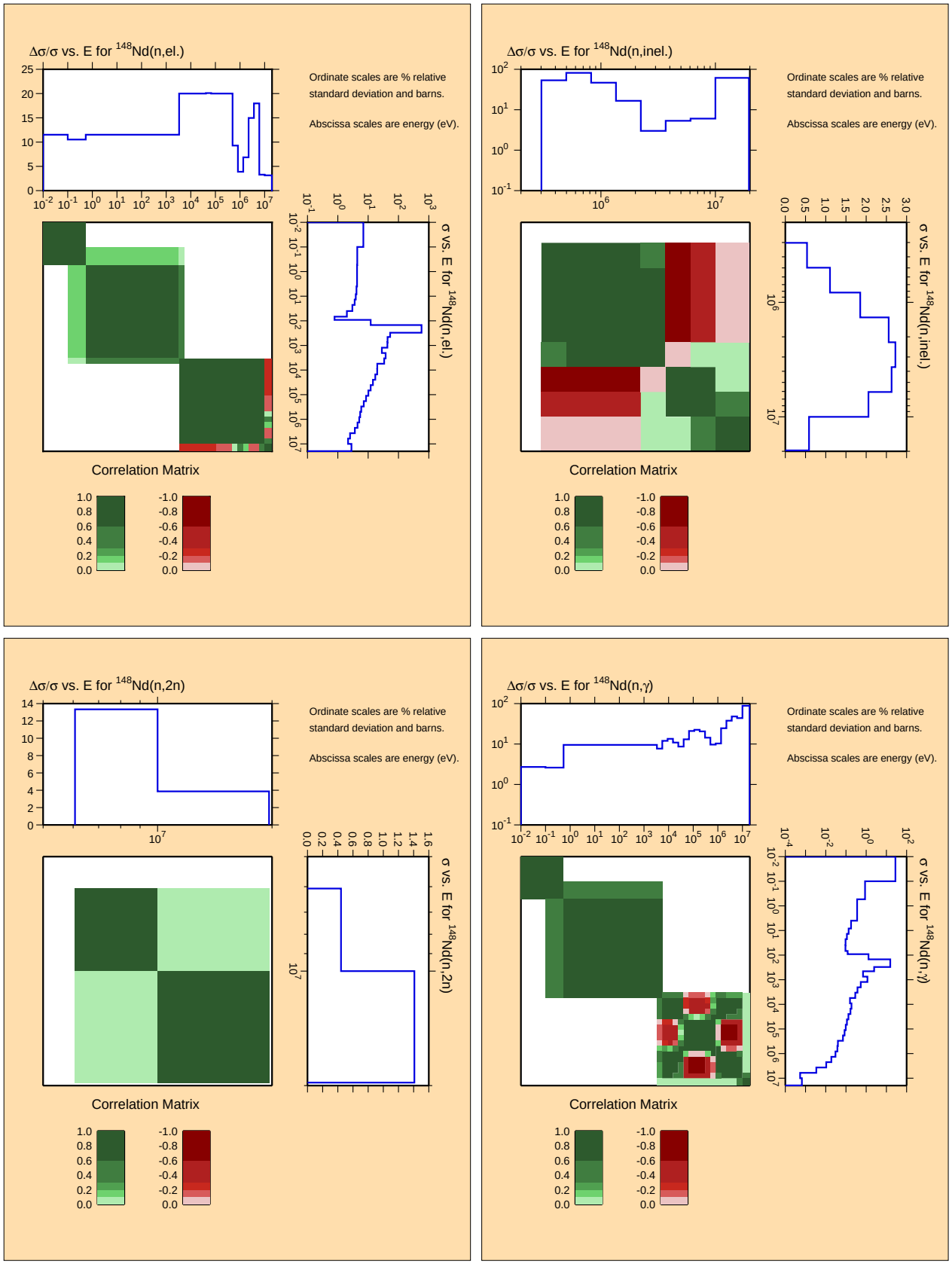

Figure A.70: Covariances for fission product ^{148}Nd.

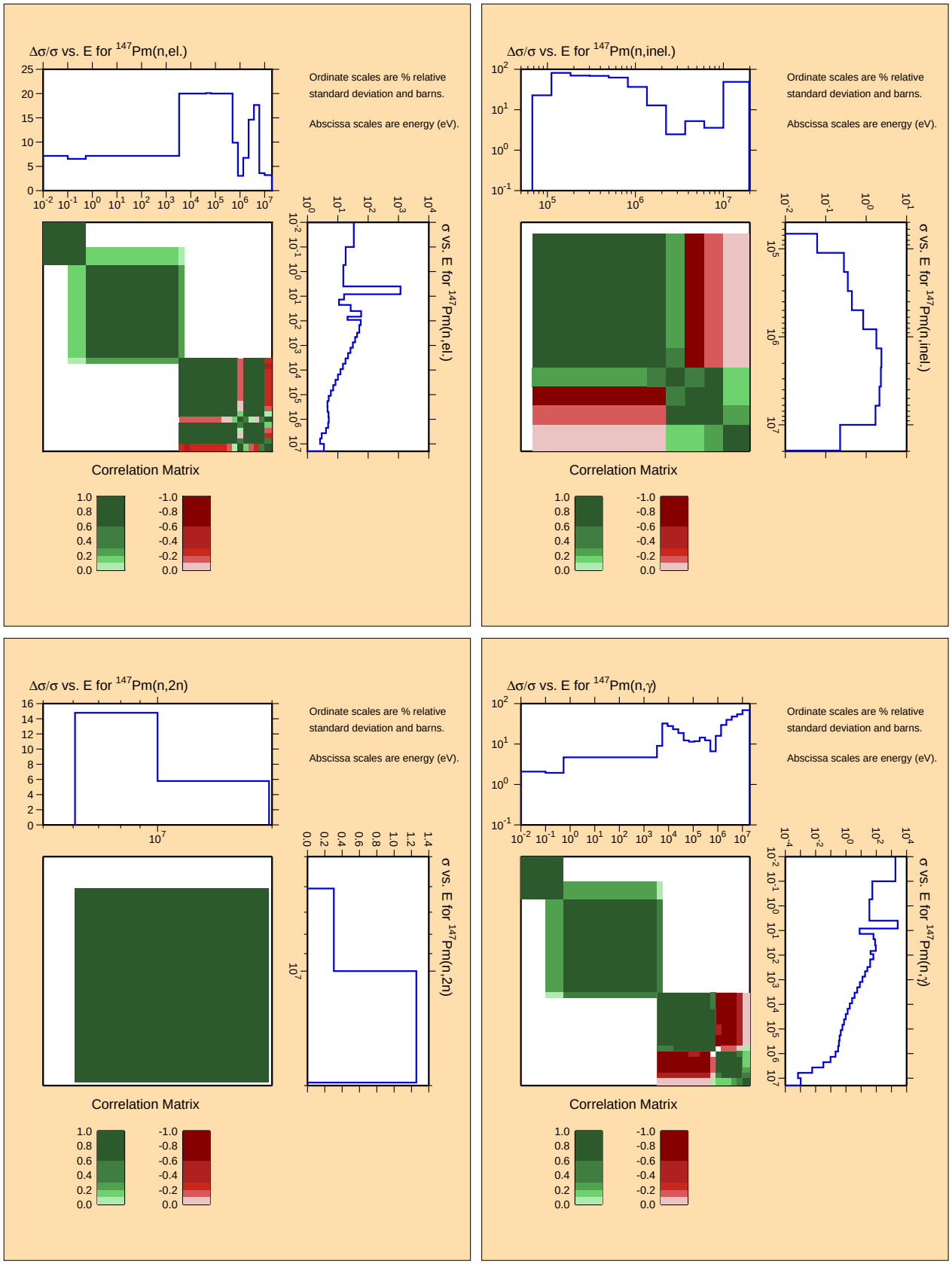

Figure A.71: Covariances for fission product ^{147}Pm.

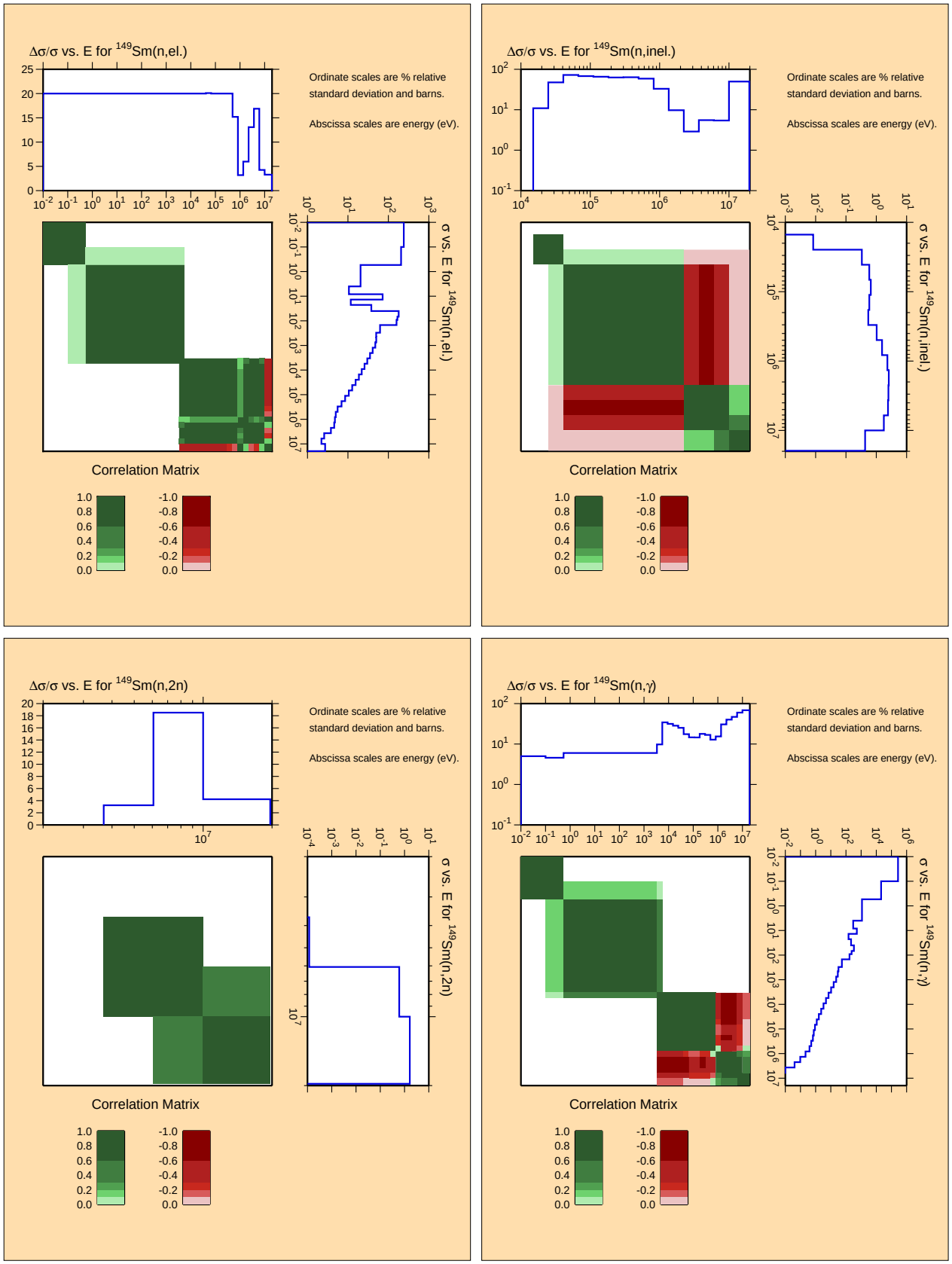

Figure A.72: Covariances for fission product ^{149}Sm.

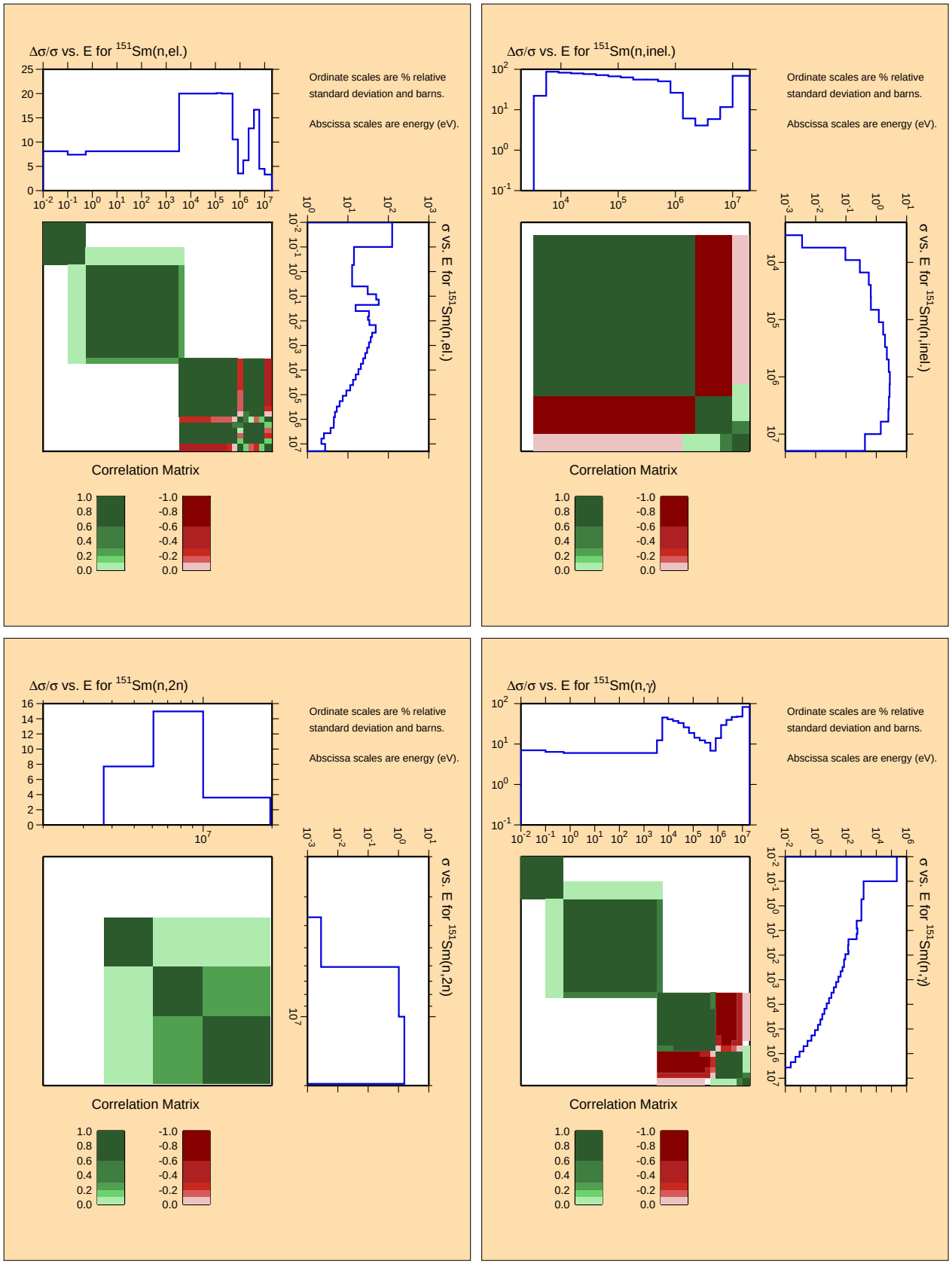

Figure A.73: Covariances for fission product ^{151}Sm.

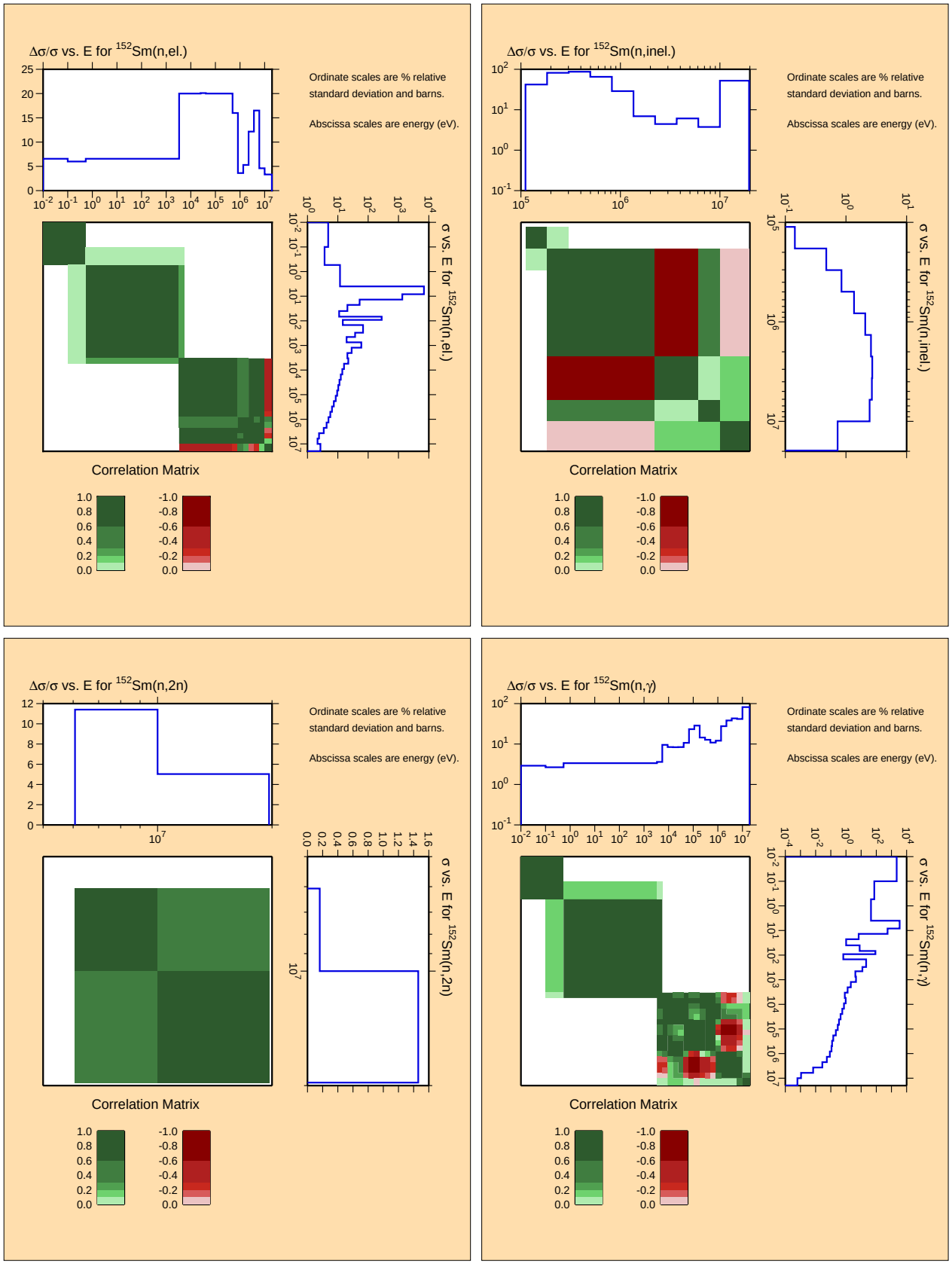

Figure A.74: Covariances for fission product ^{152}Sm.

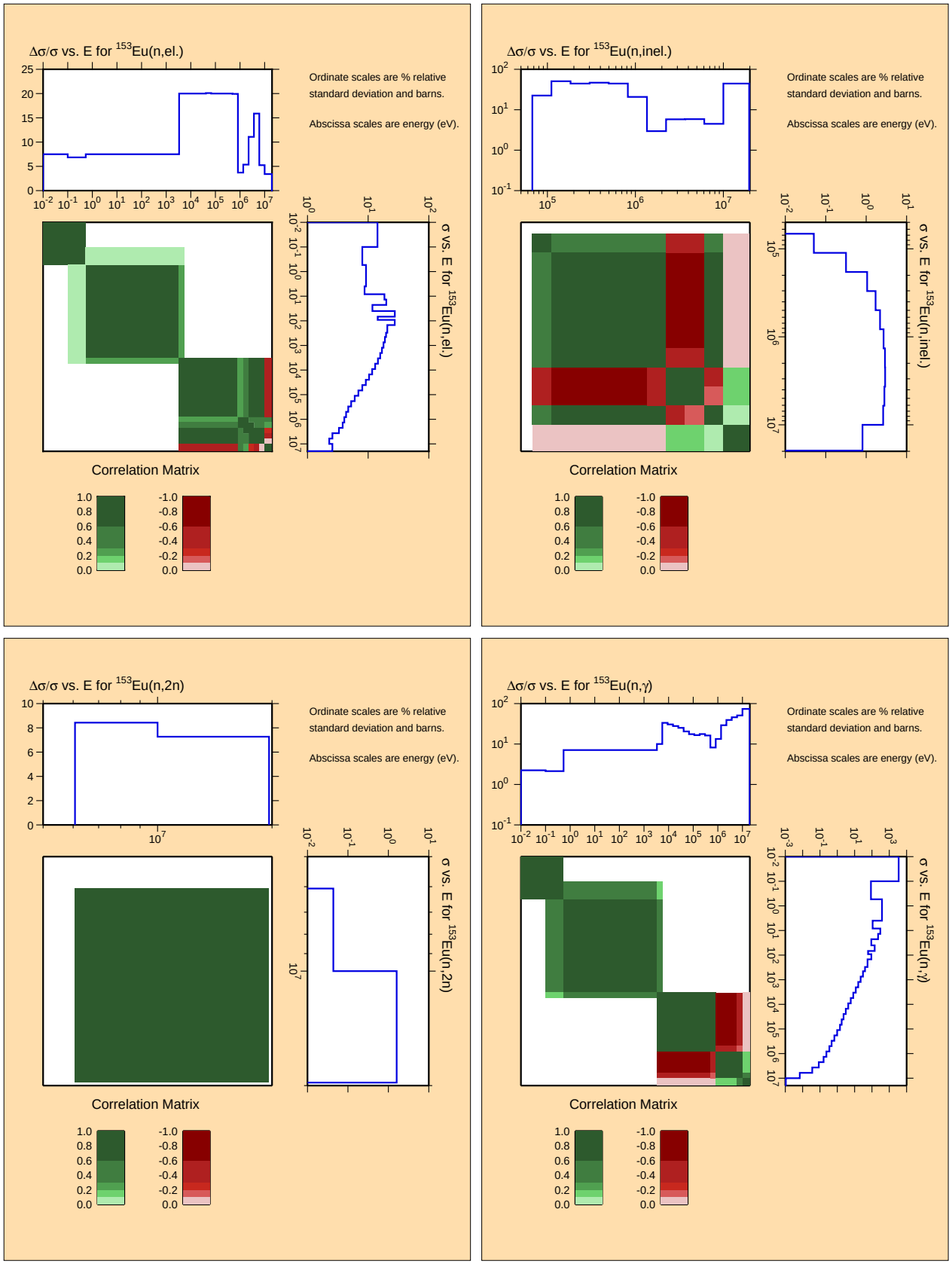

Figure A.75: Covariances for fission product ^{153}Eu.

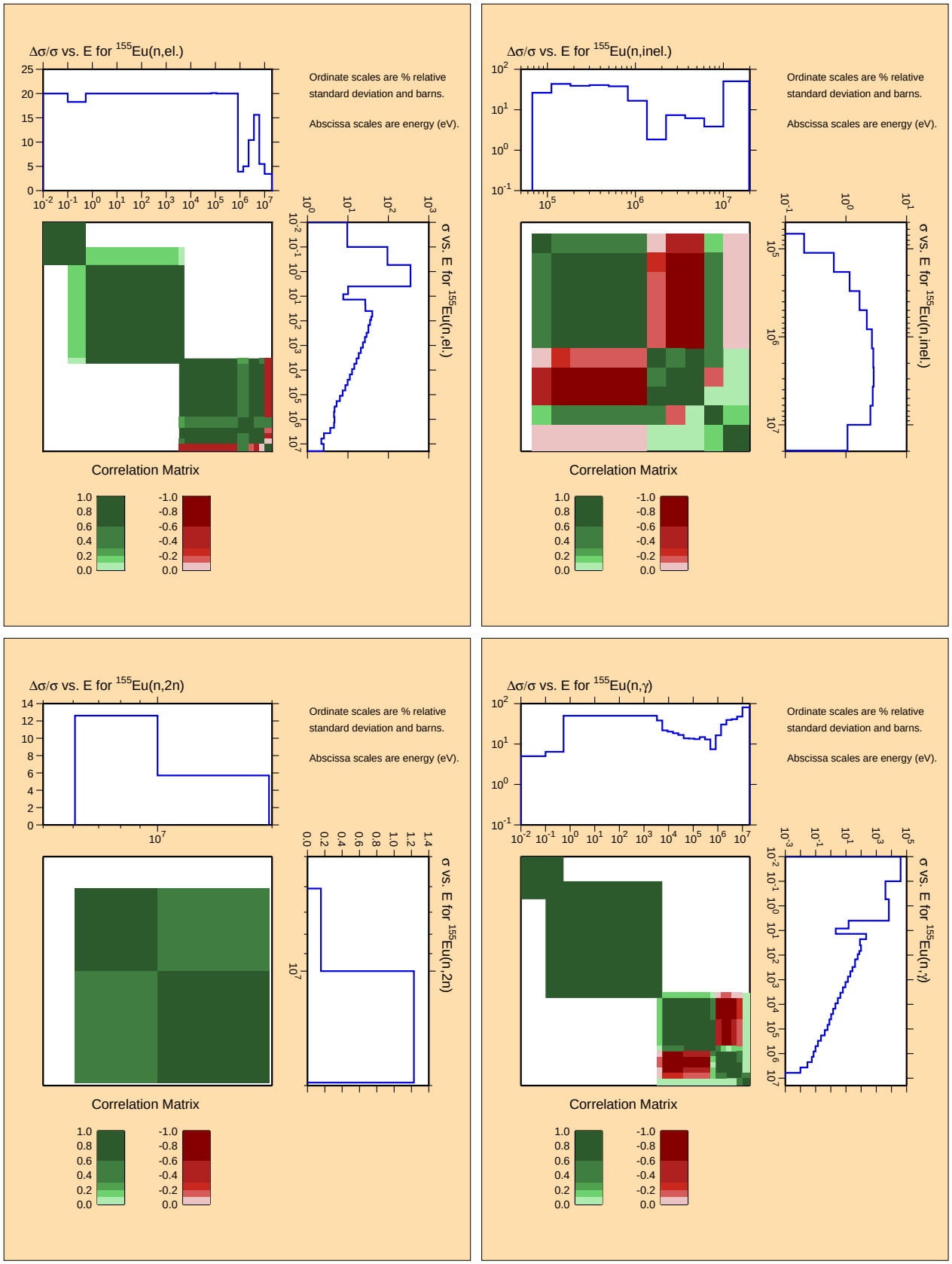

Figure A.76: Covariances for fission product ^{155}Eu.

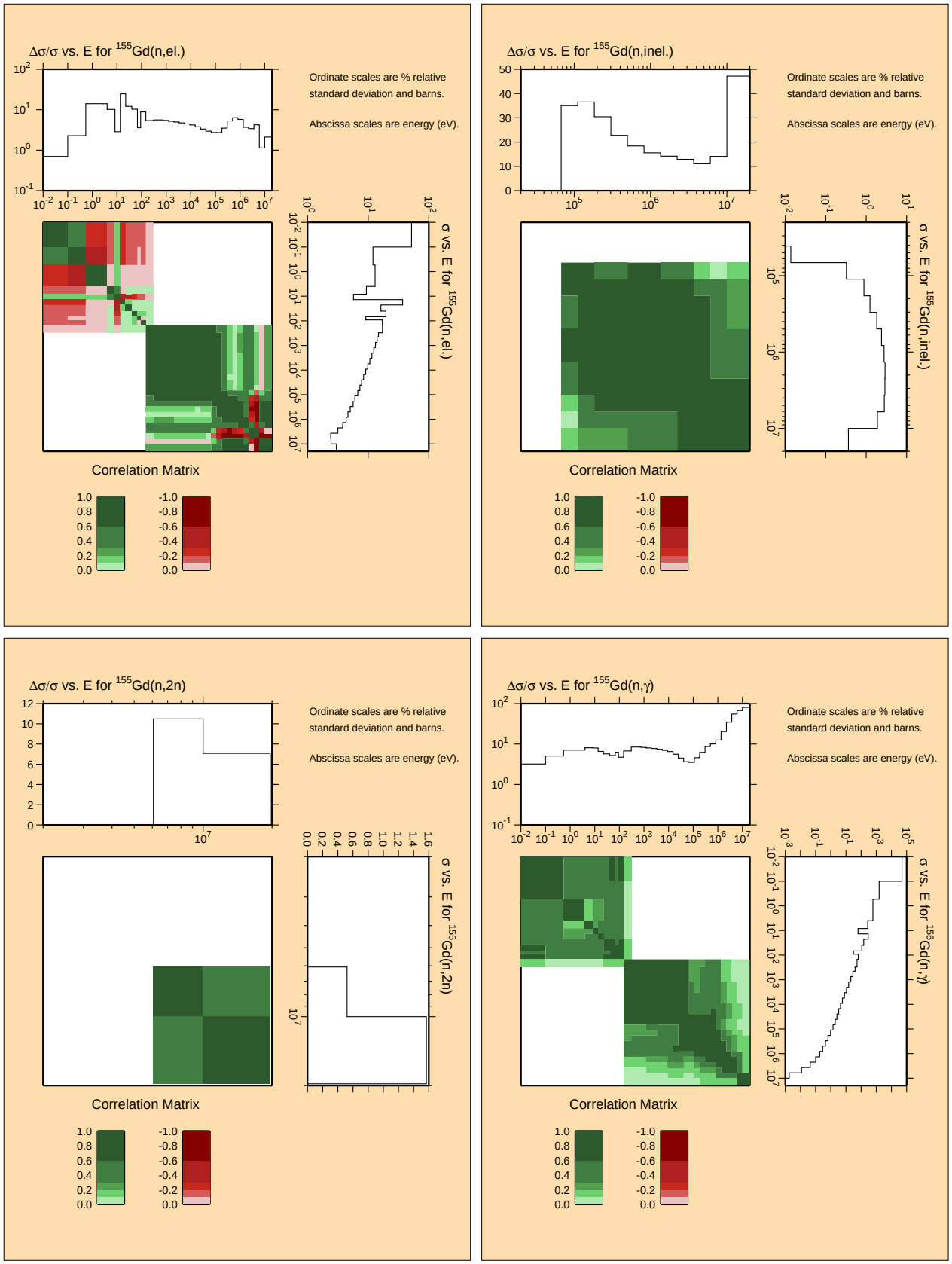

Figure A.77: Covariances for structural material ^{155}Gd.

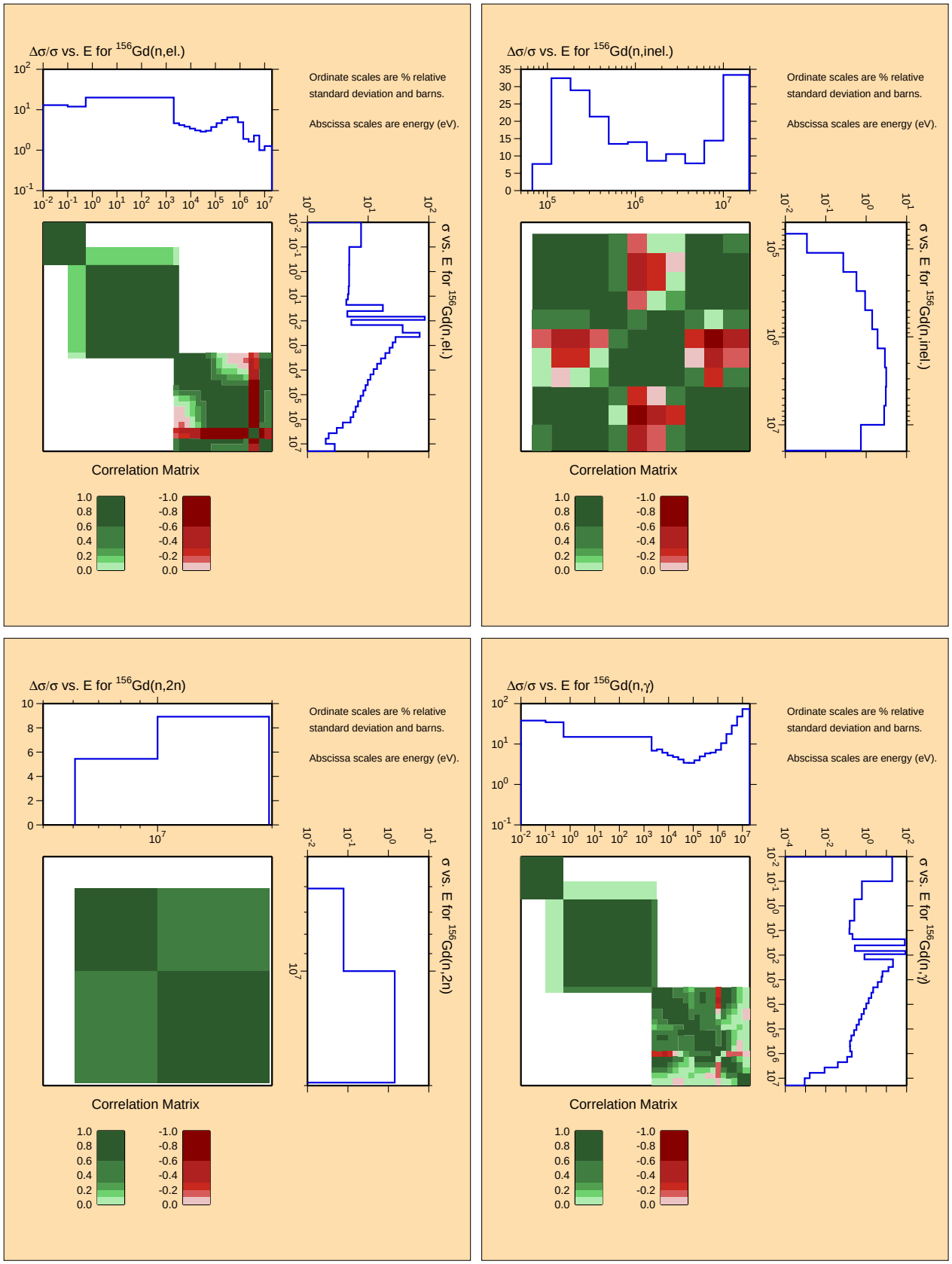

Figure A.78: Covariances for structural material ^{156}Gd.

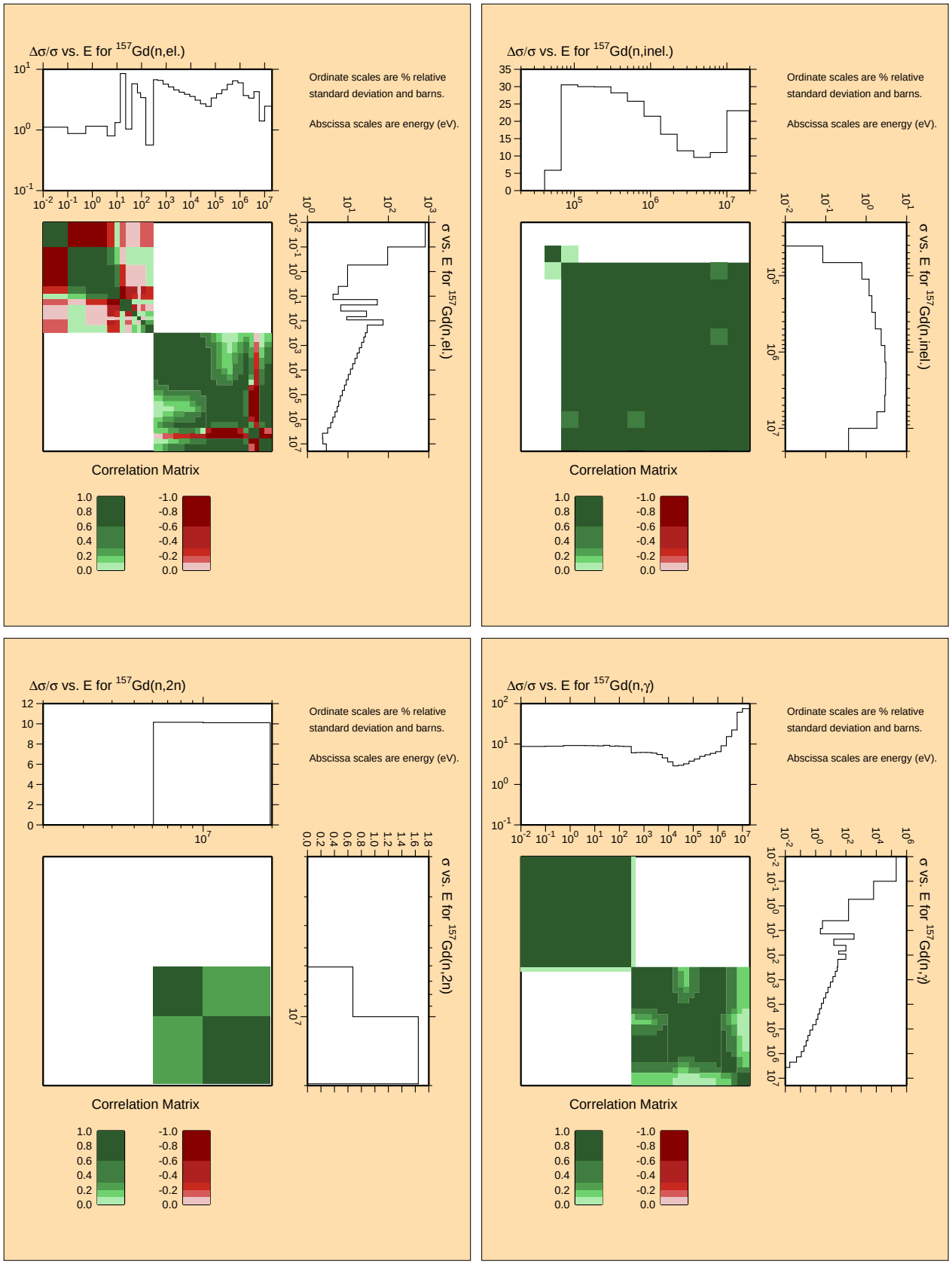

Figure A.79: Covariances for structural material ^{157}Gd.

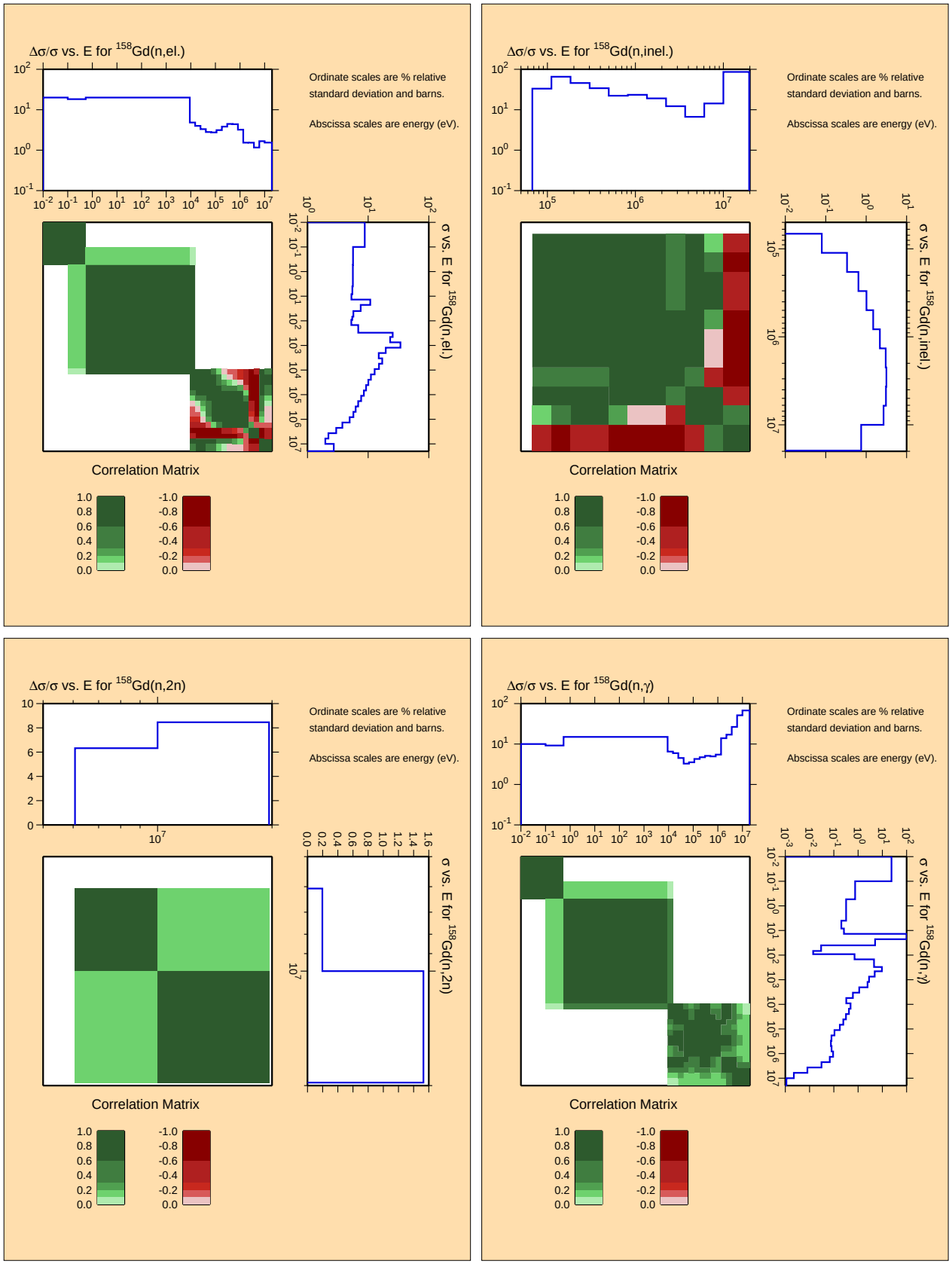

Figure A.80: Covariances for structural material ^{158}Gd.

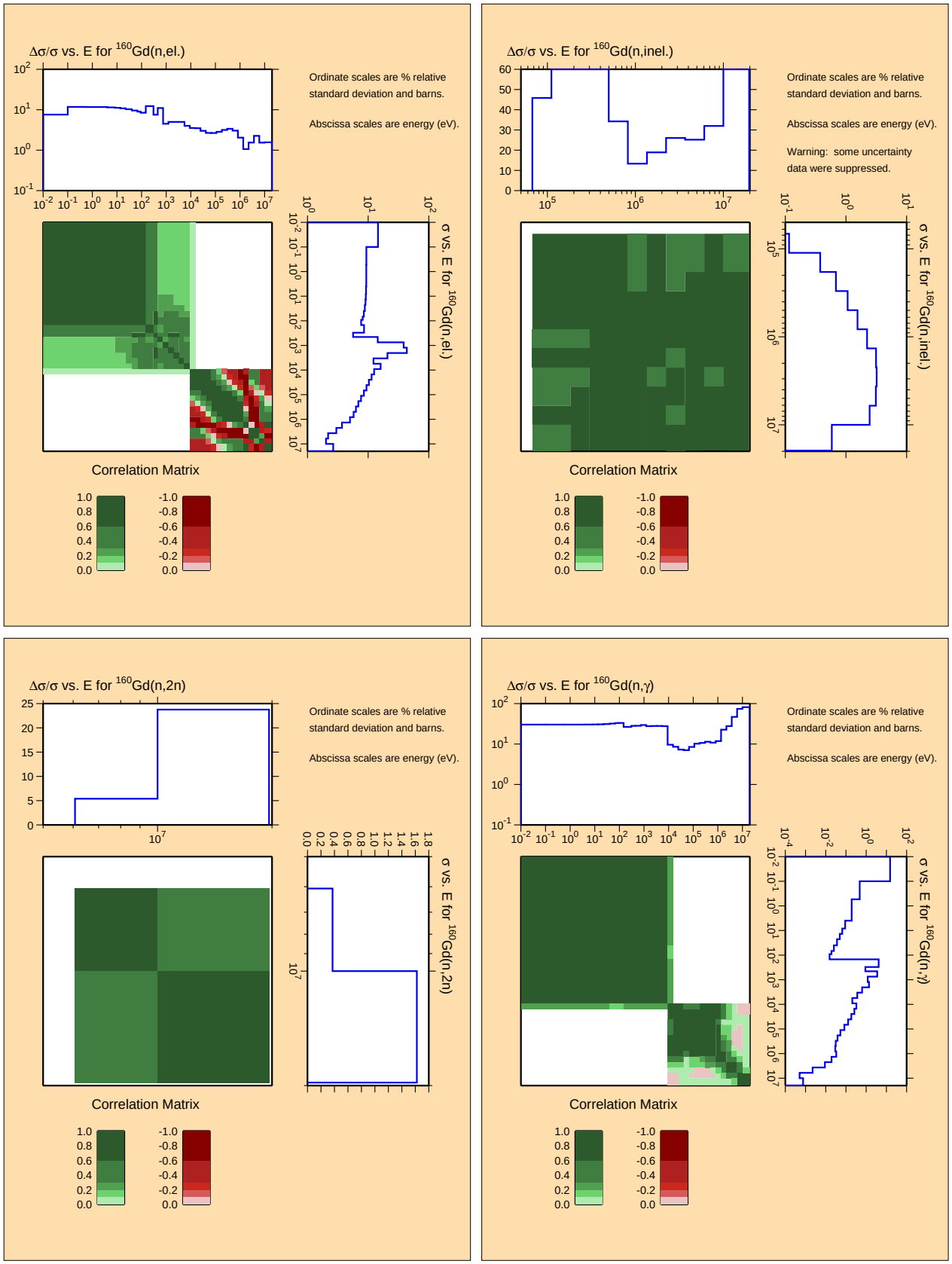

Figure A.81: Covariances for structural material ^{160}Gd.

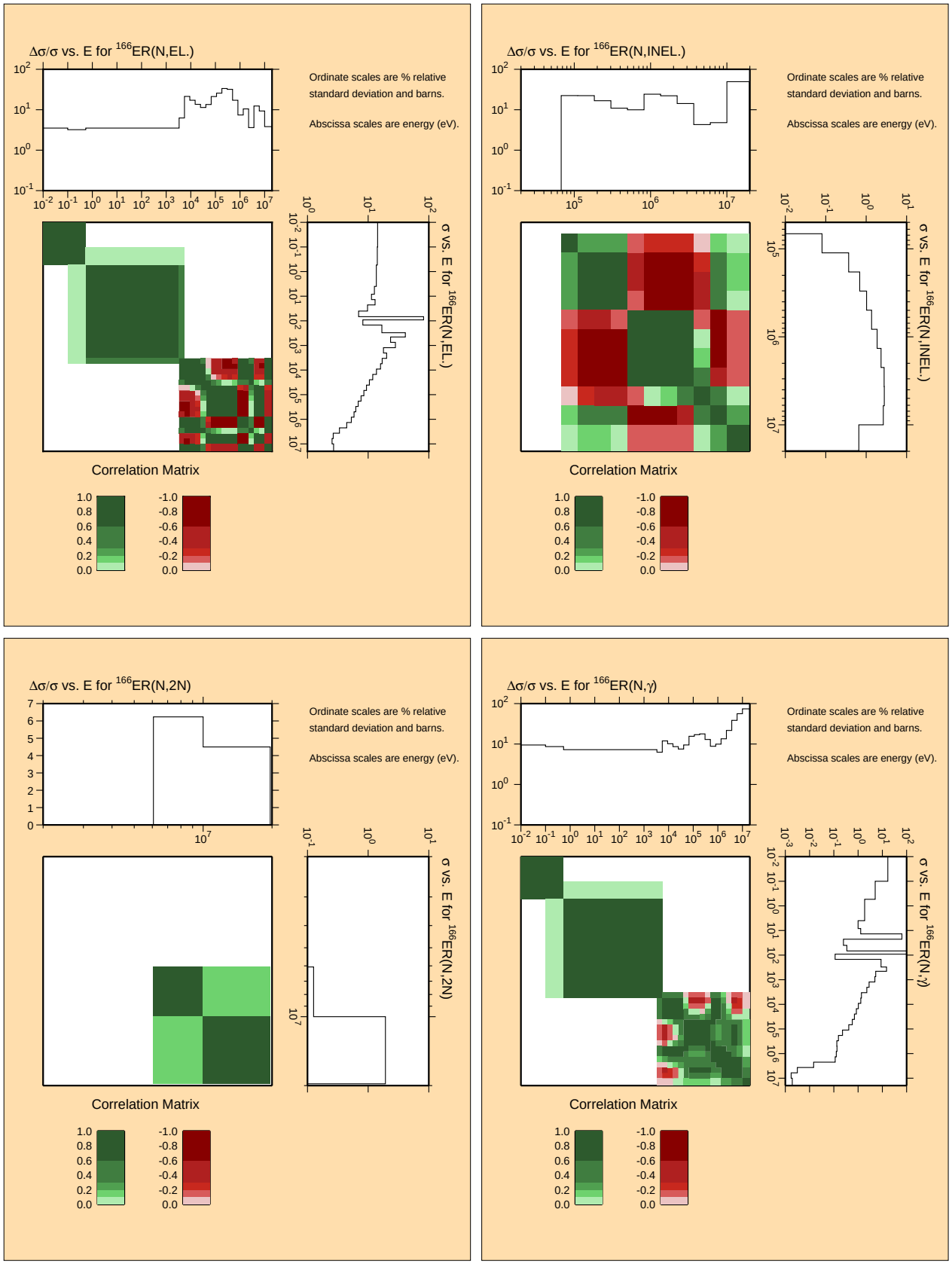

Figure A.82: Covariances for structural material ^{166}Er.

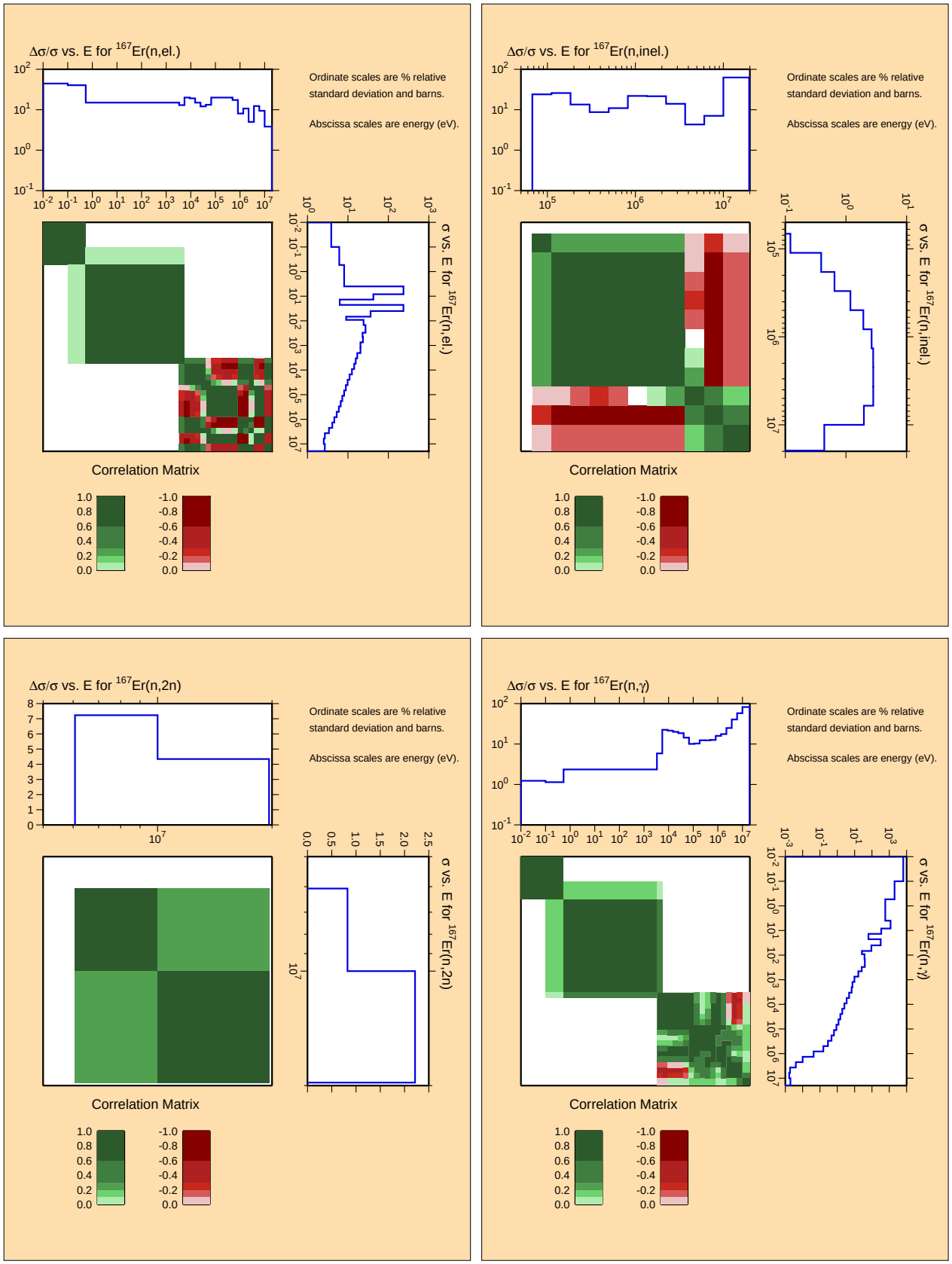

Figure A.83: Covariances for structural material ^{167}Er.

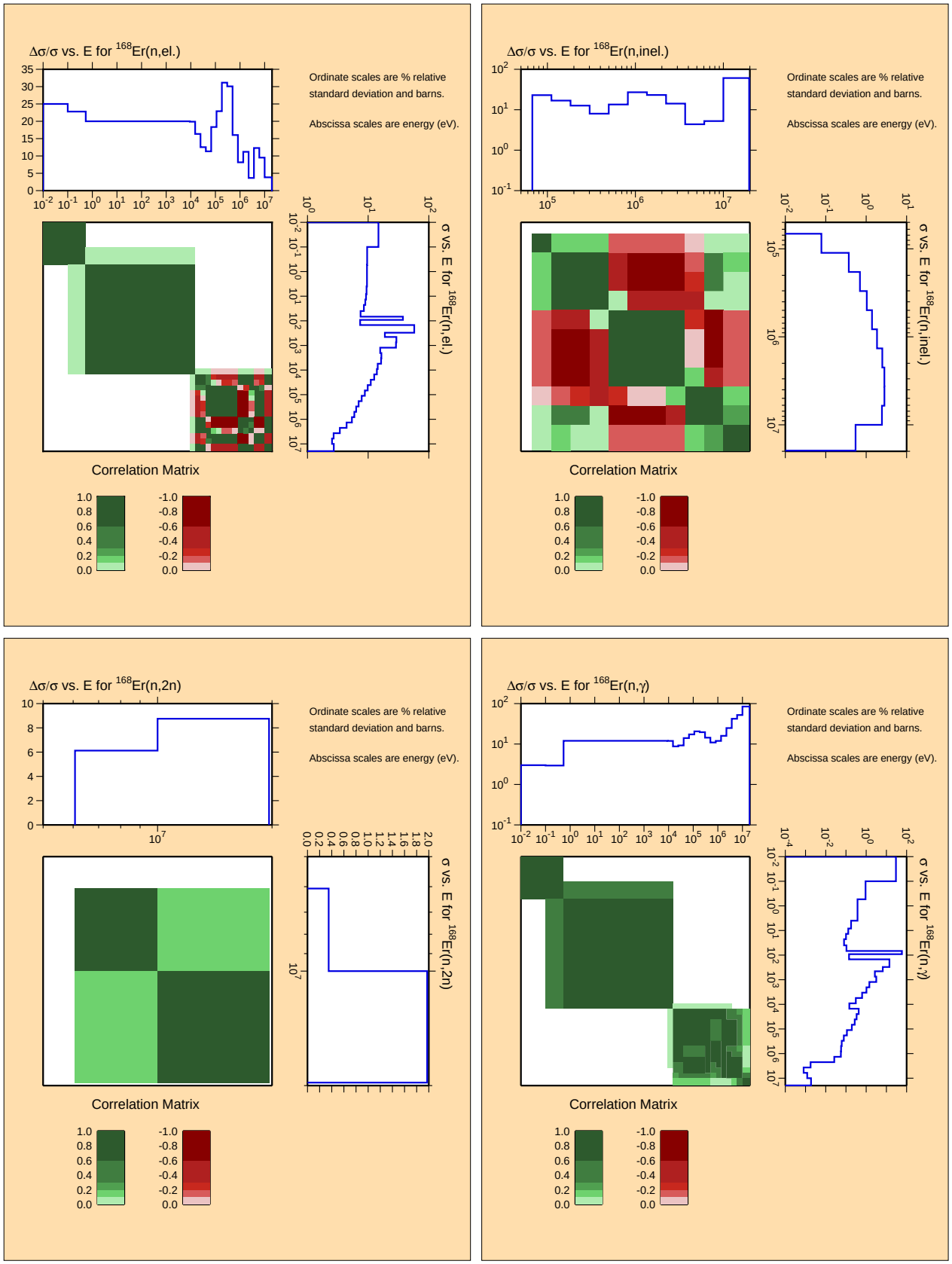

Figure A.84: Covariances for structural material ^{168}Er.

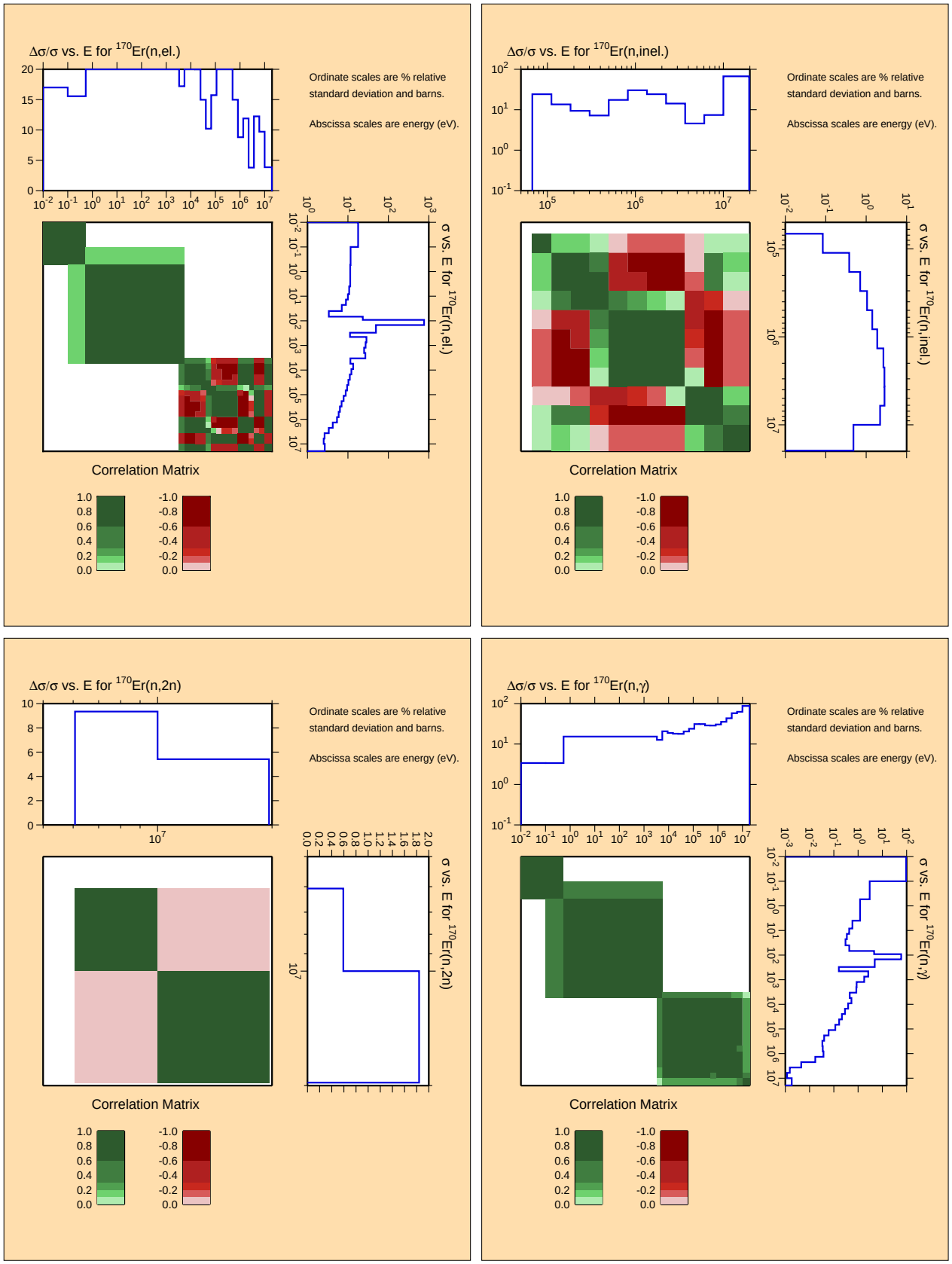

Figure A.85: Covariances for structural material ^{170}Er.

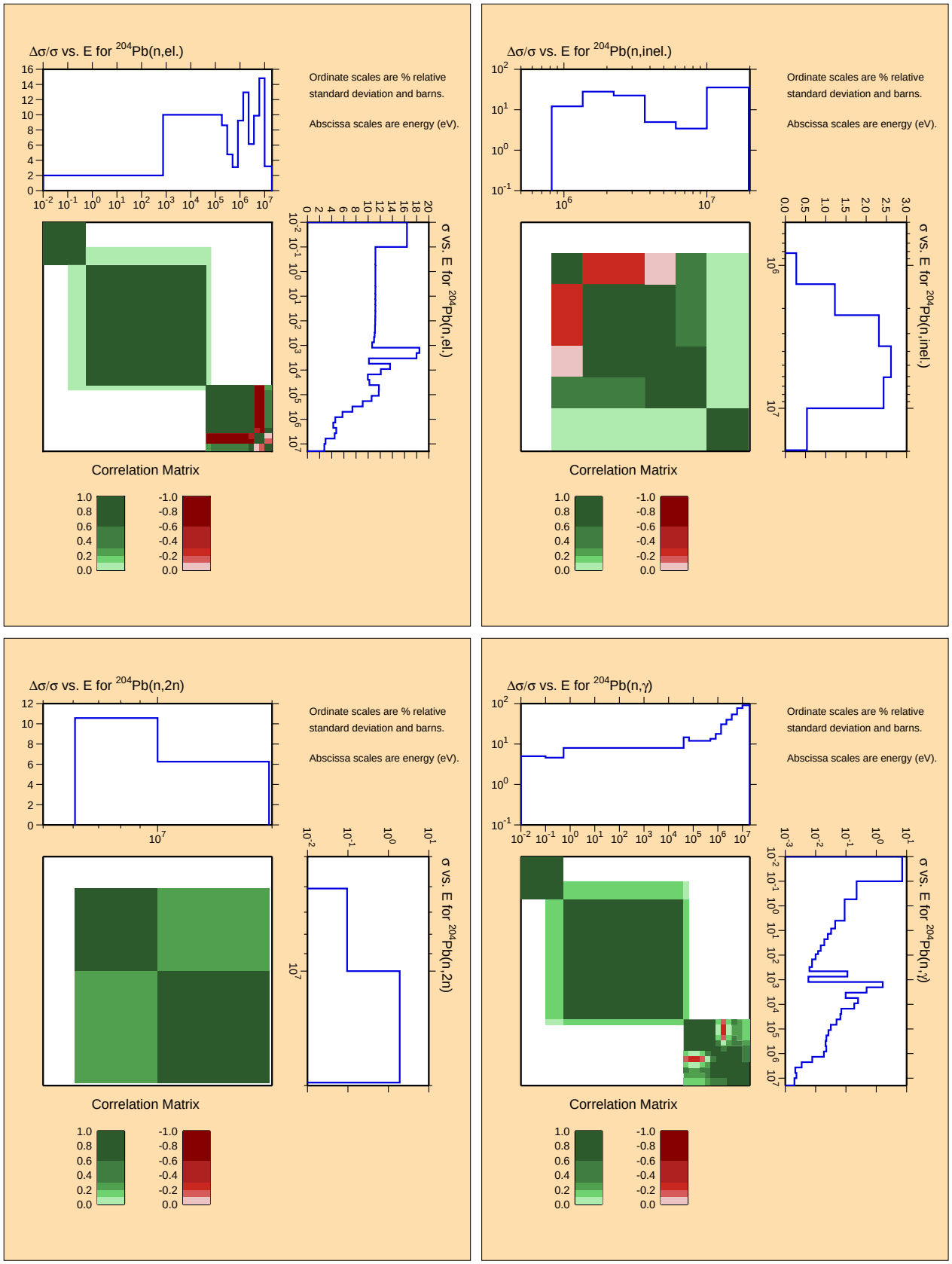

Figure A.86: Covariances for structural material ^{204}Pb.

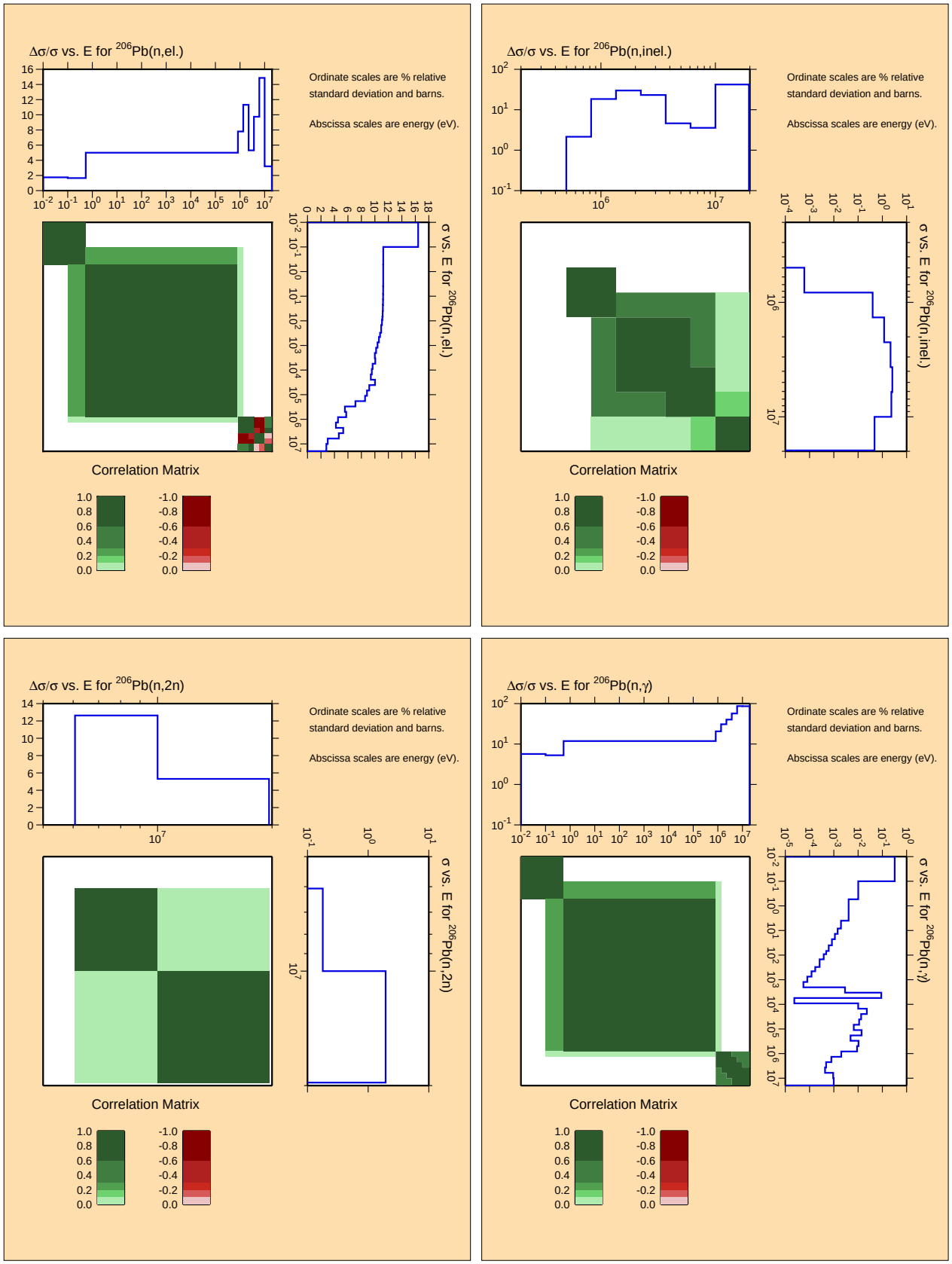

Figure A.87: Covariances for structural material ^{206}Pb.

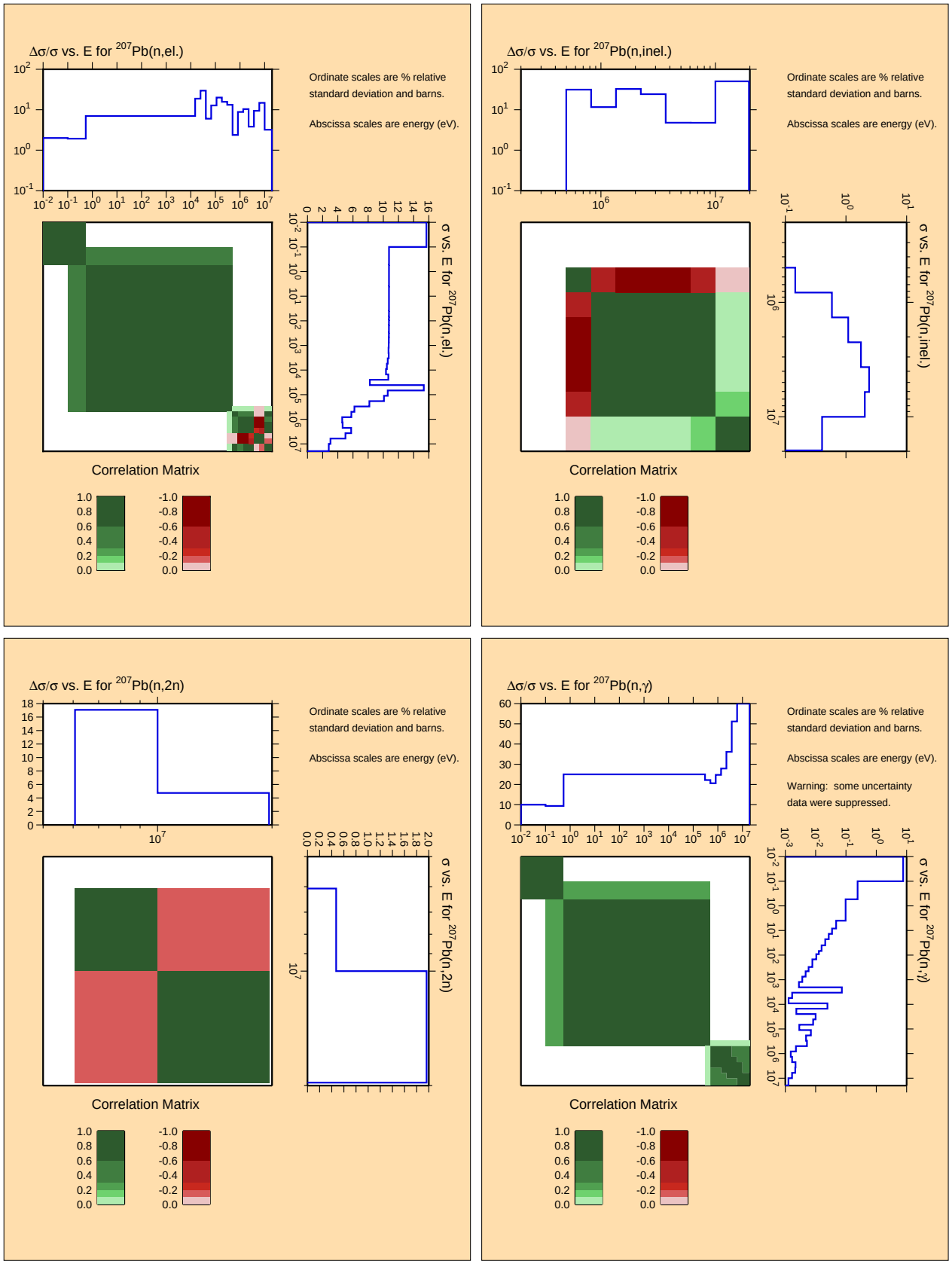

Figure A.88: Covariances for structural material ^{207}Pb.

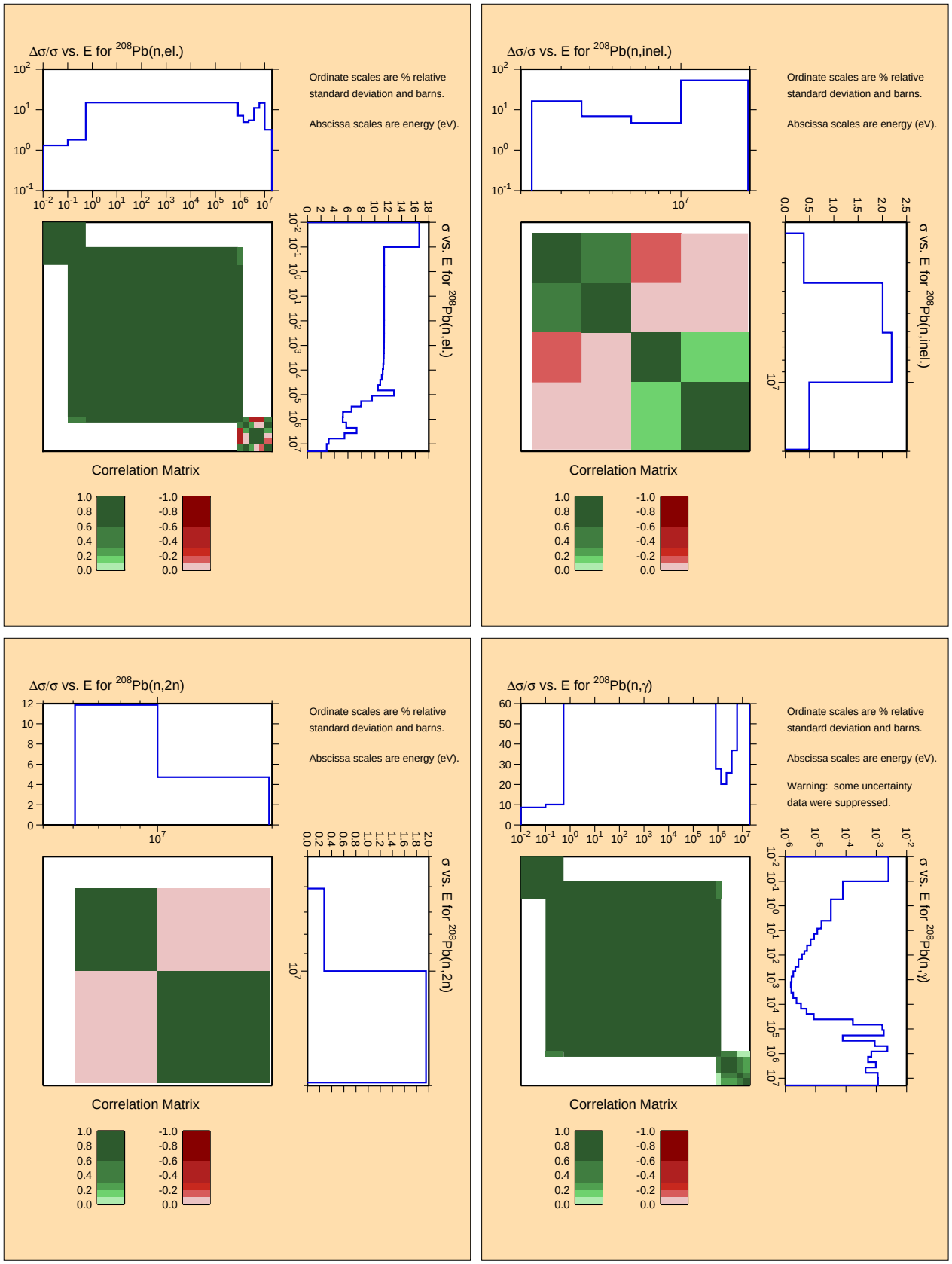

Figure A.89: Covariances for structural material ^{208}Pb.

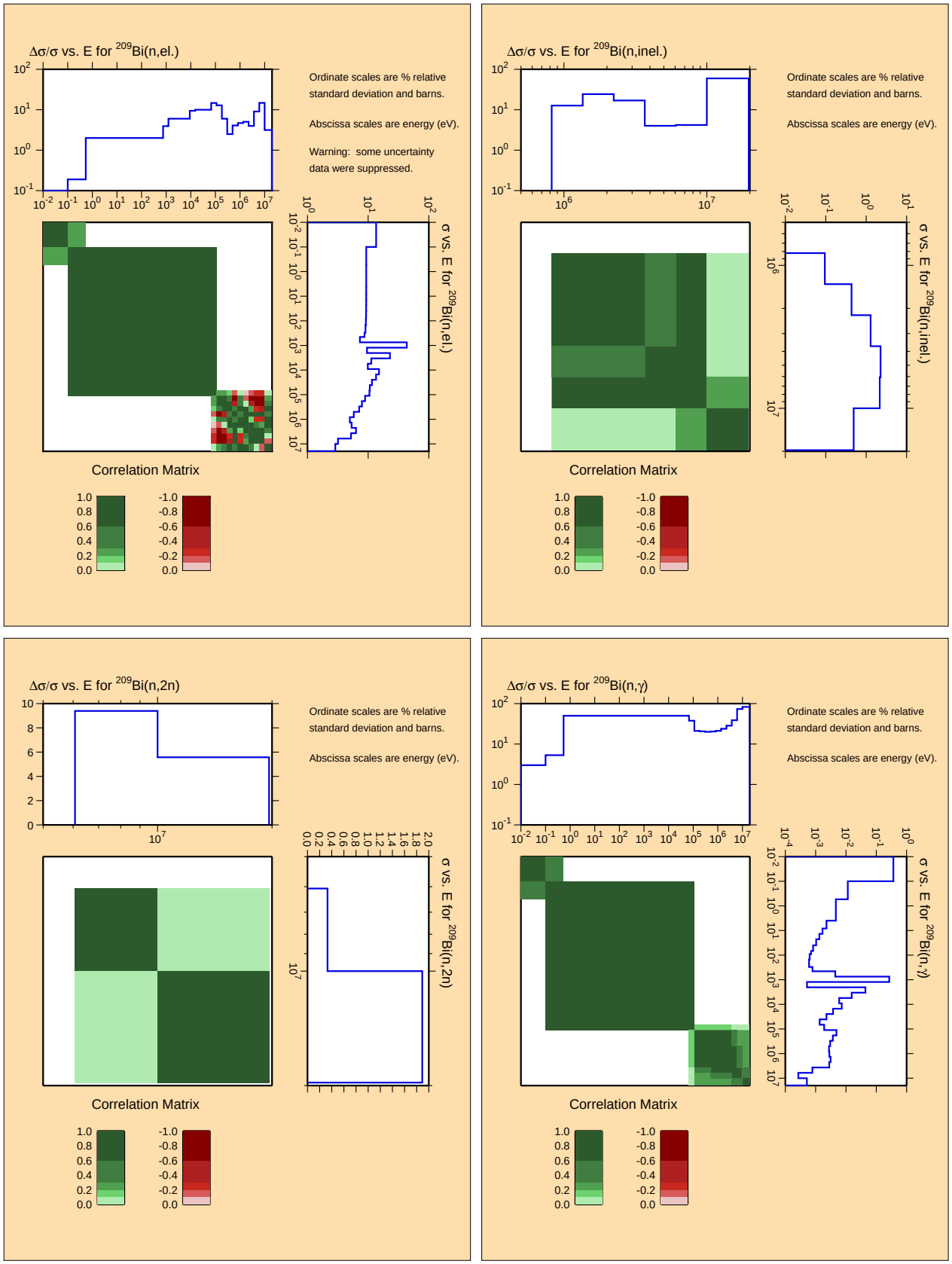

Figure A.90: Covariances for structural material ^{209}Bi.

A.2.3 Actinides

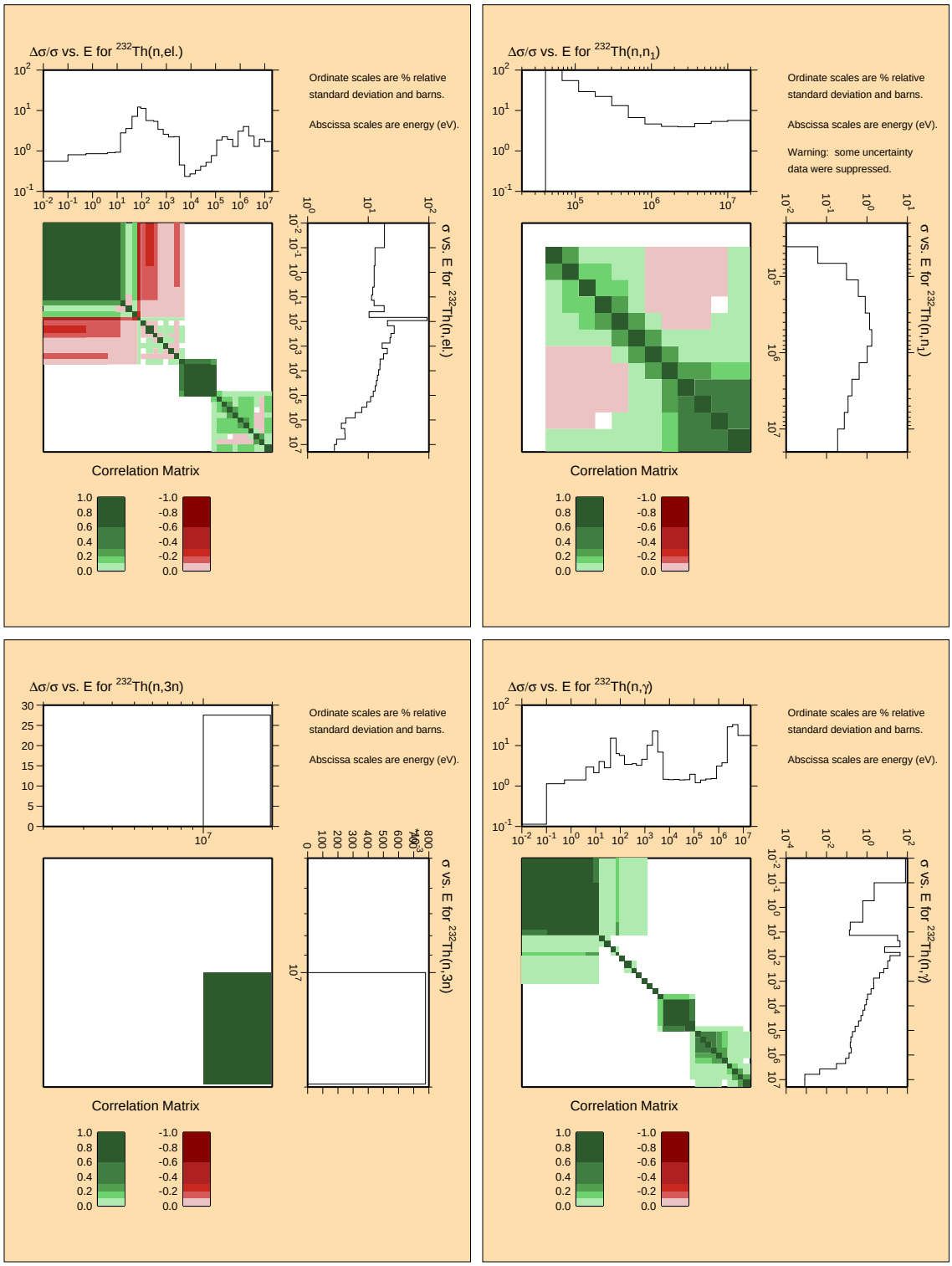

Figure A.91: Covariances for actinide ^{232}Th.

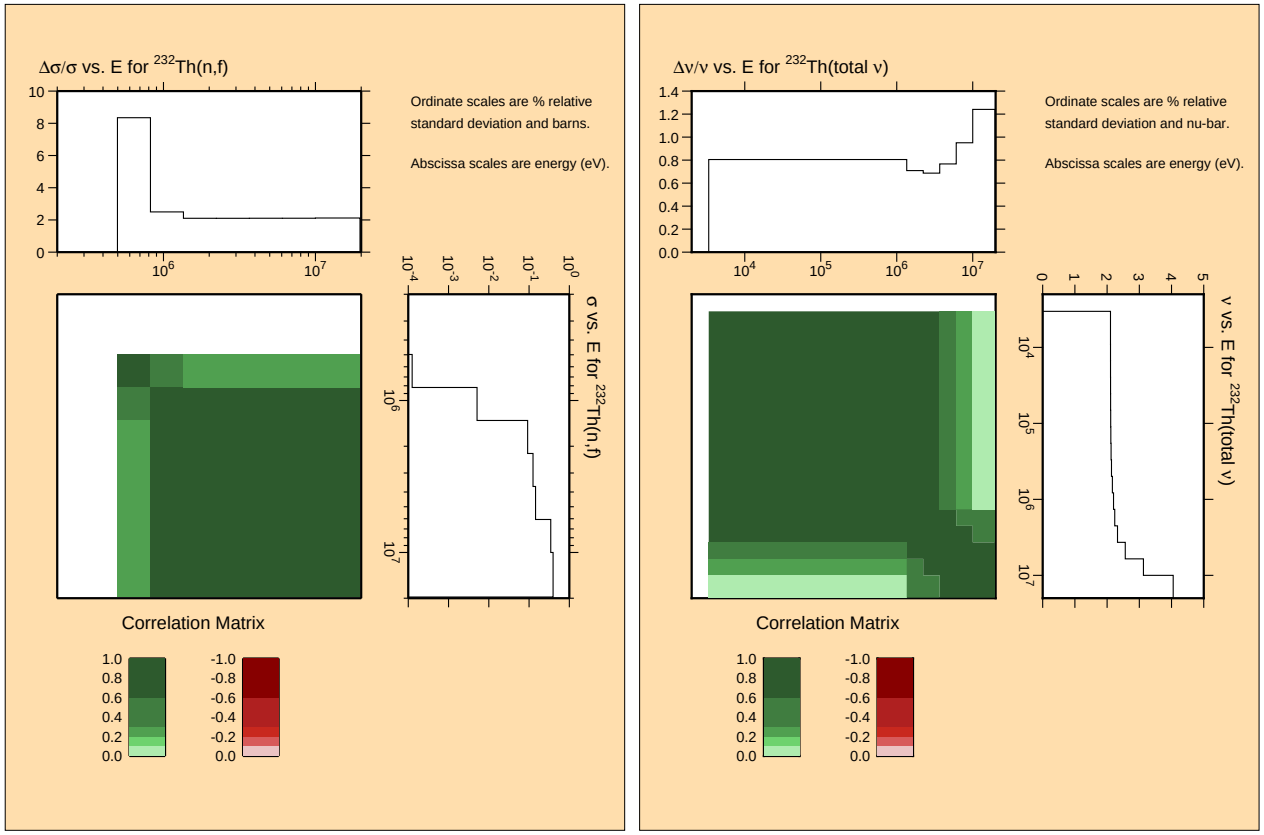

Figure A.91: Covariances for actinide ^{232}Th (continued).

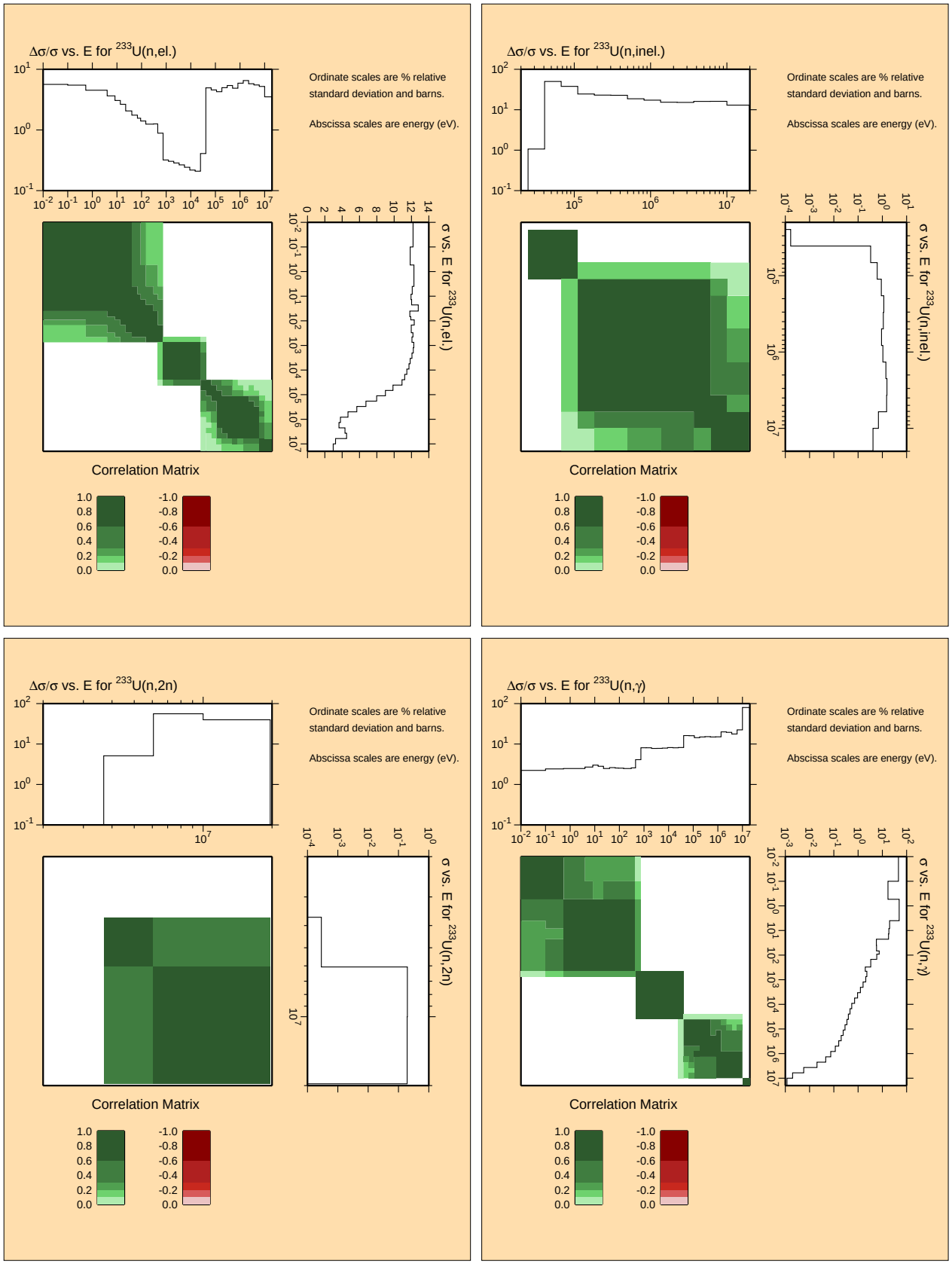

Figure A.92: Covariances for actinide ^{233}U.

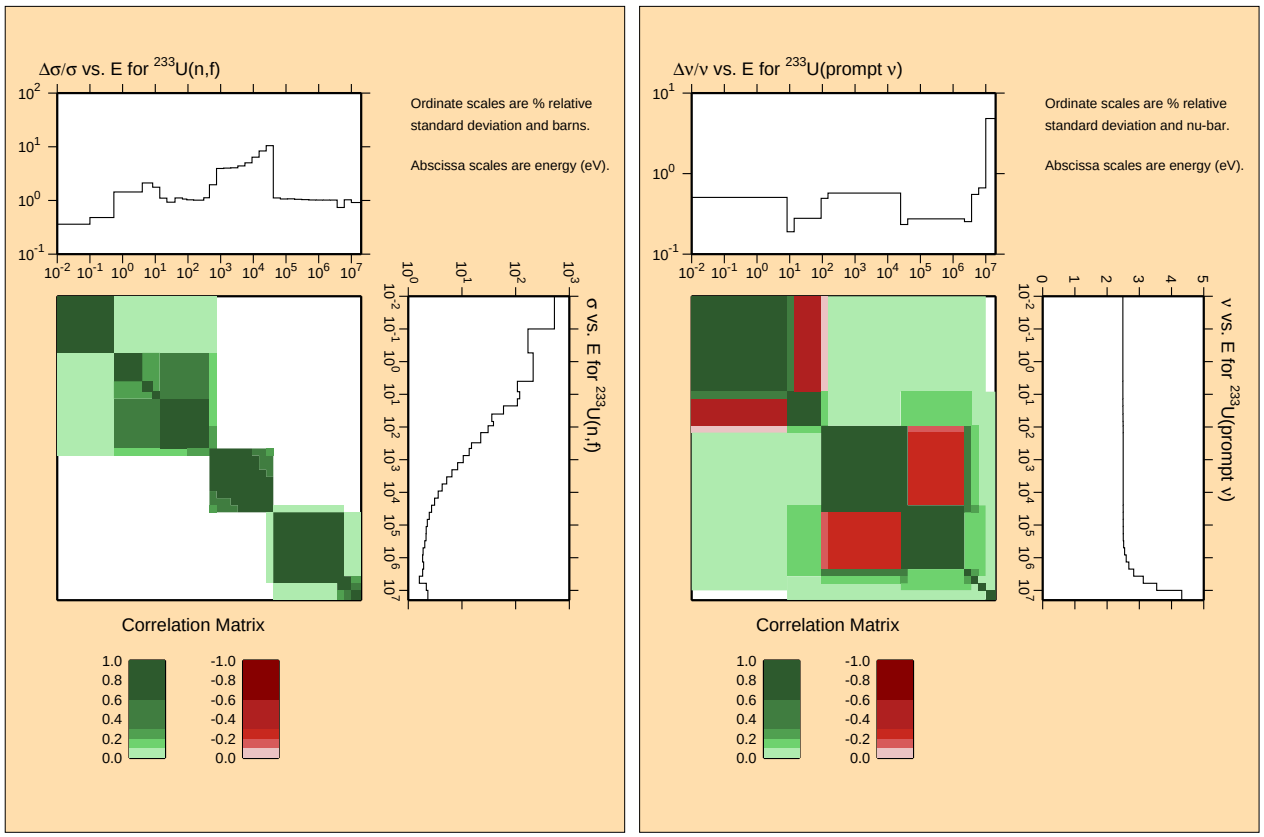

Figure A.92: Covariances for actinide ^{233}U (continued).

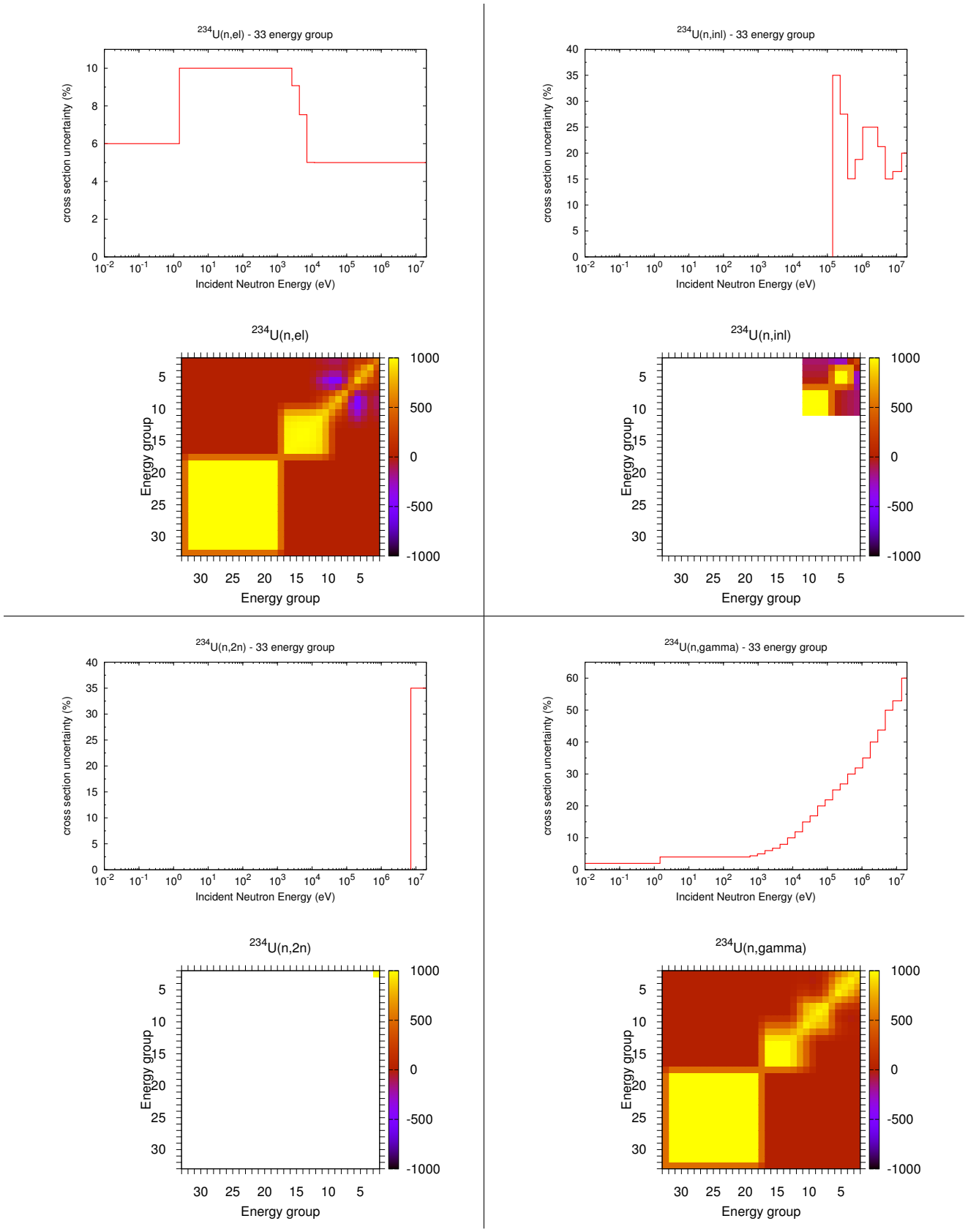

Figure A.93: Covariances for actinide ^{234}U.

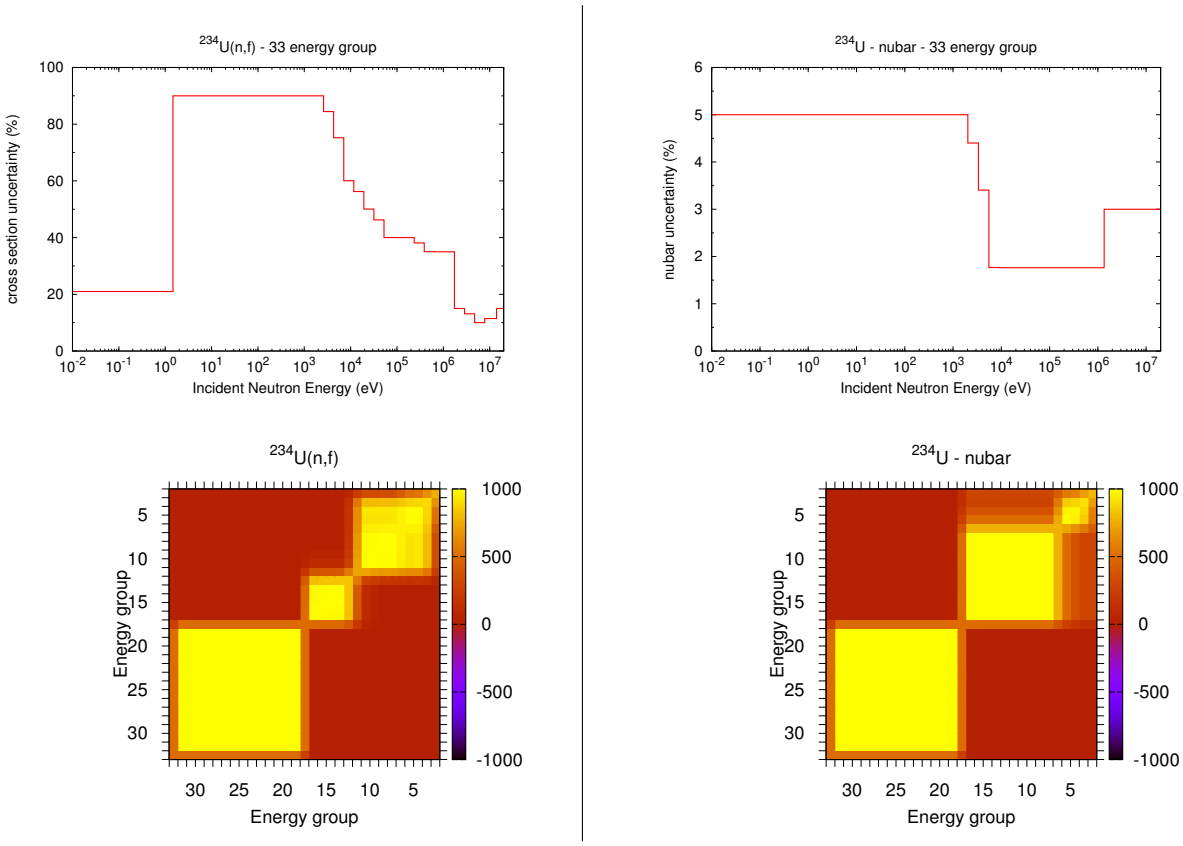

Figure A.93: Covariances for actinide ^{234}U (continued).

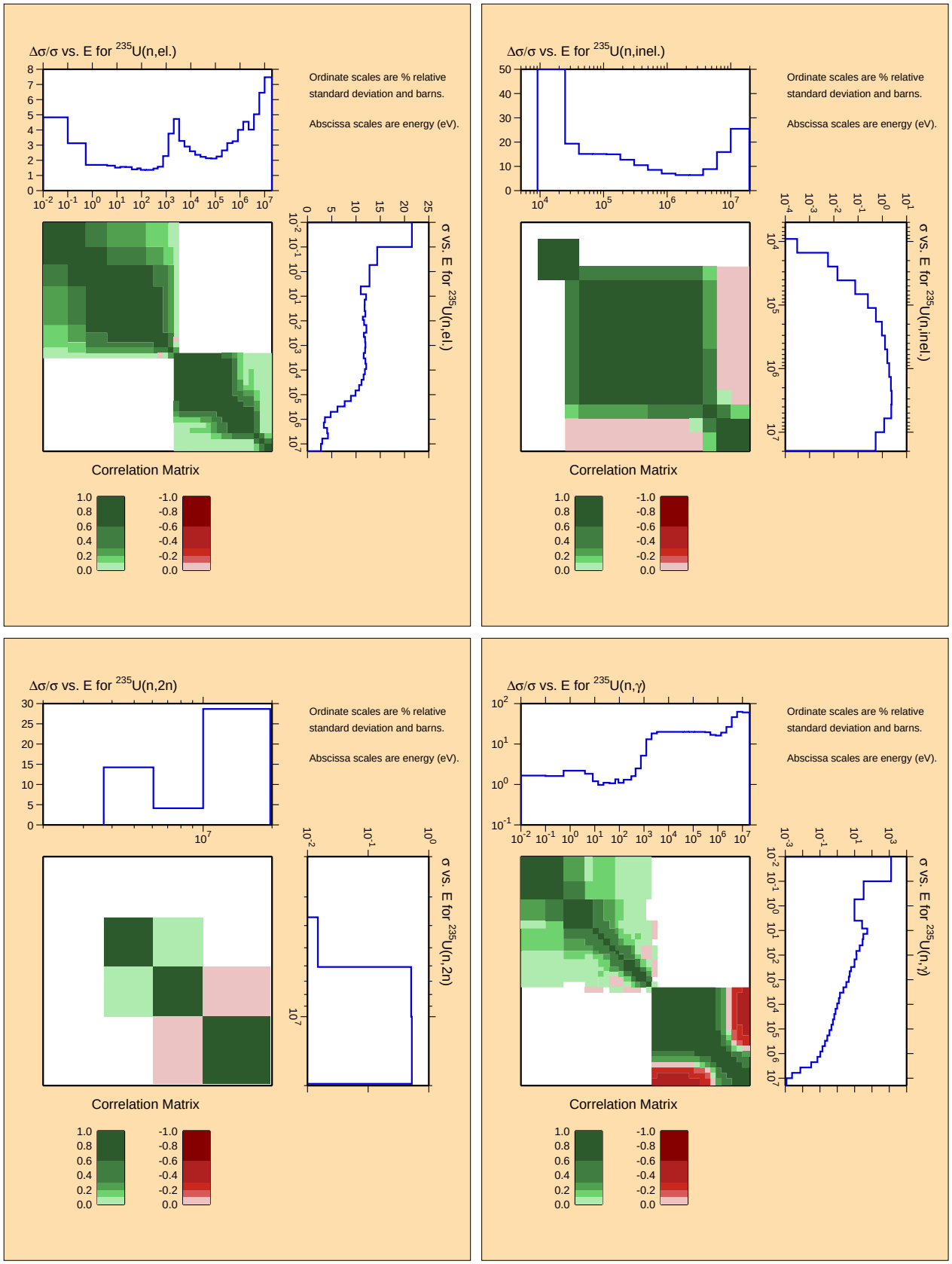

Figure A.94: Covariances for actinide ^{235}U.

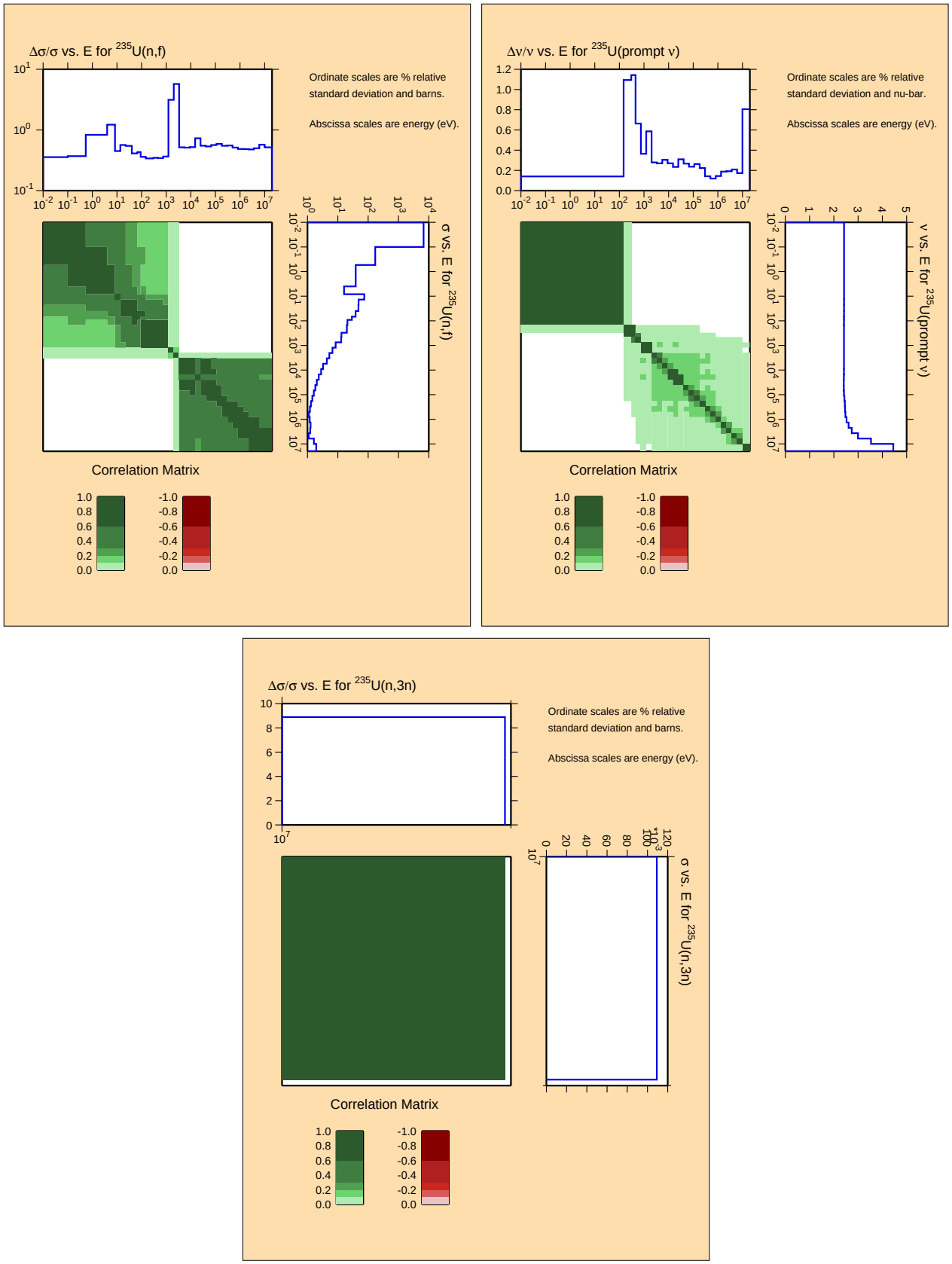

Figure A.94: Covariances for actinide ^{235}U (continued).

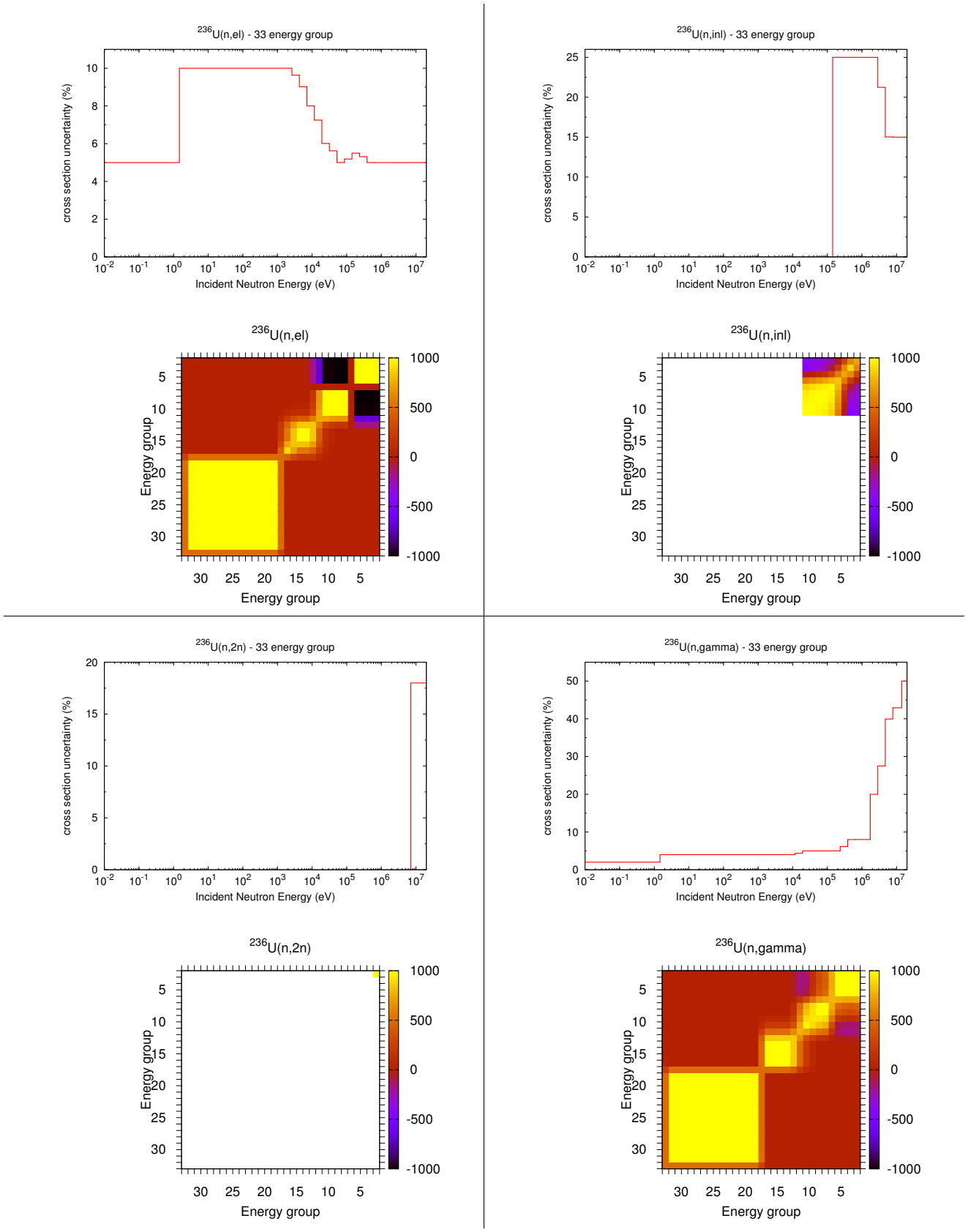

Figure A.95: Covariances for actinide ^{236}U.

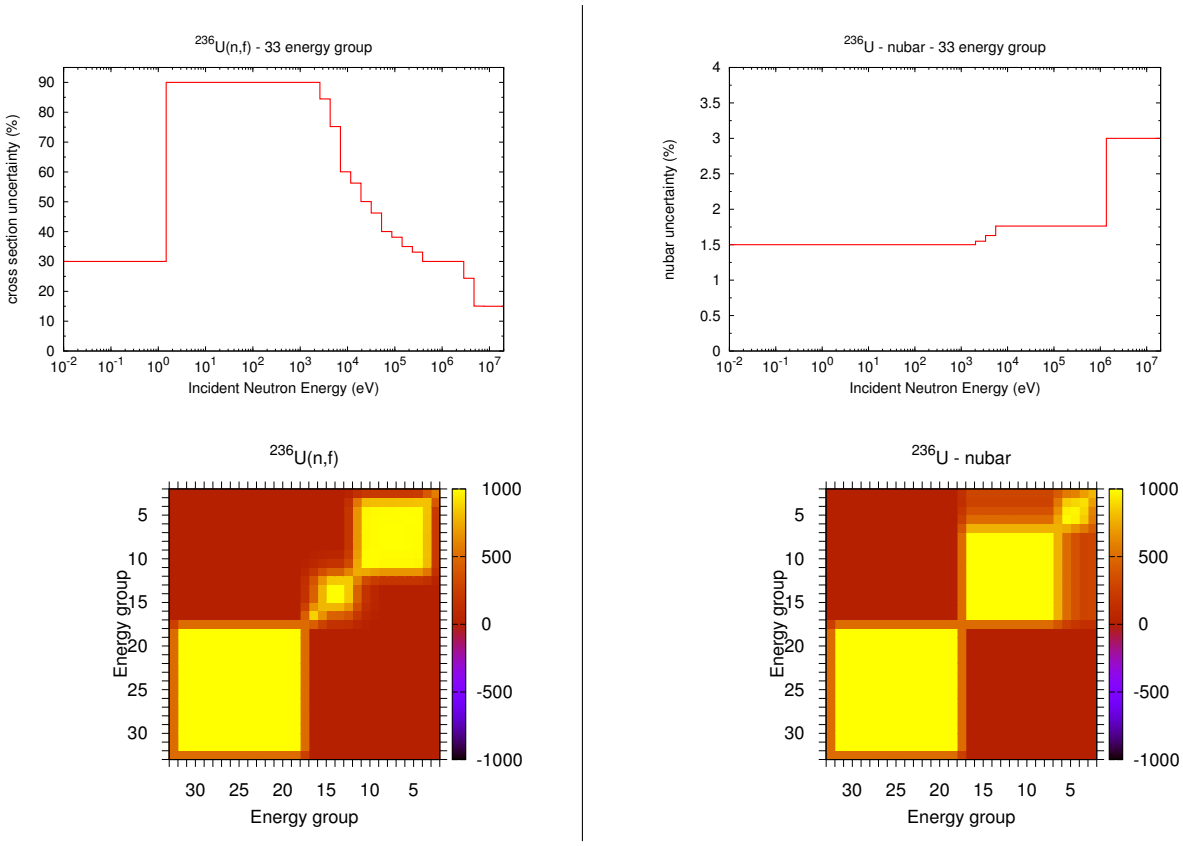

Figure A.95: Covariances for actinide ^{236}U (continued).

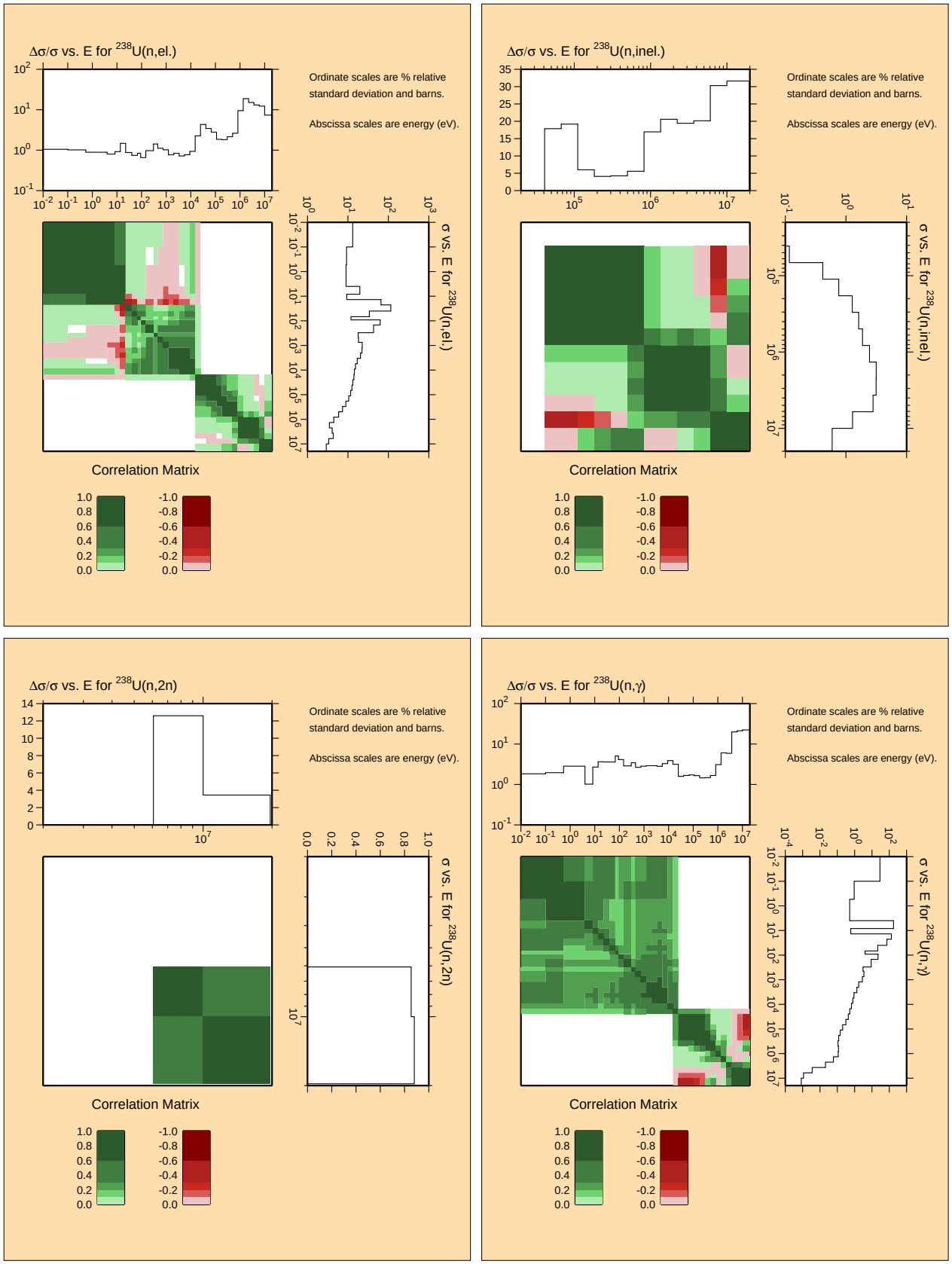

Figure A.96: Covariances for actinide ^{238}U.

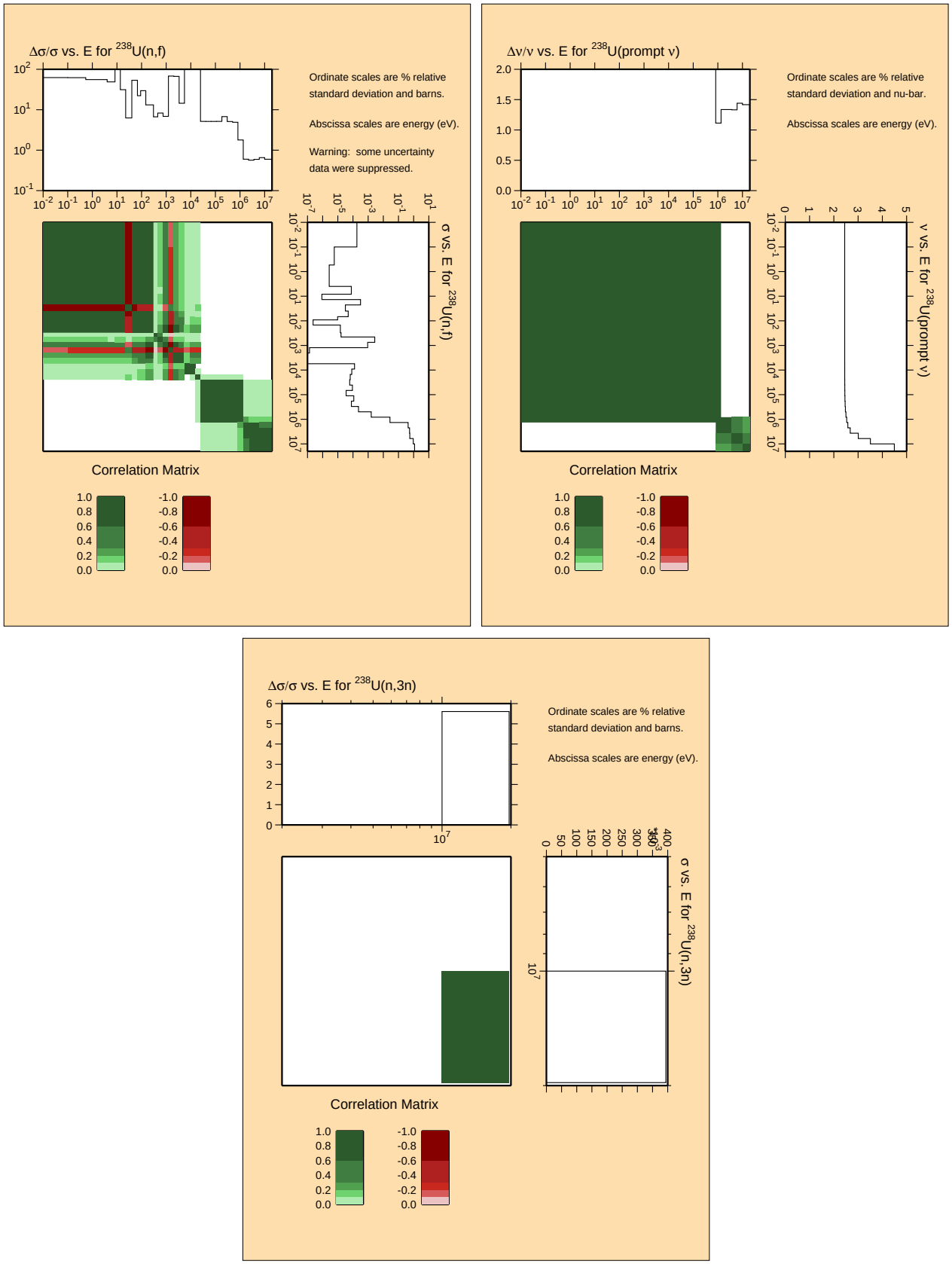

Figure A.96: Covariances for actinide ^{238}U (continued).

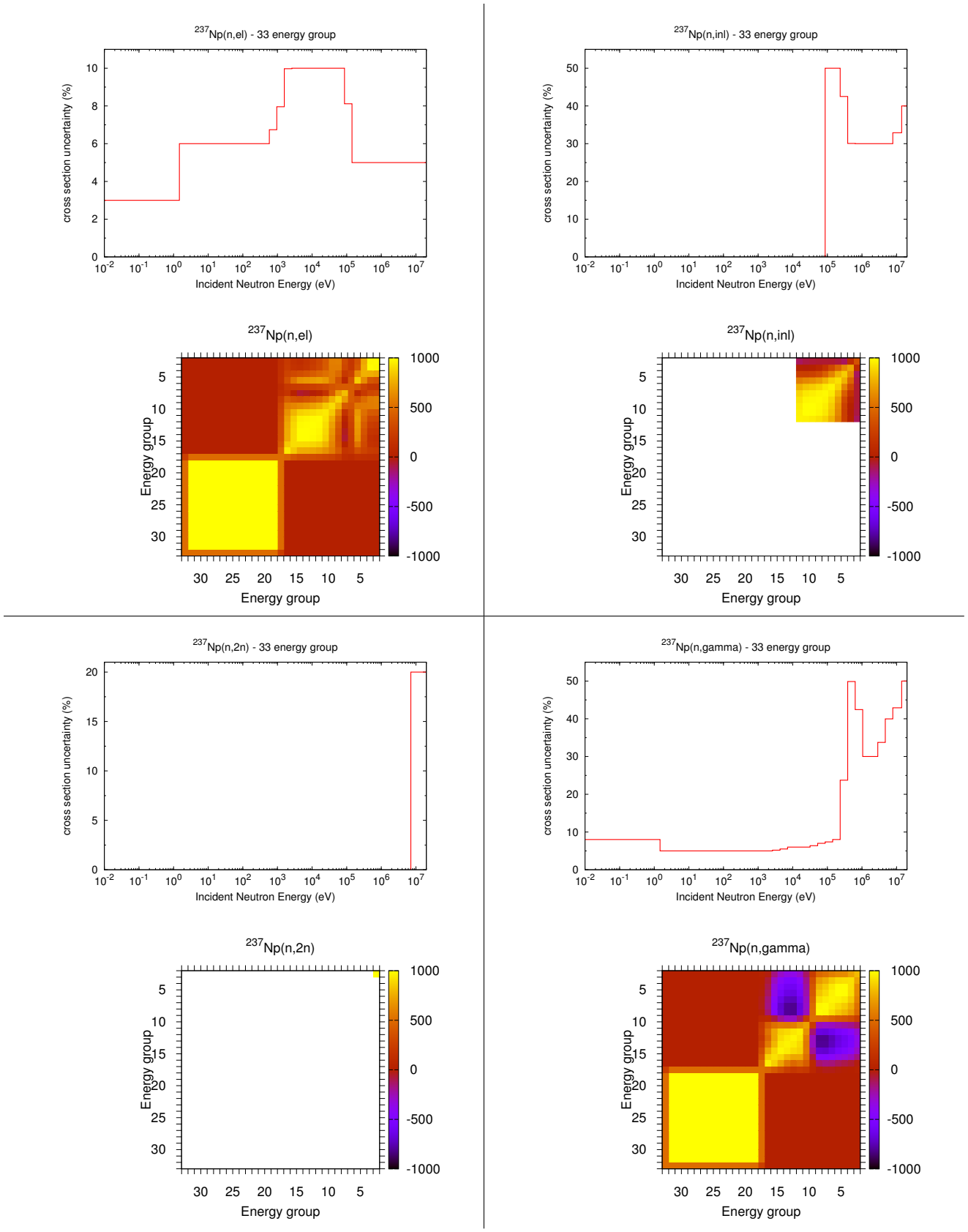

Figure A.97: Covariances for actinide ^{237}Np.

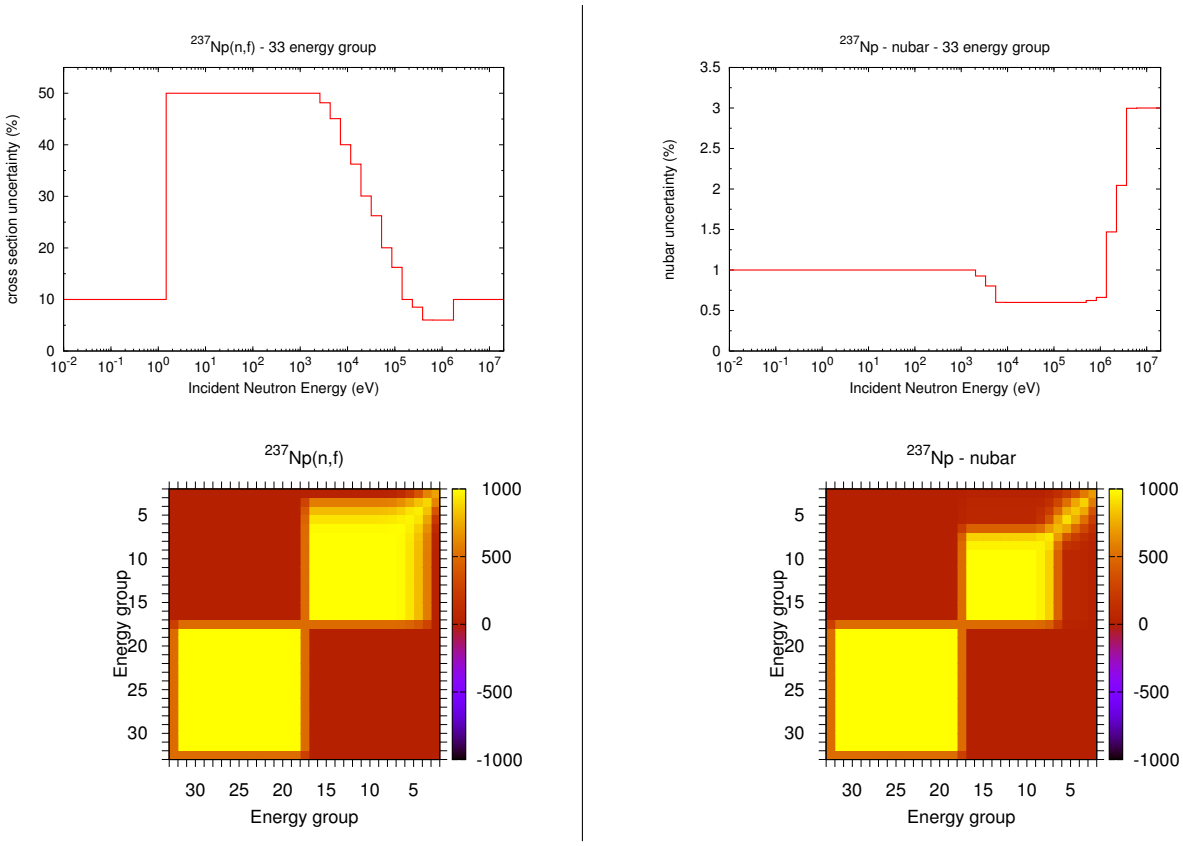

Figure A.97: Covariances for actinide ^{237}Np (continued).

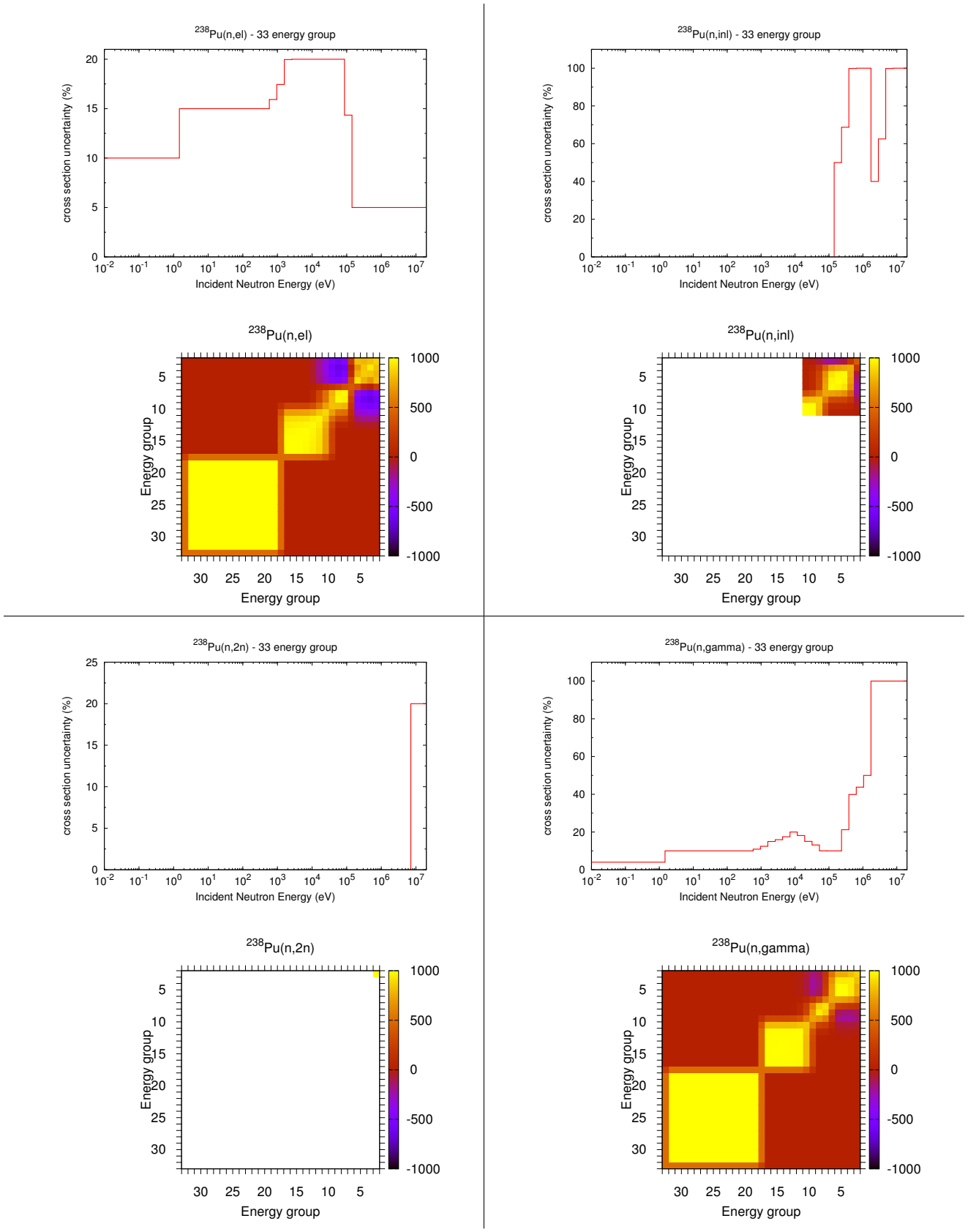

Figure A.98: Covariances for actinide ^{238}Pu.

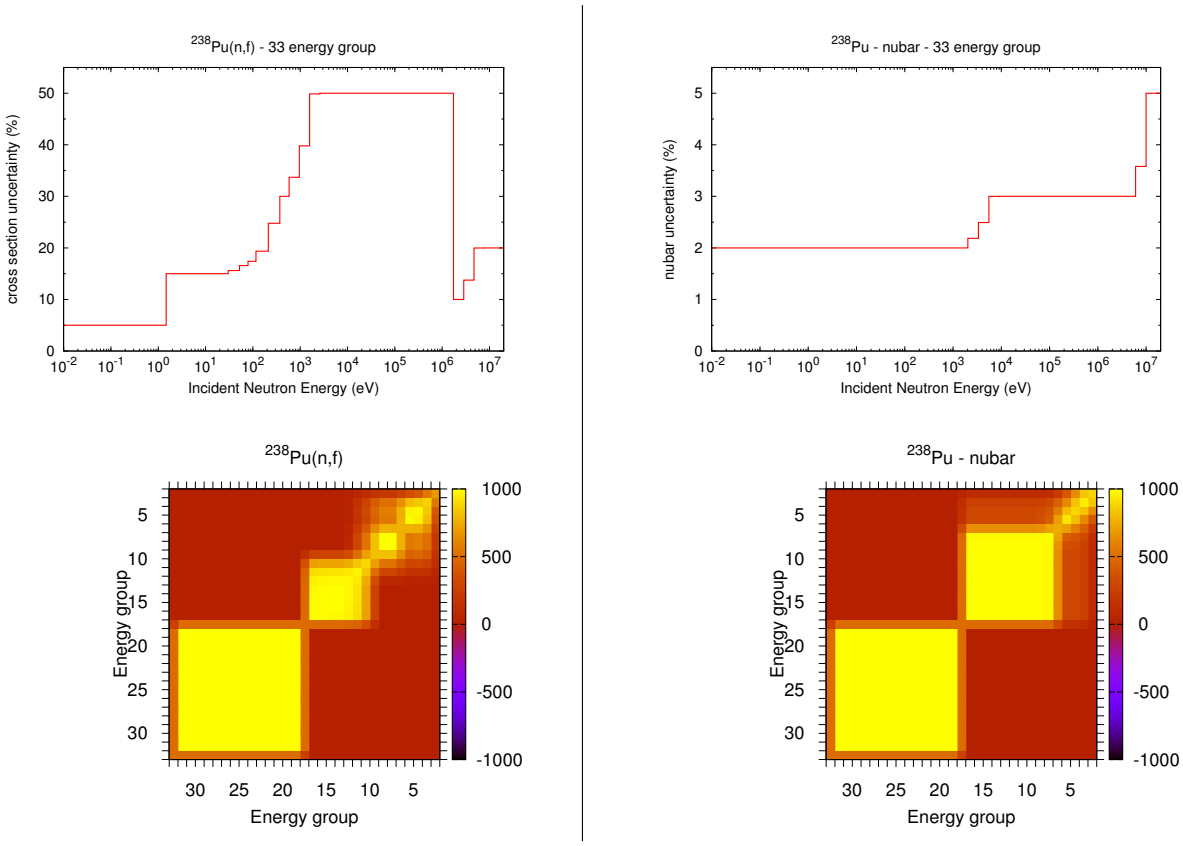

Figure A.98: Covariances for actinide ^{238}Pu (continued).

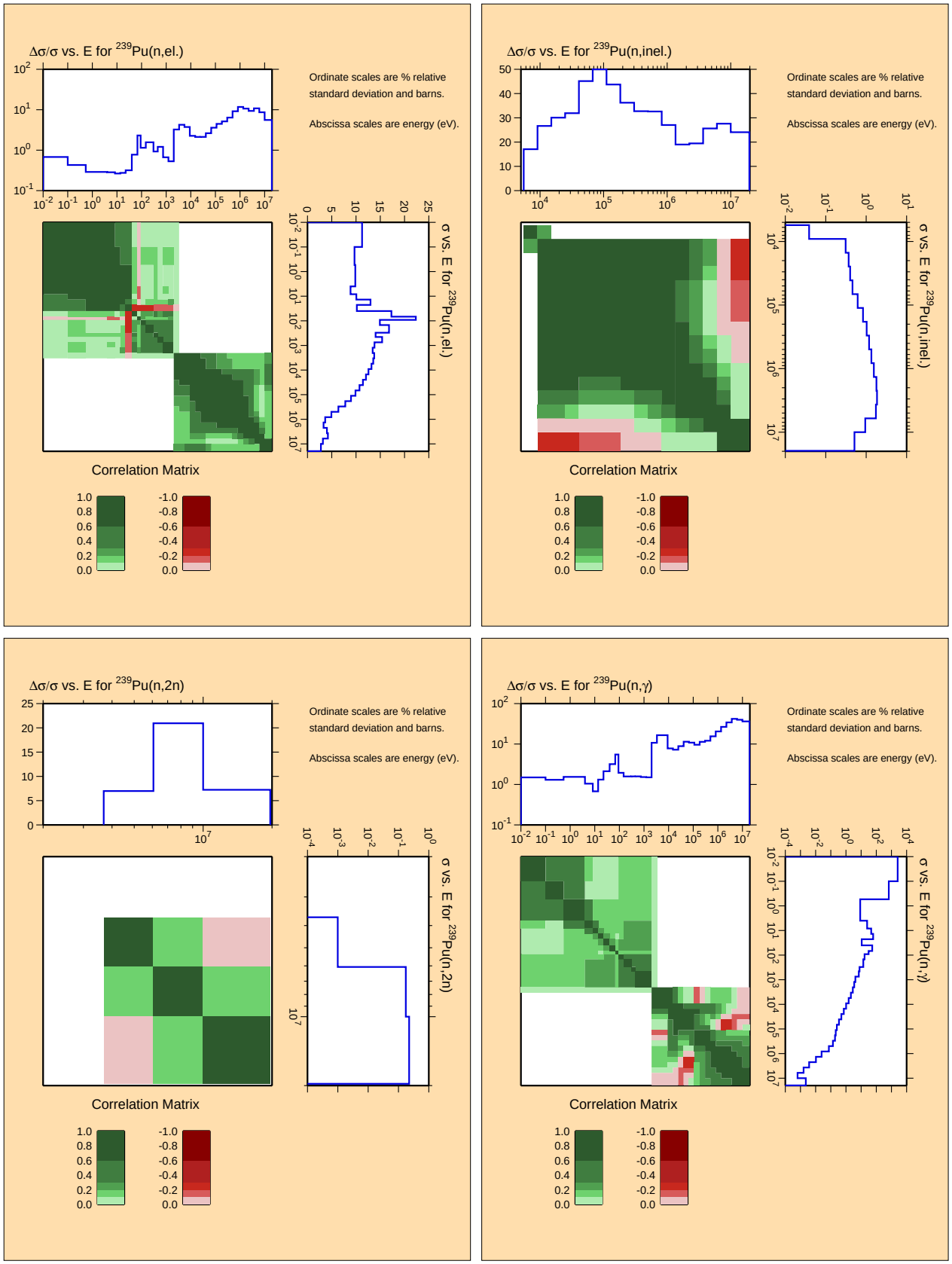

Figure A.99: Covariances for actinide ^{239}Pu.

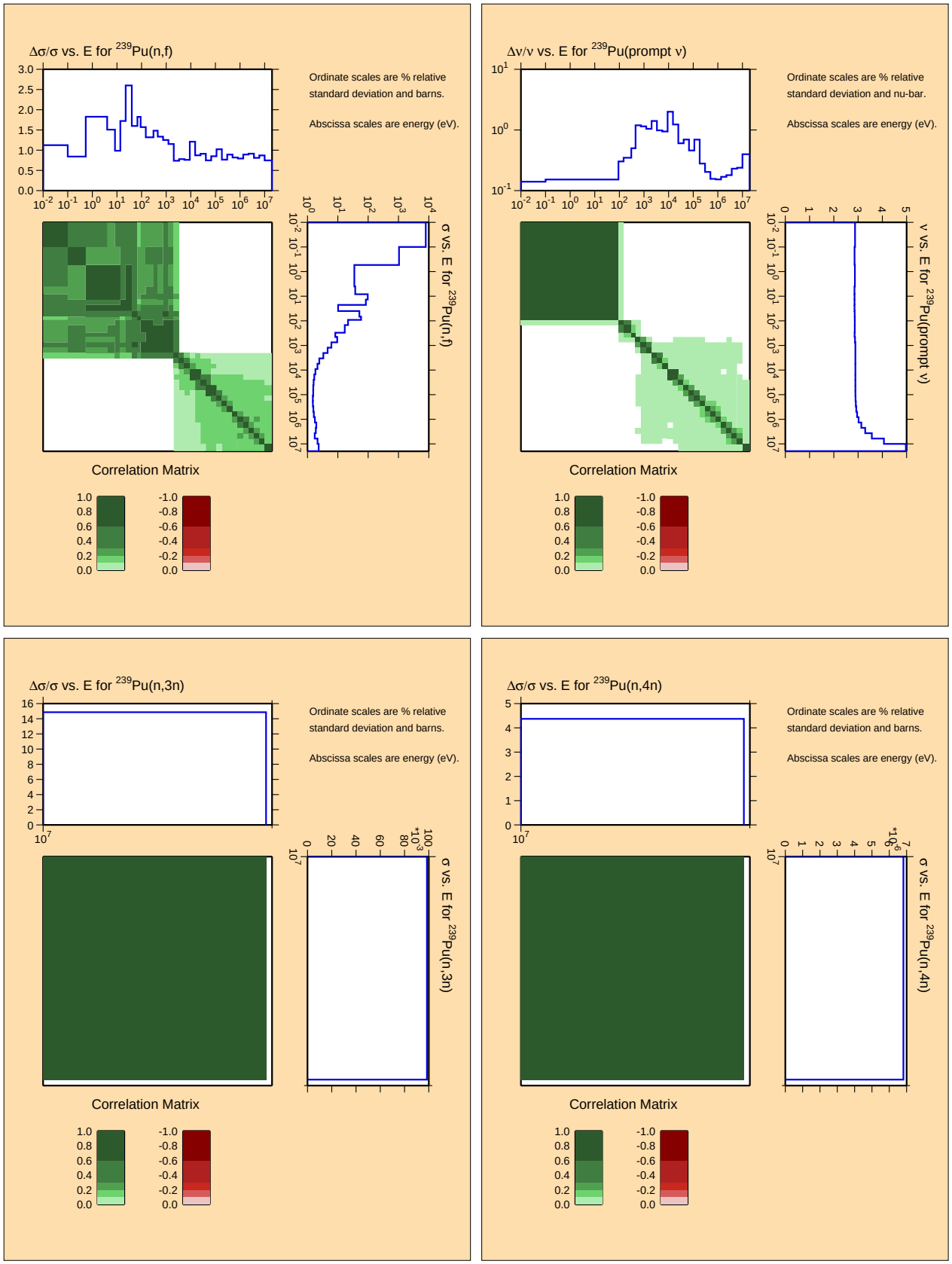

Figure A.99: Covariances for actinide ^{239}Pu (continued).

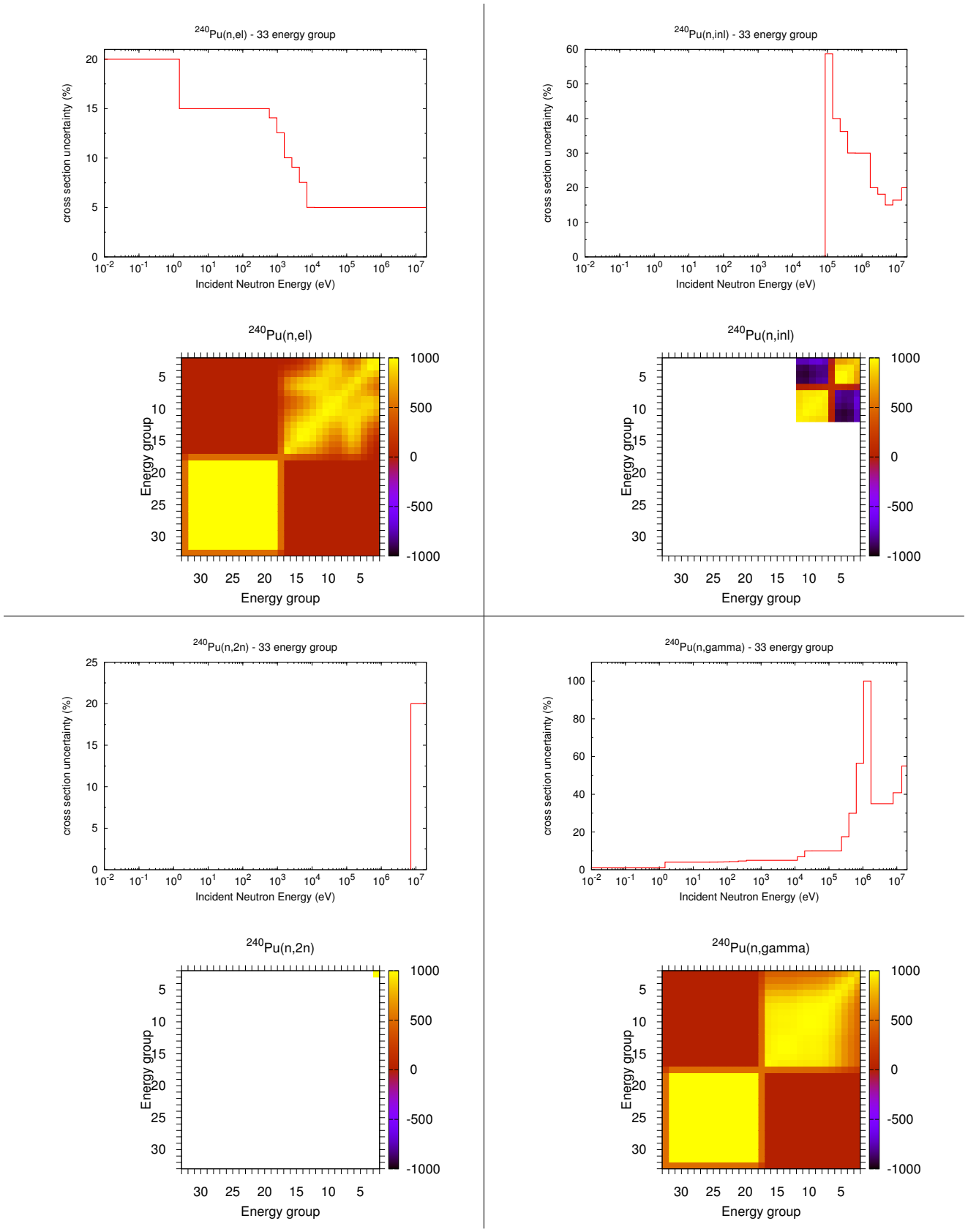

Figure A.100: Covariances for actinide ^{240}Pu.

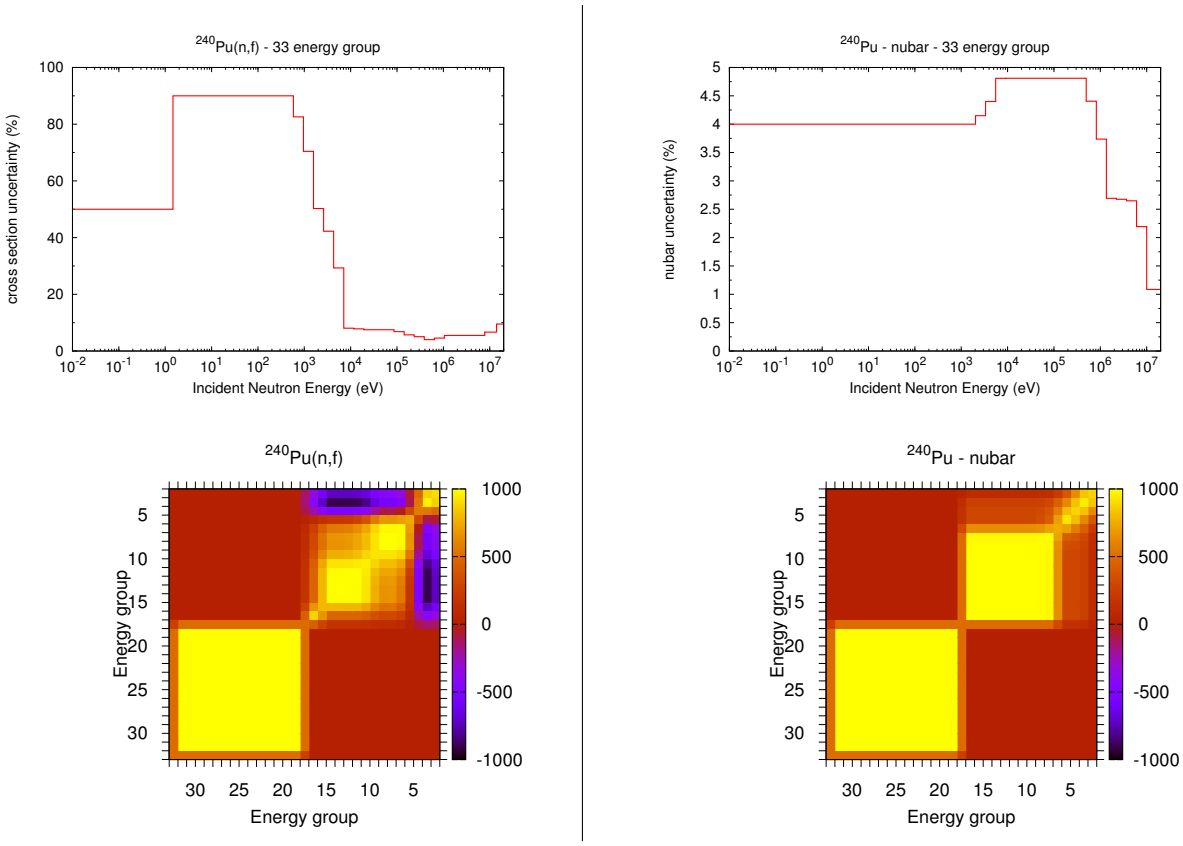

Figure A.100: Covariances for actinide ^{240}Pu (continued).

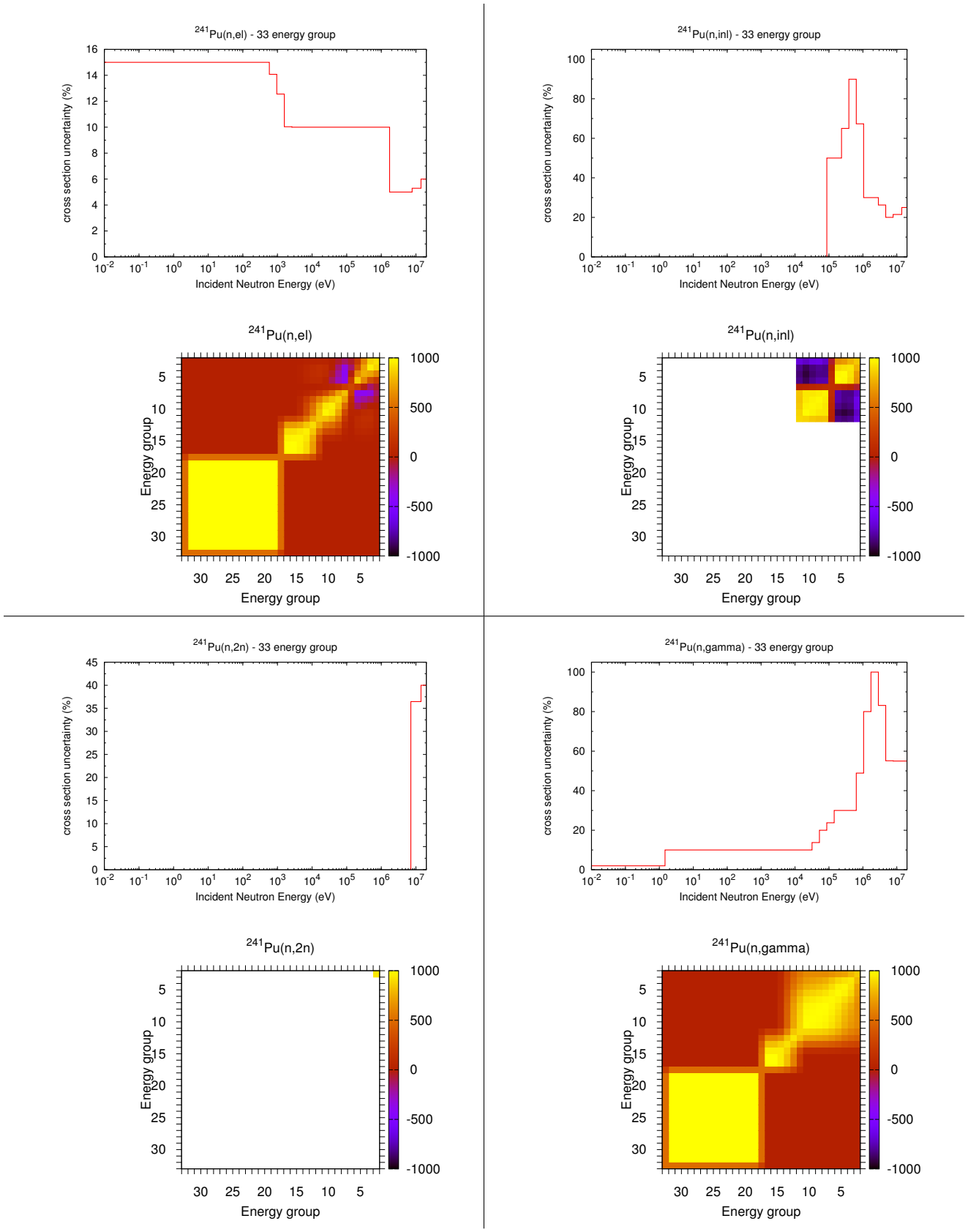

Figure A.101: Covariances for actinide ^{241}Pu.

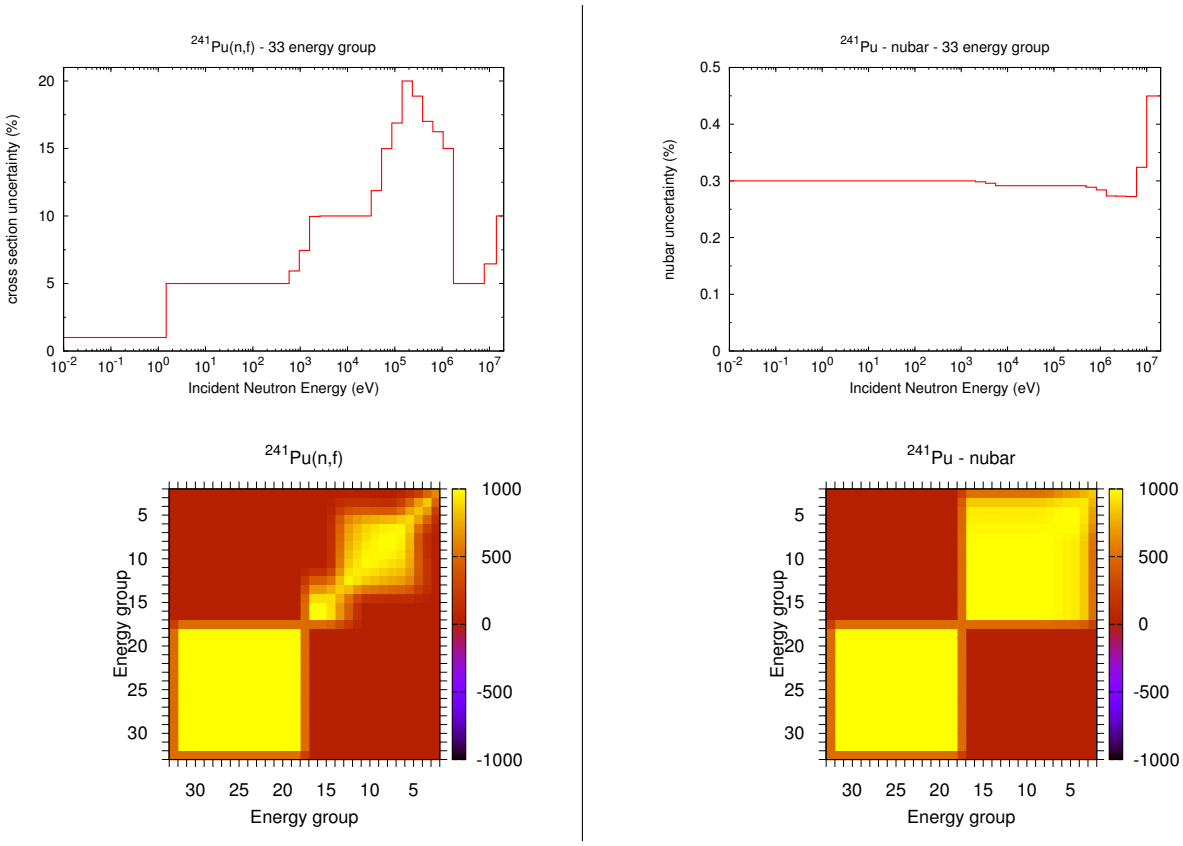

Figure A.101: Covariances for actinide ^{241}Pu (continued).

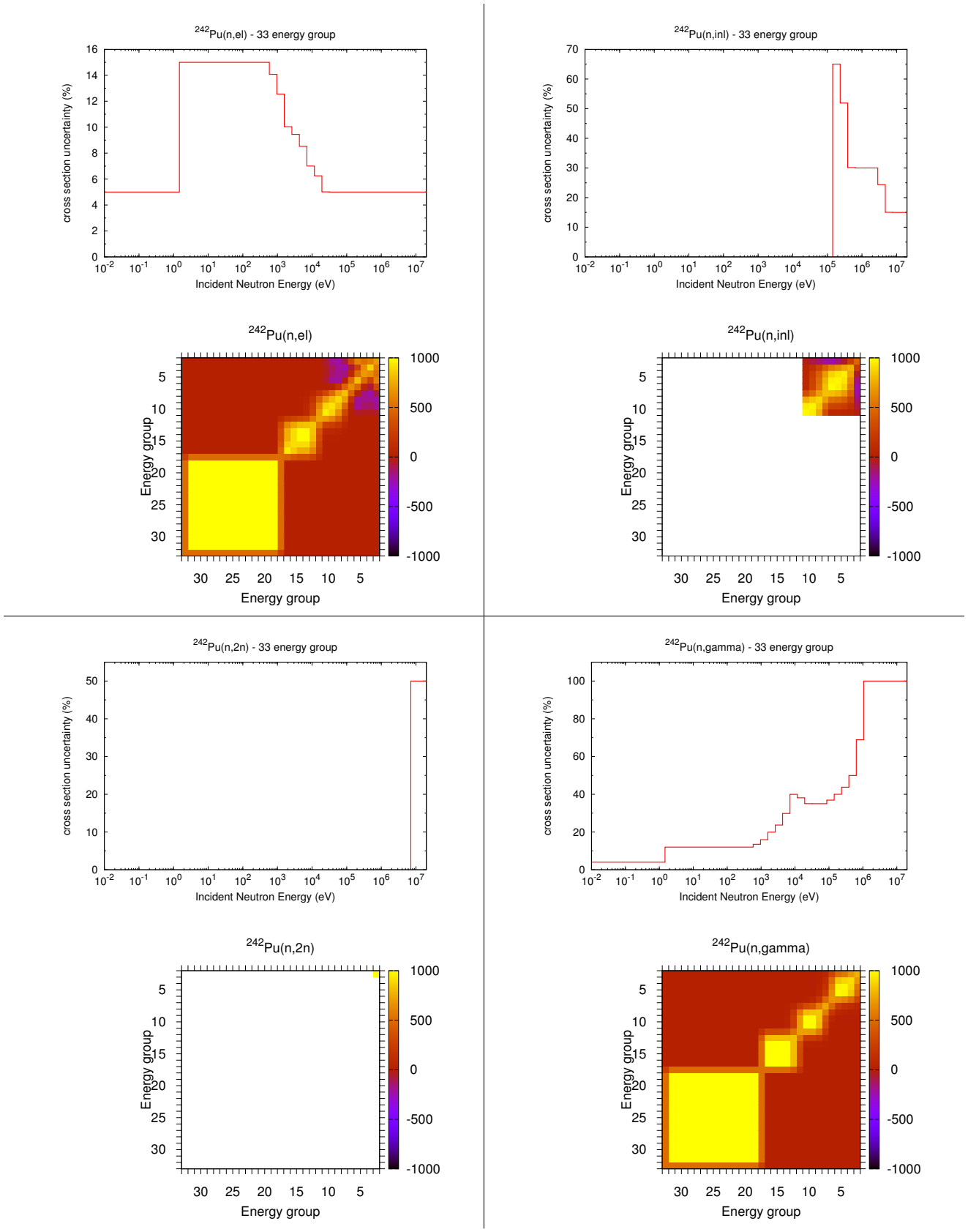

Figure A.102: Covariances for actinide ^{242}Pu.

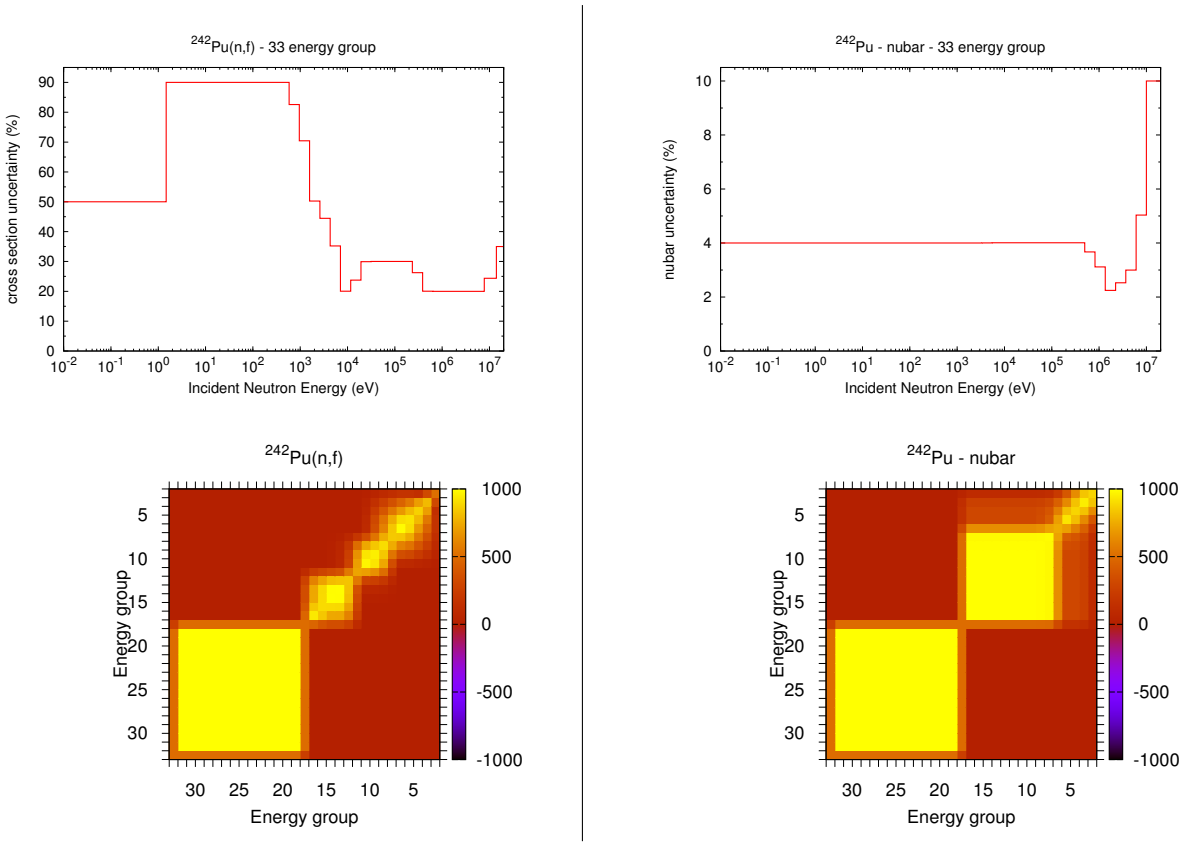

Figure A.102: Covariances for actinide ^{242}Pu (continued).

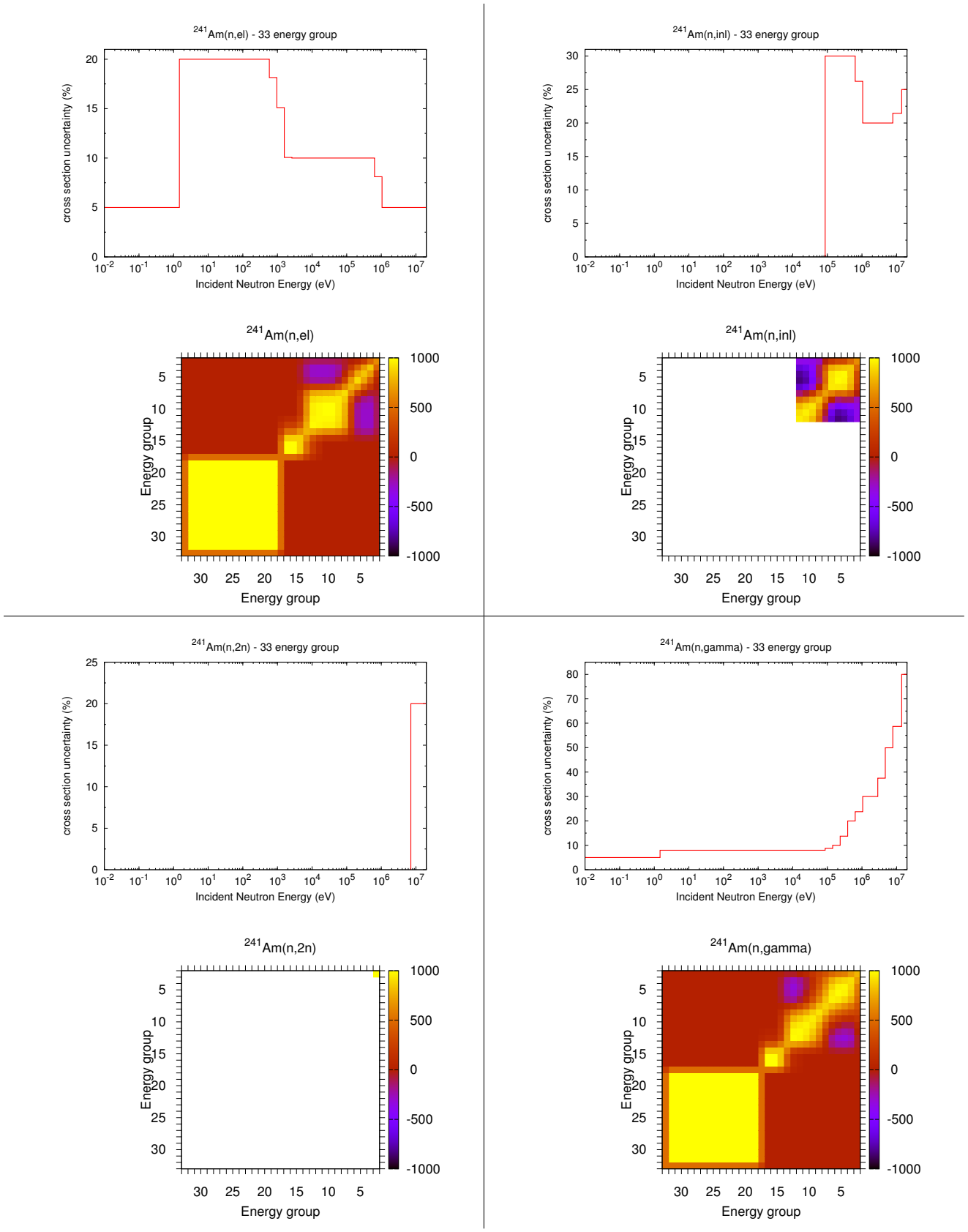

Figure A.103: Covariances for actinide ^{241}Am.

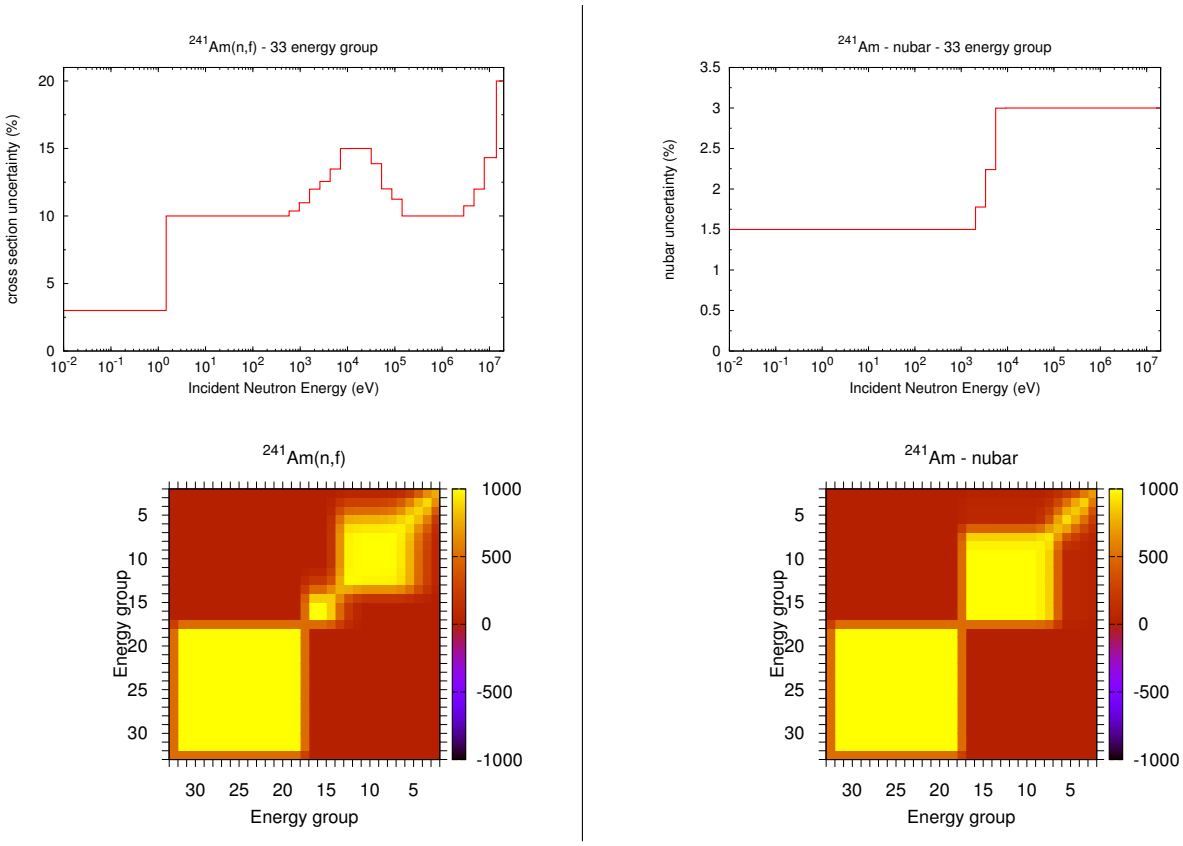

Figure A.103: Covariances for actinide ^{241}Am (continued).

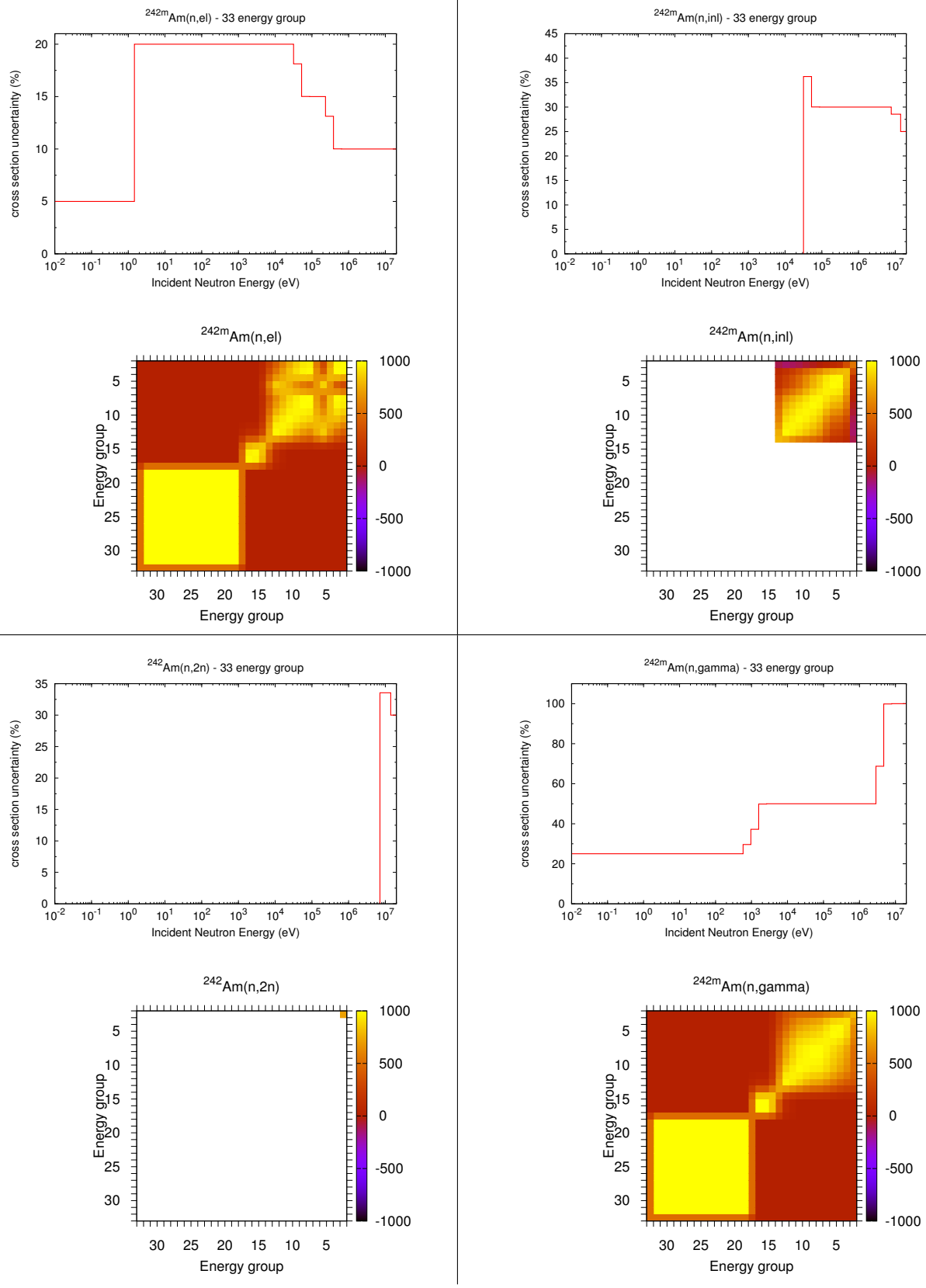

Figure A.104: Covariances for actinide ^{242m}Am.

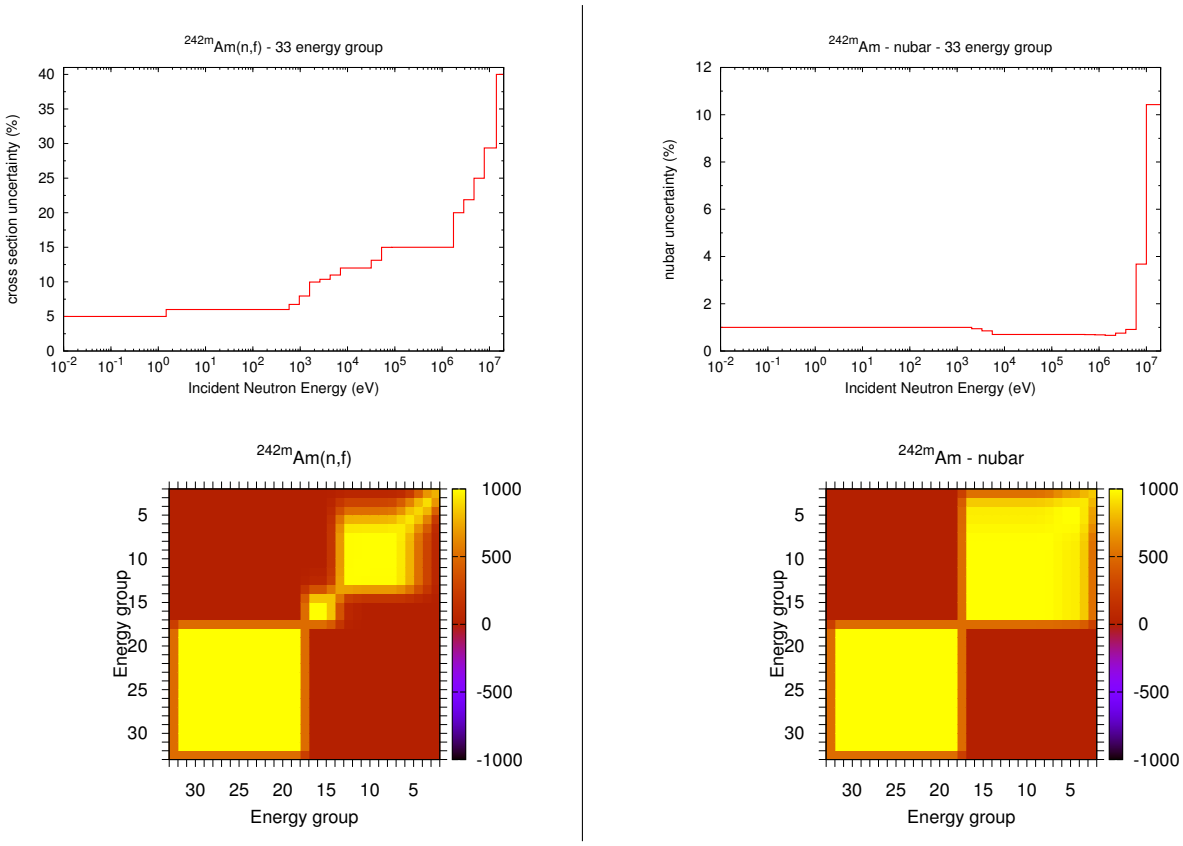

Figure A.104: Covariances for actinide ^{242m}Am (continued).

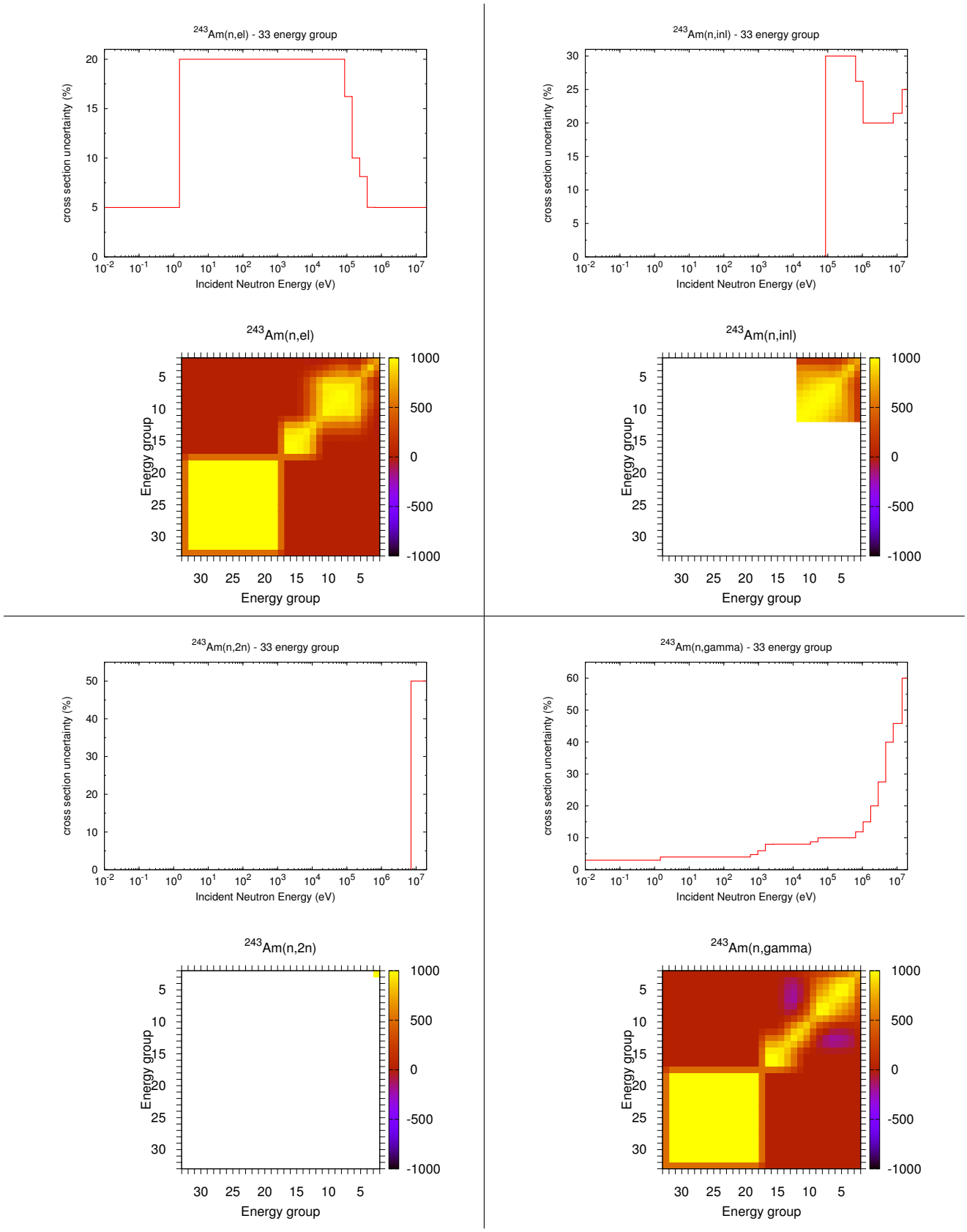

Figure A.105: Covariances for actinide ^{243}Am.

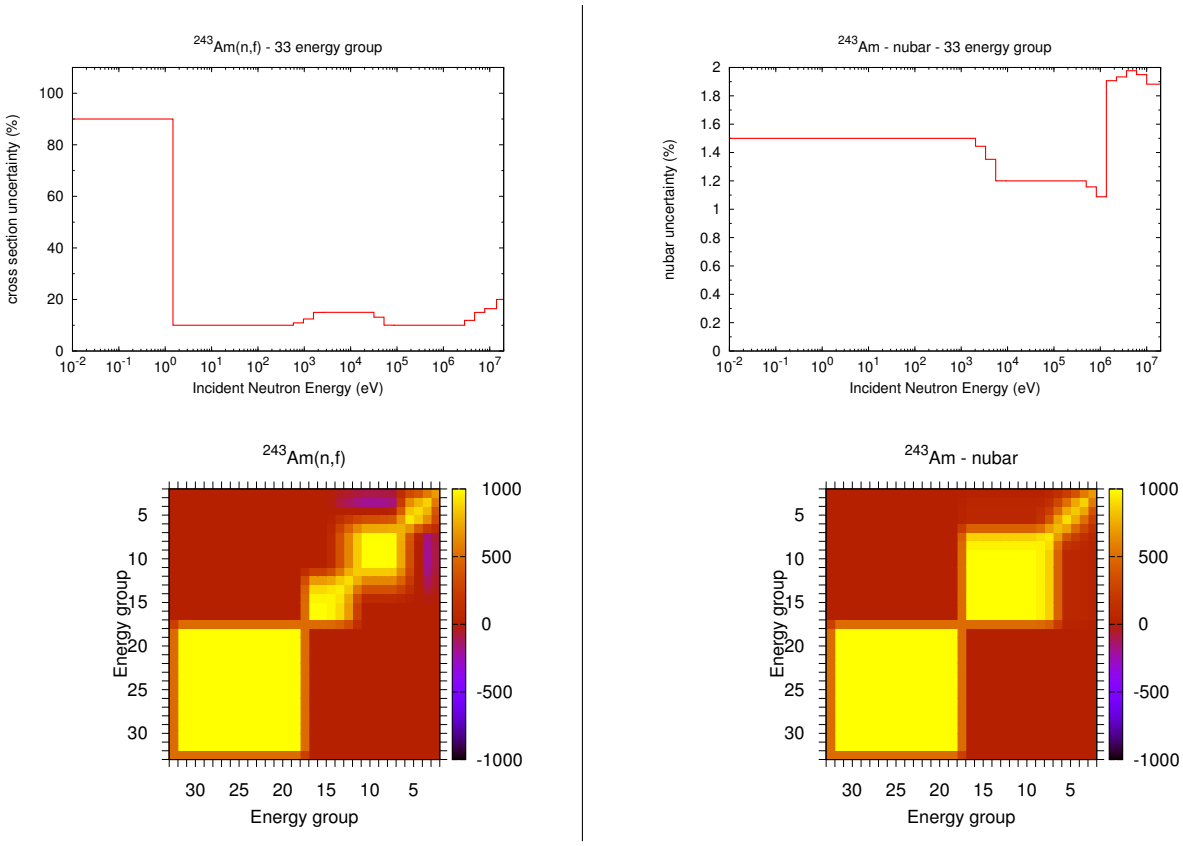

Figure A.105: Covariances for actinide ^{243}Am (continued).

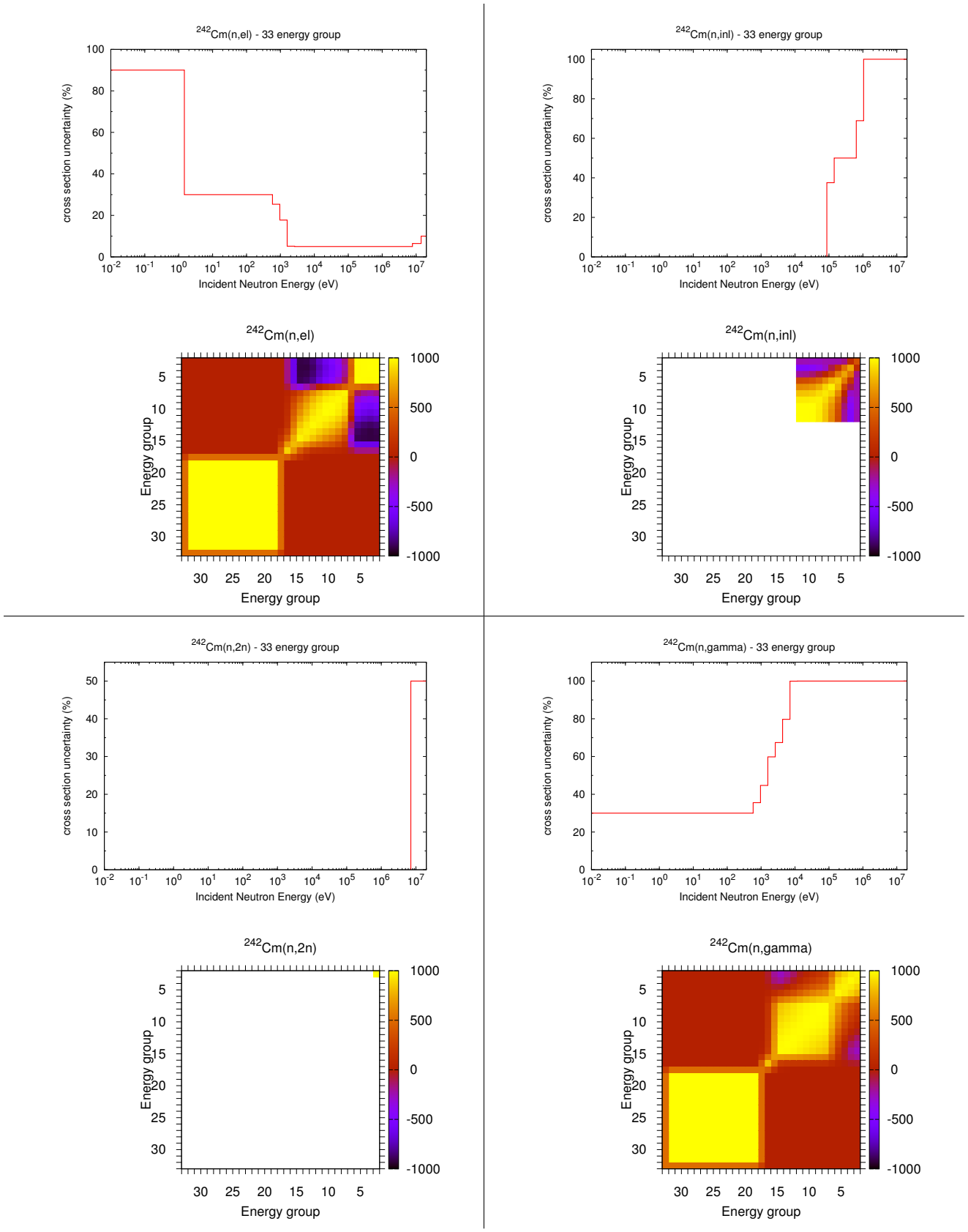

Figure A.106: Covariances for actinide ^{242}Cm.

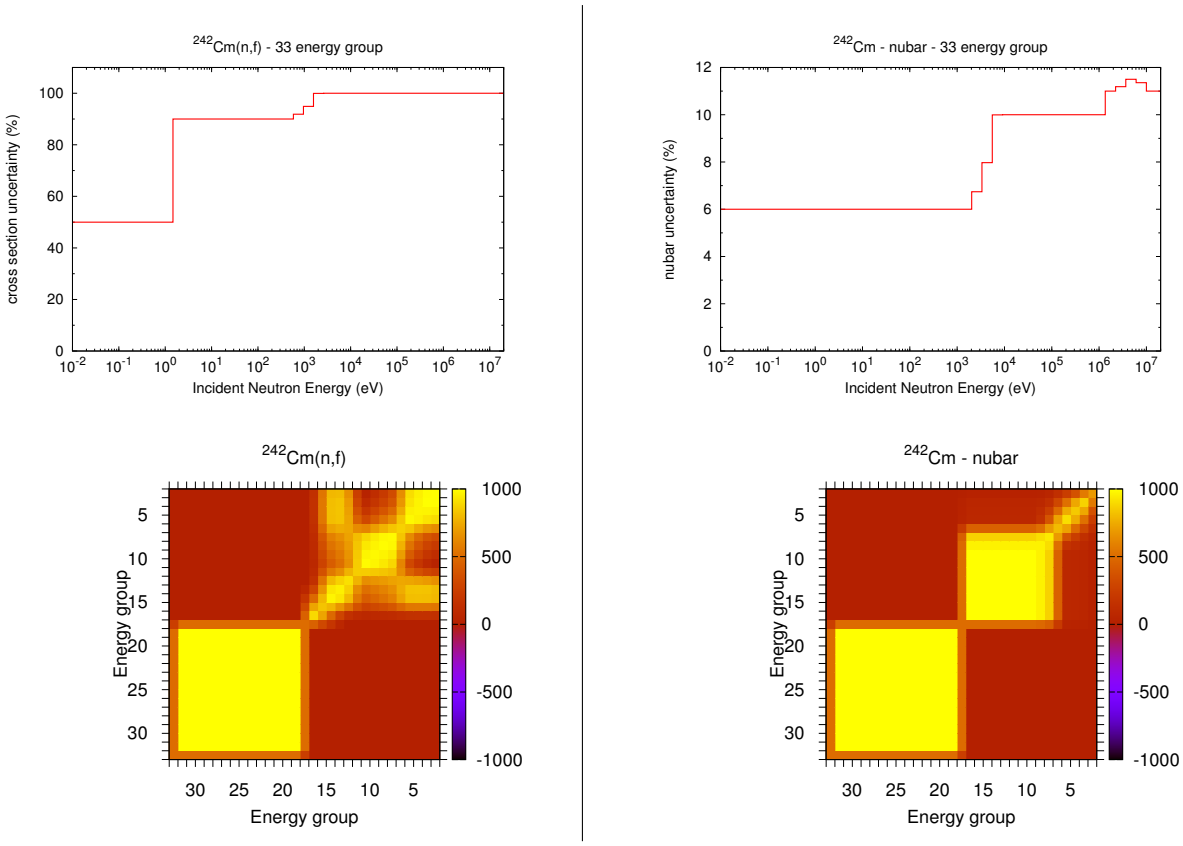

Figure A.106: Covariances for actinide ^{242}Cm (continued).

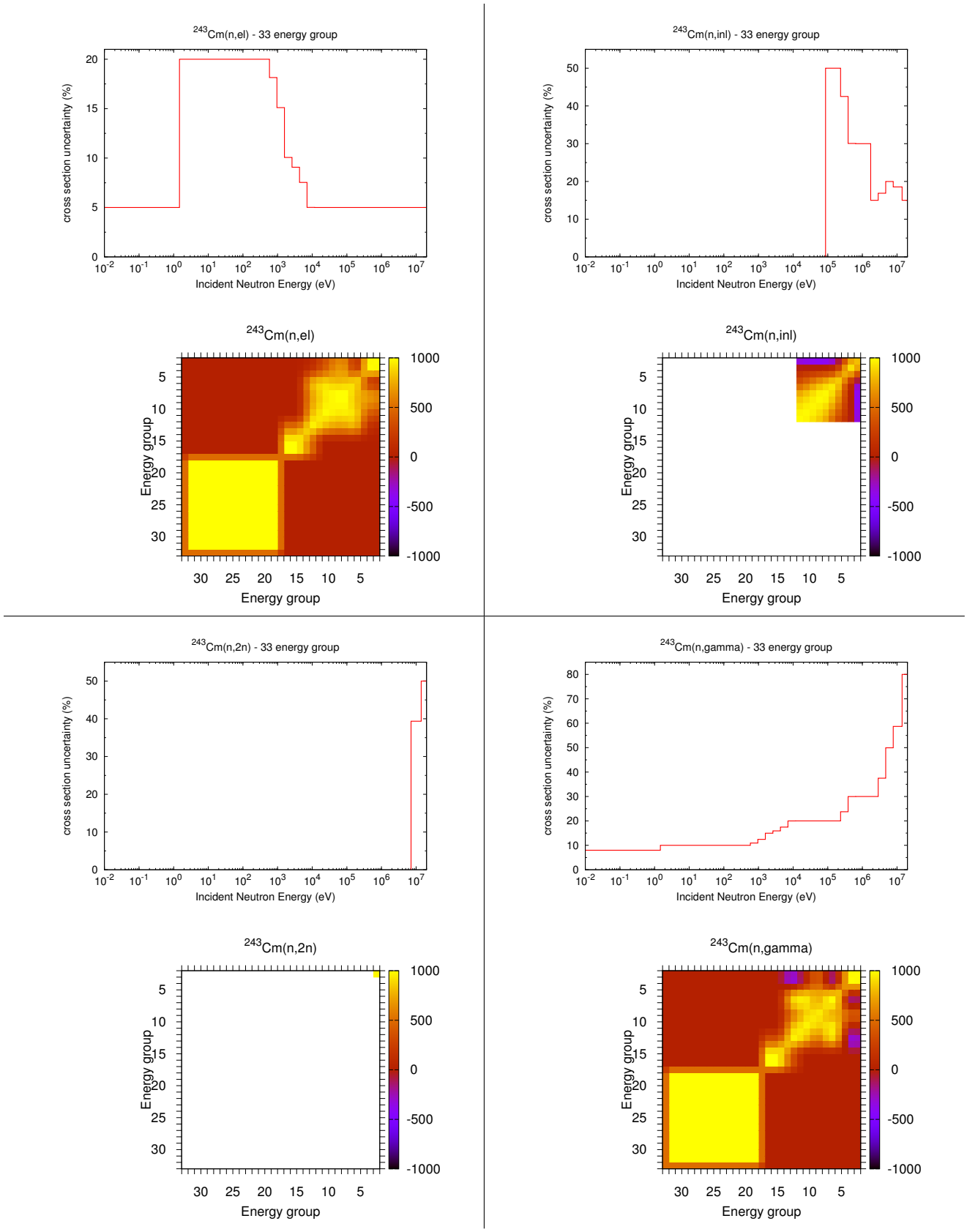

Figure A.107: Covariances for actinide ^{243}Cm.

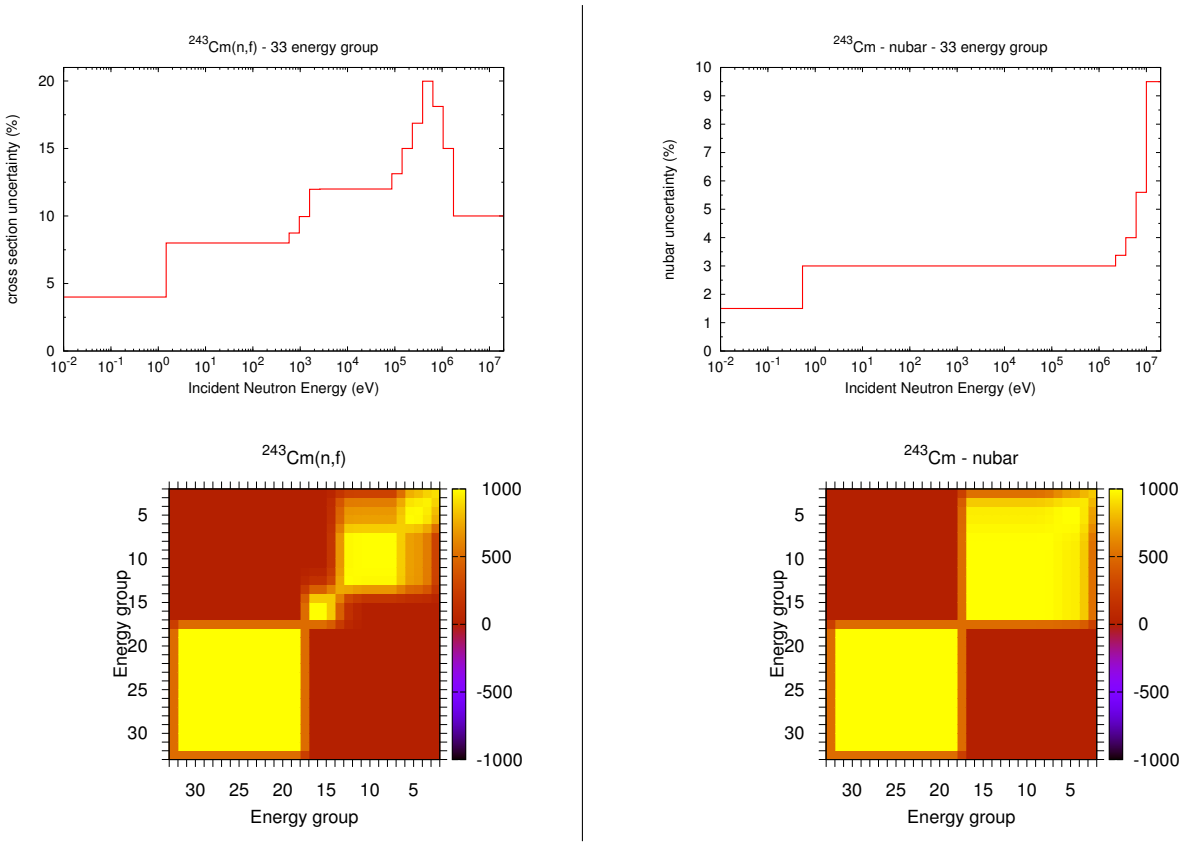

Figure A.107: Covariances for actinide ^{243}Cm (continued).

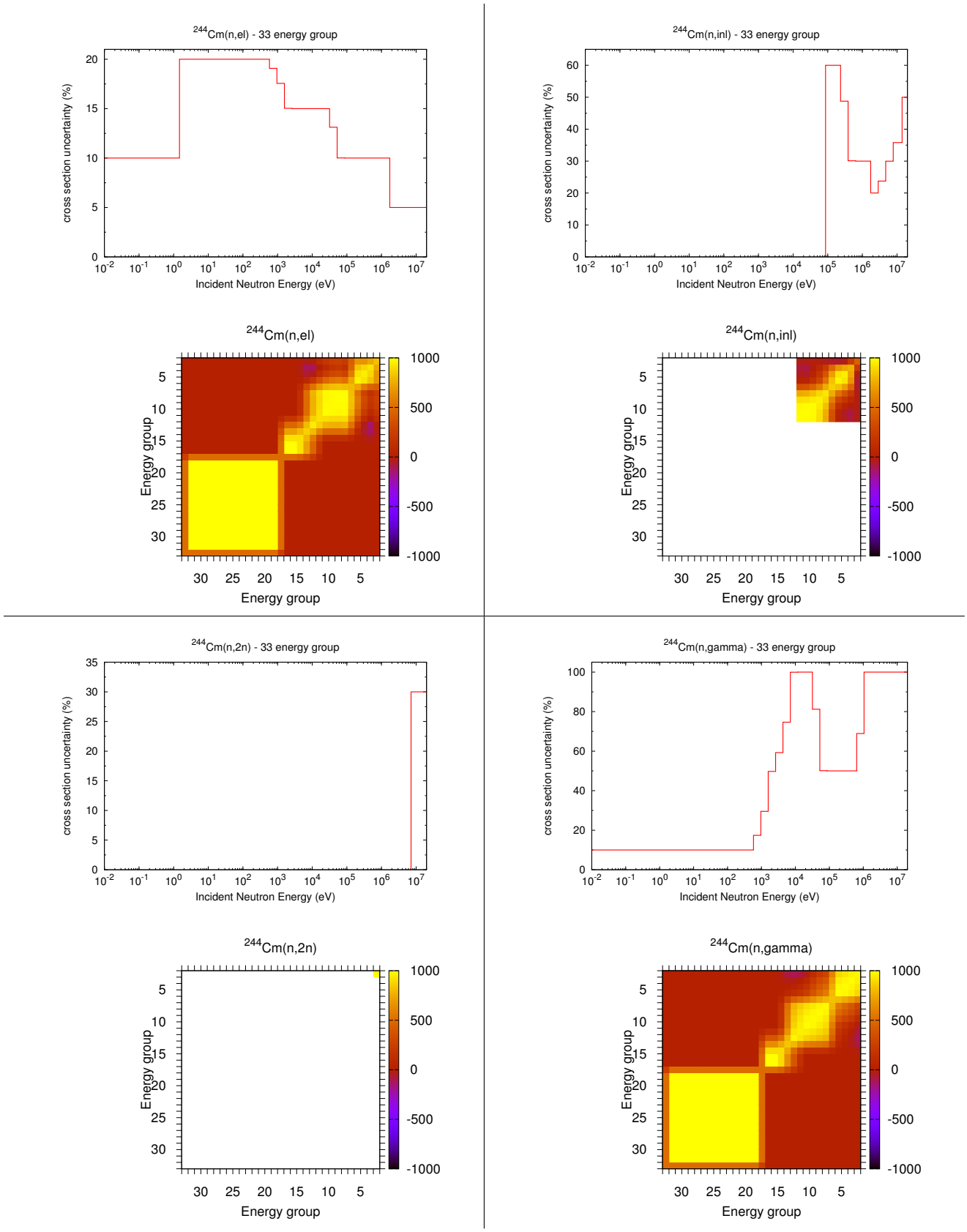

Figure A.108: Covariances for actinide ^{244}Cm.

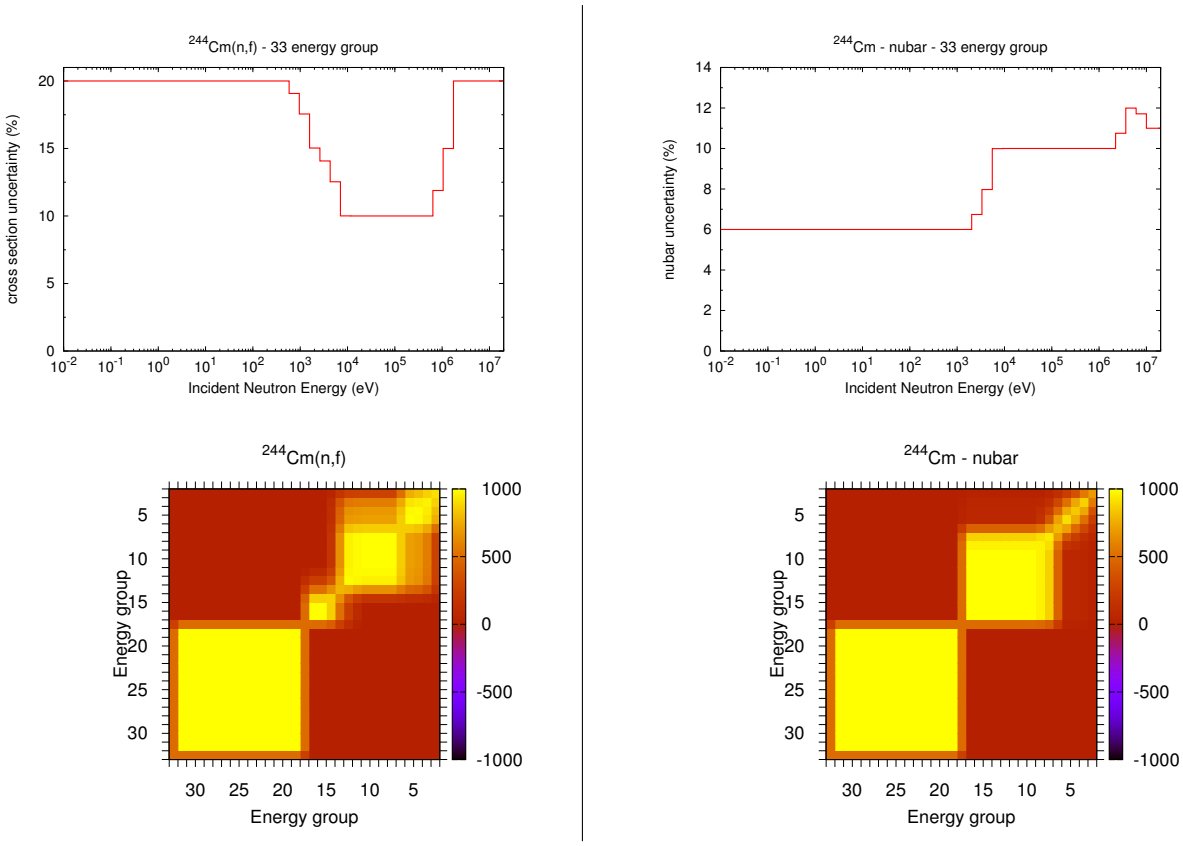

Figure A.108: Covariances for actinide ^{244}Cm (continued).

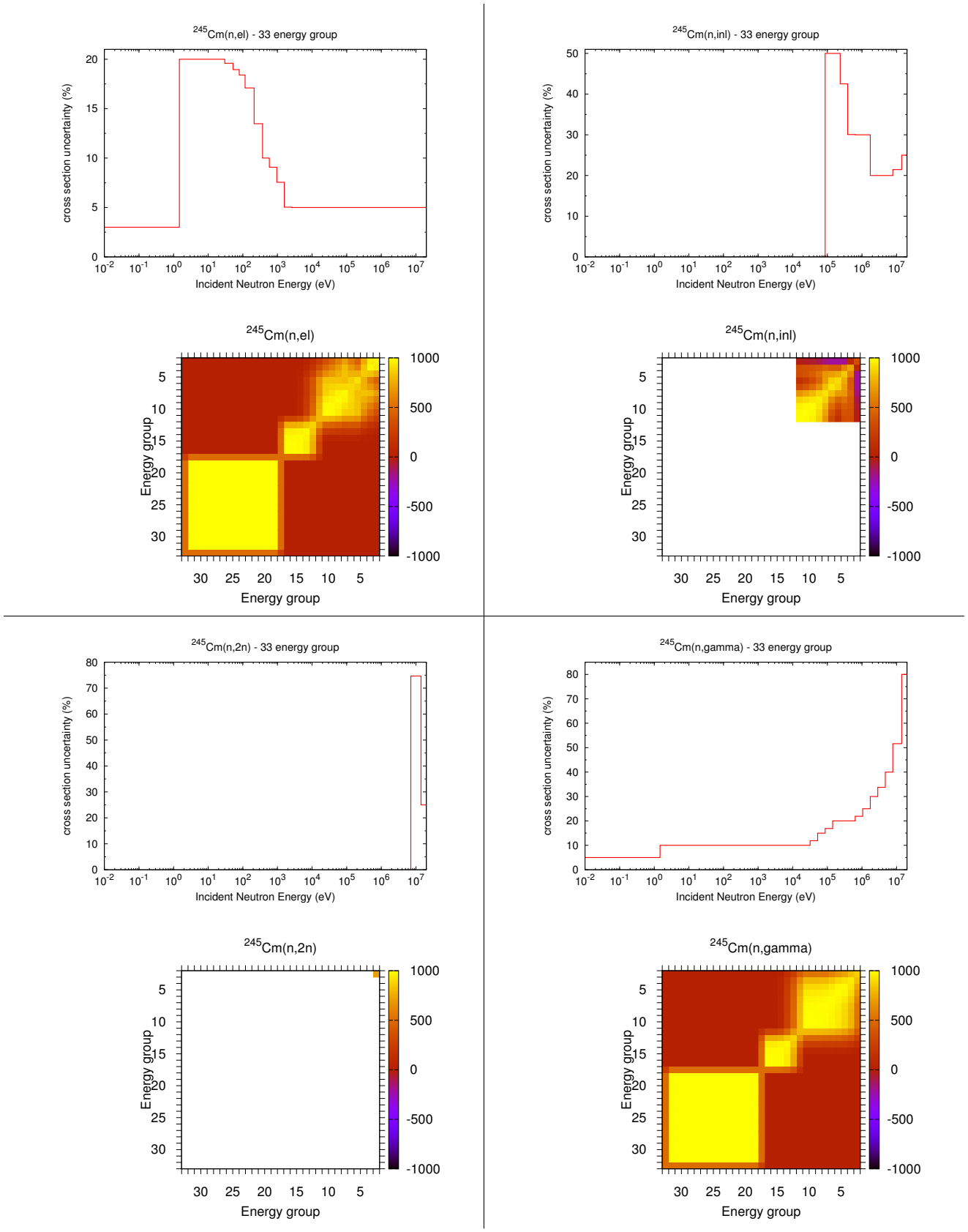

Figure A.109: Covariances for actinide ^{245}Cm.

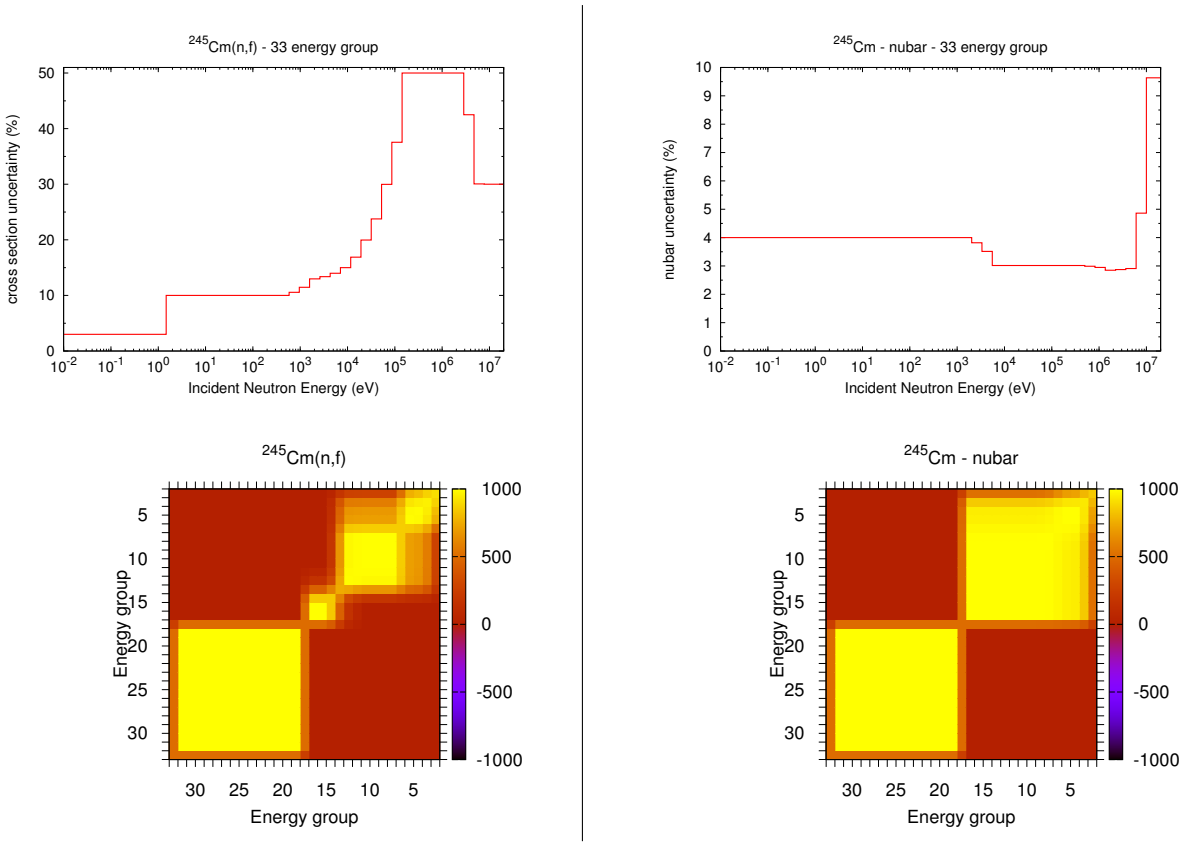

Figure A.109: Covariances for actinide ^{245}Cm (continued).

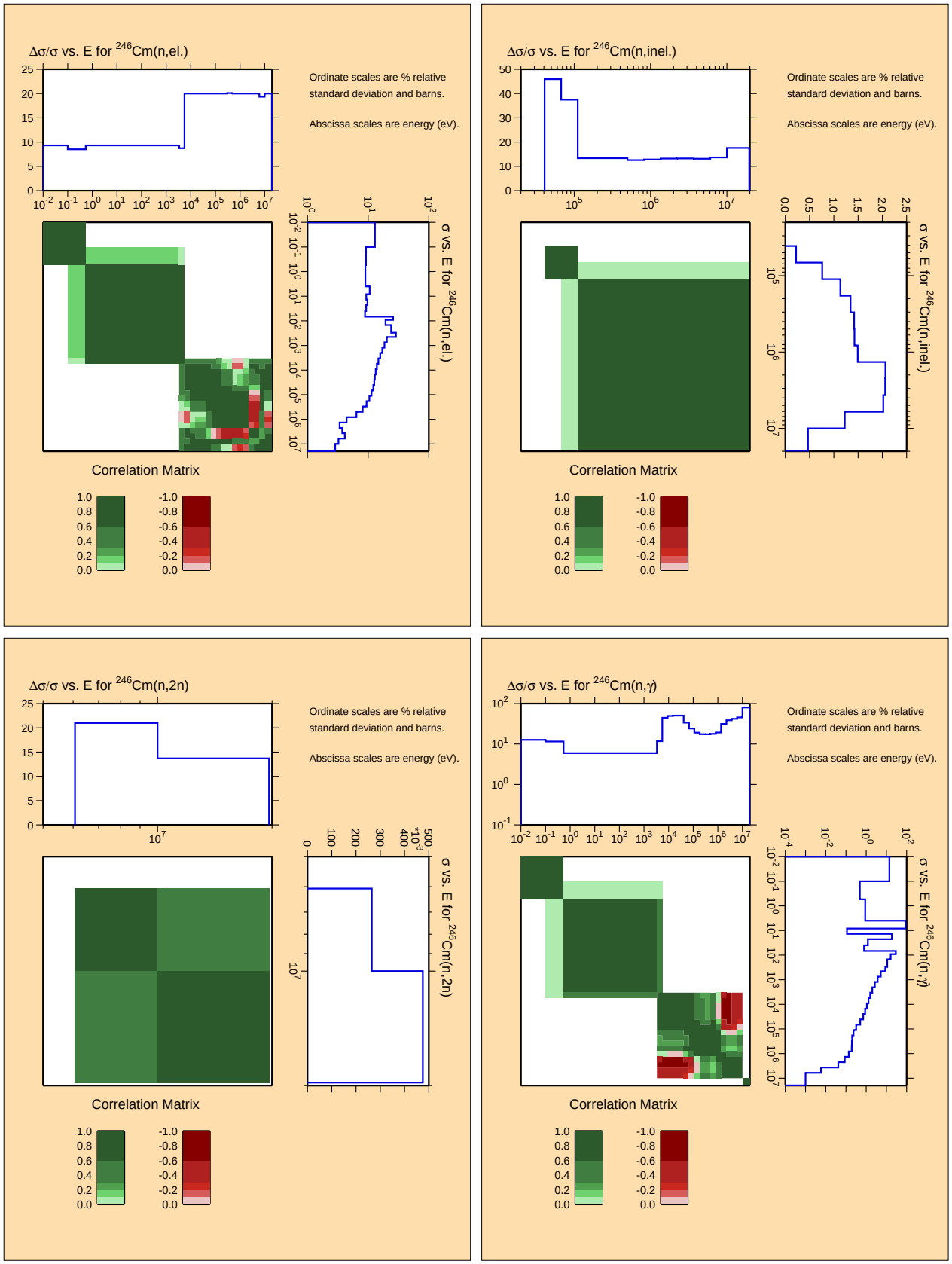

Figure A.110: Covariances for actinide ^{246}Cm.

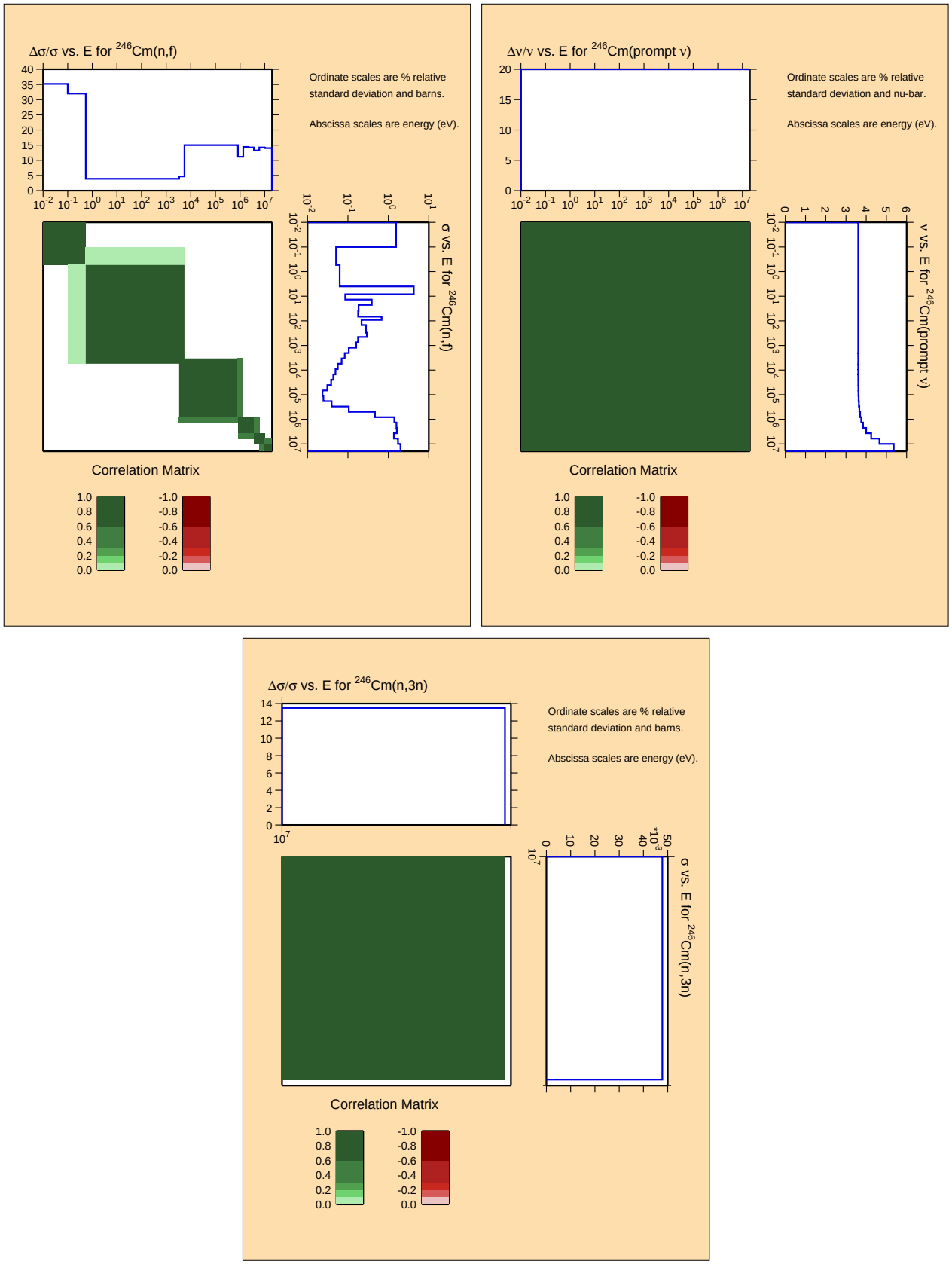

Figure A.110: Covariances for actinide ^{246}Cm (continued).

A.2.4 Mubars and Fission Spectra

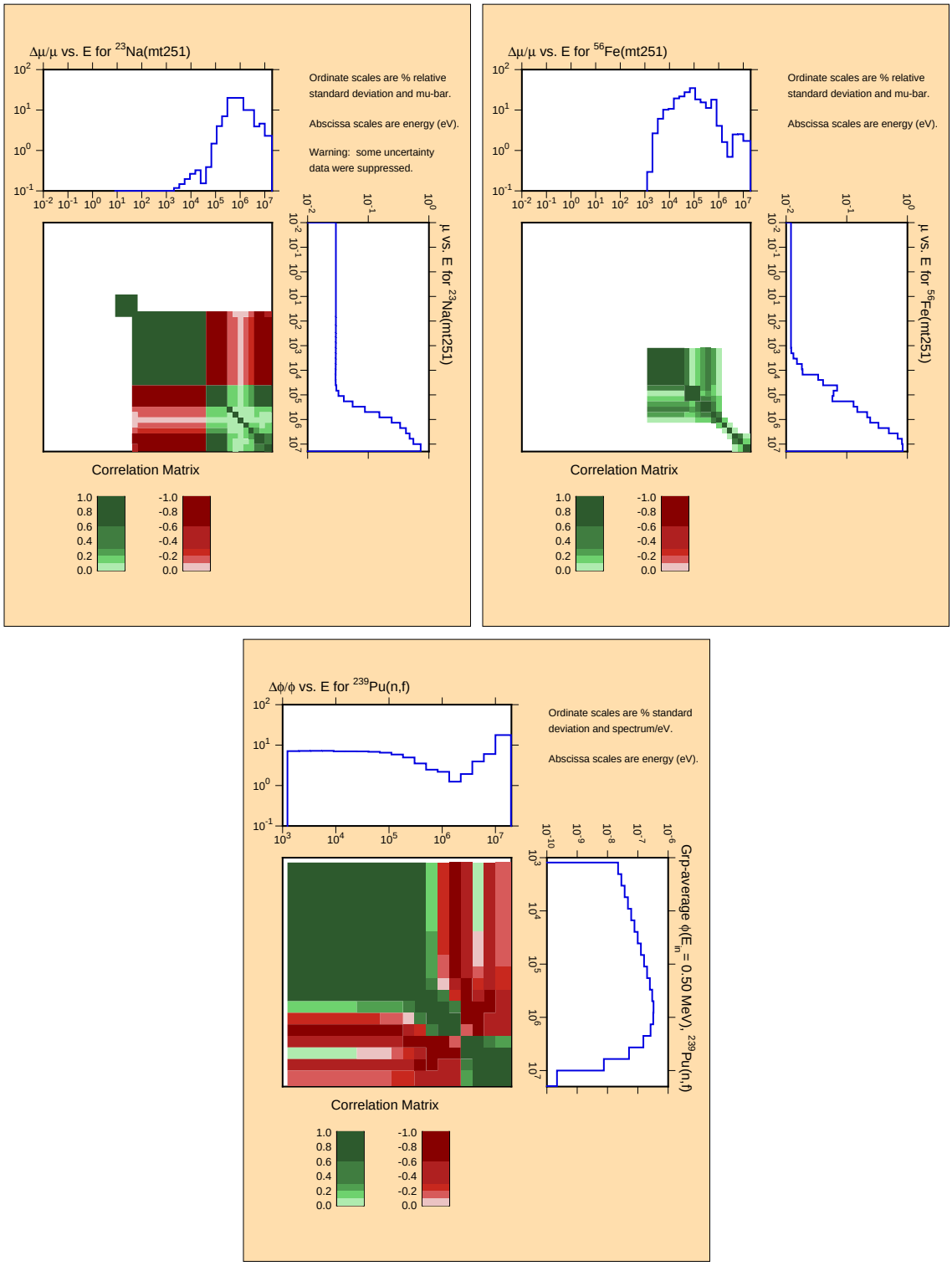

Figure A.111: $\bar{\mu}$ and fission spectra covariances.

Appendix B

^{240}Pu evaluation

In subsequent pages we reproduce recent report by LANL describing new evaluation of ^{240}Pu.

APPENDIX B

LANL TECHNICAL REPORT LA-UR-09-08071

N+^{240}PU EVALUATION AND UNCERTAINTY QUANTIFICATION

P.Talou and P.G.Young

T-2, Nuclear Physics Group,
Theoretical Division, Los Alamos National Laboratory

September 15, 2009

EVALUATION OF NEUTRON-INDUCED REACTION CROSS SECTIONS ON ^{240}PU

The total (MT=1), fission (MT=18), and radiative capture (MT=102) cross sections are based mainly on experimental data, complimented by nuclear model calculations. The experimental data were analyzed with the covariance code GLUCS (He80). Model parameters for the calculations were obtained by optimization with the experimental data.

The ECIS94 coupled-channels optical model code (Ra94) was used with a slightly modified version of the Sukovitskii optical model potential (Su04) for all discrete (n,n) and (n,n') cross section and angular distribution calculations, as well as for calculating neutron transmission coefficients for the reaction theory calculations. The modification we made to the Sukovitskii potential consisted of decreasing the λ parameter in the imaginary surface derivative potential, W_d, from 0.01759 to 0.010. This change brought the calculated total cross section into better agreement with experimental data near E_n=10 MeV.

Reaction theory calculations, utilizing the GNASH (Yo98) and COMNUC (Du70) Hauser-Feshbach codes, were used for (n,xn) reactions, again with the model parameters optimized to experimental data. The GNASH calculations also include pre-equilibrium contributions.

The JENDL Actinoid evaluation (Iw08) was also used to complement the present work in various places.

Total, Elastic, Non-Elastic and (n,xn) Cross Sections

For the total cross section between 0 and 40 keV, data were obtained from the JENDL actinoid evaluation (Iw08), but were renormalized slightly to match the covariance analysis above 40 keV. The shape of the cross sections below 40 keV follows the Sukovitskii optical model calculation closely.

From 40 keV and up to 30 MeV: the evaluation of the neutron total cross section in the MeV region resulted from a covariance analysis with the GLUCS code (He80) of the experimental data. Experimental data used were those of (Po81), (Po83), and (Sm72). We used the optical model results from our modified version of the Sukovitskii potential (Su04) as the prior in the GLUCS analysis, and the analysis results are very close to the optical model values at all energies. The evaluated total cross section is a smooth curve through the covariance analysis results, and above 8 MeV is identically equal to the optical model calculation.

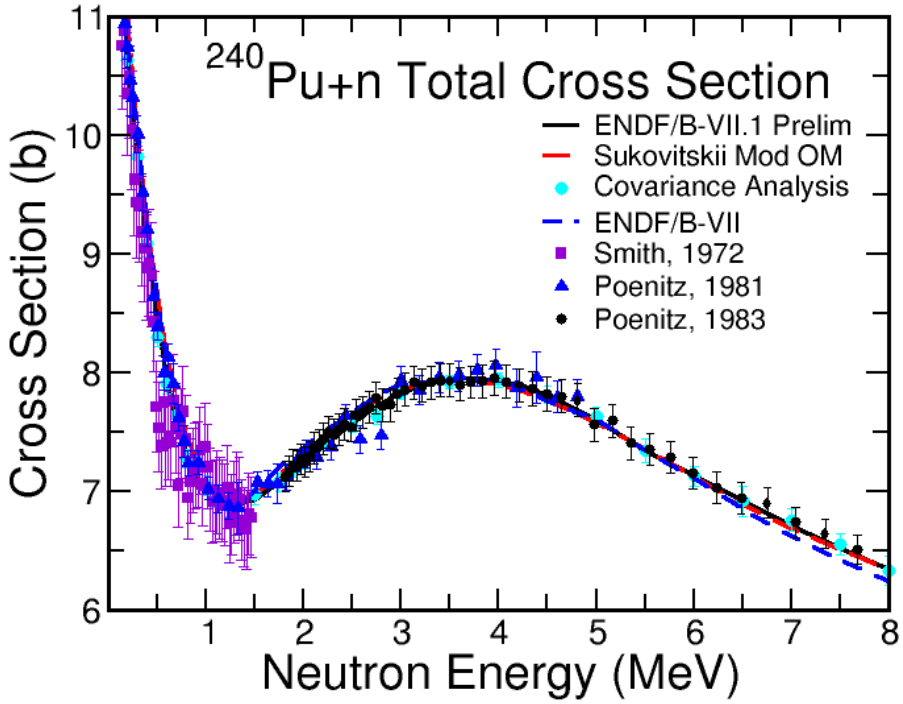

Figure 1 - Total cross section for n+^{240}Pu reaction. The present calculations are shown as a black line, and the GLUCS covariance analysis of experimental data points is shown as cyan dots.

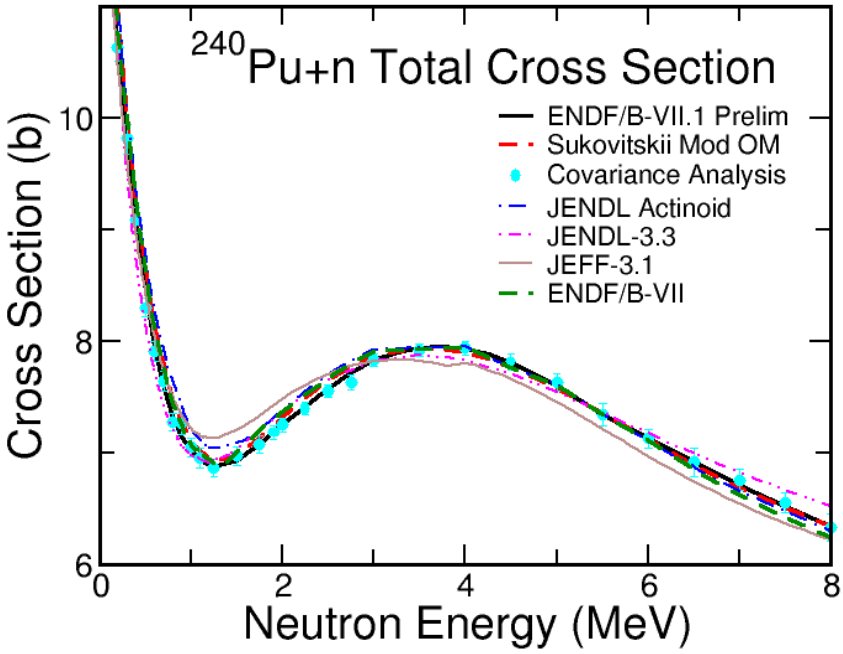

Figure 2 - Same as Fig.1 but as a comparison to other existing evaluations.

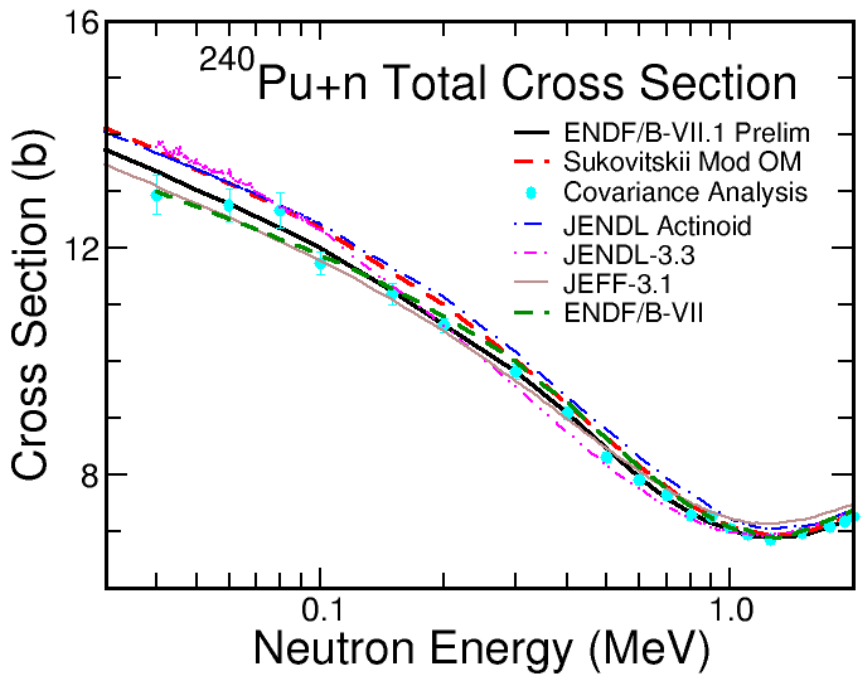

Figure 3 - A closer look at the low energy region.

The elastic cross section is obtained by subtracting the nonelastic cross section (MT=3) from the total cross section (MT=1). It is consistent with the modified Sukovitskii (Su04) optical results.

The (redundant) non-elastic cross section is the sum of MT=4,16,17,18,37,102.

The total inelastic cross section (MT4) is simply the sum of all discrete inelastic cross sections (MT51-91), including the continuum.

The (n,xn) cross sections (and energy-angle distributions) result from our GNASH (Yo98) calculations. The (n,2n) cross section is somewhat higher near 14 MeV than the earlier ENDF/B-VII, JEFF-3.1, and JENDL-3.3 evaluations but is lower than the recent JENDL actinoid (Iw08) evaluation.

Discrete Inelastic Level Cross Sections (MT=51-90)

MT=51-54: the ground-state rotational band direct and compound nucleus cross sections were taken from ECIS96 calculations with our modified version of the Sukovitskii optical model potential (Su04).

MT=55-71: Compound nucleus cross sections were taken from ECIS96 calculations with our modified version of the Sukovitskii optical model potential (Su04).

MT=72-90: Cross sections for grouped collective 2^+ and 3^- states are assumed to be the same as for ^{238}U(n,n') reactions and were taken for the ENDF/B-VII.0 ^{238}U evaluation. Those data, in turn, are based on DWBA/vibrational model calculations performed with the ECIS94 code (Ra94), assuming a set of 2+ or 3- vibrational states. Deformation parameters were determined by matching the 14-MeV Baba measurements (Ba89) of neutron emission spectra at various angles. The calculations were used to extrapolate the 14-MeV cross sections to lower and higher energies, and to obtain the MF=4 angular distributions for each assumed state. The spins, parities, and deformation parameters used in the calculations are given in the table below. These results affect the evaluation in the excitation energy range E_x=1.17-3.91 MeV.

MT	Ex (MeV)	J	π	β
	0.00000000	0.0	+1	0.0000E+00
72	1.17000000	3.0	-1	3.8087E-02
73	1.25000000	2.0	+1	3.0175E-02
74	1.44000000	3.0	-1	5.6001E-02
75	1.59000000	3.0	-1	3.8111E-02
76	1.75000000	3.0	-1	3.9460E-02
77	1.85000000	3.0	-1	3.5265E-02
78	1.95000000	3.0	-1	4.0750E-02
79	2.15000000	3.0	-1	4.7400E-02
80	2.30000000	3.0	-1	5.3002E-02
81	2.39000000	4.0	+1	8.8154E-03
82	2.49000000	2.0	+1	2.5122E-02
83	2.94000000	2.0	+1	2.7150E-02
84	3.18900000	2.0	+1	2.5287E-02

85	3.38800000	2.0	+1	2.5070E-02
86	3.53800000	2.0	+1	1.5390E-02
87	3.63700000	2.0	+1	1.6125E-02
88	3.73700000	2.0	+1	1.6472E-02
89	3.83700000	2.0	+1	1.4293E-02
90	3.90900000	2.0	+1	1.5091E-02

Inelastic Continuum Neutron Cross Section (MT=91)

The inelastic continuum neutron cross section is based on the GNASH Hauser-Feshbach statistical/pre-equilibrium calculations, described above. Note that MT=91 thresholds at 1.14 MeV. Therefore, discrete states with excitation energies above 1.14 MeV (MT=72-90) lie in the MT=91 continuum region.

Neutron Elastic Scattering Angular Distributions (MF4, MT2)

The elastic scattering angular distribution are based on coupled-channels calculations for the ground-state rotational band using the ECIS96 code (Ra94). The calculations used our modified version of the Sukovitskii optical model potential (Su04). For MT=51-54, the ground-state rotational band direct and compound nucleus angular distributions were taken from ECIS96 calculations with our modified version of the Sukovitskii optical model potential.

Above that (for MT=55-71), the compound nucleus angular distributions were obtained from ECIS96 calculations with our modified version of the Sukovitskii optical model potential.

Finally, for the assumed collective 2^+ and 3^- states (MT=72-90), the angular distributions were obtained from vibrational model calculations for the n+^{238}U reactions using the ECIS94 code (Ra94), as described above.

Fission Cross Section (MT=18 and MT=19, 20, 21 and 38)

From 0 - 550 keV, the fission cross section was taken from the JENDL Actinoid evaluation. These data agree well with the results of a GLUCS covariance analysis of the experimental data from 60 keV - 30 MeV, where they overlap.

From 550 keV - 30 MeV, the (n,f) cross section is based on a smooth curve through the GLUCS covariance analysis results. These results are influenced strongly by the extensive measurements of Staples et al. (St98). At some energies in this range, the present evaluation differs appreciably from the ENDF/B-VII.0, JEFF-3.1, JENDL-3.3, and JENDL Actinoid evaluations. The GNASH analysis closely follows the evaluation at most energies.

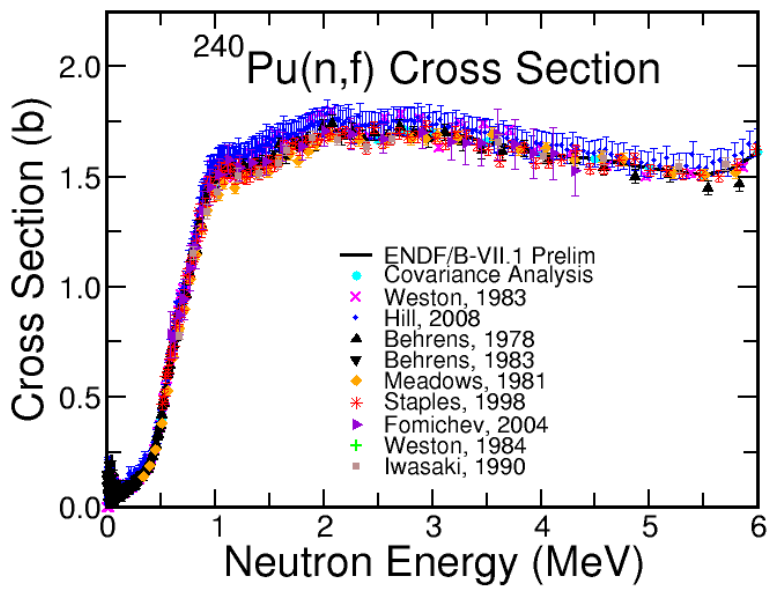

Figure 4 - Fission cross section of n+^{240}Pu. The present work is the result of a smoothing of a GLUCS analysis of experimental data.

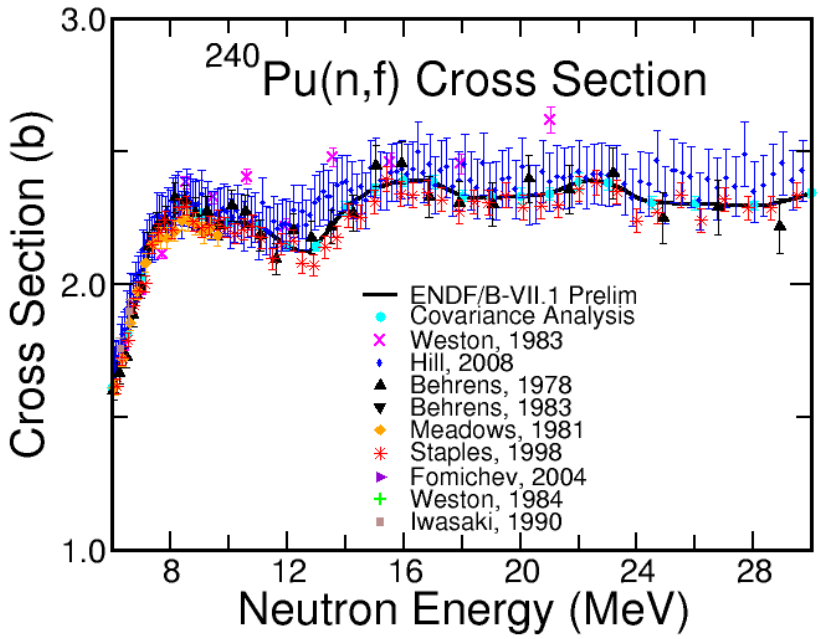

Figure 5 - Same as Fig.4 but for energies up to 30 MeV.

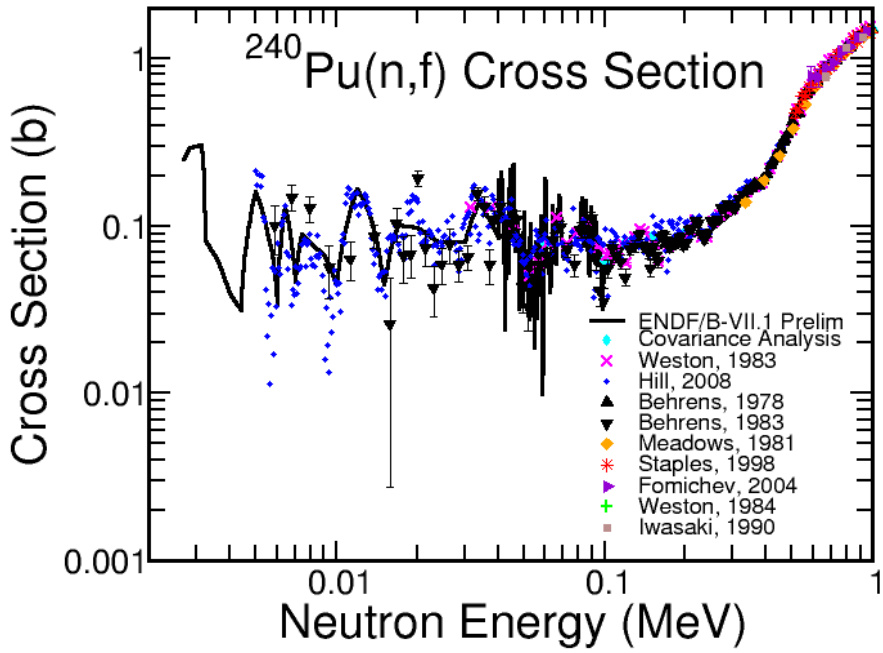

Figure 6 - Below 550 keV, the JENDL Actinoid evaluation was adopted. It agrees very well with our GLUCS analysis from 60 keV and up, where they overlap.

At higher energies, the multi-chance fission cross sections are obtained by scaling the GNASH calculations of the MT=19, 20, 21, 38 cross sections by the ratio of the new evaluated MT=18 cross section to the GNASH total fission cross section.

Neutron Radiative Capture Cross Section (MT=102)

From 0 to 30 keV, the radiative capture cross section is taken from the JENDL Actinoid evaluation, which is consistent near 30 keV with our GLUCS covariance analysis between 20 and 300 keV.

From 30 to 400 keV, our evaluation is based on a smooth curve through the result of our covariance analysis of the available experimental data.

The 0.4 to 2 MeV energy range is treated as a s
mooth transition of the data below 0.4 MeV to the ENDF/B-VII.0 evaluation at 2.0 MeV.

And from 2 to 30 MeV, the evaluation is taken from the ENDF/B-VII.0 evaluation to 20 MeV and smoothly extrapolated to 30 MeV.

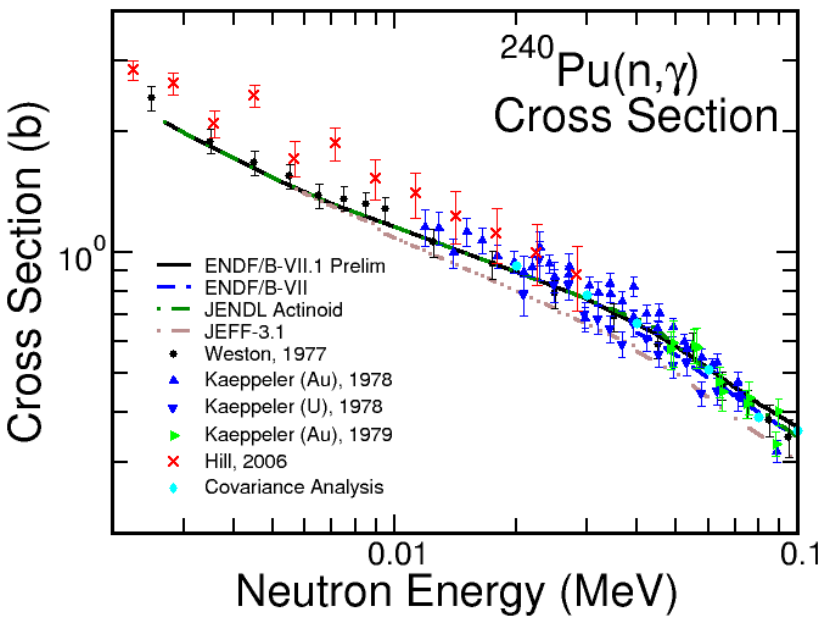

Figure 7 - Neutron radiative capture cross section of n+^{240}Pu, compared with experimental data and other evaluations. Below 30 keV, the JENDL Actinoid evaluation was adopted.

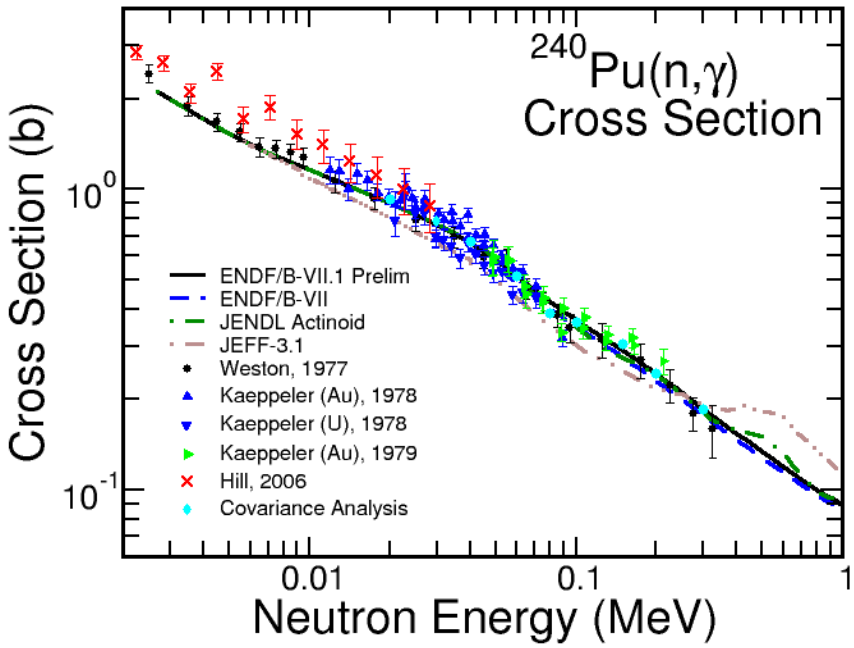

Figure 8 - Same as Fig. 7 for higher incident neutron energies.

PROMPT FISSION NEUTRONS
AVERAGE NEUTRON MULTIPLICITY, SPECTRUM AND COVARIANCE EVALUATION

The average prompt neutron multiplicity <ν> as a function of incident neutron energy is evaluated from a covariance analysis of existing experimental data. The status of the ENDF/B-VII.0 file (MF1, MT456) is shown in Figs.9 and 10 compared with experimental data and the JEFF-3.1 and JENDL-Actinoid evaluations. The ENDF/B-VII.0 evaluation clearly deviates from the low-energy data points. The experiment by Barton (1961) at thermal energy is however in contradiction with all evaluations.

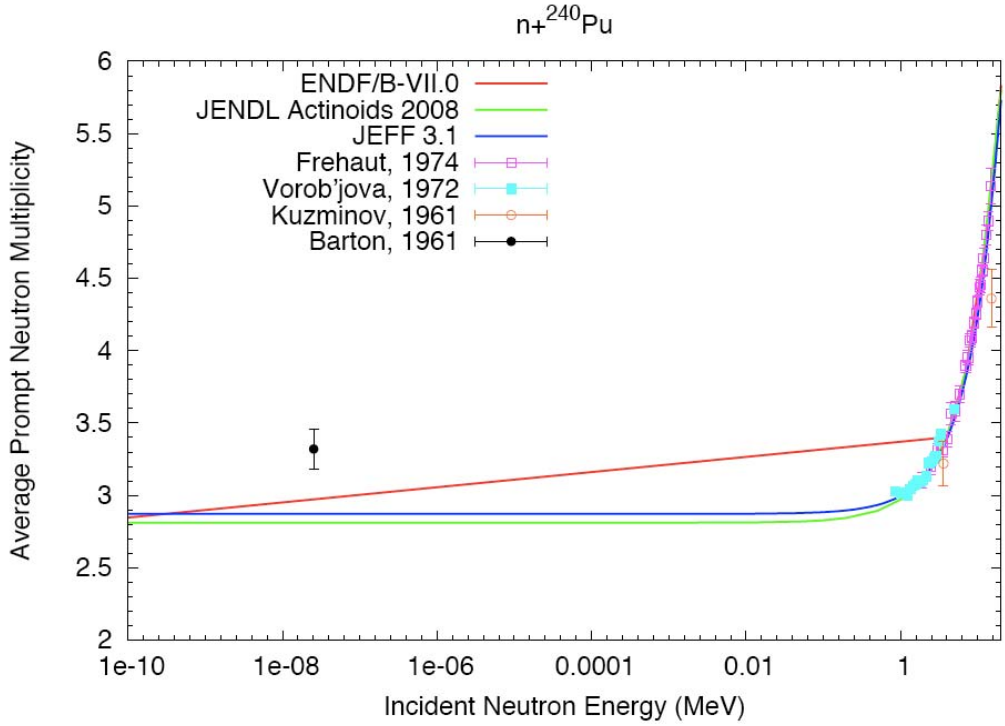

Figure 9 - Comparison of ENDF/B-VII.0 evaluation with existing experimental data sets and latest Japanese JENDL- Actinoid and European JEFF-3.1 evaluations.

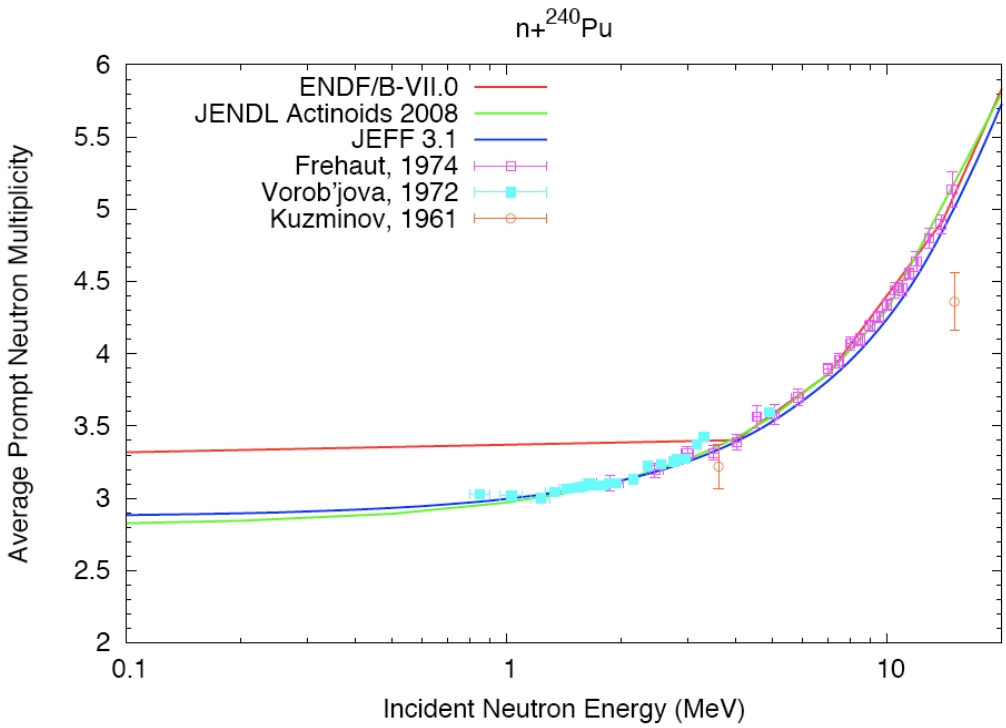

Figure 10 - A closer look from Figure 9 in the 1 to 10 MeV region.

We have performed a new covariance evaluation of the experimental data using the GLUCS code (He80). The results are very close to the JENDL-Actinoid file. In addition, a covariance matrix was produced and saved in file MF31, MT456. Figures 11 and 12 show the result of this evaluation for incident energies from 0 to 6 MeV, and from 6 to 30 MeV, respectively.

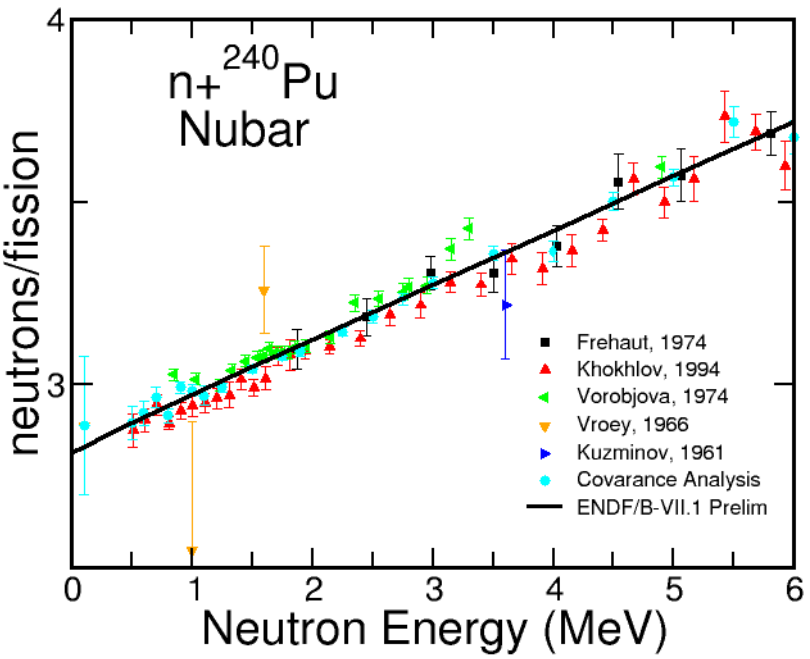

Figure 11 - The present evaluation (solid black line) compared to experimental data in the 0 to 6 MeV region.

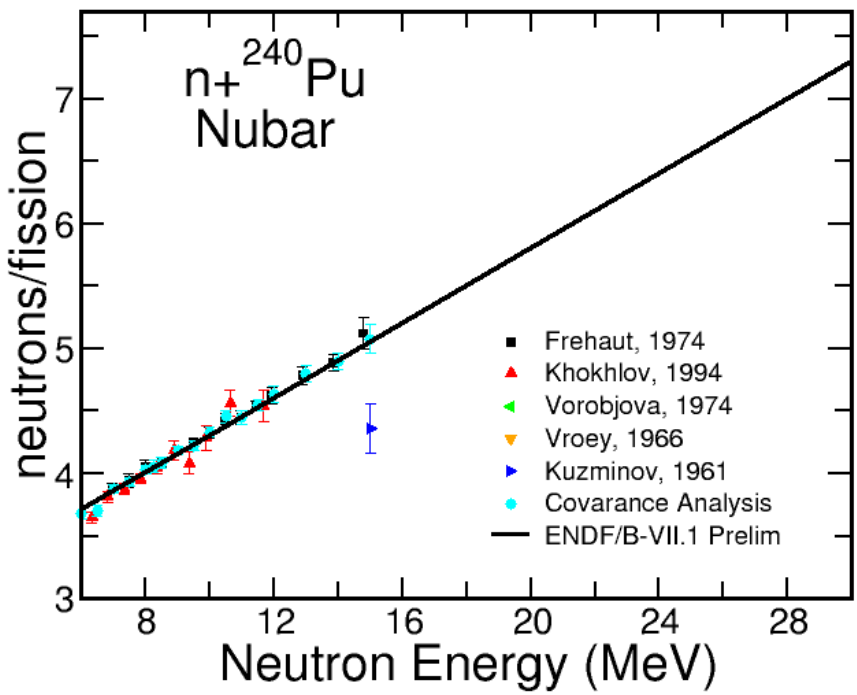

Figure 12 - Same as Fig.11 but for incident neutron energies from 6 to 30 MeV.

The Los Alamos or Madland-Nix (MN) model was used to evaluate the prompt fission neutron spectrum (PFNS) for incident neutron energies from thermal up to 20 MeV. Unfortunately no direct experimental measurement of the n+^{240}Pu PFNS exist, and only <◎> values can help constrain the model parameters values.

Table I summarizes the values of the MN model parameters used in this work. At high energies (> ~6 MeV), multiple-chance fission is treated, and the nth-chance fission probabilities are extracted from GNASH calculations. These are shown in Fig.13.

Table 1 - Values of the parameters used in the Madland-Nix model calculations. From left to right, the parameters are ZAID of the parent fissioning nucleus; the ZAID of the light fragment; the average total

kinetic energy; the average energy release, the constant entering in the level density parameter calculation; the average neutronaverage energy release, the constant entering in the level density parameter calculation; the average neutron average neutron binding energy; the average neutron separation energy; and the average total ◎-ray energy. They are given for the three chances fission considered in this work (up to 20 MeV).

	$ZAID_p$	$ZAID_{LF}$	<TKE> (MeV)	$\langle E_r \rangle$ (MeV)	C=A/<a>	$\langle B_n \rangle$ (MeV)	$\langle S_n \rangle$ (MeV)	$\langle E_\gamma \rangle$ (MeV)
1st-chance	94241	40101	178.2	198.0	10.5	5.241	5.202	6.77
2nd-chance	94240	40100	177.0	197.5	10.0	6.534	5.110	6.74
3rd-chance	94239	40100	175.5	197.0	9.5	5.646	5.217	6.71

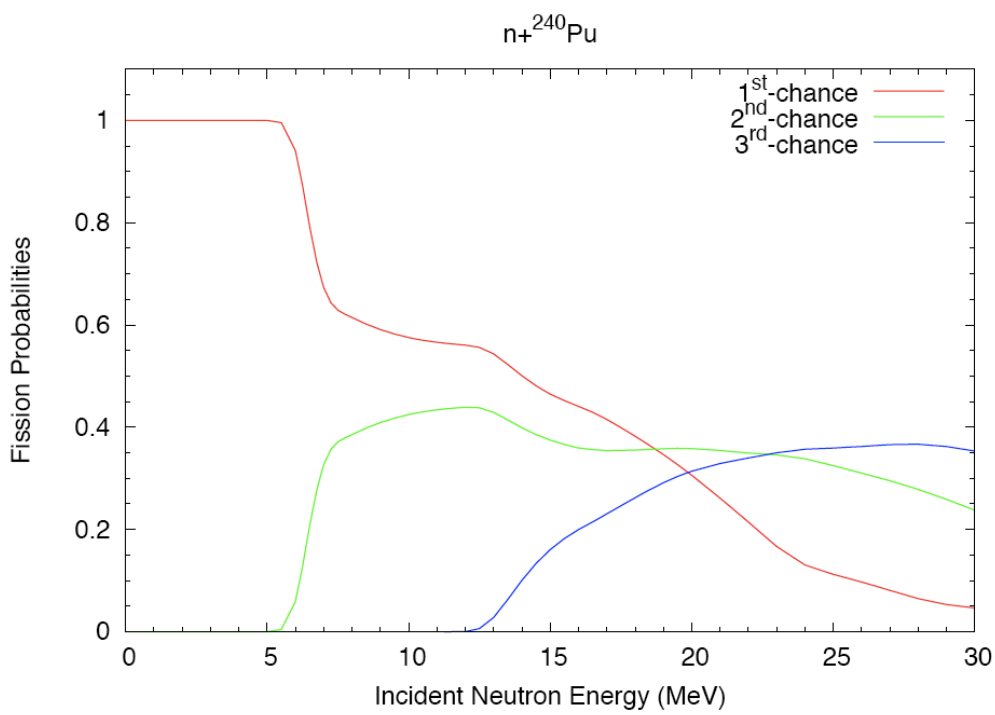

Figure 13 - First, second and third-chance fission probabilities obtained from GNASH calculations, and used in the PFNS evaluation.

The average neutron multiplicity calculated using these MN model parameter values is shown in Figs. 14 and 15 (black full triangles). It follows the GLUCS results except at the highest energies (above 15 MeV) where it lies lower than the GLUCS values. However, at these energies, no experimental data exist for <ν>.

The PFNS obtained with these MN model parameters is shown in Fig.16 as a ratio to ENDF/B-VII.0 values, which are represented as simple Maxwellians with temperature dependent upon the incident neutron energy. For comparison, the JENDL-Actinoid results are also shown on this figure. Note the spike in the 15 MeV PFNS from the JENDL evaluation due to pre-equilibrium neutrons, not considered in the present work.

Following the same methodology as for evaluating cross-section uncertainties, we have used the KALMAN code, which implements a Bayesian statistical approach, to evaluate the covariance matrix associated with the PFNS of ^{240}Pu with 0.5 MeV incident neutron energies.

However, quantifying the uncertainties associated with the evaluated PFNS based solely on experimental data on <ν> values and *a priori* model parameter values is very difficult and leads to unreasonably large uncertainties. In order to obtain more reasonable results, we have added some "dummy" experimental data points in our analysis. Those data points follow exactly the calculation, but are given some guessed uncertainties at selected outgoing energy points. This is shown in Fig.17. For instance, we have assumed an uncertainty of 15% at the mean outgoing energy, and 40% at 10 keV and 10 MeV.

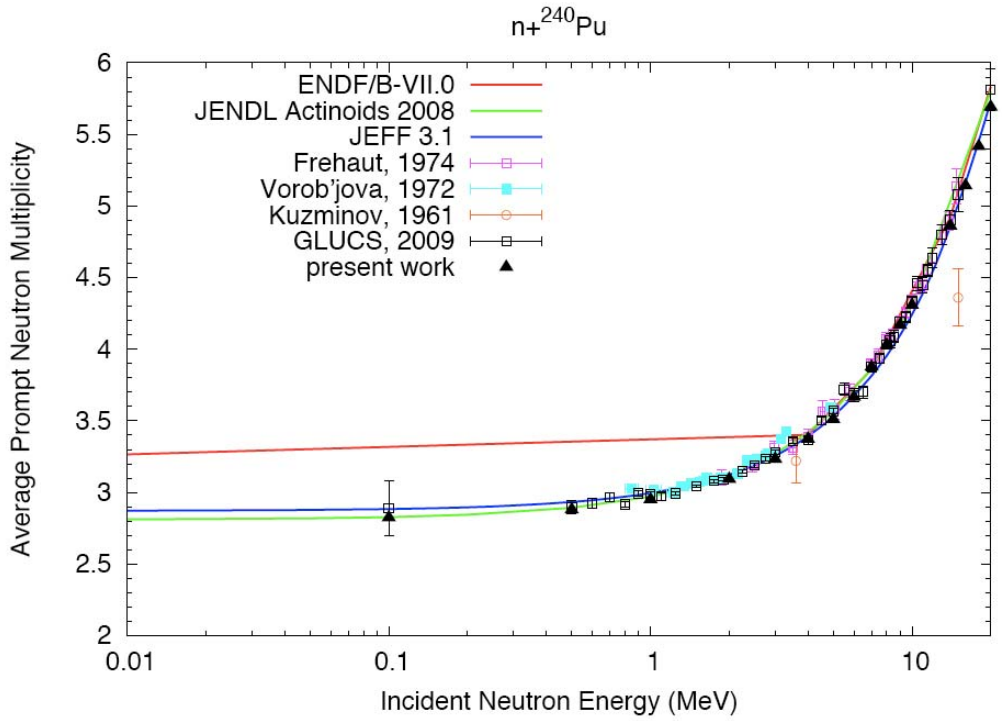

Figure 14 - Average neutron multiplicity values obtained with Madland-Nix model calculations (black triangles). The GLUCS covariance analysis results are shown as black empty squares.

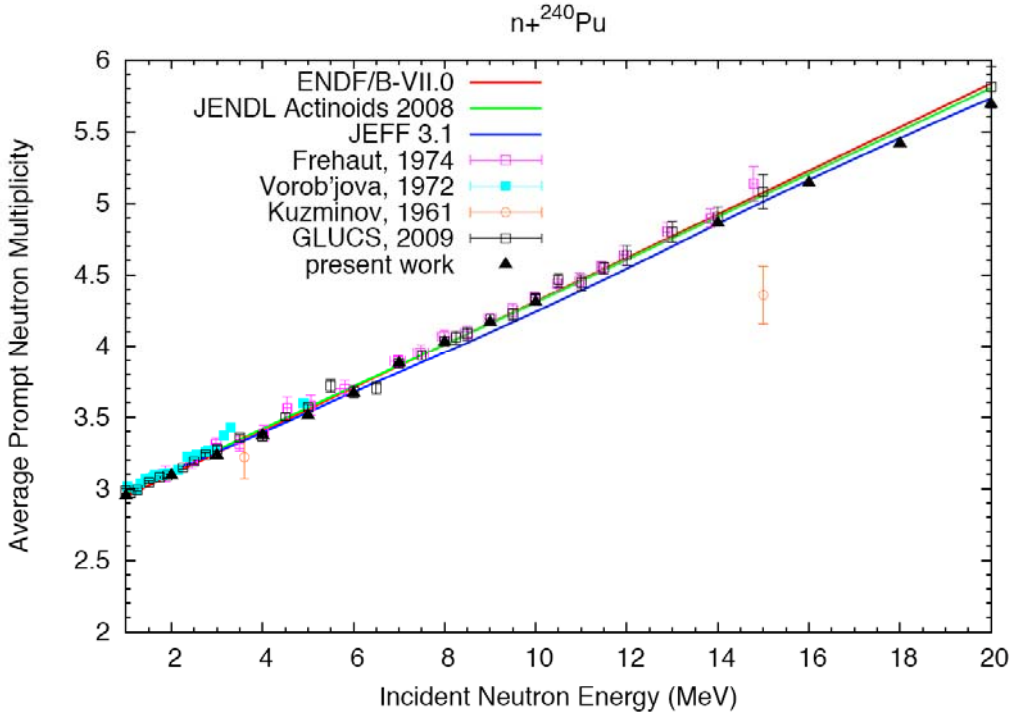

Figure 15 - Same as Fig.14 but with a linear x-axis.

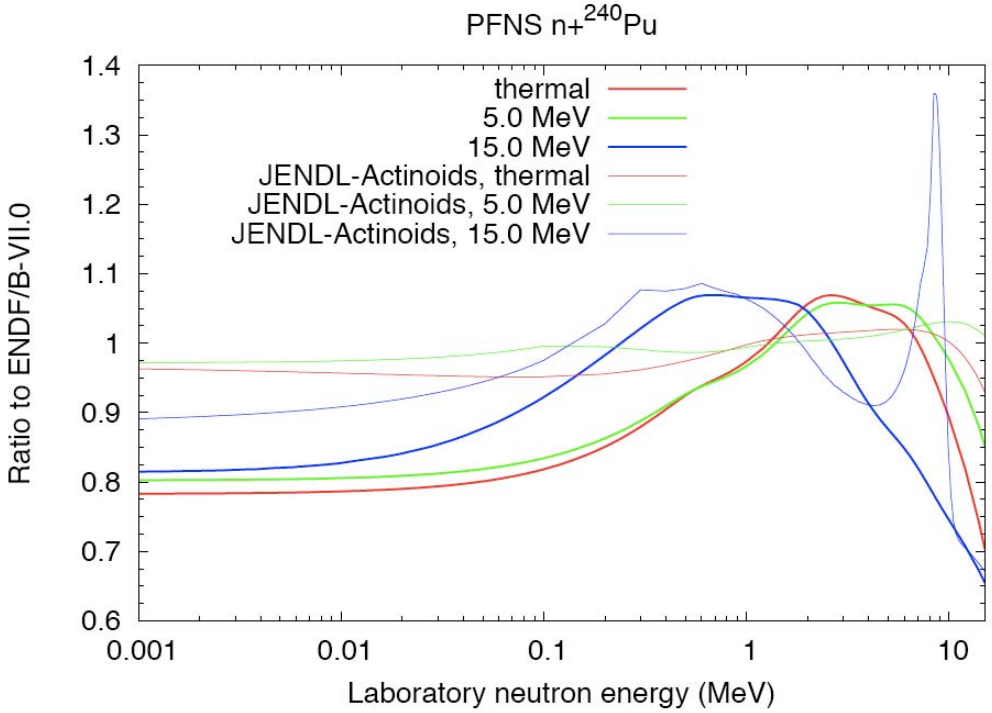

Figure 16 - Prompt Fission Neutron Spectra calculated using the MN model, for several incident energies (thermal, 5.0 and 15.0 MeV), and shown as a ratio to ENDF/B-VII.0 Maxwellian values. The JENDL-Actinoid results are also shown for comparison.

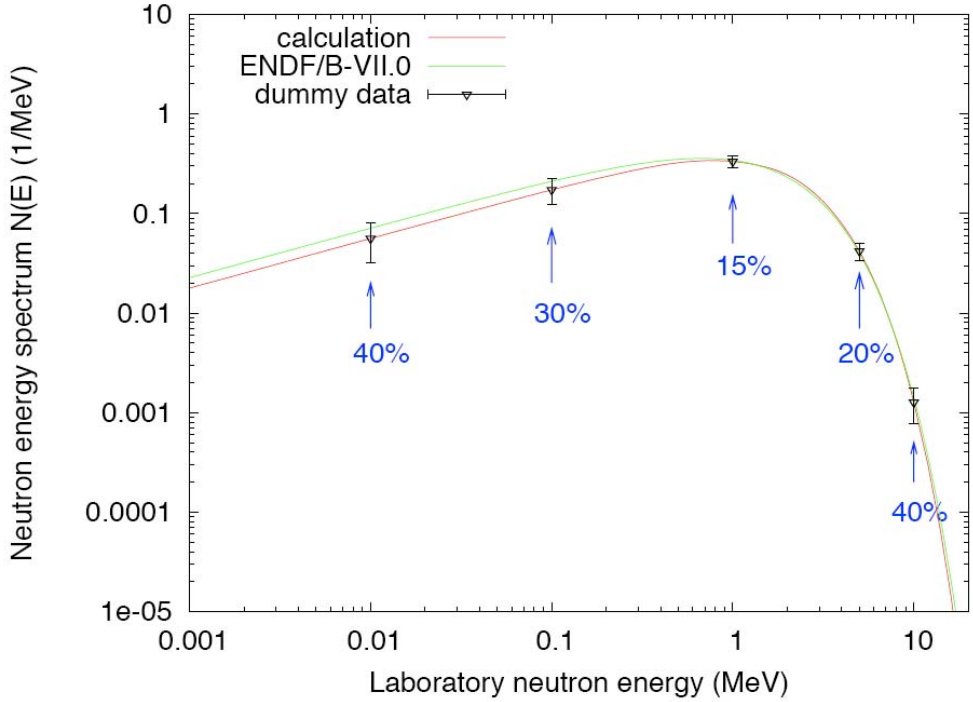

Figure 17 - Assumed uncertainties on *dummy experimental* data points at selected outgoing energies for the n (0.5 MeV)+^{240}Pu PFNS.

The result of our KALMAN analysis is shown in Figs. 18 and 19, which represent the calculated standard deviations and correlation matrix, respectively.

These final results were transformed into ENDF format, and stored as files MF5, MT18 for the spectrum, and MF35, MT18 for its associated covariance matrix.

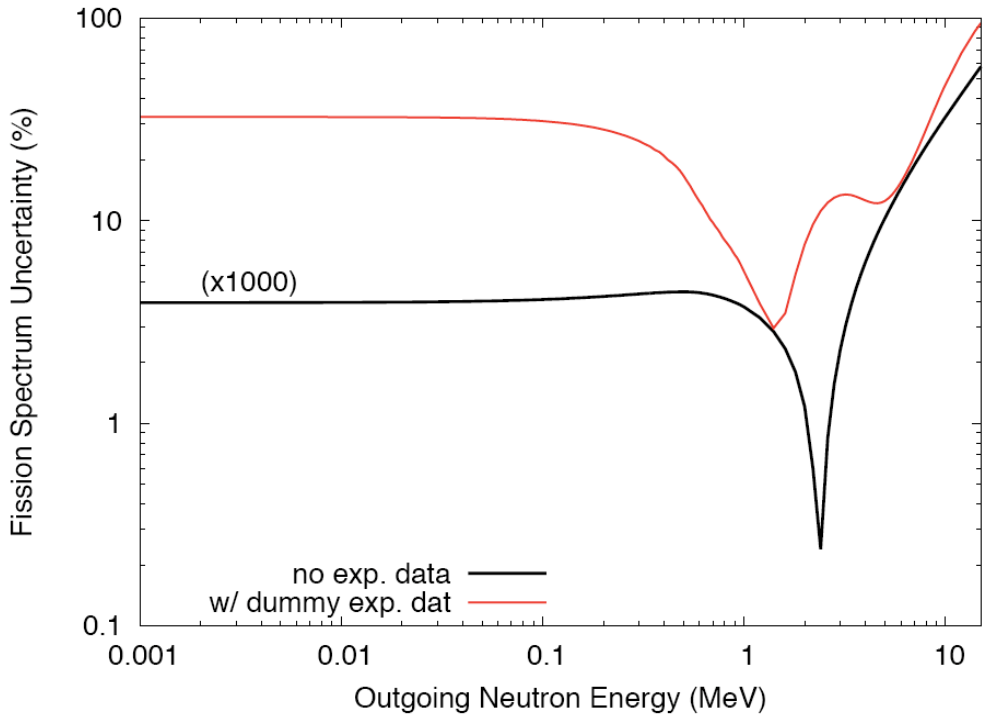

Figure 18 - Fission spectrum standard deviations obtained after a KALMAN analysis.

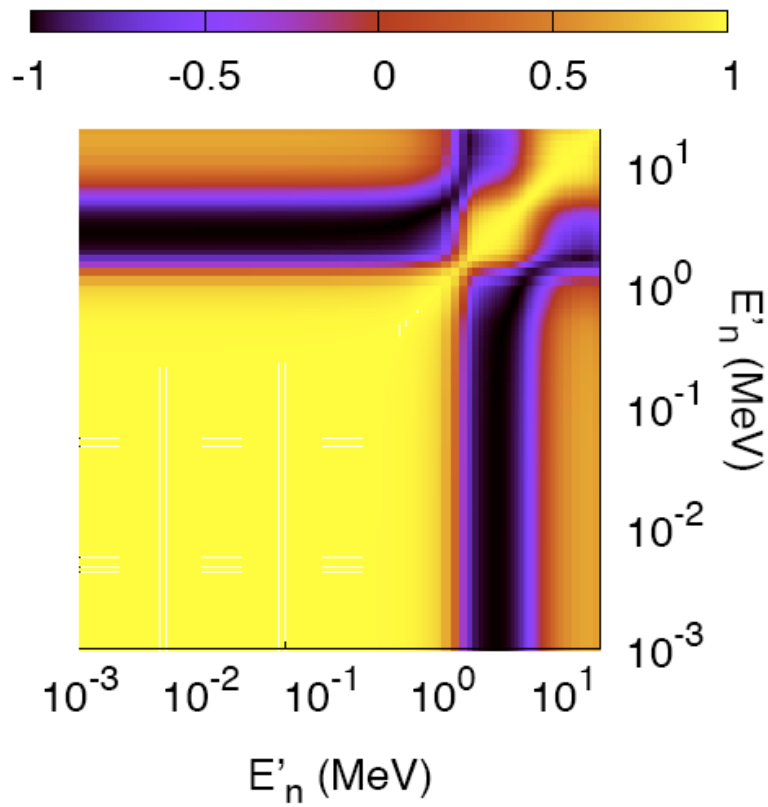

Figure 19 - Correlation matrix of the n(0.5 MeV)+^{240}Pu PFNS. The negative elements in this correlation matrix are due to the normalization of the PFNS.

UNCERTAINTY QUANTIFICATION ON N+^{240}PU REACTION CROSS SECTIONS

We have performed an uncertainty quantification analysis of the n+^{240}Pu reaction cross sections, using the GNASH code for computing the cross sections, and the KALMAN code to perform a Bayesian analysis combining experimental data sets and model calculations. The exact same methodology was used in our earlier investigations of n+$^{235,\ 238}$U and n+^{239}Pu.

REFERENCES

- **[Ba89]** M. Baba, H. Wakabayashi, N. Itoh, K. Maeda, and N. Hirakawa, "Measurements of Prompt Fission Neutron Spectra and Double-Differential Neutron Inelastic Scattering Cross Sections for 238-U and 232-Th," IAEA Int. Nucl. Data report INDC(JPN)-129 (1989).

- **[Du70]** C.L.Dunford, AI-AEC-12931 (1970).

- **[He80]** D. M. Hetrick and C. Y. FU, "GLUCS: A Generalized Least-Squares Program for Updating Cross-Section Evaluations with Correlated Data Sets," Oak Ridge National Laboratory report ORNL/TM-7341 (ENDF-303) (1980).

- **[Iw08]** O. Iwamoto, N. Otuka, S. Chiba, et al., re-evaluation of n+^{240}Pu data for JENDL (2008).

- **[Po81]** W. P. Poenitz, J. F. Whalen, and A. B. Smith, NSE **78**, 333 (1981).

- **[Po83]** W. P. Poenitz and J. F. Whalen, ANL-NDM-80 (1983).

- **[Ra94]** J. Raynal, "Notes on ECIS94," Centre d'Etudes Nucleaires (Saclay) report CEA-N-2772 (1994).

- **[Sm72]** A. B. Smith, J. F. Whalen, and P. Lambropoulos, NSE **47**, 19 (1972).

- **[St98]** P. Staples and K. Morley, NSE **129**, 149 (1998).

- **[Su04]** Sukovitskii et al., J. Phys. G: Nucl. Part. Phys. **30**, 905-920 (2004).

- **[Yo98]** P. G. Young, E. D. Arthur, and M. B. Chadwick, "Comprehensive Nuclear Model Calculations: Theory and Use of the GNASH Code," Proc. Workshop on Nuclear Reaction Data and Nuclear Reactors, ICTP, Trieste, Italy, 15 April - 17 May 1996 [Ed: A. Gandini and G. Reffo, World Scientific Publ. Co., Singapore (1998)] p. 227-404.